INTERNATIONAL SCHOOL FOR ADVANCED STUDIES

Cell death neuroprotection and repair mechanisms in a model of rat spinal cord injury *in vitro*

Thesis submitted for the degree of "Doctor Philosophiae"

Academic year 2012-2013

Candidate:

Elena Bianchetti

Supervisor:

Prof. Andrea Nistri

Co-supervisor:

Prof. Miranda Mladinic

Scuola Internazionale Superiore di Studi Avanzati (SISSA/ISAS)

Via Bonomea 265 – 34136 Trieste, Italy

Dedicated to my beloved Trieste.

«La nostra bella Trieste!
I have often said that angrily, but tonight I feel it true.
I long to see the lights twinkling along the Riva
as the train passes Miramar.
After all, Nora, it is the city which has sheltered us.»

«La nostra bella Trieste!
Spesso l'ho detto con rabbia, ma stasera sento che è vero.
Ho voglia di vedere le luci che brillano lungo la Riva
mentre il treno passa Miramare.
Dopo tutto, Nora, è la città che ci ha dato rifugio.»

James Joyce, *letter to Nora*,1909.

LIST OF CONTENTS

DECLARATION

The data reported in the present thesis have been published (or currently under review) in the articles listed herewith. The candidate's specific contribution to each paper is listed below. In each one of these articles the candidate has contributed to the interpretation, discussion of the data and writing the manuscript:

1) Mechanisms underlying cell death in ischemia-like damage to the rat spinal cord in vitro.
Bianchetti E, Mladinic M, Nistri A.
Cell death and disease (2013).

The candidate has performed all the experimental work of this paper.

2) Unusual increase in lumbar network excitability of the rat spinal cord evoked by the PARP-1 inhibitor PJ-34 through inhibition of glutamate uptake.
Nasrabady SE, Kuzhandaivel A, Akrami A, **Bianchetti E**, Milanese M, Bonanno G, Nistri A.
Neuropharmacology (2012).

The candidate has performed the immunohistochemistry analysis of this paper.

3) ATF3 is a novel nuclear marker for migrating ependymal stem cells in the rat spinal cord.
Mladinic M, **Bianchetti E**, Dekanic A, Mazzone GL, Nistri A.
Manuscript under review (2013).

The candidate has performed the isolated spinal cord preparations, proteins extraction and western blot, some immunohistochemistry and the confocal analysis of this paper.

ABSTRACT

Nowadays, new spinal cord injury (SCI) cases are frequently due to non traumatic causes, especially vascular disorders. A prerequisite to developing mechanism-based neuroprotective strategies for acute SCI is a full understanding of the early pathophysiological changes to prevent later disability and paralysis. The immediate damage spreads from the initial site through excitotoxicity and metabolic dysfunction (ischemia, free radicals and neuroinflammation) to surrounding tissue (secondary damage). Using an *in vitro* neonatal rat spinal cord model, an experimental protocol (pathological medium, PM) has been developed to mimic the profound metabolic perturbation (hypoxia, aglycemia, oxidative stress, acidosis, toxic free radicals) occurring *in vivo* after ischemic SCI, a condition surprisingly worsened by extracellular Mg^{2+} (1 mM). The current study sought to identify the cells affected by PM (with Mg^{2+}), and the associated molecular death pathways in the spinal lumbar region which contains the locomotor networks. The results indicated that 1 h PM+Mg^{2+} application induced delayed pyknosis chiefly in the spinal white matter via overactivation of poly (ADP-ribose) polymerase 1 (PARP1), suggesting cell death mediated by the process of parthanatos and also via caspase 3-dependent apoptosis. Grey matter damage was less intense and concentrated in dorsal horn neurons and motoneurons which became nuclear-immunoreactive for the mitochondrial apoptosis-inducing factor. Moreover, TRPM2 channel expression was enhanced 24 h later in dorsal horn and motoneurons, while TRPM7 channel expression concomitantly decreased. Conversely, TRPM7 expression grew earlier (3 h) in white matter cells, while TRPM2 remained undetectable. Our results show that extracellular Mg^{2+} amplified the white matter cell death via parthanatos and apoptosis, and motoneuronal degeneration via PARP1-dependent pathways with distinct changes in their TRPM expression. In fact, the PARP-1 inhibitor PJ34, when applied 30 min after the moderate excitotoxic insult, could protect spinal networks controlling locomotion in more than 50 % of preparations. Interestingly, the drug per se strongly increased spontaneous network discharges without cell damage. Glutamate ionotropic receptor blockers suppressed this phenomenon reversibly. Our results suggest that pharmacological inhibition of PARP-1 could prevent damage to the locomotor networks if this procedure had been implemented early after the initial lesion and when the lesion was limited. PJ34 had also a positive effect on PM+Mg^{2+} treated spinal cords, especially in the white matter after 24 h, both alone or administered together with caspase-3 inhibitor. The neonatal rat *in vitro* SCI model was also useful to study the activation of endogenous

spinal stem cells. We identified the ATF3 transcription factor as a novel dynamic marker for ependymal stem/progenitor cells (nestin, vimentin and SOX2 positive) located around the central canal of the neonatal or adult rat spinal cord. While quiescent ependymal cells showed cytoplasmic ATF3 expression, over 6-24 h *in vitro* these cells mobilized and acquired intense nuclear ATF3 staining. The migration of ATF3-nuclear positive cells preceded the strong proliferation of ependymal cells occurring after 24 h *in vitro*. Pharmacological inhibition of MAPK-p38 and JNK/c-Jun, upstream effectors of ATF3 activation, prevented the mobilization of ATF3 nuclear-positive cells. Excitotoxicity or ischemia-like conditions did not enhance migration of ependymal cells at 24 h. ATF3 is, therefore, suggested as a new biomarker of activated migrating stem cells in the rat spinal cord *in vitro* that represents an advantageous tool to study basic properties of endogenous stem cells.

INTRODUCTION

1. SPINAL CORD INJURY

1.1 Definition, statistics and symtomps

Spinal cord injury (SCI) is due to damage to the spinal cord that causes dysfunction, with loss of sensory and motor function distal to the point of injury (Hulsebosch, 2002). SCI, either traumatic or non-traumatic, often produces long-terme effects with lifelong consequences, associated with severe disabilities which are of great concern to the person affected, but also to their family and society as whole (van den Berg et al., 2010). SCI is particularly troubling because it predominantly occurs in young, otherwise healthy individuals, with injury occurring with the greatest frequency in those between 15 and 25 years of age. SCI occurs worldwide with an estimated annual incidence of 15–40 cases per million per year and every 5 cases, 4 affect males (Rowland et al., 2008). Total direct costs of caring for individuals with spinal-cord injury exceed $7 billion per year in the USA (McDonald and Sadowsky, 2002). SCI may induces one or more of the following symptoms: paralysis, loss of sensation such us the possibility to feel cold, heat and touch, hyper reflexia or spasms, loss of bowel and bladder control, loss of sexual function and pain. The spinal cord is divided in cervical, thoracic, lumbar and sacral segments. Depending on what group of muscles, organs and sensation are affected, paralysis can be referred to as tetraplegia (or quadriplegia), when the level of injury is above the first thoracic vertebra, or paraplegia, when the level of injury occurs below the first thoracic spinal nerve (Figoni, 1984; Harkey et al., 2003). Of the estimated 12,000 new cases of quadriplegia and paraplegia that occur in the United States each year, 5000 die (Sekhon and Fehlings, 2001). Despite significant improvements in the early medical and surgical management and progress in neuroscience research, at the present day the pathophysiology of the SCI remains largely unknow and there are no effective treatments to improve neurological outcomes following SCI (Rowland et al., 2008).

2.EPIDEMIOLOGY OF SCI.

2.1 Complete and incomplete SCI

No matter of its origin, and in relation to the forces involved in the injury (Harkey et al.,

2003), from a clinical point of view a SCI can be complete, with no motor or sensory functions below the level of injury, or incomplete, when motor or sensory functions below the level of injury remains. The clinical scale established by American Spinal Injury Association (ASIA) divides patients in five categories, from A to E, depending on the severity of neurological loss:

A = Complete. No sensory or motor function is preserved in the sacral segments S4-5. This will result in complete paraplegia or tetraplegia.
B = Sensory Incomplete. Sensory but not motor function is preserved below the neurological level and includes the sacral segments S4-5 and no motor function is preserved more than three levels below the motor level on either side of the body.
C = Motor Incomplete. Motor function is preserved below the neurological level, and more than half of key muscle functions below the neurological level of injury have a muscle grade less than 3.
D = Motor Incomplete. Motor function is preserved below the neurological level, and at least half of key muscle functions below the neurological level of injury have a muscle grade more than 3.
E = Normal. Sensory and motor functions are normal, in all segments.
(http://www.asia-spinalinjury.org/elearning/ISNCSCI_ASIA_ISCOS_low.pdf).

2.2 Traumatic SCI

According to National Spinal Cord Injury Statistical Center (NSCISC) report, published in 2012, in the United States the three leading causes of spinal cord injury from 2010 to 2012 were traumatic (figure 1). Vehicular accidents, including cars and motorcycles, ranked as the leading cause of SCI (36.5%), even if there was a steady decrease in this percentage of SCI causes from 46.9 percent (1990-1994) to 36.5 percent (2010-2012). Falls ranked second (28.5%) followed by acts of violence, primarily gunshot wounds (14.3%). A decrease in the percentage of SCI due to sports-related activities from 14.4 to 9.2% occurred during the last twenty years. During the last decade there has been a significant increase in SCI as consequence of falls, probably due to aging of the population (https://www.nscisc.uab.edu/reports.aspx). A progressive increase of traumatic spinal cord diseases among older adults has been observed, from 79.4 per million older adults in 2007 to 87.7 by the end of 2009, but remained steady among younger adults (Selvarajah et al., 2013).

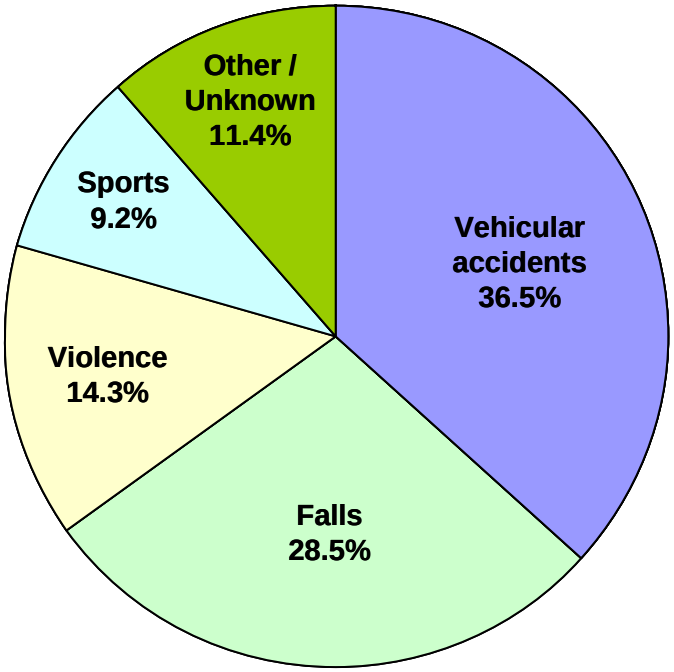

Fig. 1. Causes of traumatic SCI from 2010 to 2012 (https://www.nscisc.uab.edu/reports.aspx).

2.3 Non-traumatic SCI

A trend has been observed toward increased incidence in non-traumatic causes of SCI, which today account for about 30-50% of spinal cord disorders (Nair et al., 2005) and constitute a major risk factor for medical complications during rehabilitation such us thrombosis, spasticity or wound infections (McKinley et al., 2002). Non-traumatic SCI originates from vertebral stenosis, tumors, vascular ischemia, inflammatory conditions or cardiovascular disorders that comprise a cluster of post- surgical paralysis after abdominal aorta surgery (van den Berg et al., 2010; Nair et al., 2005). Although non-traumatic lesions are usually incomplete, the clinical symptoms are severe, and include paralysis and sensory dysfunction (van den Berg et al., 2010; Nair et al., 2005; Bianchetti et al., 2013), while traumatic SCI is four times more common in men than in women, gender is not a significant factor in non-traumatic diseases, even if women with SCI tend to suffer more from pain and depression (Nair et al., 2005). In contrast with traumatic SCI, there is a steady increase in incidence rate of non-traumatic SCI with advancing age. This may be due to the fact that etiologies in non-traumatic injuries are particularly associated with age-related conditions, such as tumor compressions, degeneration or vascular problems (van den Berg et al., 2010).

3. PHASES OF SCI

A detailed understanding of the pathophysiological processes occourring after acute SCI is a fundamental issue, as a prerequisite to develop mechanism-based neuroprotective strategies. Several elements of the injury response, including inflammatory response and reactive astrogliosis, have been found to act pathologically (Rowland et al., 2008). The interval from spinal cord injury to death ranges from 20 minutes to 9 months (Tator and Koyanagi, 1997). SCI responses that occur after injury have been divided into three phases: the immediate (or primary), secondary and chronic injury processes (Hulsebosch, 2002; Tator, 1995).

3.1 Primary injury phase (1-2 h)

The primary phase of a traumatic SCI involves the initial mechanical insult, causes fracture and/or dislocation of the spinal column which directly imparts force to the spinal cord, disrupting axons plus damage to blood vessels and cell membranes (Hulsebosch, 2002; Rowland et al., 2008), and last up to 2 h (Norenberg et al., 2004). Within minutes following injury, the first sign is edema of the cord, due to exudation of fluid from capillaries, usually accompanied by parenchymal hemorrhages of the white and grey matter (Kakulas, 2004; Quencer et al., 1986). The resulting ischemia may extend both caudal by and rostral by to the injury site (Tator and Koyanagi, 1997). During this initial process, necrosis of the central grey matter is usual, due to the direct damage of the cell membranes and ischemia (Hulsebosch, 2002; Kakulas, 2004). At the same time, the injured nerve cells respond with an upregulation of proinflammatory cytokines TNFα and IL-β resulting in activated microglia (Papa et al., 2013; Pineau and Lacroix, 2007) and with an injury-induced barrage of action potentials together with electrolytic shifts, involving the monovalent and divalent cations Na^+ (intracellular concentrations increase), K^+ (extracellular concentrations increase), and Ca^{2+} (intracellular concentrations increase to toxic levels), that contribute to failure in normal neural function and spinal shock (Hulsebosch, 2002). The consequent depolarization induces a massive release of neurotrasmitters, including glutamate, whose extracellular concentration can rise to excitotoxic levels and open glutamate receptor-operated ion channels, e.g. NMDA and AMPA (Wrathall et al., 1996). The pathology of SCI is due to secondary phenomena and not due directly to the primary traumatic event (Lipton

and Rosenberg, 1994); there may be a window of opportunity during the immediate phase for downregulating the harmful cascade of secondary events (Norenberg et al., 2004).

3.2 Secondary injury phase (2h to 2 weeks)

A typical feature of SCI is the delayed onset of a secondary lesion, with cell death affecting the initially spared neighboring tissue through complex mechanisms. It is the phase likely to be most amenable to neuroprotective interventions for practical reason, because it is typically the earliest point at which patients arrive at an appropriate center to receive treatment (Rowland et al., 2008). Secondary injury can be subdivided into early acute and subacute stages (Hulsebosch, 2002; Rowland et al., 2008). Two to 48 h following injury are the early acute phase, where the ischemic cellular death, increasing edema and inflammation continue after the immediate phase. The vascular dysfunction resulting in ischemia, ionic disregulation, free radical production and glutamate-mediated excitotoxicity is fully developed, inducing neuronal and glial cell death (Kakulas, 2004; Lipton and Rosenberg, 1994; Tator and Koyanagi, 1997). The inflammatory process involves cell populations including astrocytes, microglia, T cells, neutrophils and monocytes (David and Kroner, 2011; Donnelly and Popovich, 2008; Papa et al., 2013). Less severe injuries show a variety of axonal and myelin changes (Tator, 1995). The subacute phase continues for a maximum of two weeks after injury. It is characterized by a strong phagocytic response that could be beneficial in removing cell debris (Donnelly and Popovich, 2008). Delayed astrocytic response starts in this phase: the periphery of the lesion becomes hypertrophic and proliferative with a strong increase in glial fibrillary acid protein expression. The number of reactive astrocytes locally increases to produce scar-associated compounds which form the glial scar with negative anatomo-pathological consequences for spinal network connections. They have also beneficial effects, promoting the restoration of ionic homeostasis (Herrmann et al., 2008; Pineau and Lacroix, 2007). Primary and secondary injury after the spinal cord insult occur following different time points, shown in figure 2.

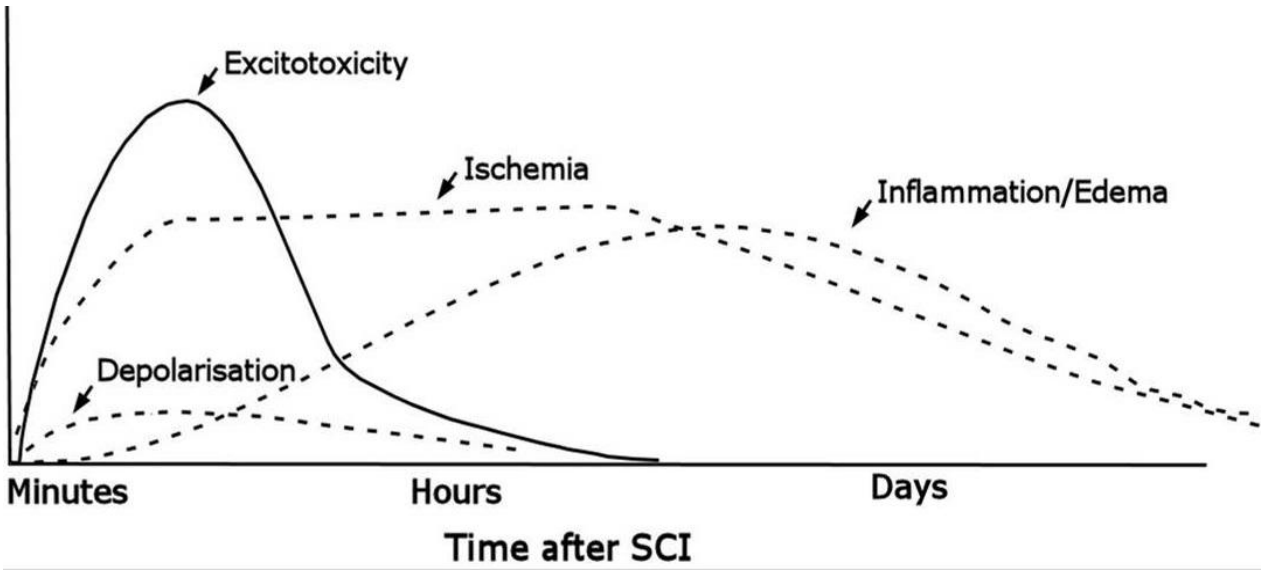

Fig. 2. Time course of primary and secondary injury after the spinal cord insult. Very early after the initial injury, excitotoxic mechanisms can damage neurones and glia. In addition, the initial damage triggers a number of events that can further contribute to the demise of the tissue, including depolarizations and the more-delayed mechanisms of inflammation, ischemia and programmed cell death (modified from Dirnagl et al., 1999).

3.3 Intermediate phase (2 weeks to 6 months)

During the intermediate phase, lasting up to 6 months, maturation of the scar produced by astrocytes continues, flanked by regenerative axonal sprouting which is, however, insufficient for recover from severe SCI (Hill et al., 2001).

3.4 Chronic phase (>6 month)

The later phase continues lifelong. In this phase there is a stabilization of the lesion with Wallerian degeneration, astroglial and mesenchymal scar formation, development of cysts and syrinx (a syrinx is a cavity superficially similar to the cyst but with a denser gliotic wall) accompanied by delayed neurological dysfunction (Norenberg et al., 2004). The “Wallerian degeneration” is a process which may take years to complete, inducing the anterograde disintegration of axons and their demyelin sheaths that have been transected following injury. It is characterized by distorted and fragmented myelin sheaths with axoplasm. Eventually the astroglial scar replaces the destroyed myelinated axon, while on the one hand, products of reactive astrocytes derived from areas of Wallerian degeneration have

been reported to dampen neurite outgrowth (Bovolenta et al., 1992; Ehlers, 2004; Norenberg et al., 2004). The spectrum of chronic spinal cord injuries encompasses myelomalacia, a pathological term referring to the softening of the spinal cord, representing the final stage.

4. MOLECULAR MECHANISMS UNDERLYING CELL DEATH AFTER SCI

Death of CNS neurons during acute injury occurs as a result of a complex combination of excitotoxicity, necrosis, apoptosis, edema and inflammatory reactions (Aarts and Tymianski, 2005a; figure 3). One process contributing to the propagation of delayed cell death after an acute SCI is ischemia, which is strongly correlated with excitotoxicity and oxidative stress.

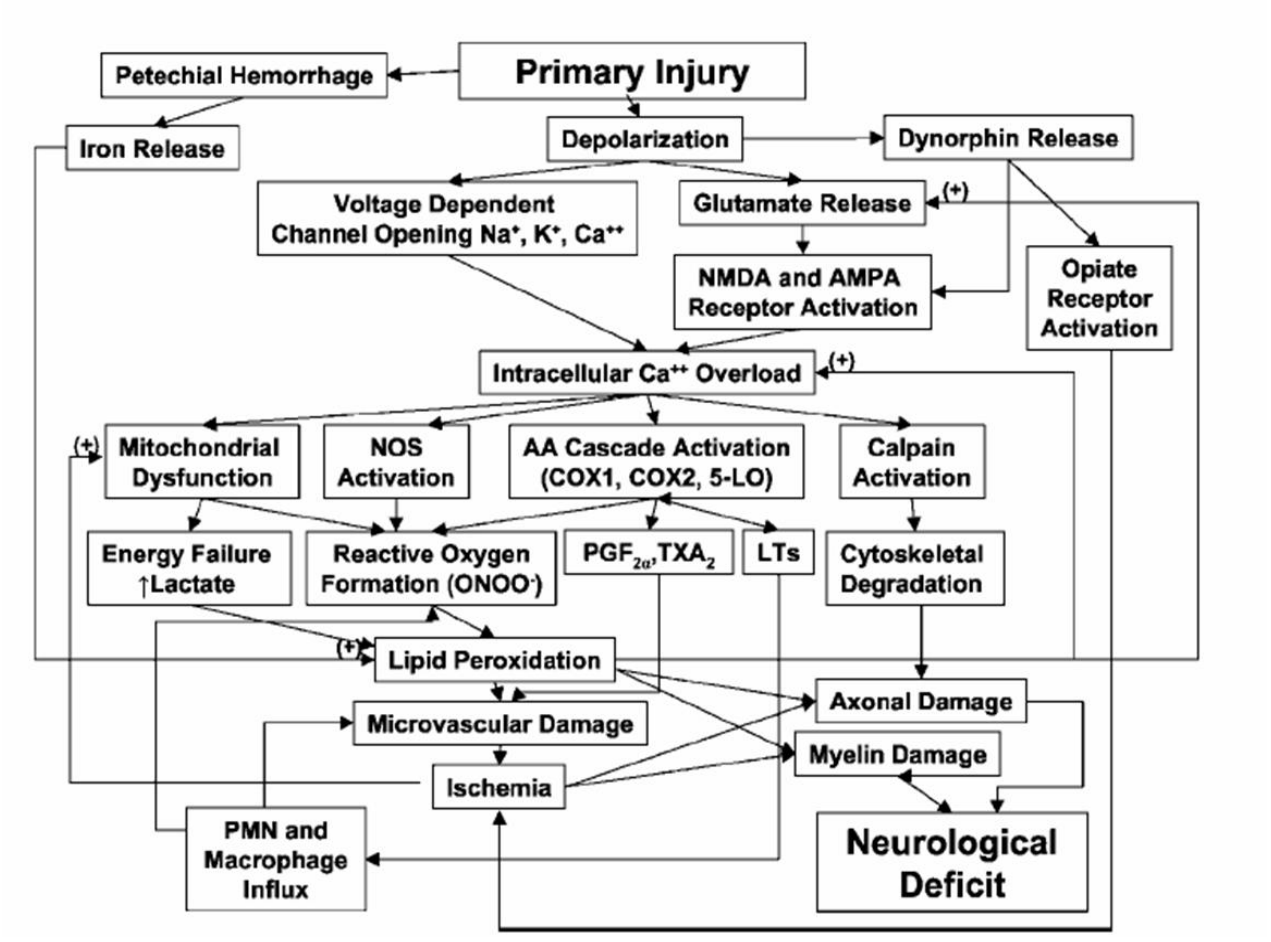

Fig. 3. Mechanisms underlying secondary spinal cord injury are complex and strength correlated (Hall and Springer, 2004).

5-LO = 5-lipoxygenase; TXA_2 = thromboxane A2; LTs = leukotrienes;

$ONOO^-$ = peroxynitrite anion; PMN = polymorphonuclear leukocyte.

4.1 Excitotoxicity

The loss of ionic homeostasis which follows SCI in few minutes and the excitotoxic process are strongly correlated. Excitotoxicity is a process of cell death caused by overactivation of excitatory aminoacid receptors often resulting in neuronal cell death (Park et al., 2004; Szydlowska and Tymianski, 2010), caused by the action of excitotoxins like neurotransmitters (Olney, 1969). Glutamate is the principal excitatory neurotransmitter in the central nervous system (CNS), released by vesicles from the presynaptic terminals into the synaptic cleft. Excitotoxic process is primarily propagated through the glutamate postsynaptic receptor family, especially ionotropic receptors (NMDA, AMPA and kainate receptors; Aarts and Tymianski, 2003; Grant et al., 1997; Kumar et al., 1991) and/or Ca^{2+} permeable receptors (TRPM2 and TRPM7; Aarts et al., 2003; Kaneko et al., 2006; Perraud et al., 2001). Activation of ionotropic receptors leads to enhanced permeability to Na^{+}, K^{+} and/or Ca^{2+}. The overload of Ca^{2+} or perturbations of intracellular Ca^{2+} compartmentalization, as shown schematically in figure 4, can activate or enhance pathways leading to cell death (Szydlowska and Tymianski, 2010). Persistent activation of NMDA receptors causes a high influx of Ca^{2+} into the postsynaptic neuron due to activation of self-destructive cascades involving many calcium-dependent enzymes. The initial reports regarding a cytotoxic role of calcium ions were published over 30 years ago. Tymianski et al. (1993) suggested the “source specificity” of Ca^{2+} loading, that is Ca^{2+} entering via NMDA channels is more toxic than that entering via other sources (Mattson, 2000; Tymianski et al., 1993). Potentially toxic cytoplasmic calcium concentrations can also occur due to its release from internal stores, either through physical damage to mitochondria and the endoplasmic reticulum, or to malfunction of receptors and channels present on their membranes. Such increases of cytoplasmic calcium concentrations can trigger a range of downstream neurotoxic cascades, including uncoupling of mitochondrial electron transfer from ATP synthesis, and activation and overstimulation of enzymes such as calpains and other proteases, protein kinases, nitric oxide synthase (NOS), calcineurin and endonucleases (Mattson, 2000; Szydlowska and Tymianski, 2010). Mitochondria sequester glutamate-induced Ca^{2+} loads producing a metabolic acidosis; metabolic stress may contribute to glutamate-induced neuronal death (Thayer and Wang, 1995). Despite the toxic role of calcium, drugs designed to block its entry into neurons have all failed to have any beneficial effects in clinical trials, because of deleterious side effects such as agitation, confusion, reduced level of consciousness, hallucinations, hypertension and, in the worst cases, mortality increased (Davis et al., 2000; Kalia et al., 2008; Lees et al.,

2000; Szydlowska and Tymianski, 2010). Further, motoneuron properties expose them to the damaging effects evoked by glutamate overactivity. In fact, AMPA receptors on motoneurons often lack the GluR2 subunit, rendering them more permeable to Ca^{2+} influx (Van Damme et al., 2002).In addition, Ca^{2+} binding proteins (parvalbumin and calbindin) are absent in upper and lower motor neurons, thus limiting the calcium buffering capacity (Ince et al., 1993). While the term “excitotoxicity” is usually applied to neurons, where glutamate has excitatory effects, it is also widely used about glial cell. Although these cells normally do not exhibit true excitability due to absence of action potentials, glutamate mediated excitotoxicity is a significant contributor to secondary injury mechanisms in white matter tissue as well (Park et al., 2004). The source of white matter glutamate includes astrocytes (Araque et al., 2000), oligodendrocytes and the reverse glutamate transporter which is a significant contributor to glutamate release (Li and Stys, 2001). Excitotoxicity is proposed to be involved in a variety of neurological diseases like spinal cord injury, stroke, traumatic brain injury (Singleton and Povlishock, 2004) and neurodegenerative diseases of the central nervous system (CNS) such as multiple sclerosis, Alzheimer's disease, amyotrophic lateral sclerosis (ALS), Parkinson's disease, and Huntington's disease.

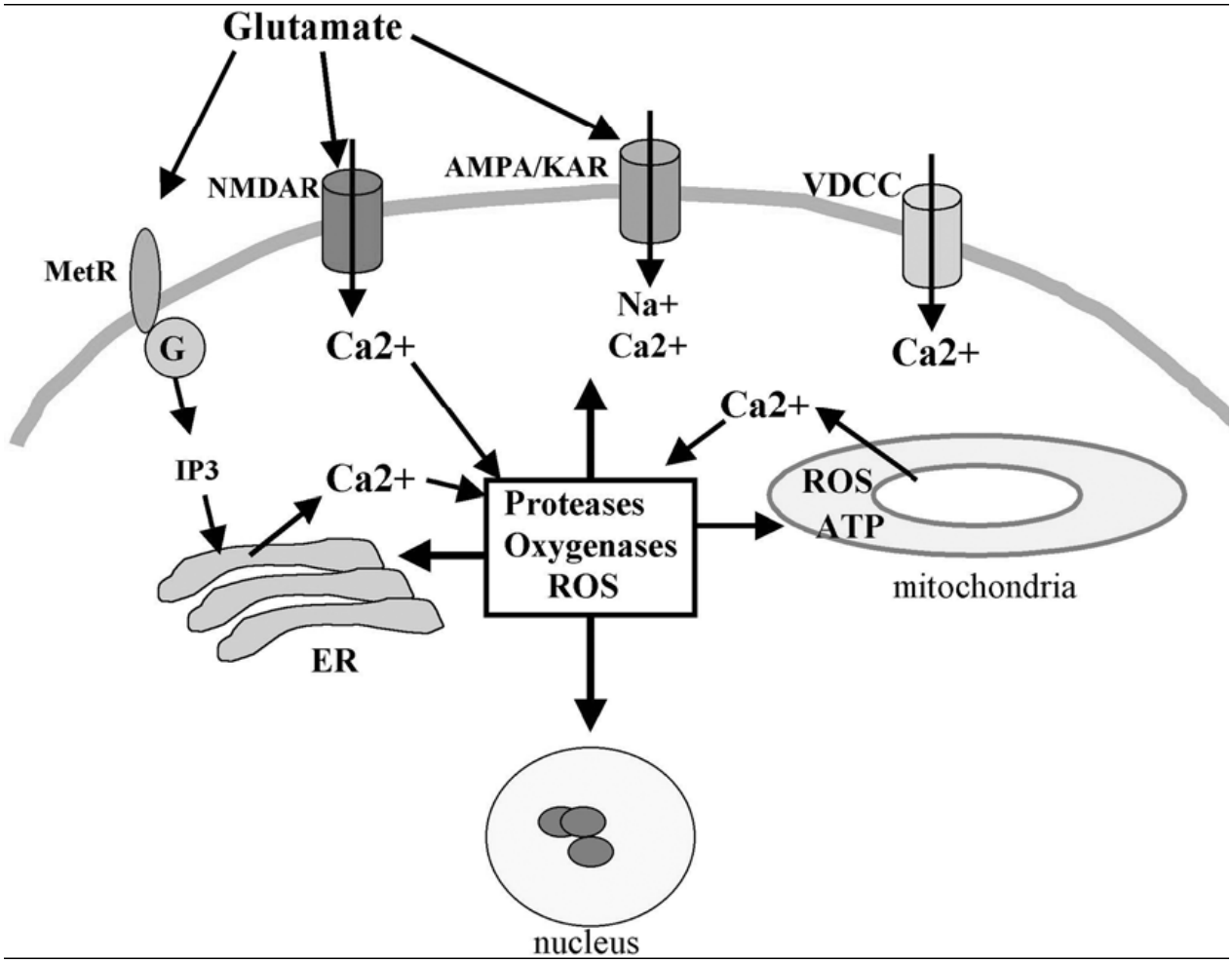

Fig. 4. Mechanisms whereby glutamate increases cytoplasmic Ca^{2+} concentrations, and modulation by endoplasmic reticulum (ER) and mitochondria. Binding of glutamate to AMPA receptors and kainate receptors (KAR) opens the receptor channels resulting in Na^{+} influx and consequent membrane depolarization and opening of voltage-dependent Ca^{2+} channels (VDCC). Some forms of AMPA receptor are also very permeable to Ca^{2+}. Binding of glutamate to NMDA receptors under depolarizing conditions opens the NMDA receptor channel resulting in large amounts of Ca^{2+} influx. Activation of metabotropic glutamate receptors (MetR) induces IP3 production and activation of IP3 receptor channels in the ER membrane resulting in release of Ca^{2+} from the ER into the cytoplasm. The increases in cytoplasmic Ca^{2+} levels in response to glutamate receptor activation can induce Ca^{2+} uptake into the mitochondria which, if excessive, can induce production of reactive oxygen species (ROS) and inhibits ATP production. By activating proteases and inducing oxidative stress, Ca^{2+} is a key mediator of excitotoxic cell death (Mattson, 2003).

4.2 Ischemia, oxidative stress and lipid peroxidation

Vascular changes are a direct consequence occurring immediately after injury. Due to the decrease in tissue perfusion and oxygenation, the injured spinal cord becomes ischemic. Ischemia is characterized by a process named “oxygen and glucose deprivation” (OGD), which cause an immediate reduction of energy available to support neuronal and glial cells (Tator, 1972). Alteration in ionic gradients results in neuronal depolarization and excessive accumulation of intracellular Ca^{2+}, acid pH and reactive oxygen species (ROS) production including $ONOO^{-}$ (Lewén et al., 2000). In SCI a strong relationship between excitotoxicity and ROS has been described, whereby free radical scavengers attenuated extracellular glutamate release up to 4 h after injury (Yamamoto et al., 1998). ROS peaks 12 h after SCI and remains elevated for 1 week, returning to the basal levels 4-5 weeks after injury (Rowland et al., 2008). Oxidative stress is an important contributor to secondary damage following SCI with radical mediated lipid peroxidation contributing to axonal disruption and death of both neurons and glia. Radical species such as hydrogen peroxide can be converted, through the Fenton reaction upon interaction with Fe^{2+} and Cu^{2+}, to hydroxyl radical, a highly reactive free radical and potent inducer of membrane lipid peroxidation (Mattson, 2003). This induction leads to fatty acid conformation alterations with the consequent severe loss of membrane integrity and edema formation, cell lysis and dysfunction of organelles, all contributing to Ca^{2+} dysregulation (Hall, 1993). A key mediator of oxidative stress induced by injury is the reactive nitric oxide (NO), a highly

diffusible free radical that has been implicated in glutamate-mediated neuronal cell death by formation of toxic peroxynitrite (Beckman et al., 1990; Dawson et al., 1994, 1991). After SCI, nitric oxide synthases (NOS) expression is increased in neutrophilis and vascular smooth muscles with a peak 24-48 h after weight-drop injury in immature rats (Clark et al., 1996; Hamada et al., 1996). Peroxynitrite has been directly associated with the induction of neuronal apoptosis in rat SCI (Xiong et al., 2007).

4.3 TRP channels and role of Mg^{2+} after injury

One mechanism of neurotoxicity, that operate independently or in parallel with excitotoxicity, involves Transient Receptor Potential (TRP) channels. The TRP ion channels are a large class of non-specific cation channels united by a common 6-transmembrane spanning core motif that forms the ion channel pore. All TRP family members are expressed abundantly in the mammalian brain (Aarts and Tymianski, 2005a). TRP family is composed of six related families of proteins, including the melastatin (TRPM) subfamily, that contains eight distinct family members, from TRPM1 to TRPM8 (McNulty and Fonfria, 2005), most of which are permeable to Ca^{2+}. TRPM channels are expressed by neurons and by other cells, including microglia, astrocytes and vascular smooth muscle cells (Rempe et al., 2009). Of these, TRPM2 and TRPM7 have been associated with cell death due to anoxia (Aarts et al., 2003; Szydlowska and Tymianski, 2010), reactive oxygen species (Ishii et al., 2007; Kaneko et al., 2006) and stroke (Aarts and Tymianski, 2005a; Sun et al., 2009). Both TRPM7 and TRPM2 channels are permeable to calcium. TRPM2 (formerly designated TRPC7 and LTRPC2; figure 5) is a non-selective cation channel permeable to Na^+, K^+ and Ca^{2+} and activated by adenosine diphosphoribose (ADPR) (Perraud et al., 2001). It is a long TRP channel containing an ADP-ribosylase domain; the homology between a small soluble protein (known as NUDT9), and the TRPM2 C-terminus (over a region now designated the NUDT9-H) played an important role in the identification of ADP-ribose as a TRPM2 gating ligand (Scharenberg, 2005). TRPM2 can be activated by H_2O_2 and agents that produce reactive oxygen/nitrogen species and it is also modulated positively by arachidonic acid, TNF-α and intracellular Ca^{2+} (Aarts and Tymianski, 2005a). TRPM2 channels have been proposed to mediate oxidative stress dependent cell death (McNulty and Fonfria, 2005).

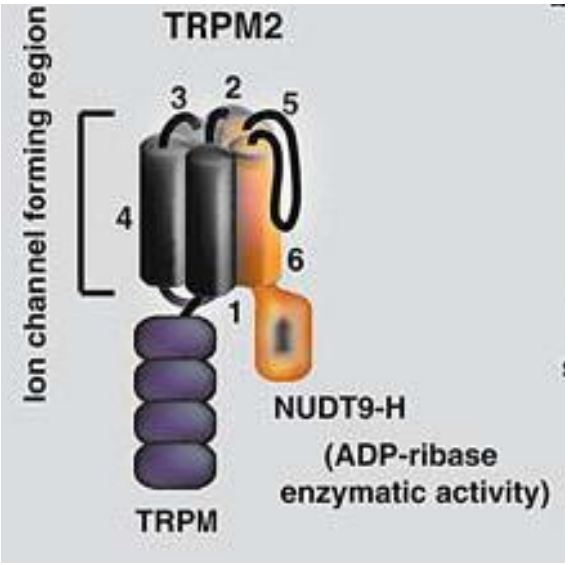

Fig. 5. Schematic appearance of a transient receptor potential (melastatin) 2 (TRPM2) monomer (Scharenberg, 2005).

The TRPM7 channel (figure 6), when heterologously expressed (Ryazanova et al., 2010), is activated by low extracellular divalent cations (Wei et al., 2007), ROS and pH changes (Wei et al., 2007), all of which occur in ischemia (Szydlowska and Tymianski, 2010). TRPM7 has been implicated in regulating Mg^{2+} homeostasis and in the permeation of trace metals into the cell (Aarts and Tymianski, 2005a; McNulty and Fonfria, 2005). The TRPM7 current is reportedly constitutively active and is suppressed by increasing concentration of Mg^{2+}, leading to the suggestion that the stimulatory effect of ATP occurs as a consequence of a drop in free Mg^{2+} in the cell (McNulty and Fonfria, 2005; Schmitz et al., 2003). TRPM7 possess an α-kinase domain at the C-terminus and activation of TRPM7 has been proposed to require ATP, a functional kinase domain and autophosphorylation of the channel. The kinase domain of TRPM7 reportedly functions in the regulation of channel function but its presence is not critical for channel gating (Aarts and Tymianski, 2005a; Chen et al., 2012; Cook et al., 2009; Schmitz et al., 2003).

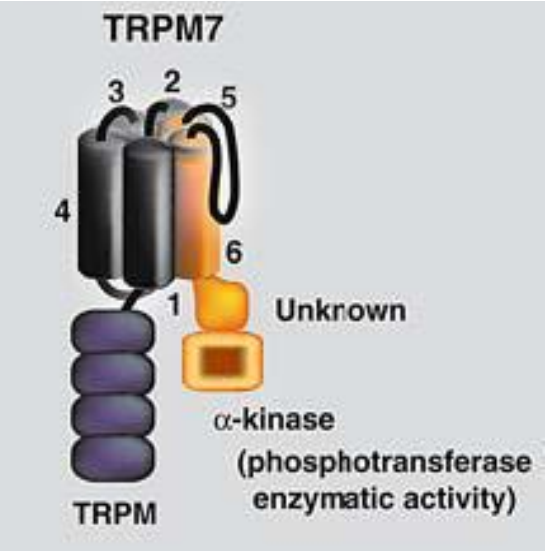

Fig. 6. Schematic appearance of a TRPM7 monomer. The region designated "unknown", which lies between the end of the sixth TM span/coiled coil region and the kinase domain, differs markedly between TRPM6 and TRPM7, and has no homology to any known proteins (Scharenberg, 2005).

In acute neuronal death, NMDA receptor activation during neuronal injury results in Ca^{2+} entry that stimulates production of nitric oxide (NO) and release of superoxide ($O2^-$) from mitochondria. NO and $O2^-$ then combine to form the highly reactive species peroxynitrite ($ONOO^-$). These free radicals, in turn, activate TRPM7 and/or heteromeric TRPM7/ TRPM2 channels resulting in further Ca^{2+} influx and production of oxygen and nitrogen free radicals. In addition, release of ADP ribose from injured mitochondria could activate TRPM2 subunits via the C-terminal ADP-ribosylase domain, as represented in figure 7. Ischemia and activation of NMDA receptors can also cause localized decreases in Ca^{2+} levels outside the cell, activating an extracellular Ca^{2+} sensing cation conductance attributed to TRPM7 (Aarts and Tymianski, 2005a).

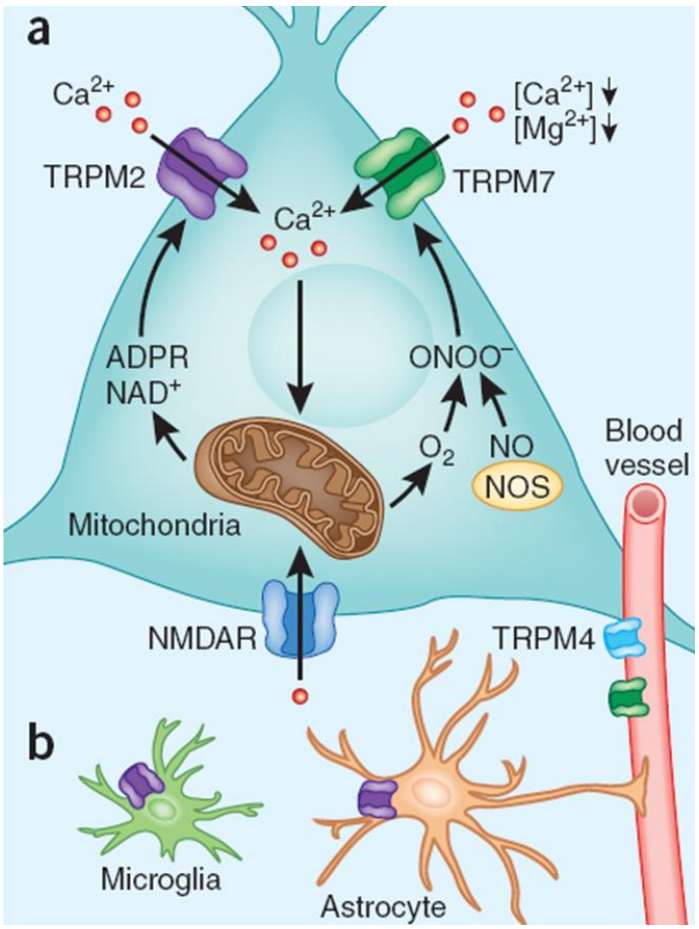

Fig. 7. The activation mechanisms of TRPM channels during ischemia. Neurons express TRPM2 and TRPM7 channels. Reduced extracellular Ca^{2+} and Mg^{2+}, which occurs during ischemia, activate TRPM7 channels, which conduct Ca^{2+} and other cations. TRPM2 channels are activated by ADPribose (ADPR), which is also induced during ischemia (Rempe et al., 2009).

Magnesium, the fourth most common cation in the body, has been the recent focus of much clinical and scholarly interest. This ion is established as a central electrolyte in a large number of reactions that either consume or produce ATP, including glycolysis, oxidative phosphorilation and cellular respiration, and plays a pivotal role in protein synthesis, cell cycle and neuronal function; it maintains the stability and integrity of the cell membrane and modulates other ion transport pumps and channels such as Na^+/K^+-ATPase. It is also referred as a physiologica calcium blocker (Aarts and Tymianski, 2005b; Cook et al., 2009; Margaryan et al., 2009; Schmitz et al., 2003; Sumoza-Toledo and Penner, 2011). Brain lesions are transiently associated with decreased extracellular Mg^{2+} concentration (van den Berg et al., 2010), even if this observation has not been systematically confirmed in humans (Lin et al., 2004). Mg^{2+} solution infusion was tested as

a neuroprotector, but it was found to worsen the outcome in patients with traumatic brain lesions (Maas and Murray, 2007; Valadka et al., 1998). This result was also observed in stroke patients (Temkin et al., 2007). In accordance with this view there are reports of the lack of effectiveness of exogenous Mg^{2+} on experimental SCI or neonatal brain injury (Muir et al., 2004; Perlman, 2006).

5. CELL DEATH PATHWAYS FOLLOWING SCI

In view of the substantial progress in the biochemical and genetic exploration of cell death, the Nomenclature Committee on Cell Death (NCCD) has proposed, in 2012, a set of recommendations for the definition of distinct cell death pathways, classified into 13 different types (table 1) (Galluzzi et al., 2012). After SCI cell death occurs through different pathways (Beattie et al., 2002; Zipfel et al., 2000). Shearing of membranes causes immediate necrotic death. Beyond this, intact and partially damaged cells are vulnerable to death for biochemical attack by free radicals and excitatory aminoacids released by dying neurons and other cells (Hall, 1996): understanding the mechanisms by which they mediate cell death after an acute SCI is mandatory, in order to provide new therapeutic targets. Cell death can occur through programmed cell death (PCD) pathways, like apoptosis, or by unprogrammed mechanisms, like necrosis. PCD mechanisms are involved in death of specific cells during development (Lockshin and William, 1965), they are fundamental during life for processes like the regulation of the immune system, but they can occur also in particular conditions, such as SCI.

	Main biochemical features	Caspase dependence	Examples of inhibitory interventions[a]
Anoikis	Downregulation of EGFR Inhibition of ERK1 signaling Lack of β1-integrin engagement Overexpression of BIM Caspase-3 (-6,-7) activation	++	BCL-2 overexpression Z-VAD-fmk administration
Autophagic cell death	MAP1LC3 lipidation SQSTM1 degradation	−−	VPS34 inhibitors AMBRA1, ATG5, ATG7, ATG12 or BCN1 genetic inhibition
Caspase-dependent intrinsic apoptosis	MOMP Irreversible $\Delta\psi_m$ dissipation	++	BCL-2 overexpression Z-VAD-fmk administration
Caspase-independent intrinsic apoptosis	Release of IMS proteins Respiratory chain inhibition	−−	BCL-2 overexpression
Cornification	Activation of transglutaminases Caspase-14 activation	+	Genetic inhibition of TG1, TG3 or TG5 Genetic inhibition of caspase-14
Entosis	RHO activation ROCK1 activation	−−	Genetic inhibition of metallothionein 2A Lysosomal inhibitors
Extrinsic apoptosis by death receptors	Death receptor signaling Caspase-8 (-10) activation BID cleavage and MOMP (in type II cells) Caspase-3 (-6,-7) activation	++	CrmA expression Genetic inhibition of caspases (8 and 3) Z-VAD-fmk administration
Extrinsic apoptosis by dependence receptors	Dependence receptor signaling PP2A activation DAPK1 activation Caspase-9 activation Caspase-3 (-6,-7) activation	++	Genetic inhibition of caspases (9 and 3) Genetic inhibition of PP2A Z-VAD-fmk administration
Mitotic catastrophe	Caspase-2 activation (in some instances) TP53 or TP73 activation (in some instances) Mitotic arrest	−−	Genetic inhibition of TP53 (in some instances) Pharmacological or genetic inhibition of caspase-2 (in some instances)
Necroptosis	Death receptor signaling Caspase inhibition RIP1 and/or RIP3 activation	−−	Administration of necrostatin(s) Genetic inhibition of RIP1/RIP3
Netosis	Caspase inhibition NADPH oxidase activation NET release (in some instances)	−−	Autophagy inhibition NADPH oxidase inhibition Genetic inhibition of PAD4
Parthanatos	PARP1-mediated PAR accumulation Irreversible $\Delta\psi_m$ dissipation ATP and NADH depletion PAR binding to AIF and AIF nuclear translocation	−−	Genetic inhibition of AIF Pharmacological or genetic inhibition of PARP1
Pyroptosis	Caspase-1 activation Caspase-7 activation Secretion of IL-1β and IL-18	++	Administration of Z-YVAD-fmk Genetic inhibition of caspase-1

Table 1. *C*lassification of regulated cell death modes, proposed by NCCD (Galluzzi et al., 2012).

Cell death pathways quite common after the primary insult of a SCI are discussed here.

5.1 Necrosis

For a long time, necrosis has been considered as a merely accidental cell death mechanism and was defined by the absence of morphological traits of apoptosis or autophagy (Galluzzi et al., 2012). It is now clear that necrosis can occur in a regulated manner (Cho et al., 2009; Degterev et al., 2005; He et al., 2009; Hitomi et al., 2008; Zhang et al., 2009), and it has a prominent role in multiple physiological and pathological settings, including ischemic injury and viral infection (Vandenabeele et al., 2010). Several triggers

can induce regulated necrosis, including alkylating DNA damage and excitotoxins (Galluzzi et al., 2012). The initiation of programmed necrosis by death receptors, such as tumour necrosis factor receptor 1, requires the kinase activity of receptor-interacting protein 1 (RIP1; also known as RIPK1) and RIP3 (also known as RIPK3), and its execution involves the active disintegration of mitochondrial, lysosomal and plasma membranes (Vandenabeele et al., 2010; figure 8). Necrosis is characterized by cell swelling, energy loss, intense mitochondrial damage, disruption of internal homeostasis and the internucleosomal DNA fragmentation, which leads to the membrane lysis with the release of intracellular constituents. The immediate consequence of these events is the inflammatory response (Cohen, 1993; Lu et al., 2000). The immediate physical injury of SCI causes necrosis at the injury level, with the premature death of cells or living tissue (Crowe et al., 1997; Katoh et al., 1996; Liu et al., 1997).

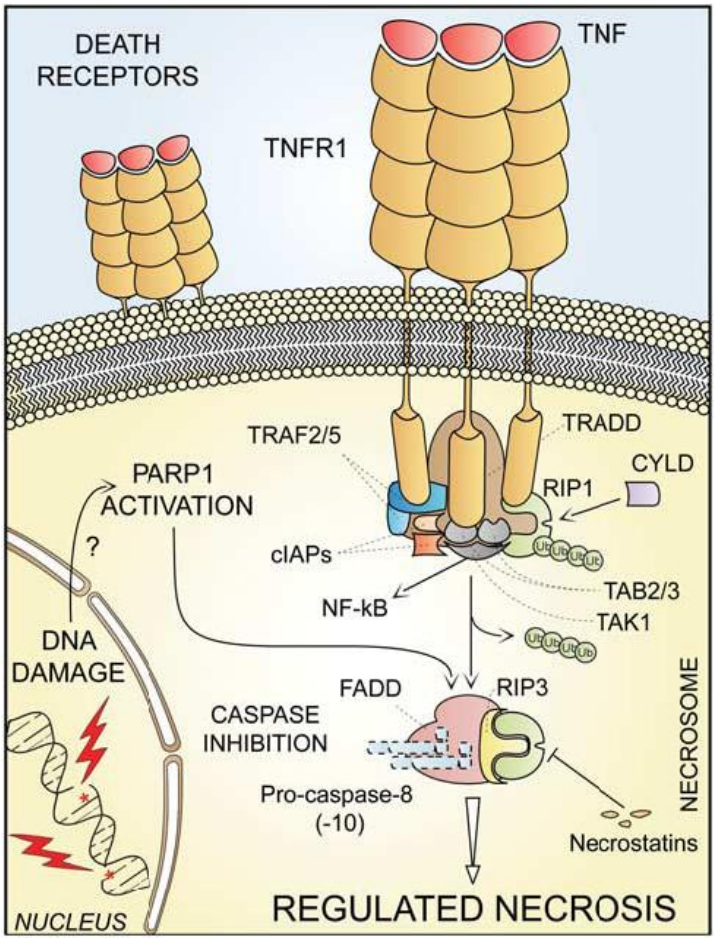

Fig. 8. Necrosis. Upon tumor necrosis factor a (TNFα) binding, the cytoplasmic tails of TNF receptor 1 (TNFR1, a prototypic death receptor) trimers recruit TNFR-associated death domain (TRADD), receptor-interacting protein kinase 1 (RIP1), cellular inhibitor of apoptosis 1 (cIAP1), cIAP2, TNFR-associated

factor 2 (TRAF2) and TRAF5. Within the so-called complex I, RIP1 is polyubiquitinated by cIAPs, thereby providing a docking site for the recruitment of transforming growth factor b (TGFb)-activated kinase 1 (TAK1), TAK1-binding protein 2 (TAB2) and TAB3 (which together deliver a pro-survival signal by activating the transcription factor NF-kB). Cylindromatosis (CYLD)-deubiquitinated RIP1 engage in physical and functional interactions with its homolog RIP3, ultimately activating the execution of necrotic cell death. Necrosis can also be induced by alkylating DNA damage (possibly by the overactivation of poly(ADP-ribose) polymerase 1, PARP1) (Galluzzi et al., 2012).

5.2 Apoptosis

Apoptosis is the best characterized PCD. Every cell is able to perform apoptosis, by ultimately controlled destruction of DNA (Nagata, 1997). Apoptosis presents well estabilished morphological signs, including cells round up, forming blebs, zeosis (appearance of boiling due to rapid bleb formation), chromatine condensation, nuclear fragmentation and budding of apoptotic bodies. Fundamental for the occurring of this apoptotic morphological changes is the activation of caspases (Yuan et al., 2003). Caspases are cysteine-aspartyl-specific proteases that cleave, with high specificity, a small subset of aspartic acid residues, and are present in the cell as inactive pro-enzymes (or zymogens) activated by proteolytic cleavage. Two types of caspases exist: initiators and effectors, depending on their point of action in the apoptotic pathway (Fuentes-Prior and Salvesen, 2004). Initiator caspases (caspase-8,-9 and -10) are the first to be activated. They exist as monomers and bind to other proteins through the “caspase activation and recruitment domain” (CARD) in caspase-9 and the “death effector domain” (DED) in caspase-8 and -10. This protein-protein interaction leads to the dimerization of the initiator caspases, activating them (Bredesen et al., 2006). The effector caspases (caspase-3 and -7) exists in the cell as inactive dimers and they are activated by clivage by the initiator caspases. The caspase subtrates cover varied molecular pathways including activation of proteolytic cascades, inactivation of DNA repair, DNA cleavage, mitochondrial permeabilization and initiation of phagocytic process to clear up dying cells, apoptotic bodies and debris (Bredesen et al., 2006; Pop and Salvesen, 2009). Apoptotic pathways can be classified as extrinsic or intrinsic (figure 9). One of these pathways (or both) may operate in determining death of glial cells in the spinal cord subjected to PM application (dysmetabolic insult) (Kuzhandaivel et al., 2011).

5.2.1. Extrinsic pathway

The extrinsic pathway is initiated by the binding of death factors to death receptors, resulting in receptor multimerization, recruitment of adaptor molecules and formation of a caspase-activating complex (Muzio et al., 1996; Salvesen and Dixit, 1997). The best studied extrinsic pathway is that of death receptor Fas, which is a member of tumor necrosis family (Itoh et al., 1991). Fas ligand (FasL) binds to death receptor Fas, resulting in receptor multimerization and consequent recruitment of the adaptor FADD (Chinnaiyan et al., 1995). FADD than interacts with caspase-8 through the caspase-8 domain DED. Interaction with FADD induces dimerization of caspase-8 to assume an active conformation (Fuentes-Prior and Salvesen, 2004). Activated caspase-8 than cleaves and activates effector caspases such as caspase-3 and -7 (Bredesen, 2000).

5.2.2. Intrinsic pathway

The components of cell-intrinsic machinery have become organized around mitochondria, which act as a hub for the apoptotic machinery. Almost all survival and death signaling pathways in post mitotic neurons are funneled through the mitochondria, where they are integrated largely by the Bcl-2 proteins (Becker and Bonni, 2004). The Bcl-2 family of proteins is a critical regulator of cell death, subdivided into the anti-apoptotic “multidomain” proteins containing BH 1-4 (Bcl-2, Bcl-$_{xL}$ etc.), the pro-apoptotic main BH 1-3 (Bax, Bak etc.), and the “BH 3 only” pro-apoptotic proteins. A major checkpoint in the common portion of this pathway is the ratio of pro-apoptotic (BAX) to anti-apoptotic (BCL-2) members. The multidomain members of the Bcl-2 family are associated with the outer mitochondrial membrane. Following an apoptotic stimulus, Bax or Bak becomes activated leading to its oligomerization with the outer mitichondrial membrane (Gross et al., 1999). Oligomerized Bax and Bak induces mitochondrial dysfunction and includes a change in the mitochondrial membrane potential, production of reactive oxygen species (ROS), formation of pores in the mitochondrial membrane with loss of mitochondrial constituents, including the intermembrane space protein cytochrome c (Gross et al., 1999; Vander Heiden and Thompson, 1999). The release of cytochrome c to the cytosol activates the adaptor apoptotic protease activating factor-1 (Apaf-1) and allows the formation of the apoptosome, a caspase-activating complex (Liu et al., 1996). The apoptosome is a large quaternary protein structure formed by cytochrome c, dATP nucleotides, Apaf-1. Once formed, the apoptosome can then recruit and activate the inactive pro caspase-9. As for FADD and caspase-8, the multimerization of pro caspase-9, is thought to contribute to its

activation (Becker and Bonni, 2004). Following caspase-9 activation, downstream effector caspases are again activated. There is also cross-talk between intrinsic and extrinsic pathways, resulting from cleavage of Bid by caspase-8 with subsequent traslocation of cleaved Bid to the mitochondria and the resultant release of cytochrome c (Bredesen, 2000; Li et al., 1998).

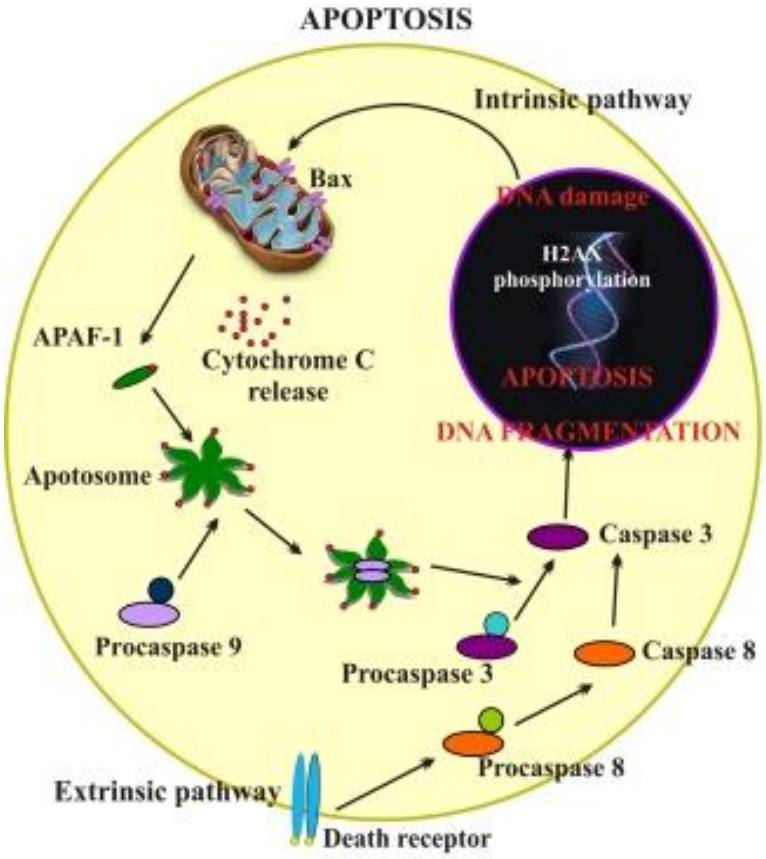

Fig. 9. **Schematic representation of apoptosis cell-death pathways.** The intrinsic pathway is initiated within the cell usually in response to cellular signals resulting from DNA damage, hypoxia, or other types of severe cell stress. These signals stimulate proapoptotic proteins (e.g., Bax) in the mitochondrial membrane leading to mitochondrial membrane permeabilization, that allows translocation of cytochrome c from the mitochondrial intermembrane space to the cytosol. Cytochrome c binds the adaptor APAF-1, forming a large multiprotein structure known as apoptosome. The initiator caspase 9 is recruited into the apoptosome and activates the downstream effector caspases 3. The extrinsic pathway begins outside the cell through the activation of specific proapoptotic receptors on the cell surface by specific molecules known as proapoptotic ligands. Such a ligand binding induces receptor clustering and recruitment of the adaptor protein Fas-associated death domain and the initiator caspases 8 as procaspases, facilitating their

autocatalytic processing and release into the cytoplasm where they activate the effector caspases 3, thereby converging on the intrinsic pathway (Kuzhandaivel et al., 2011).

5.2.3. Other apoptotic pathways

Evidence suggests that additional pathways of apoptosis may also exist. Caspases, in fact, are not exclusively cytosolic enzymes, but they can target or translocate to multiple cellular sites, including the nucleus, mitochondria, endoplasmic reticulum and Golgi apparatus (Jürgensmeier et al., 1998; Mancini et al., 2000). For example, endoplasmic reticulum specific apoptosis has been shown to be mediated by caspase-12 (Nakagawa et al., 2000).

5.2.4. Apoptosis after SCI

Many studies have been done with different SCI models to identify apoptosis (Crowe et al., 1997; Katoh et al., 1996; Liu et al., 1996; Shuman et al., 1997) stemming from the evidence of apoptosis after ischemia and traumatic brain injury (Rink et al., 1995). Twentyfour hours after moderate weight drop contusion injury, damaged cord tissue shows evidences of apoptosis, especially in the white matter tracts at the injury epicenter (Beattie et al., 2000). Cells positive for the TUNEL assay, which is a common method for detecting DNA fragmentation that results from apoptotic signaling cascades, have been seen after cord compression with an increased Bcl-2 expression (anti-apoptotic protein), indicating that protection from apoptosis was being induced by injury (Liu et al., 1996). Also neurons are involved in apoptotic cell death following SCI (Liu et al., 1997; Yong et al., 1998). Neuronal apoptosis occurs from 4 to 24 hours after injury (Liu et al., 1997). Apoptosis is also reported in human traumatic SCI and is accompanied by the activation of caspase-3 (Emery et al., 1998) and extensive studies with different SCI models also confirmed the morphological data for apoptosis in neurons after injury (Abe et al., 1999; Yong et al., 1998). Glial cells, especially oligodendrocytes, may dye by apoptosis many days or even weeks following injury (Emery et al., 1998; Knoblach et al., 2005; Springer et al., 1999; Takagi et al., 2003) and death of oligodendrocytes by apoptosis contributes to the demyelination of intact axons (Beattie et al., 2000; Shuman et al., 1997). Loss of axons removes trophic support needed by the oligodendrocytes (Barres et al., 1993; Raff et al., 1993), or the degeneration products of the axons are somehow toxic to the oligodendrocytes. The lesion centre early after injury is interested also by astrocytic apoptosis (Davis et al., 2007; Yoshino et al., 2004) and microglial apoptosis (Colak et al.,

2005; Koda et al., 2002; Shuman et al., 1997). Apoptosis can be involved in the secondary injury, starting at the immediate phase along with necrosis, and continuing to other phases with making damage to white matter, oligodendrocytes and microglia. This later phase confined principally to the white matter that involves both oligodendrocytes and microglia. Further, it seems likely that the oligodendrocyte death might be associated with axonal death induced by the injury (Beattie et al., 2000, 2002).

5.3 Parthanatos

Parthanatos shares molecular and morphological features with apoptosis and necrosis, but it is the result of a distinct molecular mechanism (David et al., 2009). It is an intrinsic PCD pathway in which Poly-ADP-ribose (PAR) plays a pivotal role (David et al., 2009). PAR is synthesized by Poly-ADP-ribose polymerase-1 (PARP-1), a nuclear enzyme which responds to DNA damage. PARP superfamily includes 17 putative isoforms based on protein sequence homology to PARP catalytic domain, PARP-1 accounts for more than 90% cellular PARP activity (Dawson and Dawson, 2004; Schreiber et al., 2006). There are three major functional domains in PARP-1 (Kameshita et al., 1984; Schreiber et al., 2006), namely:

1. an N-terminal DNA-binding domain (42 kDa), containing two zinc-finger motifs and a nuclear localization sequence (NLS), which recognizes both double- and single-stranded DNA breaks,
2. a central automodification domain (16 kDa) which is thought to be the target of self-poly-ADP-ribosylation,
3. a C-terminal catalytic domain (55 kDa) containing both the NAD binding site and the catalytic domain which synthesizes PAR.

PARP-1 basal enzymatic activity is low, but nicks and breaks of the DNA strand potently activate PARP-1, thereby facilitating DNA repair (Lautier et al., 1993; Smulson et al., 2000). PARP-1, in fact, can bind to a huge variety of DNA structures, including single and double strand breaks, crossovers, cruciforms and supercolis, as well as some specific double-stranded sequences (Kim et al., 2005) and its activity is stimulated dramatically in the presence of variety of allosteric activators, including damaged DNA, some undamaged DNA structures, nucleosomes and a variety of protein-binding partners (D'Amours et al.,

1999; Kun et al., 2002; Oei and Shi, 2001). Once activated, PARP-1 enzymatic activity has a varied targets, including PARP-1 itself, core histones, the linker histone H1, and a variety of transcription-related factors that interact with PARP-1 (D'Amours et al., 1999; Huletsky et al., 1989; Kraus and Lis, 2003; Ogata et al., 1981) and are involved in DNA damage, detection and repair, cell death, modification of chromatin structure, transcriptional regulation, insulator function and mitosis (Ariumi et al., 1999; Pavri et al., 2005; Poirier et al., 1982; Yu et al., 2004). PARP-1 also catalyzes the polymerization of ADP-ribose units from donor NAD^+ on target proteins (Hayaishi and Ueda, 1977). The ADP-ribose units are linked to each other via glycosidic ribose-ribose bonds, so the resulting PAR polymers may be linear or branched (D'Amours et al., 1999), usually heterogeneous in terms of length and extent of branching with roughly one branch every per 20-50 ADP-ribose residues. However, it has been reported that PAR polymers of increasing complexity and molecular weight are more toxic (Andrabi et al., 2006). PAR once bound to its target protein may alter protein activity by functioning as a site-specific covalent modification, a protein binding matrix or a steric block (Kim et al., 2005). Poly-ADP-ribose glycohydrolase (PARG) is the major enzyme responsible for the catabolism of PAR chains. PARG hydrolyze the glycosidic linkages between the ADP-ribose units of PAR (Jagtap and Szabó, 2005; Kim et al., 2005).

In physiological conditions, in cases of low level of DNA damage, PARP-1 takes part in genomic repair acting as a survivor factor (Masson et al., 1998; Ruscetti et al., 1998). Despite this, in presence of massive DNA damage and/or stress, PARP-1 acts to promote cell death. PARP-1 activation can be due to oxidative stress by overproduction of nitric oxide (NO), which reacts with superoxide anion to produce the oxidant peroxynitrite and causes DNA damage that activates PARP-1 (Dawson et al., 1991; Xia et al., 1996). It has been observed that PARP-1 induces cell death through parthanatos in pathological condition like stroke, trauma, and ischemia/reperfusion injury in various organs (Lorenzo and Susin, 2007; Mandir et al., 2000; Szabó and Dawson, 1998). According with Berger (1985), massive DNA damage causes PARP-1 overactivation, which rapidly depletes NAD pools with an impairment of NAD-dependent metabolic pathways, including glycolysis and mitochondrial respiration. The consequent depletion of ATP production and energy shortage is aggravated by the fact that NAD shortage activates nicotinamide phosphoribosyl transferase and nicotinamide mononucleotide adenylyl transferase that consume ATP to re-synthesize NAD. This altered metabolism contributes to the generation of a lethal cycle (Berger et al., 2004; Chiarugi, 2005). PARP-1 mediates cell

death also through translocation of apoptosis inducing factor (AIF) (Andrabi et al., 2008; David et al., 2009; Lorenzo and Susin, 2007; Wang et al., 2009). After overactivation of PARP-1, PAR is translocated from the nucleus to the cytosol, where it causes AIF release from mitochondria (Andrabi et al., 2006; Koh et al., 2005; Wang et al., 2011). The released AIF is then translocated to the nucleus, where it interacts with DNA and/or RNA to induce chromatine condensation or large scale DNA fragmentation (Susin et al., 1999; Ye et al., 2002). How PAR translocates from the nucleus to the cytosol and how it induces the release of AIF is, at present, unknown. In mitochondria there are two pools of AIF; about 80% of AIF is localized to the inner membrane and inner membrane space that does not bind PAR. However, 20-30% of mitochondrial AIF is localized to the cytosolic side of the outer mitochondrial membrane where it is available to bind PAR and be released during parthanatos (Wang et al., 2011). A schematic representation of parthanatos is shown in figure 10.

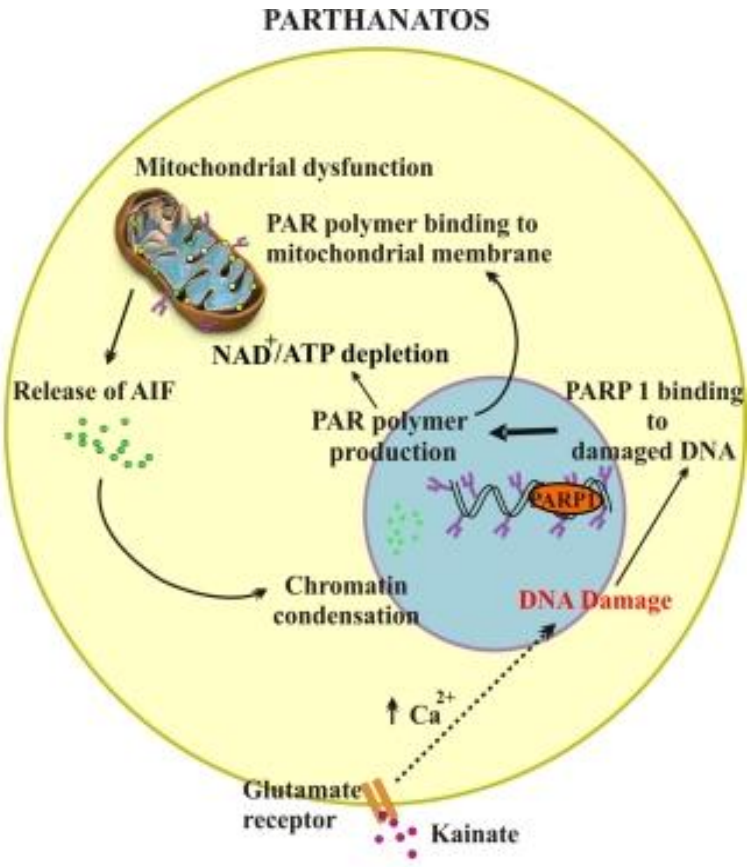

Fig. 10. **Schematic representation of parthanatos cell-death pathways** mediated by PARP-1 hyperactivation. Following an injury, intracellular increase in free Ca^{2+} activates downstream cascades leading to peroxynitrite formation. This readily induces DNA damage, thereby activating PARP-1 that initiates the synthesis of PAR chains. PAR

interacts with the mitochondrial membrane to change its membrane potential, thus allowing AIF translocation to the nucleus, a process leading cell death. An additional lethal mechanism may originate from excessive PARP-1 activation to deplete the NAD pool and cause severe ATP starvation and cell energy failure with the outcome of cell death (Kuzhandaivel et al., 2011).

5.3.1. Parthanatos after SCI

Many studies with different SCI models identified PARP-1-dependent cell death after SCI, the presence of which was initially associated with the overproduction of nitric oxide and reactive oxygen species (Genovese and Cuzzocrea, 2008; Genovese et al., 2005; Scott et al., 2004; Wu et al., 2007). Oxidative stress as cause of parthanatos has been proposed also after ischemic and traumatic brain injury (David et al., 2009; Eliasson et al., 1997) even if the injury occurs in the perinatal brain (Hagberg et al., 2004). PARP-1 mediated neuronal cell death is confirmed by the therapeutic efficacy of gene inactivation or pharmacological inhibition of PARP-1 in experimental models of stroke, cerebral ischemia, neurotrauma, Parkinson's desease and excitotoxicity (Mandir et al., 1999, 2000; Szabó and Dawson, 1998; Whalen et al., 1999). In fact, PARP inhibitors protect neurons from NMDA and NO mediated toxicity (Zhang et al., 1994). PARP-1 KO mice are strongly resistant to NMDA exitotoxicity and stroke (Mandir et al., 2000). Studies performed in our laboratory have recently demonstrated the presence of parthanatos in neuronal cells and also in the white matter in excitotoxic or non-traumatic models of SCI (Bianchetti et al., 2013; Kuzhandaivel et al., 2010a, 2011; Nasrabady et al., 2011a, 2012).

6. SPINAL CORD MODELS *IN VITRO*

In addition to *in vivo* animal models of SCI (Onifer et al., 2007), there are growing attempts to develop new *in vitro* models that can supply useful data, to understand basical mechanisms of SCI pathophysiology. *In vitro* models can be cell cultures, organotypic cultures or isolated spinal cord preparations. The main advantage for *in vitro* models is the fact that they simplify the complexity of *in vivo* SCI pathophysiology, and they can point to the identification of specific injury processes without interference by blood pressure changes and/or general anesthesia. Primary cultures from spinal cord tissue have been

applied to reproduce *in vitro* excitotoxicity (Van Den Bosch et al., 2000; Taylor et al., 2007) and ischemia (Kaushal and Schlichter, 2008). Despite this, these models present many disadvantages like influences caused by the culturing media and the difficulty in controlling the cell microenvironment, fundamental for axon growth and regeneration (Abu-Rub et al., 2010; Silani et al., 2000). Many reports are based on organotypic spinal cultures (Guzmán-Lenis et al., 2009), *in vitro* spinal slices (Zhang et al., 2010) and even the incision model very similar to the one reported here (Que et al., 2011). The main advantage of the organotypic system is that they maintain the basic cytoarchitecture of the tissue with the dorsal–ventral orientation of spinal segments. They also allow long-term studies (weeks) in which plastic changes in network properties can be explored in relation to changes in the local environment (Sibilla and Ballerini, 2009). These cultures, however, cannot generate locomotor-like patterns, and cannot readily relate molecular changes to complex network function. Acute slices of the spinal cord can be used for functional studies, even though they have limited viability *in vitro*, may pose barriers to drug diffusion and it is also impossible to ascertain if there had been any specific damage to locomotor networks.

6.1. Neonatal rat isolated spinal cord preparation developed in our lab

Our group has recently developed a novel model of *in vitro* SCI, in order to investigate the rapid evolution of early secondary damage (Taccola et al., 2008). It is an *in vitro* model, based on neonatal rat isolated spinal cord, in which we can mimic both non traumatic and incomplete SCI (Kuzhandaivel et al., 2010a, 2010b; Taccola et al., 2008, 2010). Our aim was to generate an experimental condition that might simulate the acute clinical setting occurring *in vivo*. In order to replicate the biochemical conditions believed to occur at the site of the lesion, we keep the isolated spinal cord inside a medium evoking excitotoxic damage (through the application of Kainic acid) or the ischemic-like damage (through the application of a pathological medium characterized by OGD, which contains reactive oxygen species, low osmolarity and acid pH conditions). After a 1-h application, the latter solution is washed out and standard Kreb's solution superfused again for up to 24 h. Sham experiments are performed by keeping the preparations for analogous times in the same experimental setup without applying a toxic medium. This model presents intrinsic limitations such as absence of immune system responses, lack of vascular supply and rat neonatal age. Despite this, it has the great advantage of correlating the functional outcome of injury with >24 h monitoring of locomotor-like activity (termed fictive locomotion) to the number, type, and topography of damaged or dead cells. It allows to preserve the entire

tissue with its laminar and intersegmental organization. This point is fundamental, due to the fact that it has been demonstrated that the extent of loss of electrophysiological function depends on the extent of the damage (Nistri et al., 2010). It is simpler than *in vivo* models even if retains cellular connections, network and activities, and it doesn't present the problem due to the general anesthesia.

7. THERAPEUTICAL APPROCHES AT THE SCI

7.1 Neuroprotection

As well as surgical intervention and rehabilitation treatments, a variety of pharmacological agents have demonstrated neuroprotective or neuroregenerative properties in animal models of acute SCI. These drugs target specific secondary pathological events like edema, ischemia, inflammation, excitotoxicity, disturbances of ionic homeostasis, excessive cytokines release, caspases and calpain activation and/or apoptosis. Following the initial traumatic insult, it is rare that axons traversing the lesion epicenter are completely transected, so some myelinated and/or demyelinated axons function persist. Preclinical studies have demonstrated, for example, that K^+/Na^+ channel antagonists improve axonal conduction of damaged axons (Baptiste and Fehlings, 2008). Additionally, many promising pharmacological strategies were applied as neuroprotective agents. A summary of the most promising drugs are shown in figure 11.

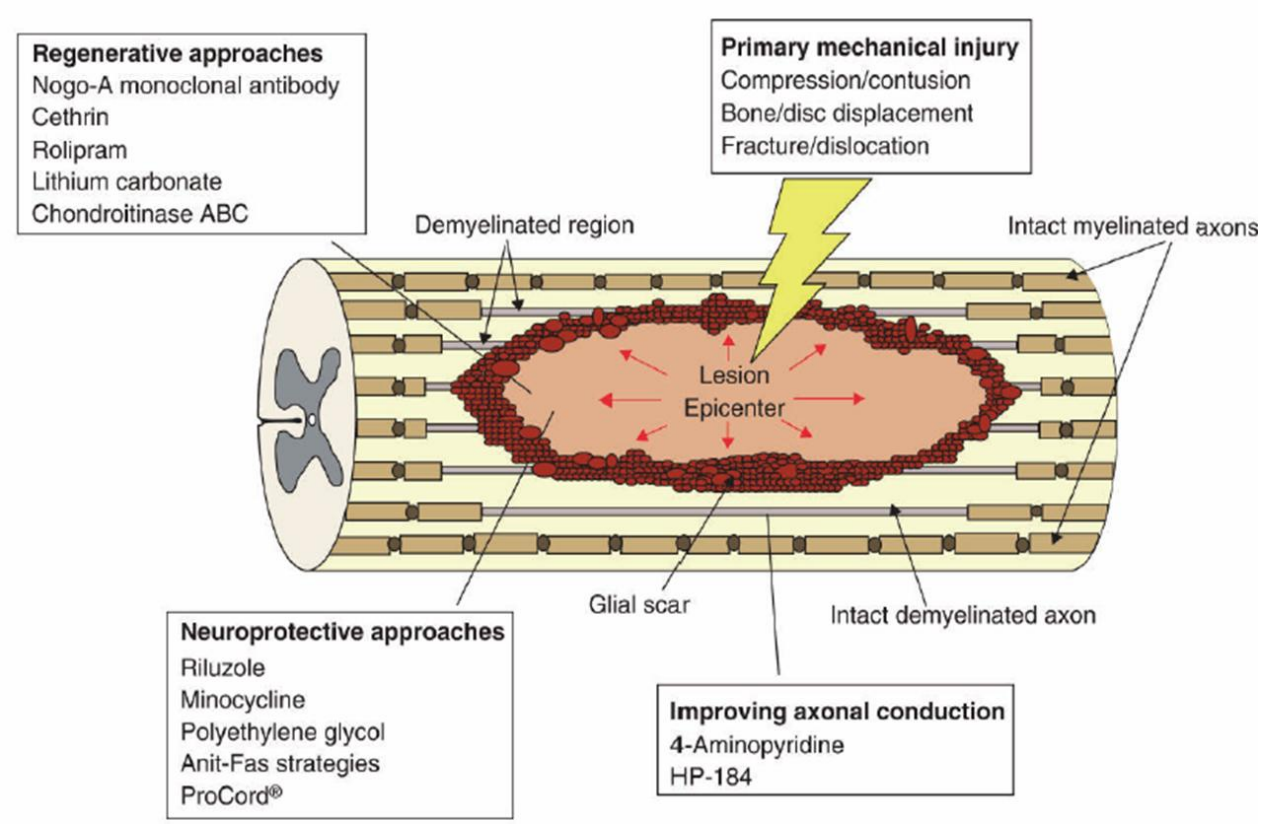

Fig. 11. Promising pharmacological strategies to attenuate SCI (Baptiste and Fehlings, 2008).

One of the most important points on which our group focused during last years has been inhibition of PARP-1 (Nasrabady et al., 2011a, 2011b, 2012). Involvement of PARP in damage following SCI is shown by the fact that PARP $^{-}/^{-}$ phenotype in brain slices demonstrated protection to glutamate-NO-mediated ischemic insults (Eliasson et al., 1997) and mice lacking PARP-1 are highly resistant to NMDA excitotoxicity (Mandir et al., 1999). Inhibition of PARP by 3-aminobenzamide (3-AB) reduces injury after transient focal ischemia in rats and attenuates NMDA-induced glutamate efflux (Lo et al., 1998). The neonatal rat isolated spinal cord, treated with high dose of kainate to induce the excitotoxicity, demonstrates a significantly decrease in number of pyknotic cells after pharmacological inhibition of PARP-1 with (6-5(H)-phenanthiridinone; PHE) (Kuzhandaivel et al., 2010a). PHE could also prevent the translocation of AIF which is the last molecular effector of PARP-1 in inducing cell death. The use of inhibitors of PARP-1 like 3-aminobenzamide (3-AB) or 5-aminoisoquinolinone (5-AIQ) in an experimental model of spinal chord trauma (*in vivo*) performed by Genovese's group (2005) decrease inflammation and tissue injury, PAR formation, neutrophil infiltration, apoptosis and the

motor disturbance. The neuroprotective effect of a novel potent inhibitor of PARP, namely N-(6-oxo-5,6-dihydrophenanthiridin-2-yl)-N-N-dimethylacetamide (PJ34), was tested by Abdelkarim et al. (2001) in the rat model of middle cerebral artery occlusion. PJ34 administration significantly reduces infarct size: the effect of the drug is maintained even if given as late as 10 minutes prior to reperfusion time. PJ34 significantly protects at 4 hours, but not in a 24 hours permanent occlusion model. They suggested that PJ34 exerts massive neuroprotective agents, with a significant pharmacological approach for the treatment of acute stroke. PJ34 also induced positive effects in another rat model of stroke, like bilateral carotid occlusion-reperfusion, including suppressing the ischemia-induced microglial activation and astrogliosis, decreased deficits in spatial memory and learning and increased neuronal density in hippocampal CA1 area. In general, it is proposed that treatment with PJ34 for several days after ischemia enhances long-term neuronal survival and neurogenesis by reducing tissue inflammation (Kauppinen et al., 2009).

7.2 Stem cells

The discovery of neural stem cells (NCSs) in the adult brain (Reynolds and Weiss, 1992) raised new hopes for the development of neural repair, either by transplantation or by recruiting endogenous NSC (Foret et al., 2010). The manipulation of endogenous spinal stem cells after injury is preferred to stem cell transplantation, since it is non invasive and avoids the need for immune suppression (Meletis et al., 2008). Neural plasticity following brain injury illustrates the potential for regeneration in the central nervous system. Lesioning of the perforant path, which innervates the outer two-thirds of the molecular layer of the dentate gyrus, triggered a marked proliferation of newborn neurons. These result indicate that injury causes an increase in newborn neurons and lamina-specific synaptic reorganization indicative of enhanced plasticity (Perederiy et al., 2013). It has been demonstrated that the ependymal region of the adult spinal cord in mammals contains a pool of stem/precursor cells (SPCs), activated and recruited after a spinal damage (Hugnot and Franzen, 2011; Weiss et al., 1996). After SCI the neural stem cells proliferate (Yamamoto et al., 2001a) and produce scar-forming astrocytes and myelinating oligodendrocytes (Meletis et al., 2008). Spinal stem cells are difficult to identify due to their heterogeneity (figure 12) and lack of specific expressional markers, since the ones currently used significantly overlap with those of mature astrocytes (McDonough and

Martínez-Cerdeño, 2012). Moreover, there is no specific marker to discriminate between quiescent and activated ependymal spinal cells, or to monitor migratory ependymal cells. The signaling pathways and genes controlling the spinal SPCs destiny remain largely unknown, both in normal and pathological situations (Hugnot and Franzen, 2011). Evidences show that brain transcription factors that regulate formation and proliferation of neural SPCs depend on the Sox family of genes, in particular Sox2 (Liu et al., 2013). Moreover, Runx1 is a transcription factors that play essential roles during development and adult tissue homeostasis. It acts to promote proliferation in olfactory sensory neuron precursor cells (Zagami et al., 2009) and it is also expressed in post-mitotic neurons in the mouse CNS, especially motoneurons of the hindbrain and spinal cord (Stifani et al., 2008). Genomics and proteomics technologies have recently identified Wnt/beta-catenin, Notch, sonic hedgehog and growth factor networks as major signaling pathways involved in maintenance, self-renewal, proliferation and neurogenesis of the neural SPCs, demonstrating the cross-talk between key molecules of these pathways and their modulations by transcription factors, miRNA and histone modifications (Yun et al., 2010). Despite this, transcription factors controlling spinal cord stem cells remain incompletely understood as they have been studied with *in vitro* primary cultures, showing common expression of various homeodomain-type (Pax6, Pax7, Nkx2.2, and Prox1) and basic helix-loop-helix (bHLH)-type (Ngn2, Mash1, NeuroD1, and Olig2) regulatory factors in the adult and embryonic rat spinal neural progenitors (Yamamoto et al., 2001b).

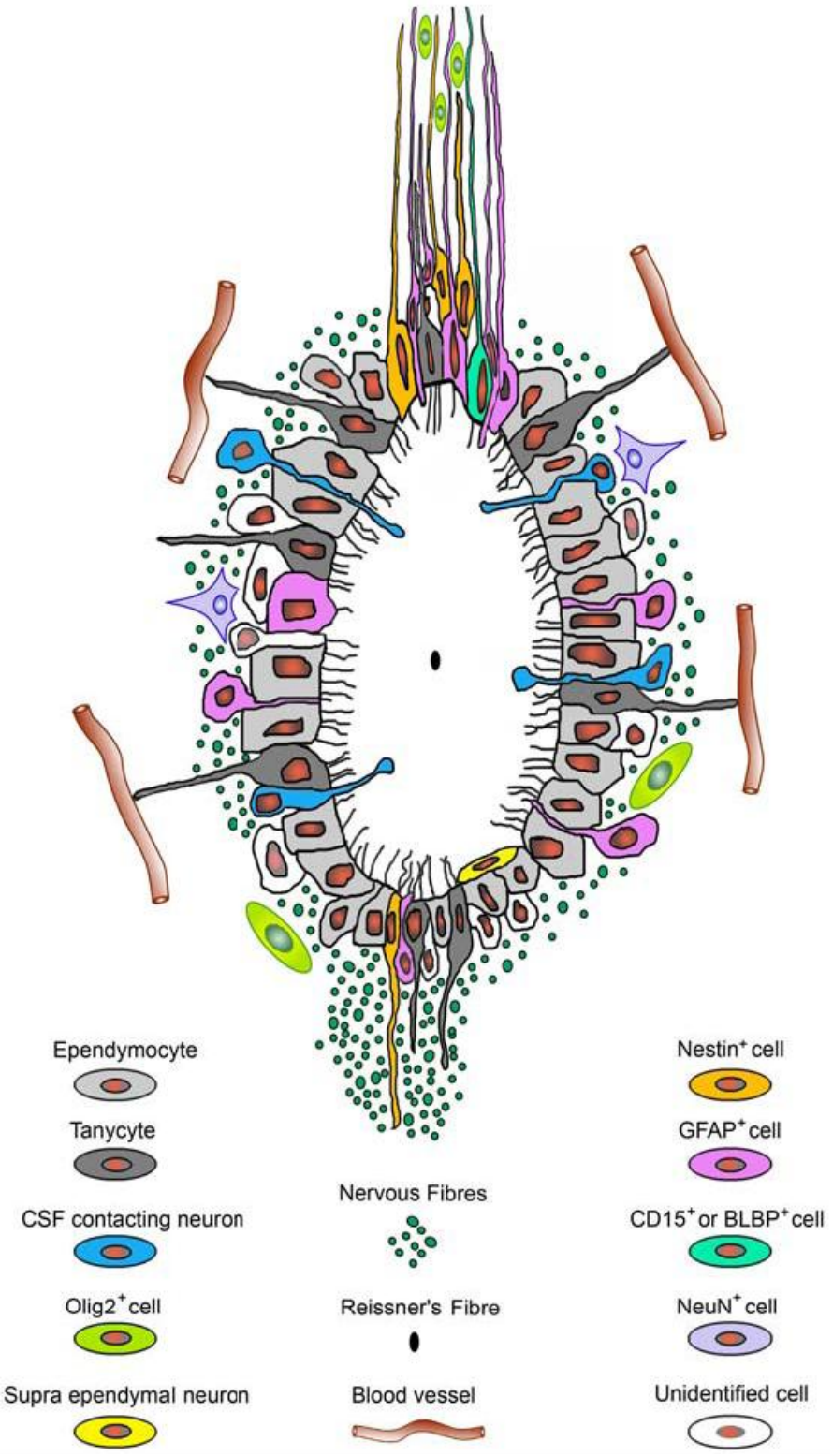

Fig. 12. Schematic drawing of the adult mouse ependymal region. The ependymal region is composed of severalcell types, which are located either in direct contact with the lumen or in a subependymal position, evoking a pseudostratified epithelium (Hugnot and Franzen, 2011).

AIMS OF THE STUDIES

The immediate damage of acute SCI spreads from the initial injury site through excitotoxicity and metabolic dysfunction (ischemia, free radicals and neuroinflammation) to spared tissue (secondary damage). As the pathophysiological mechanisms of SCI remain largely unknown, the aims of our studies were:

- identifying the molecular and cellular processes underlying this pathology.

- enquire whether the increased severity of spinal damage evoked by PM+Mg^{2+} was due to recruitment of additional cell death pathways, their identity and the potential TRPM2 and/or TRPM7 involvement.

As well as surgical intervention and rehabilitation treatment, a variety of pharmacological agents have demonstrated neuroprotective or neuroregenerative properties in animal models of acute SCI. Also the manipulation of endogenous spinal stem cells after injury raised new hopes for the development of reparative therapies, either by transplantation or by recruiting of endogenous NSC. Thence, we also studied:

- the potential neuroprotective effect of PARP-1 inhibitors in SCI models.

- the efficacy of ATF3 as a marker for the migration of ependymal stem cells of the spinal cord.

Methods, materials and results

Section 1

Mechanisms underlying cell death in ischemia-like damage to the rat spinal cord in vitro.

Bianchetti E, Mladinic M, Nistri A.

Cell death and disease (2013).

OPEN

Citation: Cell Death and Disease (2013) 4, e707; doi:10.1038/cddis.2013.237

www.nature.com/cddis

Mechanisms underlying cell death in ischemia-like damage to the rat spinal cord *in vitro*

E Bianchetti[1], M Mladinic[1,2,3] and A Nistri*[,1,2]

New spinal cord injury (SCI) cases are frequently due to non-traumatic causes, including vascular disorders. To develop mechanism-based neuroprotective strategies for acute SCI requires full understanding of the early pathophysiological changes to prevent disability and paralysis. The aim of our study was to identify the molecular and cellular mechanisms of cell death triggered by a pathological medium (PM) mimicking ischemia in the rat spinal cord *in vitro*. We previously showed that extracellular Mg^{2+} (1 mM) worsened PM-induced damage and inhibited locomotor function. The present study indicated that 1 h of PM + Mg^{2+} application induced delayed pyknosis chiefly in the spinal white matter via overactivation of poly (ADP-ribose) polymerase 1 (PARP1), suggesting cell death mediated by the process of parthanatos that was largely suppressed by pharmacological block of PARP-1. Gray matter damage was less intense and concentrated in dorsal horn neurons and motoneurons that became immunoreactive for the mitochondrial apoptosis-inducing factor (the intracellular effector of parthanatos) translocated into the nucleus to induce chromatin condensation and DNA fragmentation. Immunoreactivity to TRPM ion channels believed to be involved in ischemic brain damage was also investigated. TRPM2 channel expression was enhanced 24 h later in dorsal horn and motoneurons, whereas TRPM7 channel expression concomitantly decreased. Conversely, TRPM7 expression was found earlier (3 h) in white matter cells, whereas TRPM2 remained undetectable. Simulating acute ischemic-like damage *in vitro* in the presence of Mg^{2+} showed how, during the first 24 h, this divalent cation unveiled differential vulnerability of white matter cells and motoneurons, with distinct changes in their TRPM expression.
Cell Death and Disease (2013) **4,** e707; doi:10.1038/cddis.2013.237; published online 4 July 2013
Subject Category: Neuroscience

The clinical scenario of new spinal cord injury (SCI) cases is changing because trauma is no more the leading cause.[1] Non-traumatic SCI originates from vertebral stenosis, tumors, or cardiovascular disorders that comprise a cluster of post-surgical paralysis after abdominal aorta surgery.[1] Although non-traumatic lesions are usually incomplete, the clinical symptoms are severe, and include paralysis and sensory dysfunction. A typical feature of SCI is the delayed onset of a secondary lesion, with cell death affecting the initially spared neighboring tissue through complex mechanisms. This is an important issue, as a prerequisite to the development of mechanism-based neuroprotective strategies for acute SCI is a detailed understanding of the early pathophysiological changes. On the assumption that brain lesions are transiently associated with decreased extracellular Mg^{2+} concentration,[2] even if this observation has not been systematically confirmed in humans,[3] Mg^{2+} solution infusion was tested and was found to worsen the outcome in patients with traumatic brain lesions.[4,5] This result was also observed in stroke patients.[6] In accordance with this view are reports on the lack of effectiveness of exogenous Mg^{2+} on experimental SCI or neonatal brain injury.[7,8]

To explore the cell death mechanisms, our laboratory has developed an *in vitro* neonatal rat spinal cord model to mimic the metabolic perturbation (hypoxia, aglycemia, oxidative stress, acidosis, and toxic free radicals with low extracellular Mg^{2+}) occurring *in vivo* after ischemic SCI.[9] This model is based on the transient application of a toxic medium (termed 'pathological medium', PM) that recapitulates the chief elements of metabolic dysfunction occurring *in vivo* and depresses locomotor network function with cell death predominantly in the white matter via an apoptotic pathway. We have observed that more extensive pyknosis with block of locomotor network activity is evoked when PM is applied with a standard concentration (1 mM) of extracellular Mg^{2+}[10] when compared with preparations treated with Mg-free PM.

[1]Department of Neuroscience, International School for Advanced Studies (SISSA), Via Bonomea Trieste, Italy; [2]SPINAL (Spinal Person Injury Neurorehabilitation Applied Laboratory), Istituto di Medicina Fisica e Riabilitazione, Udine, Italy and [3]Department of Biotechnology, University of Rijeka, Rijeka, Croatia
*Corresponding author: A Nistri, Department of Neuroscience, International School for Advanced Studies (SISSA), Via Bonomea 265, Trieste 34136, Italy. Tel: +39 040 3787718; Fax: +39 040 3787702; E-mail: nistri@sissa.it
Keywords: magnesium; PAR; AIF; parthanatos; TRPM2; TRPM7
Abbreviations: AIF, apoptosis-inducing factor; AUs, arbitrary units; ChAT, choline acetyltransferase; DAPI, 4,6-diamidino-2-phenylindole; DTT, dithiothreitol; EDTA, ethylenediaminetetraacetic acid; ELISA, enzyme-linked immunosorbent assay; H2AX, phospho-histone2A.X(Ser139); HEPES, 4-(2-hydroxyethyl)-1-piperazineethanesulfonic acid; L3, lumbar spinal cord segment 3; NeuN, neuronal nuclei; PM, pathological medium; PBS, phosphate-buffered solution; PJ34, N-(5,6-dihydro-6-oxo-2-phenanthridinyl)-2-acetamide; PMSF, phenylmethylsulfonyl fluoride; SNP, sodium nitroprusside; SCI, spinal cord injury; PAR, poly-ADP-ribose; PARP-1, poly (ADP-ribose) polymerase 1; ROI, region of interest; SMI 32, neurofilament H non-phosphorylated monoclonal antibody; T13, thoracic spinal cord segment 13; TRIS, tromethamine; TRPM2, transient receptor potential cation channel, subfamily M, member 2; TRPM7, transient receptor potential cation channel, subfamily M, member 7
Received 27.3.13; revised 28.5.13; accepted 03.6.13; Edited by A Verkhratsky

Although Mg^{2+} is essential for numerous enzymatic reactions,[11] novel targets of Mg^{2+} on the central nervous system have emerged. In particular, Mg^{2+} gates the activity of TRPM7, a bifunctional protein containing a protein kinase fused to an ion channel[12] and having a key role in neuronal death caused by oxidative stress and excitotoxicity.[13] Further, TRPM2 (a member of the same channel family and modulated by Mg^{2+}) is involved in the delayed death of brain neurons after experimental ischemia.[13–15] The aim of the present report was to investigate whether the increased severity of spinal damage evoked by PM + Mg^{2+} was due to recruitment of additional cell death pathways, as well as study their identity and the potential involvement of TRPM2 and TRPM7.

Results

Cell death induced by PM + Mg^{2+}. Our previous report[10] indicated that a 1-h application of PM containing 1 mM Mg^{2+} induces, 24 h later, significant damage to the *in vitro* spinal cord. This observation was confirmed by detecting extensive pyknosis in the white matter region at 24 h (see arrow in the example of Figure 1a). Figure 1b indicates the four ROIs used for these experiments, whereas Figure 1c quantifies these data. Significant pyknosis already emerged 3 h after washing out the toxic medium (Figure 1c). It is noteworthy that sham preparations (kept in standard Krebs for up to 24 h) or mock preparations (bathed for 1 h in Mg-free Krebs solution to which 1 mM Mg^{2+} was added to test for any artifact due to solution application and washout procedure) showed no significant pyknosis (Figure 1c). Thus, unlike the outcome with PM without Mg^{2+} (Figure 1c), the presence of this divalent cation worsened an ischemia-like metabolic perturbation, and cell damage developed over 24 h.

Characterization of the white matter damage evoked by PM + Mg^{2+}. Using biomarkers previously employed to characterize spinal injury,[16,17] we next investigated the type of cell damage evoked by PM + Mg^{2+} by studying immunoreactivity to phospho-histone2A.X(Ser139) (H2AX a marker of DNA double-strand breaks)[18] and active-caspase 3 (a marker of apoptosis)[19] in the white matter ROI where extensive pyknosis was found (Figure 1c). Figure 2a shows that the percentage of H2AX-positive cells in the white matter region was higher in treated than in sham preparations at 3 or 24 h. Nevertheless, unlike the number of pyknotic nuclei (Figure 1c), the number of H2AX-positive elements did not increase from 3 to 24 h (Figure 2a), suggesting the presence of early DNA double-strand lesions in keeping with former studies.[18,20] By comparing the 24-h data in Figures 1c and 2a, it seems likely that the PM + Mg^{2+} damage affected the vast majority of white matter elements, as about 75% of them showed pyknosis and 25% had H2AX immunoreactivity. Interestingly, in the same ROI, immunopositivity for active caspase 3 (an important executor of apoptosis), although limited to $<5\%$ of the cells, was larger than that in the sham condition (Figure 2b).

The poor expression of active caspase 3 was an unexpected result, as PM (without Mg^{2+}) is known to damage the spinal white matter primarily via caspase-dependent apoptosis.[16] When the spinal damage is evoked by excitotoxicity, the main process of cell death is a non-apoptotic mechanism termed parthanatos caused

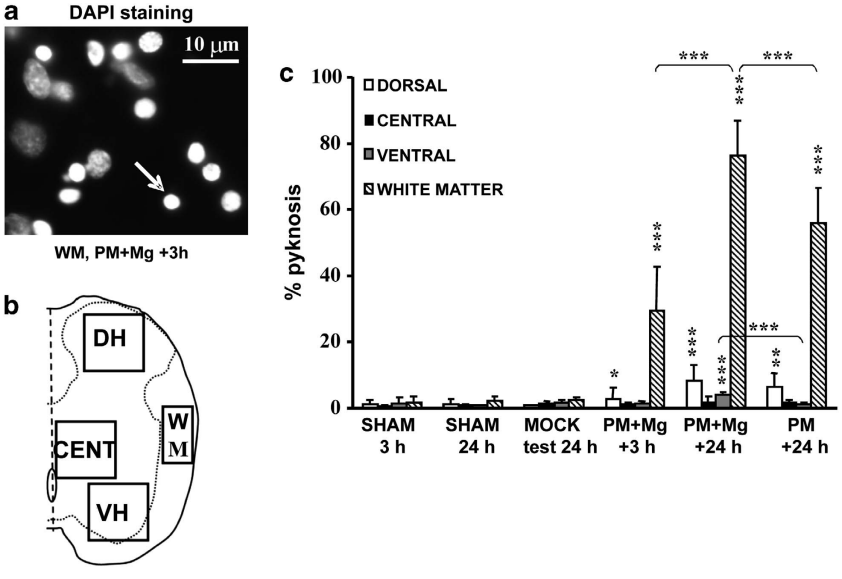

Figure 1 Pyknosis in the rat spinal cord *in vitro* following transient (1 h) application of pathological medium with or without Mg^{2+}. (**a**) Example of the spinal cord pyknosis (see arrow) in the white matter 3 h after washout of PM + Mg^{2+}. Scale bar: 10 μm. (**b**) Schematic representation of the four spinal ROIs used for analysis. DH, dorsal horn; CENT, central area; VH, ventral horn; WM, white matter. (**c**) Histograms show percentage of pyknotic cells in the four ROIs shown in (**b**). Mock data refer to preparations in which washout of incubating medium was performed to test for any potential mechanical damage related to this procedure. Note: statistically significant increase in the white matter pyknotic cell number in the samples treated with PM with or without Mg^{2+} *versus* sham preparations at 3 or 24 h after washout. Data are the average taken from nine sections from three rats. The Mann–Whitney test was used after performing an ANOVA Tukey test; $^{*}P = 0.022$; $^{**}P = 0.004$; $^{***}P < 0.001$

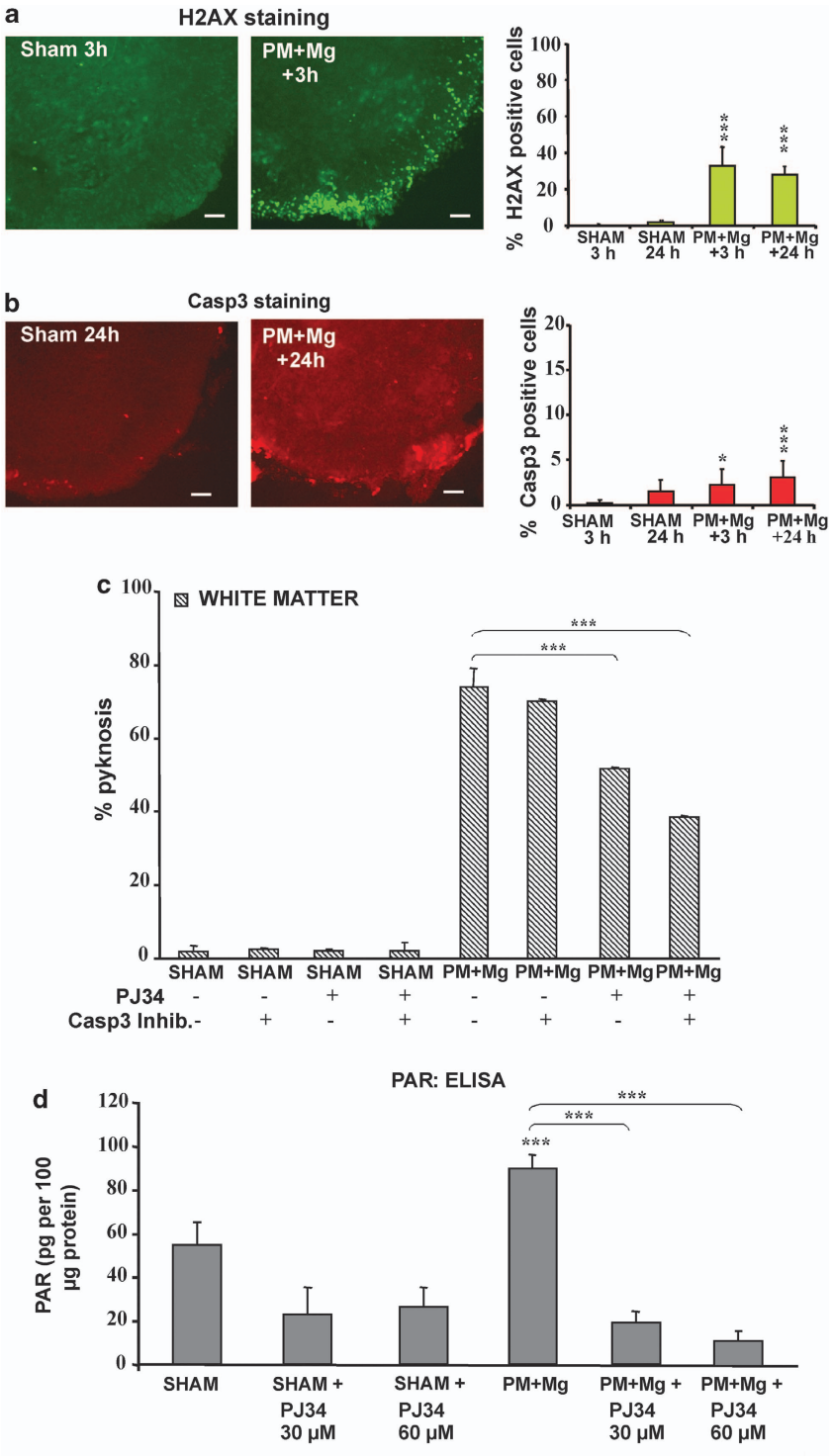

Figure 2 Characterization of white matter damage evoked by PM + Mg^{2+}. (**a**) Left, examples of immunostaining for H2AX in the ventral quadrant of the spinal cord in which the white matter shows minimal signal positivity in sham conditions. Scale bar: 30 μm; right, percentage of H2AX-positive cells in the ventrolateral white matter after PM + Mg^{2+}; $n = 9$ sections, ***$P < 0.001$. (**b**) Left, examples of immunostaining for active caspase 3 in the same ROIs as shown in (**a**); right, percentage of caspase 3-positive cells in the ventrolateral white matter after PM + Mg^{2+}; $n = 9$ sections, *$P = 0.034$; ***$P < 0.001$. (**c**) Histograms showing pyknotic nuclei after addition (on PM + Mg^{2+} washout) of caspase 3 inhibitor (1 μM), PJ34 (60 μM), or both. $n = 9$; ***$P < 0.001$. For data shown in (**a**), (**b**) and (**c**), the Mann–Whitney test was used after performing an ANOVA Tukey test. (**d**) Histograms show PAR tissue levels in various experimental conditions. For each test, data are from three spinal cords tested in duplicate; one-way Anova Tukey test; ***$P < 0.001$

by excessive activation of PARP-1 (poly (ADP-ribose) polymerase 1) to synthesize toxic concentrations of PAR (poly-ADP-ribose) that disrupt cell energy stores.[21] Therefore, in the present report we investigated whether, in the white matter ROI, PM + Mg^{2+} could stimulate excessive production of PAR, which is known to induce pyknosis.[21,22] Thus, we tested whether application of a selective inhibitor of either PARP-1 activity or caspase-3 might protect white matter elements from PM + Mg^{2+} toxicity. To this end, we used PJ34 (N-(5,6-dihydro-6-oxo-2-phenanthridinyl)-2-acetamide) to block PARP-1[23] and the caspase peptide inhibitor (caspase 3 inhibitor II, Z-DEVD-fmk) to block apoptosis,[24] which were applied (for 24 h) either alone or in combination immediately after washing out PM + Mg^{2+}. Figure 2c summarizes these data: whereas the caspase inhibitor alone did not significantly reduce pyknosis (5% change; see Figure 2c), PJ34 significantly ($P<0.001$) decreased pyknosis by >25%, an effect even stronger (>35%) when the two pharmacological blockers were applied together ($P<0.001$), indicating partial convergence of these two cell death processes. Neither inhibitor had any effect on sham preparations (Figure 2c). Figure 2d indicates that PJ34 applied at a concentration of 60 μM was a strong inhibitor of the tissue generation of PAR measured with an enzyme-linked immunosorbent assay (ELISA). Halving the concentration of PJ was less effective.

Figure 3a illustrates an example of co-staining with 4,6-diamidino-2-phenylindole (DAPI) and the PAR antibody of a pyknotic white matter cell 24 h after PM + Mg^{2+} application. Figure 3b shows that, among the total DAPI-stained elements, the percentage of PAR-positive cells in white matter ROI (hatched bars) had already increased significantly ($P<0.001$) 3 h after PM + Mg^{2+}, and it remained elevated ($P<0.001$) 24 h later. Figure 3b (filled bars) also quantifies co-occurrence of PAR immunopositivity together with pyknosis for the total number of pyknotic cells; it is clear that PM + Mg^{2+} induced a significant ($P<0.001$) increase in the association between PAR and pyknosis at 3 and 24 h. In fact, few cells were PAR positive without pyknotic nucleus at either time (open bars). This finding suggested that PM + Mg^{2+} had transformed the white matter damage from the apoptosis previously detected with PM alone[10] to a process with parthanatos characteristics. We thus wondered whether an analogous process might have developed in the gray matter.

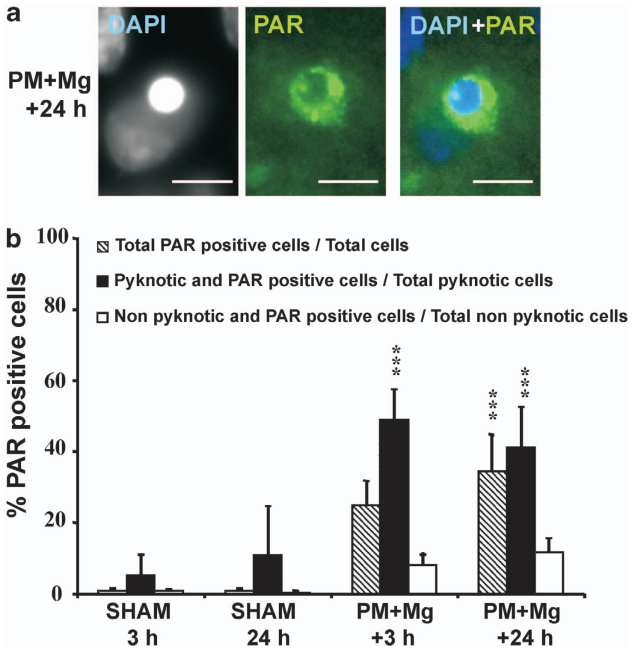

Figure 3 PAR immunoreactivity in the white matter after PM + Mg^{2+}. (**a**) Example of co-staining with DAPI (left) and PAR immunoreactivity (middle) of a pyknotic white matter cell 24 h after PM + Mg^{2+} application; right panel shows overlapped images; scale bar: 10 μm. (**b**) Histograms show percentage of PAR-positive cells (hatched bars) over total DAPI-stained elements, co-occurrence of PAR immunopositivity and pyknosis (filled bars) and total number of pyknotic cells (open bars). $n=9$; the Mann–Whitney test was used after performing an ANOVA Tukey test; ***$P<0.001$

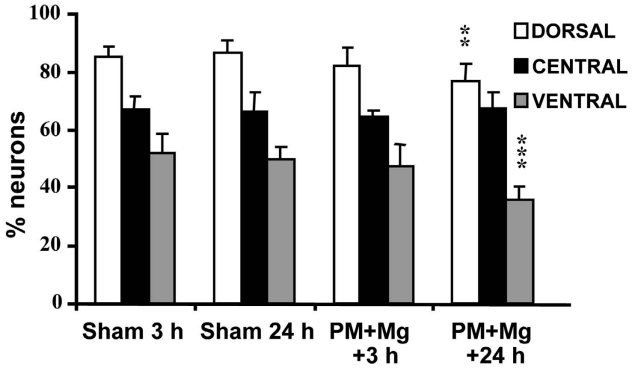

Figure 4 Characterization of neuronal damage evoked by PM + Mg^{2+}. Histograms show percentage of neurons (NeuN-positive cells) observed in three ROIs in control or after PM + Mg^{2+} washout (3 or 24 h). The Mann–Whitney test was used after performing an ANOVA Tukey test, $n=9$; **$P=0.003$; ***$P<0.001$

Characterization of gray matter damage evoked by PM + Mg^{2+}. Despite the comparatively modest extent of the lesion to the gray matter induced by PM + Mg^{2+} (see Figure 1c), this protocol is known to inhibit locomotor network function.[10] To further analyze neuronal damage, the present study quantified the percentage of NeuN-positive neurons in dorsal, central, and ventral ROIs at 3 and 24 h after PM + Mg^{2+}. Figure 4 demonstrates that significant neuronal loss was absent at 3 h, and became apparent at 24 h as far as the dorsal and ventral ROIs were concerned. Thus, in accordance with pyknosis data (Figure 1c), PM + Mg^{2+} had an early effect on white matter elements, and a later one on gray matter cells, which, in the ventral horn, constitute a small minority of the spinal cell population.[25]

As, among gray matter regions, the late damage by PM + Mg^{2+} appeared to mostly affect the ventral ROI that contains motoneurons, namely, the essential output elements of the locomotor network, we next investigated dysfunctional changes in motoneurons, identified as large (>25 μm somatic diameter) cells located in the ventral horn and immunopositive for choline acetyltransferase (ChAT, the cytoplasmic ACh synthetic enzyme), and for SMI32, a marker for motoneuron cytoskeleton.[26,27] Figure 5a shows that the number of ChAT-positive motoneurons did not change following PM + Mg^{2+} at 3 or 24 h, whereas the average intensity of the SMI32 signal was significantly ($P<0.001$) decreased at 3 and 24 h (Figure 5b). This observation suggests that, despite the

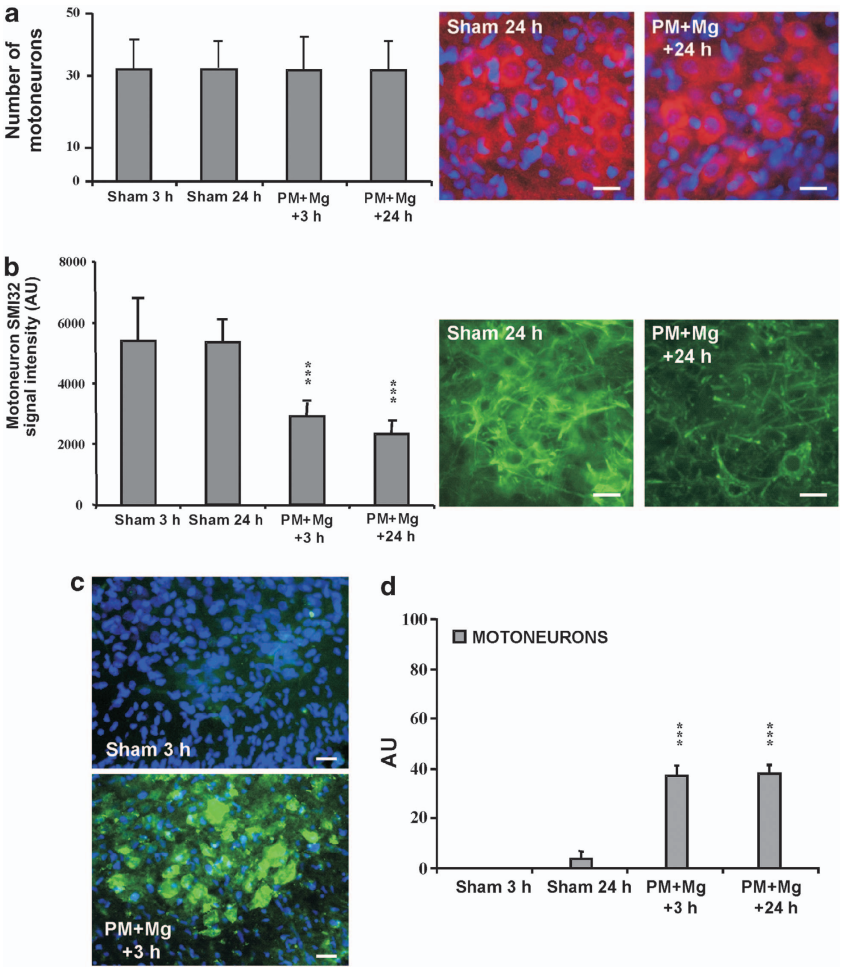

Figure 5 Characterization of motoneuron damage evoked by PM + Mg^{2+}. (**a**) Histograms show motoneuron numbers counted with ChAT immunostaining. Inset shows an example of ChAT-stained ventral horn cells in sham-24 or PM + Mg-24 conditions. Bar = 30 μm. (**b**) Histograms show motoneuron SMI32 signal intensity that was already decreased 3 h after PM + Mg^{2+} washout; a *t*-test was performed after an ANOVA Tukey test; ***$P<0.001$. Inset shows an example of SMI32-stained ventral horn cells in sham-24 h or PM + Mg-24 h conditions. Bar = 30 μm. (**c**) Examples of PAR immunoreactivity detected in motoneurons 3 h after PM + Mg^{2+}; scale bar: 30 μm. (**d**) Histograms show motoneuron PAR signal intensity enhanced after PM + Mg^{2+}; a Mann–Whitney test was performed after an ANOVA Tukey test, ***$P<0.001$. For all experiments, data are from nine spinal sections from three rats

unaltered number of motoneurons, these cells showed signs of cytoskeleton damage.

Neuronal distress can strongly activate PARP-1 to generate toxic levels of PAR ('parthanatos').[28,29] In accordance with this notion, a significant increase in PAR immunoreactivity was detected in motoneurons early after PM + Mg^{2+}, as exemplified in Figure 5c and quantified in Figure 5d. It is noteworthy that the PAR signal intensity did not increase further at 24 h.

The toxic action of PAR is typically executed via translocation of the transcription factor apoptosis-inducing factor (AIF) from the mitochondria to the nucleus[22,29,30] and it thus represents a delayed cell death signal. We examined the expression and translocation of AIF in motoneurons as indicated in Figures 6a and b. In sham conditions, the confocal line scan of the motoneuron cell body (see line across cell soma in Figure 6a, left) demonstrated that its DAPI staining was confined to the cell nucleus (blue line; Figure 6a, right), whereas AIF (red line in Figure 6a, right) was poorly expressed throughout the cell. In contrast, 24 h after PM + Mg^{2+} (Figure 6b), whereas DAPI staining was still restricted to the nucleus, AIF immunoreactivity was diffused and extended to the cell nucleus as well. Detection of AIF in the motoneuron nucleus was accompanied by loss of expression of the nuclear transcription factor NeuN as shown in Figure 6c (see open arrow). Finally, Figure 6d indicates that, 24 h after PM + Mg^{2+}, about 30% of motoneurons showed AIF nuclear translocation. All together, these observations suggest that, despite the persistence of ChAT immunoreactivity, a significant fraction of motoneurons displayed multiple signs of distress 24 h after PM + Mg^{2+}, consistent with the onset of a parthanatos-like process.

Expression of TRPM7 or TRPM2 after PM + $Mg2^{+}$ application. TRPM7 and TRPM2 are members of a large family of ion channels[31] believed to play an important role in the neurodegeneration evoked by ischemia *in vivo* or by ischemia-like conditions *in vitro*.[13,14,32–35] In the present study, we found undetectable TRPM7 immunopositivity in the white matter from freshly frozen preparations (Figure 7a, open circle), or under 3 and 24 h sham conditions (Figure 7a,

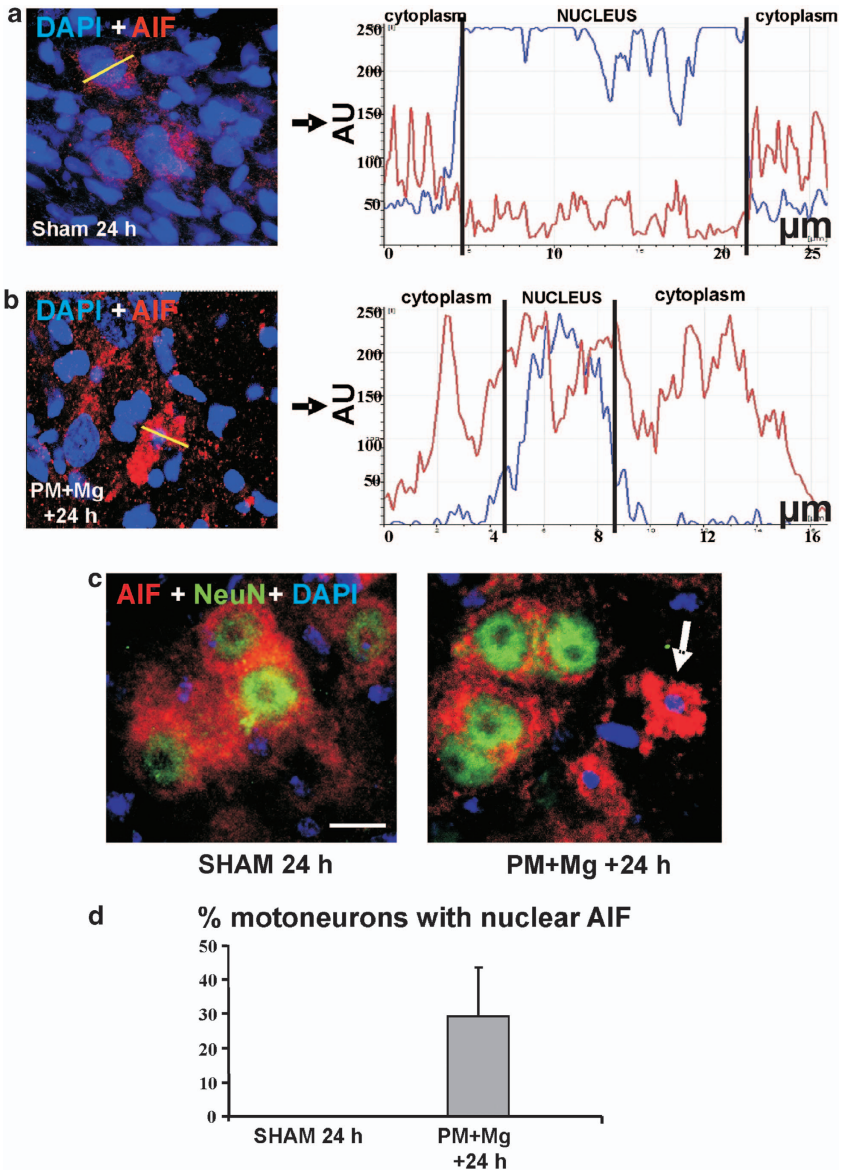

Figure 6 AIF signal in motoneurons after PM + Mg^{2+}. (**a**) An example of AIF cytoplasmic distribution in sham motoneurons (left), with confocal line scan analysis plotted on the right for the cell indicated by an open bar on the left. Note strong nuclear distribution of DAPI (blue) *versus* AIF. (**b**) Analogous presentation of data referred to sample 24 h after PM + Mg^{2+}. Note DAPI signal colocalized with AIF in the nucleus. (**c**) Examples of DAPI (blue) co-staining with AIF (red; left columns) or NeuN (green; right columns) under sham conditions (top row) or after PM + Mg^{2+} (bottom row). Under sham conditions, the AIF signal was cytoplasmic and the NeuN signal was nuclear. After PM + Mg^{2+}, the AIF signal is expressed by the motoneuron nucleus that has lost NeuN immunoreactivity. Scale bar: 30 μm. (**d**) Histograms show percentage of motoneurons expressing nuclear AIF after PM + Mg^{2+}. For all experiments, data are from nine spinal sections from three rats (see white arrow)

open squares), or immediately after washing out PM + Mg^{2+} (Figure 7a, filled triangle). Vice versa, a strong signal became apparent 3 h after PM + Mg^{2+} washout and remained stable 24 h later (Figure 7a, filled triangles). White matter TRPM7 immunoreactivity was most frequently detected in pyknotic cells (see arrows in Figure 7b) as quantified in Figure 7c (filled bars). In the white matter ROI, there was no significant TRPM2 immunoreactivity under treated or sham conditions (not shown). Thus, it appeared that about half of the white matter elements that died (pyknosis) after PM + Mg^{2+} treatment also expressed strong positivity to TRPM7.

In contrast to these data from the white matter ROI, in the three gray matter ROIs we found baseline positivity to TRPM7 (Figures 8a and b) and TRPM2 (Figure 8c). After washing out PM + Mg^{2+}, the TRPM7signal was found significantly lower 24 h later (Figures 8a and b) in the dorsal horn ROI ($P<0.001$) and in the motoneuron ROI ($P=0.002$). Conversely, for the same ROIs, TRPM2 immunopositivity appeared to move in the opposite direction with a delayed increase 24 h after washing out PM + Mg^{2+} (Figure 8c).

Discussion

The focus of the present study was the role of extracellular Mg^{2+} in the genesis of cell death after transient application of a solution mimicking ischemia conditions. The present data

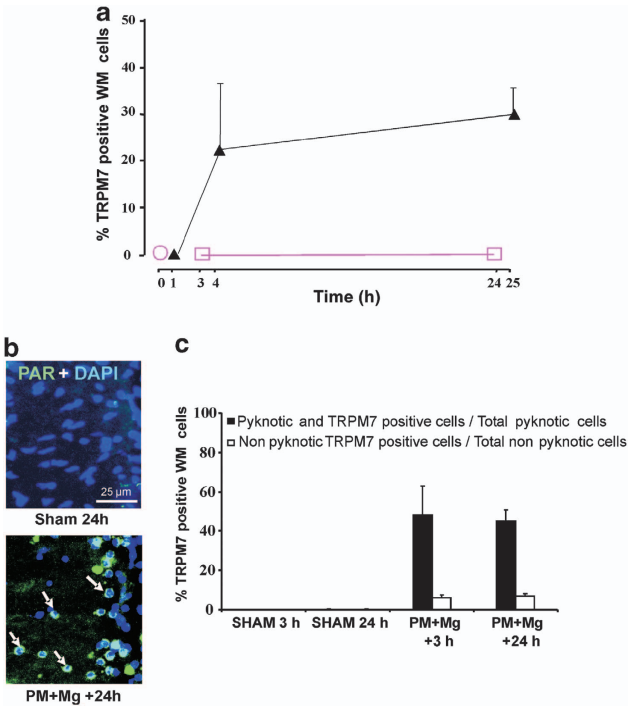

Figure 7 White matter expression of TRPM7 after $PM + Mg^{2+}$ application. (**a**) Plot of the number of TRPM7-positive white matter cells against time following $PM + Mg^{2+}$ (filled triangles). TRPM7 immunopositivity was undetectable in the white matter from freshly frozen preparations (open circle at time 0) or under sham conditions (open squares at 3 and 24 h). (**b**) Examples of TRPM7-positive white matter cells (see arrows) after $PM + Mg^{2+}$. (**c**) Histograms show percentage of TRPM7-positive/pyknotic white matter cells calculated with respect to the total number of pyknotic elements (filled bars). Open bars show percentage of TRPM7-positive cells without pyknosis over total number of non-pyknotic cells. We also quantified co-occurrence of TRPM7 immunopositivity together with pyknosis for the total number of pyknotic cells. All data are from nine spinal sections from three rats

indicate that the presence of this divalent cation contributed to enhancing and widening the delayed damage to the white and gray matters of the rat spinal cord by facilitating a distinct cell death pathway.

A model of non-traumatic injury. The growing number of non-traumatic causes of SCI[1] led us to examine the processes responsible for early cell death after the *in vitro* insult. Our previous investigations indicated that applying a toxic solution containing free oxygen radicals with no oxygen or glucose supply especially damaged the white matter elements, with moderate impairment of locomotor-like patterns that were still present at regular frequency but with clearly lower amplitude.[9,10] Nevertheless, when the same toxic solution contained the standard extracellular Mg^{2+} concentration, the histological damage was intensified and locomotor patterns were inhibited.[10] The present report sought to characterize the processes responsible for this damage enhancement.

$PM + Mg^{2+}$ evoked lesion of white matter elements. This solution was confirmed to produce stronger damage than the original PM (without added Mg^{2+}), as pyknosis was seen in about 80% of the ROI white matter elements and was accompanied by early phosphohistone positivity to indicate relatively rapid DNA damage.[18] The canonical marker of apoptosis, namely, activated caspase 3,[19] was evident in a small minority of white matter cells only. Perhaps the damage had evolved so quickly that cell death had become apparent before any extensive apoptosis could be produced. In keeping with this view was our observation that a pharmacological inhibitor of apoptosis[24] did not arrest pyknosis, although it reduced pyknosis when coapplied with PJ34, the inhibitor of PARP-1,[23] which is essential for DNA damage repair and whose hyperactivation generates the toxic product PAR.[23,28,29] PAR was already strongly increased 3 h after the end of $PM + Mg^{2+}$ application, suggesting a narrow time window before irreversible cell damage could occur (demonstrated by colocalization of PAR and pyknosis). When PJ34 is administered early during the lesion protocol, a degree of functional neuroprotection is observed[36] in accordance with the present data. In general, the present results suggest that the presence of Mg^{2+} during the ischemic-like protocol aggravated the damage to the white matter cells by promoting the activation of at least one major cell death pathway, namely, parthanatos.

Gray matter damage by $PM + Mg^{2+}$. Alongside low-scale pyknosis, most NeuN-positive neurons exhibited a gradient of neuronal loss: the strongest in the ventral horn, a modest one in the dorsal horn, and apparently none in the central region. Motoneurons, however, did not disappear, as their typical marker ChAT was preserved even 24 h later. These cells were, nevertheless, showing signs of distress because their SMI32 positivity was decreased, suggesting disturbance of their cytoskeleton. Conversely, a traumatic lesion *in vivo* is associated, a few days later, with loss of ChAT, followed by upregulation of SMI32 expression by surviving motoneurons, taken as an index of cell repair.[37] The differential evolution of ChAT and SMI32 in the present study compared with *in vivo* experiments is unlikely due to motoneuronal maturation, as neonatal motoneurons already show adult somatic size.[38] Accordingly, in the *in vitro* rat spinal cord model, the number of SMI32- and ChAT-positive cells and their staining pattern remain constant in the first week of life.[25] Further, AIF-dependent cell death mediates neuronal death after hypoxia–ischemia in the neonatal rat brain[39] as much as in the adult brain.[22] Hence, dynamic changes in these two biomarkers may indicate distinct processes and time course underlying either degenerative mechanisms or restoration.

Concomitant with the fall in SMI32 signal was the detection of rising PAR immunoreactivity in the same cells. This was likely a sign of impending death, as it was accompanied by strong AIF translocation into the nucleus, a known effector of cell death.[29] Interestingly, AIF nuclear translocation was closely associated with loss of NeuN positivity. NeuN is an intrinsic component of the neuronal nuclear matrix,[40] whose fast degradation (already at 1 h after injury)[41] precedes cytoskeletal changes (identified, for instance, with SMI32 positivity) in injured motoneurons.[37]

These results imply that various motoneuron biomarkers should be tested for assessing damage in pathological conditions, as their significance in the diagnosis of cell death is time-dependent. Thus, we surmise that the development of

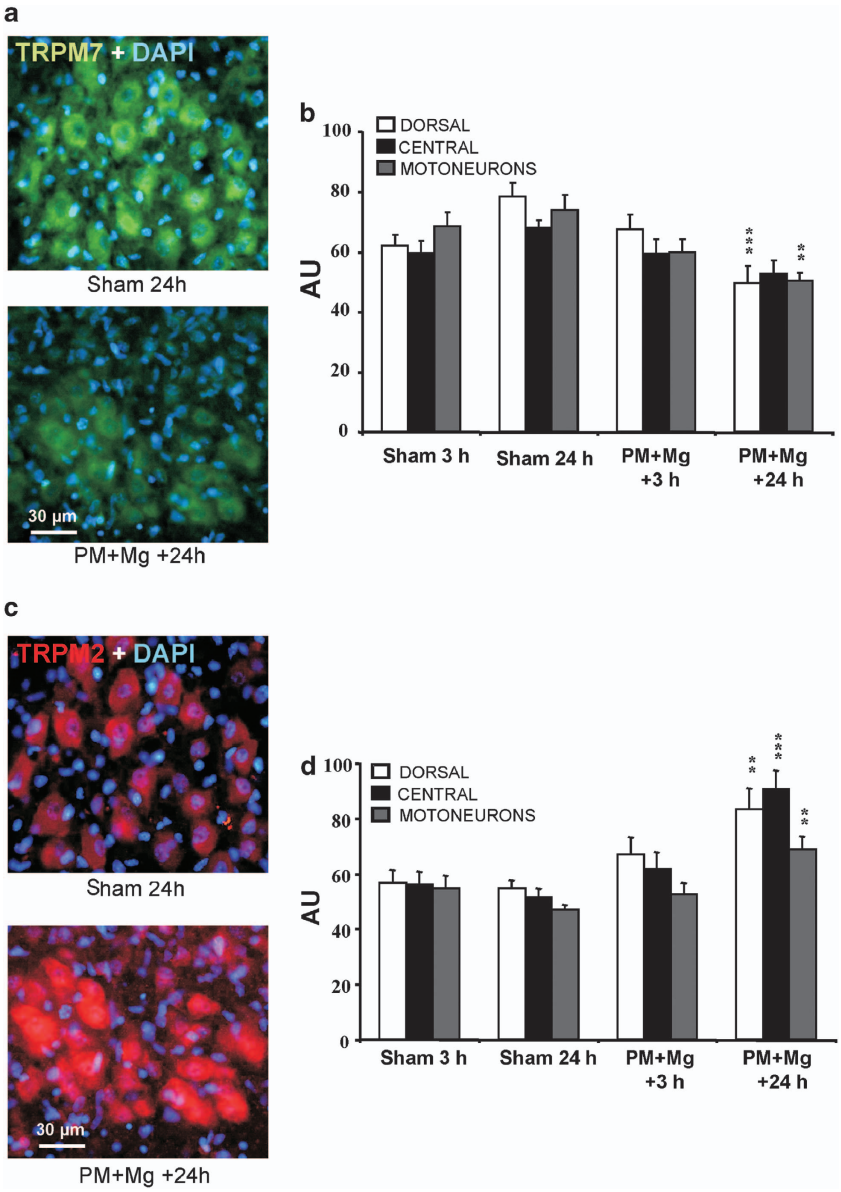

Figure 8 Gray matter expression of TRPM7 or TRPM2 after PM + Mg^{2+} application. (**a**) Examples of TRPM7 immunoreactivity in the ventral horn under sham conditions or 24 h after PM + Mg^{2+}. (**b**) Histograms show distribution of TRPM7 immunoreactivity in dorsal, central and motoneuron ROIs. Note the significant fall in average signal intensity 24 h after PM + Mg^{2+} for dorsal and motoneuron ROIs; $^{**}P = 0.002$; $^{***}P < 0.001$. (**c**) Examples of TRPM2 immunoreactivity in ventral horn under sham conditions or 24 h after PM + Mg^{2+}. (**d**) Histograms show distribution of TRPM2 immunoreactivity in dorsal, central and motoneuron ROIs. Note the significant increase in TRPM2 signal in all three ROIs examined; one-way Anova Tukey test, $^{**}P = 0.004$; $^{***}P < 0.001$. All data are from nine spinal sections from three rats

parthanatos in motoneurons occurred on a slower time base than in the white matter. Nevertheless, these pathological changes have a strong negative impact on locomotor network function.[10]

TRPM2 and TRPM7 roles in the PM + Mg^{2+} effects. These two membrane channels have recently been investigated for their contribution to ischemic cell death in the brain.[13,35] These channels are gated open by intracellular PAR, reactive oxygen species and Mg^{2+} (as under normal conditions such channels are minimally activated).[13,14,42–44] For these reasons, we studied how these channels were expressed during our experimental protocol. In view of reports on the ubiquitous occurrence of TRPM7 expression,[45] their immunohistochemical absence in the white matter under sham conditions was not anticipated. This phenomenon could not be attributed to loss of protein expression by keeping the preparation *in vitro* because analogous lack of signal was found when the tissue was frozen immediately after dissection. It seems feasible that immaturity of the neonatal spinal cord was a factor for poor TRPM7 expression in controls. It was, however, clear that already 3 h after PM + Mg^{2+} exposure a large number of white matter cells (with pyknotic nucleus) were positive to

TRPM7. Our interpretation is that metabolic distress in the presence of Mg^{2+} triggered rapid trafficking of TRPM7 proteins to the cell membrane, where their activation might have contributed to the observed damage.

Unlike the white matter cells, in the gray matter, baseline expression of TRPM7 fell in motoneurons and dorsal neurons 24 h after PM + Mg^{2+} when low-scale pyknosis was manifested. TRPM2 expression (that could not be observed in the white matter) showed an opposite pattern with a late rise in gray matter neurons, which was especially strong in the central region. It is not feasible to relate the intensity of immunoreactivity to channel activation; thus, the present results about differential TRPM7 and TRPM2 signal intensities cannot be extrapolated to a specific role of these proteins in neuronal survival or death. Nonetheless, the present observations indicate a significant dichotomy in TRPM7 and TRPM2 channel expression, whose molecular mechanism remains to be clarified. Future studies are necessary to investigate the functional activity of TRPM2 or TRPM7 channels under the present experimental protocols. This goal is, however, complex because of the difficulty to isolate, in an intact network system, the contribution of these conductances in the absence of selective inhibitors, the widespread dysfunction of motoneurons and the lack of knockout rat models.

Even if both TRPM7 and TRPM2 channels have been proposed to be mediators of neuronal death after ischemia,[46] the time dependence of their differential activation is not known under the present conditions. As TRPM2 channels are inhibited by intracellular glutathione,[47] TRPM2 overexpression was perhaps related to metabolic dysfunction that developed early for the superficial motoneurons. The effects of the toxic solution on deep central neurons were likely delayed with morphological preservation of such cells that had shown the strongest TRPM2 expression. One hypothesis is that the TRPM2 activation would eventually lead to central neuron damage occurring at the time point beyond the 24-h *in vitro* survival of the isolated control spinal cord, and thus outside our experimental range. As TRPM2 channels are characterized by small conductance,[14] it would follow that a small-scale influx of these cations might determine the delayed trigger of parthanatos.

Role of extracellular Mg^{2+}. From the point of view of an *in vitro* spinal model, it is apparent that the standard concentration (1 mM) of Mg^{2+} amplified white matter damage and extended it to the gray matter. The reason might reside in the differential expression of TRPM7 and TRPM2, plus the degree of PAR hyperproduction at the early stage of damage, because the concentrations of PAR and intracellular Mg^{2+} are potent modulators of the activity of these channels.[13,46] Recent studies with *in vitro* brainstem neurons have proposed that changes in intracellular Mg^{2+} concentrations occurring during pathological states can affect the conductance of neuronal Cx36 gap junctions[48] and presumably shape the damage outcome. Although chemical synaptic inputs and Cx36-dependent electrical synapses contribute to synchronization of spinal motoneuron function,[49] the expressions of Cx36 and Cx32 mRNA and proteins are sparse and unchanged after rat SCI.[50] The complexity of the processes underlying ischemia-induced damage in the spinal cord even when studied with an *in vitro* model implies diversity of molecular pathways with distinct time dependence and cell specificity, factors that contribute to the difficulty of implementing successful neuroprotection *in vivo*.[51–53] The present report suggests that the extracellular level of Mg^{2+} largely affects cell death mechanisms in the spinal cord and extends damage to motoneurons by facilitating the onset of parthanatos.

Materials and Methods

Rat spinal cord preparation. The experiments were performed on neonatal Wistar rats of postnatal age 0–1 days in accordance with the guidelines of the National Institutes of Health and the Italian act D.Lgs. 27/1/92 no. 116 (implementing the European Community directives no. 86/609 and 93/88), and the protocols were approved by the SISSA ethical committee for animal experimentation. We minimized the number of animals used in order to allow clear statistical analysis. Spinal cords were carefully dissected out from pups under urethane anesthesia (0.2 ml i.p. of a 10% w/v solution) at room temperature, with continuous superfusion with Kreb's solution containing (in mM) the following: NaCl, 113; KCl, 4.5; $MgCl_2 7H_2O$, 1; $CaCl_2$, 2; NaH_2PO_4, 1; $NaHCO_3$, 25; glucose, 11; gassed with 95% O_2/5% CO_2, pH 7.4 at room temperature (22 °C), as described previously.[26]

Protocol for spinal cord lesion. Our aim was to generate an experimental condition that might mimic the acute clinical setting when the metabolic insult is often temporary because of intensive care treatment to correct the metabolic derangement. In accordance with our studies[10,11] and to simulate the biochemical conditions believed to occur at the site of the lesion, we used a metabolic perturbation protocol consisting of the transient application of PM (see below) with the addition of 1 mM Mg^{2+}.[10] This protocol is known to induce a pathological condition that includes locomotor network inhibition and histological damage.[10] Thus, a solution containing 10 mM H_2O_2, 500 μM sodium nitroprusside (SNP) and 1 mM Mg^{2+} and lacking oxygen and glucose was applied for 1 h. $NaHCO_3$ was omitted and 4-(2-hydroxyethyl)-1-piperazineethanesulfonic acid (HEPES) was added to reach the pH range of 6.75–6.80 (with 0.1 N NaOH) and the osmolarity was lowered to 230–240 mOsm. This solution recapitulates the biochemical derangement believed to occur in the spinal cord after acute non-traumatic injury.[9]

After a 1-h application of PM + Mg^{2+}, the latter solution was washed out and standard Kreb's solution was superfused again for up to 24 h, after which preparations were fixed as previously reported[9] and processed for histology as detailed below. Sham experiments were performed by keeping the preparations for analogous times in the same experimental setup without applying a toxic medium.

Quantification of dead cells. Using a Zeiss Axioskop2 microscope (Oberkochen, Germany) and Metavue software (Metamorph suite sold by Molecular Devices, Sunnyvale, CA, USA), cell counting was performed after DAPI staining or NeuN positivity (for neurons). Data were counted with 'eCELLence' (Glance Vision Tech., Trieste, Italy) software.[9,10] For each histological cross-section of the spinal cord, four different regions were investigated: dorsal gray matter (Rexed laminae I–IV), central gray matter (Rexed laminae V–VII and X), ventral gray matter (Rexed laminae VIII–IX) and ventrolateral white matter. In each region, three to six fields of 280 × 280-μm (gray matter) or 100 × 280-μm (white matter) area were analyzed. For each experimental group, three spinal cords were analyzed and, for each spinal cord, 3–4 different sections from T13 to L3 (thoracic spinal cord segment 13 to lumbar spinal cord segment 3) segments were examined. Pyknosis was readily observed as a change in nuclear morphology resulting from chromatin condensation.[54]

Immunofluorescence procedure. Immunostaining was performed as previously described.[9,26] Briefly, paraformaldehyde-fixed spinal cords were cryoprotected with 30% sucrose and sectioned (30 μm) with a sliding microtome. In accordance with our former studies, we analyzed spinal regions between T13 and L3 segments. For all antibodies (except anti-PAR), after incubation in blocking solution (5% normal goat serum, 5% bovine serum albumin, 0.3% Triton-X 100) for 1 h at room temperature, the primary antibody was incubated at 4 °C overnight. Before incubating tissue sections with the PAR antibody, an

antigen-retrieval procedure was performed by treating (20 min at 60 °C) samples with Tromethamine (TRIS)—Ethylenediaminetetraacetic acid (EDTA)—TWEEN 80 (pH = 8.5). To preserve the structure of spinal cord slices that could be damaged by the antigen retrieval procedure, the TRIS–EDTA–TWEEN was washed out with cold phosphate-buffered solution (PBS) five times to stop the reaction before mounting the slices for immunostaining. The primary antibodies were visualized using secondary anti-mouse Alexa fluor 488 or 594 antibodies (1 : 500; see Supplementary Table 1). Sections were finally stained with DAPI for 20 min and analyzed as detailed below.

All antibodies (except TRPM2 and TRPM7) have been previously used and validated for immunostaining with our preparations (for ChAT, NeuN, SMI32, see Taccola *et al.* [9] and Cifra *et al.*[25]; for AIF, cleaved caspase-3, H2AX and PAR, see Kuzhandaivel *et al.*[16,21]). The TRPM2 antibody was validated by Hara *et al.*[55] and the TRPM7 antibody by Everaerts *et al.*[56]

Immunofluorescence data analysis. For each spinal section, images of the dorsal and ventral horns, the area around the central canal and the ventrolateral white matter were acquired with a LEICA 6000 microscope ($\times 40$ lens) using identical capture settings throughout, and ensuring that signals were clearly below saturation and yielding a good signal/noise ratio. For each spinal region, the acquisition procedure was repeated four times at *z* axis intervals of 1 μm. In order to analyze all these images, we used the 3D Volocity software (Perkin Elmer, London, UK) applied to four regions of interest (ROIs). For the dorsal, central and white matter regions, the ROI size was 200×100 μm. For motoneurons, we drew by hand a ventral horn region that comprised large-diameter (>25 μm) neurons. For each gray matter ROI, using the 'voxel spy' facility of the software, we calculated the background fluorescence and included in the analysis only those signals that were higher than this threshold value. Owing to the large degree of cell meshing in the neuropile, the ROI signal intensity was evaluated on a gray scale and expressed in arbitrary units (AUs). The data were averaged from three histological sections from each one of three rats. In the case of white matter quantification, it was possible to observe individual cells that were counted and averaged for three sections from each one of three rats.

This approach was employed for quantifying data concerning immunopositivity to PAR, ChAT, SMI32, TRPM2 and TRPM7. For caspase 3, phosphohistone and NeuN data, we used previously published procedures with a Zeiss Axioskop2 microscope and Metavue software.[16]

Analysis of AIF translocation. Images of single motoneurons were acquired with a LEICA confocal microscope, using 0.5-μm z sectioning as reported by Oh *et al.*[57] After reconstructing the cell image, we selected a single central optical section that comprised the largest nuclear staining with DAPI. Thereafter, we performed a line scan of such an image to verify the distribution of AIF immunofluorescence signal in the nucleus and in the cytoplasmic compartment. The number of reconstructed motoneurons showing AIF nuclear translocation was quantified with ImageJ (http://rsb.info.nih.gov/ij).

Nuclear and mitochondrial protein extraction. The nuclear extraction was prepared in accordance with published reports.[21,58] Thus, isolated spinal cords were washed with ice-cold 250-STMDPS buffer (50 mM Tris-HCl, pH 7.4, 250 mM sucrose, 5 mM $MgCl_2$, 1 mM dithiothreitol (DTT), 1 mM phenylmethylsulfonyl fluoride (PMSF), 25 μg/ml spermine and 25 μg/ml spermidine) and then submerged in the same. After 15 strokes in a Dounce homogenizer, the extract was centrifuged at 800 *g* for 15 min. The pellet (Pellet I) was used to prepare the nuclear fraction. The supernatant was again centrifuged at 6000 *g* for 15 min to remove mitochondria (Pellet II). To prepare the nuclear fraction, Pellet I was homogenized with a single stroke in a Dounce homogenizer in 2 M-STMDPS buffer (50 mM Tris-HCl, pH 7.4, 2 M sucrose, 5 mM $MgCl_2$, 1 mM DTT, 1 mM PMSF, 25 μg/ml spermine, and 25 μg/ml spermidine) and fractionated at 80 000 *g* for 5 min. The resulting pellet was resuspended in nuclear extract buffer (20 mM HEPES, pH 7.9, 1.5 mM $MgCl_2$, 0.5 M NaCl, 0.2 mM EDTA, and 20% glycerol) and used as the nuclear fraction (Pellet I). Pellet II was resuspended in hypotonic lysis buffer (10 mM HEPES, pH 7.9, 1 mM DTT, plus the protease inhibitor cocktail; Sigma, Milan, Italy) and incubated on ice for 30 min. The suspension was sonicated to lyse mitochondria. Protein concentrations were determined for the nuclear fraction and the mitochondrial lysate using the standard bicinchoninic acid assay following the manufacturer's protocol (Sigma). For each individual experiment, three spinal cords were used. The purity of the extracted nuclear fraction was validated by looking for (with western immunoblotting) any mitochondrial contamination indicated by the cytochrome *C* oxidase IV protein (Abcam, Cambridge, UK) in accordance with the method of Beirowski *et al.*[59] These samples were then used for ELISA.

ELISA quantification of PAR. To obtain evidence for PARP-1 activation and pharmacological inhibition by N-(5, 6-Dihydro-6-oxo-2-phenanthridinyl)-2-acetamide (PJ34), we quantified its product PAR in accordance with Nasrabady *et al.*[60] For this purpose, lysates of spinal cords treated with PM + Mg and/or PJ34, or in sham conditions, were collected 24 h later and their PAR levels were measured using the PARP *in vivo* pharmacodynamic assay II (http//www.trevigen.com/protocols) following the manufacturer's protocol (Trevigen, Bologna, Italy). This assay is based on ELISA immunoreactivity resulting in chemiluminescence signals recorded with a Glomax multi-detection system (Promega, Milan, Italy). Whenever tests were performed for the action of PJ34, this substance was added to the cell lysis buffer to avoid inhibitor dilution as per the manufacturer's instructions. All samples were run in duplicate. After background subtraction (blank samples), the net PAR levels were quantified using a standard linear plot ($r = 0.98$) based on the immunoreactivity induced by known concentrations (20–1000 pg/ml) of PAR. Data were expressed as pg/ml/100 μg of protein (estimated as indicated below).

Drugs. SNP and PJ34 were purchased from Sigma; H_2O_2 was obtained from Carlo Erba Reagents (Milan, Italy); and active caspase 3 inhibitor II was obtained from CalBiochem-Millipore (Billerica, MA, USA).

Data analysis. The data are shown as mean ± S.D. Statistical analysis was carried out with SigmaStat 3.1 (Systat Software, Chicago, IL, USA). Parametric and nonparametric data were first distinguished with a normality test (Anova Tukey) and analyzed with the Student *t*-test and the Mann–Whitney test, respectively, in accordance with the software choice. The significance level was always $P < 0.05$, and *n* indicates the number of tissue sections.

Conflict of Interest

The authors declare no conflict of interest.

Acknowledgements. We thank our colleague Dr. A Kuzhandaivel for her help with the ELISA assay, Dr. Micaela Grandolfo for support with quantitative image analysis and Dr. Andrea Tomicich for software support. This work was supported by a grant from the government of the Friuli Venezia Giulia Region (SPINAL project).

1. van den Berg ME, Castellote JM, Mahillo-Fernandez I, de Pedro-Cuesta J. Incidence of spinal cord injury worldwide: a systematic review. *Neuroepidemiology* 2010; **34**: 184–192.
2. Lin MC, Huang YL, Liu HW, Yang DY, Lee CP, Yang LL *et al.* On-line microdialysis-graphite furnace atomic absorption spectrometry in the determination of brain magnesium levels in gerbils subjected to cerebral ischemia/reperfusion. *J Am Coll Nutr* 2004; **23**: 561S–565SS.
3. Valadka AB, Goodman JC, Gopinath SP, Uzura M, Robertson CS. Comparison of brain tissue oxygen tension to microdialysis-based measures of cerebral ischemia in fatally head-injured humans. *J Neurotrauma* 1998; **15**: 509–519.
4. Maas AI, Murray GD. Magnesium for neuroprotection after traumatic brain injury. *Lancet Neurol* 2007; **6**: 20–21.
5. Temkin NR, Anderson GD, Winn HR, Ellenbogen RG, Britz GW, Schuster J *et al.* Magnesium sulfate for neuroprotection after traumatic brain injury: a randomised controlled trial. *Lancet Neurol* 2007; **6**: 29–38.
6. IMAGES.. Magnesium for acute stroke (Intravenous Magnesium Efficacy in Stroke Trial): randomised controlled trial. *Lancet* 2004; **363**: 439–445.
7. Perlman JM. Intervention strategies for neonatal hypoxic-ischemic cerebral injury. *Clin Ther* 2006; **28**: 1353–1365.
8. Saeki H, Matsumoto M, Kaneko S, Tsuruta S, Cui YJ, Ohtake K *et al.* Is intrathecal magnesium sulfate safe and protective against ischemic spinal cord injury in rabbits? *Anesth Analg* 2004; **99**: 1805–1812.
9. Taccola G, Margaryan G, Mladinic M, Nistri A. Kainate and metabolic perturbation mimicking spinal injury differentially contribute to early damage of locomotor networks in the *in vitro* neonatal rat spinal cord. *Neuroscience* 2008; **155**: 538–555.

10. Margaryan G, Mladinic M, Mattioli C, Nistri A. Extracellular magnesium enhances the damage to locomotor networks produced by metabolic perturbation mimicking spinal injury in the neonatal rat spinal cord *in vitro*. *Neuroscience* 2009; **163**: 669–682.
11. Ryazanova LV, Rondon LJ, Zierler S, Hu Z, Galli J, Yamaguchi TP *et al.* TRPM7 is essential for Mg^{2+} homeostasis in mammals. *Nat Commun* 2010; **1**: 109.
12. Schmitz C, Perraud AL, Johnson CO, Inabe K, Smith MK, Penner R *et al.* Regulation of vertebrate cellular Mg^{2+} homeostasis by TRPM7. *Cell* 2003; **114**: 191–200.
13. Aarts MM, Tymianski M. TRPMs and neuronal cell death. *Pflugers Arch* 2005; **451**: 243–249.
14. Kühn FJ, Heiner I, Lückhoff A. TRPM2: a calcium influx pathway regulated by oxidative stress and the novel second messenger ADP-ribose. *Pflugers Arch* 2005; **451**: 212–219.
15. Sumoza-Toledo A, Penner R. TRPM2: a multifunctional ion channel for calcium signalling. *J Physiol* 2011; **589**: 1515–1525.
16. Kuzhandaivel A, Margaryan G, Nistri A, Mladinic M. Extensive glial apoptosis develops early after hypoxic-dysmetabolic insult to the neonatal rat spinal cord *in vitro*. *Neuroscience* 2010; **169**: 325–338.
17. Kuzhandaivel A, Nistri A, Mazzone GL, Mladinic M. Molecular mechanisms underlying cell death in spinal networks in relation to locomotor activity after acute injury *in vitro*. *Front Cell Neurosci* 2011; **5**: 9.
18. Plesca D, Mazumder S, Almasan A. DNA damage response and apoptosis. *Methods Enzymol* 2008; **446**: 107–122.
19. Cohen GM. Caspases: the executioners of apoptosis. *Biochem J* 1997; **326**: 1–16.
20. Cook PJ, Ju BG, Telese F, Wang X, Glass CK, Rosenfeld MG. Tyrosine dephosphorylation of H2AX modulates apoptosis and survival decisions. *Nature* 2009; **458**: 591–596.
21. Kuzhandaivel A, Nistri A, Mladinic M. Kainate-mediated excitotoxicity induces neuronal death in the rat spinal cord *in vitro* via a PARP-1 dependent cell death pathway (Parthanatos). *Cell Mol Neurobiol* 2010; **30**: 1001–1012.
22. Wang Y, Dawson VL, Dawson TM. Poly(ADP-ribose) signals to mitochondrial AIF: a key event in parthanatos. *Exp Neurol* 2009; **218**: 193–202.
23. Abdelkarim GE, Gertz K, Harms C, Katchanov J, Dirnagl U, Szabó C *et al.* Protective effects of PJ34, a novel, potent inhibitor of poly(ADP-ribose) polymerase (PARP) in *in vitro* and *in vivo* models of stroke. *Int J Mol Med* 2001; **7**: 255–260.
24. Vandenabeele P, Vanden Berghe T, Festjens N. Caspase inhibitors promote alternative cell death pathways. *Sci STKE* 2006; **2006:** pe44.
25. Cifra A, Mazzone GL, Nani F, Nistri A, Mladinic M. Postnatal developmental profile of neurons and glia in motor nuclei of the brainstem and spinal cord, and its comparison with organotypic slice cultures. *Dev Neurobiol* 2012; **72**: 1140–1160.
26. Mladinic M, Nistri A, Taccola G. Acute spinal cord injury *in vitro*: insight into basic mechanisms. In Aldskogius H (ed) *Animal Models in Spinal Cord Repair. Springer Science + Business Media, LLC.* Humana Press: Heidelberg/New York, 2013, pp 39–63.
27. Carriedo SG, Yin HZ, Lamberta R, Weiss JH. *In vitro* kainate injury to large SMI-32 + spinal neurons is Ca2 + dependent. *Neuroreport* 1995; **6**: 945–948.
28. Andrabi SA, Kim NS, Yu SW, Wang H, Koh DW, Sasaki M *et al.* Poly(ADP-ribose) (PAR) polymer is a death signal. *Proc Natl Acad Sci USA* 2006; **103**: 18308–18313.
29. Yu SW, Andrabi SA, Wang H, Kim NS, Poirier GG, Dawson TM *et al.* Apoptosis-inducing factor mediates poly(ADP-ribose) (PAR) polymer-induced cell death. *Proc Natl Acad Sci USA* 2006; **103**: 18314–18319.
30. Susin SA, Lorenzo HK, Zamzami N, Marzo I, Snow BE, Brothers GM *et al.* Molecular characterization of mitochondrial apoptosis-inducing factor. *Nature* 1999; **397**: 441–446.
31. Venkatachalam K, Montell C. TRP channels. *Annu Rev Biochem* 2007; **76**: 387–417.
32. McNulty S, Fonfria E. The role of TRPM channels in cell death. *Pflugers Arch* 2005; **451**: 235–242.
33. Miller BA. The role of TRP channels in oxidative stress-induced cell death. *J Membr Biol* 2006; **209**: 31–41.
34. Nicotera P, Bano D. The enemy at the gates. Ca2 + entry through TRPM7 channels and anoxic neuronal death. *Cell* 2003; **115**: 768–770.
35. Sun HS, Jackson MF, Martin LJ, Jansen K, Teves L, Cui H *et al.* Suppression of hippocampal TRPM7 protein prevents delayed neuronal death in brain ischemia. *Nat Neurosci* 2009; **12**: 1300–1307.
36. Nasrabady SE, Kuzhandaivel A, Mladinic M, Nistri A. Effects of 6(5H)-phenanthridinone, an inhibitor of poly(ADP-ribose)polymerase-1 activity (PARP-1), on locomotor networks of the rat isolated spinal cord. *Cell Mol Neurobiol* 2011; **31**: 503–508.
37. Penas C, Casas C, Robert I, Forés J, Navarro X. Cytoskeletal and activity-related changes in spinal motoneurons after root avulsion. *J Neurotrauma* 2009; **26**: 763–779.
38. Carrascal L, Nieto-Gonzalez JL, Cameron WE, Torres B, Nunez-Abades PA. Changes during the postnatal development in physiological and anatomical characteristics of rat motoneurons studied *in vitro*. *Brain Res Brain Res Rev* 2005; **49**: 377–387.
39. Zhu C, Qiu L, Wang X, Hallin U, Candé C, Kroemer G *et al.* Involvement of apoptosis-inducing factor in neuronal death after hypoxia-ischemia in the neonatal rat brain. *J Neurochem* 2003; **86**: 306–317.
40. Dent MA, Segura-Anaya E, Alva-Medina J, Aranda-Anzaldo A. NeuN/Fox-3 is an intrinsic component of the neuronal nuclear matrix. *FEBS Lett* 2010; **584**: 2767–2771.
41. Giordano G, Sánchez-Pérez AM, Montoliu C, Berezney R, Malyavantham K, Costa LG *et al.* Activation of NMDA receptors induces protein kinase A-mediated phosphorylation and degradation of matrin 3. Blocking these effects prevents NMDA-induced neuronal death. *J Neurochem* 2005; **94**: 808–818.
42. Chen HC, Su LT, González-Pagán O, Overton JD, Runnels LW. A key role for Mg^{2+} in TRPM7's control of ROS levels during cell stress. *Biochem J* 2012; **445**: 441–448.
43. Cook NL, Van Den Heuvel C, Vink R. Are the transient receptor potential melastatin (TRPM) channels important in magnesium homeostasis following traumatic brain injury? *Magnes Res* 2009; **22**: 225–234.
44. Scharenberg AM. TRPM2 and TRPM7: channel/enzyme fusions to generate novel intracellular sensors. *Pflugers Arch* 2005; **451**: 220–227.
45. Penner R, Fleig A. The Mg^{2+} and Mg^{2+}-nucleotide-regulated channel-kinase TRPM7. *Handb Exp Pharmacol* 2007; **179**: 313–328.
46. Xie YF, Macdonald JF, Jackson MF. TRPM2 calcium and neurodegenerative diseases. *Int J Physiol Pathophysiol Pharmacol* 2010; **2**: 95–103.
47. Belrose JC, Xie YF, Gierszewski LJ, MacDonald JF, Jackson MF. Loss of glutathione homeostasis associated with neuronal senescence facilitates TRPM2 channel activation in cultured hippocampal pyramidal neurons. *Mol Brain* 2012; **5**: 11.
48. Palacios-Prado N, Hoge G, Marandykina A, Rimkute L, Chapuis S, Paulauskas N *et al.* Intracellular magnesium-dependent modulation of gap junction channels formed by neuronal connexin36. *J Neurosci* 2013; **33**: 4741–4753.
49. Tresch MC, Kiehn O. Synchronization of motor neurons during locomotion in the neonatal rat: predictors and mechanisms. *J Neurosci* 2002; **22**: 9997–10008.
50. Lee IH, Lindqvist E, Kiehn O, Widenfalk J, Olson L. Glial and neuronal connexin expression patterns in the rat spinal cord during development and following injury. *J Comp Neurol* 2005; **489**: 1–10.
51. Faden AI, Stoica B. Neuroprotection: challenges and opportunities. *Arch Neurol* 2007; **64**: 794–800.
52. Savitz SI, Fisher M. Future of neuroprotection for acute stroke: in the aftermath of the SAINT trials. *Ann Neurol* 2007; **61**: 396–402.
53. Thuret S, Moon LD, Gage FH. Therapeutic interventions after spinal cord injury. *Nat Rev Neurosci* 2006; **7**: 628–643.
54. Burgoyne LA. The mechanisms of pyknosis: hypercondensation and death. *Exp Cell Res* 1999; **248**: 214–222.
55. Hara Y, Wakamori M, Ishii M, Maeno E, Nishida M, Yoshida T *et al.* LTRPC2 Ca^{2+} – permeable channel activated by changes in redox status confers susceptibility to cell death. *Mol Cell* 2002; **9**: 163–173.
56. Everaerts W, Vriens J, Owsianik G, Appendino G, Voets T, De Ridder D *et al.* Functional characterization of transient receptor potential channels in mouse urothelial cells. *Am J Physiol Renal Physiol* 2010; **298**: F692–F701.
57. Oh YK, Shin KS, Kang SJ. AIF translocates to the nucleus in the spinal motor neurons in a mouse model of ALS. *Neurosci Lett* 2006; **406**: 205–210.
58. Cox B, Emili A. Tissue subcellular fractionation and protein extraction for use in mass-spectrometry-based proteomics. *Nat Protoc* 2006; **1**: 1872–1878.
59. Beirowski B, Babetto E, Gilley J, Mazzola F, Conforti L, Janeckova L *et al.* Non-nuclear Wld(S) determines its neuroprotective efficacy for axons and synapses *in vivo*. *J Neurosci* 2009; **29**: 653–668.
60. Nasrabady SE, Kuzhandaivel A, Nistri A. Studies of locomotor network neuroprotection by the selective poly(ADP-ribose) polymerase-1 inhibitor PJ-34 against excitotoxic injury to the rat spinal cord *in vitro*. *Eur J Neurosci* 2011; **33**: 2216–2227.

Supplementary Information accompanies this paper on Cell Death and Disease website (http://www.nature.com/cddis)

Methods, materials and results

Section 2

Unusual increase in lumbar network excitability of the rat spinal cord evoked by the PARP-1 inhibitor PJ-34 through inhibition of glutamate uptake.

Nasrabady SE, Kuzhandaivel A, Akrami A, **Bianchetti E**, Milanese M, Bonanno G, Nistri A.

Neuropharmacology (2012).

Neuropharmacology 63 (2012) 415–426

Contents lists available at SciVerse ScienceDirect

Neuropharmacology

journal homepage: www.elsevier.com/locate/neuropharm

Unusual increase in lumbar network excitability of the rat spinal cord evoked by the PARP-1 inhibitor PJ-34 through inhibition of glutamate uptake

Sara Ebrahimi Nasrabady [a], Anujaianthi Kuzhandaivel [a,1], Athena Akrami [a], Elena Bianchetti [a], Marco Milanese [b], Giambattista Bonanno [b,c], Andrea Nistri [a,d,*]

[a] Neuroscience department, International School for Advanced Studies (SISSA), Trieste, Italy
[b] Unit of Pharmacology and Toxicology, Department of Experimental Medicine, University of Genoa, Genoa, Italy
[c] Center of Excellence for Biomedical Research (CEBR), Genoa, Italy
[d] SPINAL (Spinal Person Injury Neurorehabilitation Applied Laboratory), Istituto di Medicina Fisica e Riabilitazione, Udine, Italy

ARTICLE INFO

Article history:
Received 12 December 2011
Received in revised form
11 April 2012
Accepted 16 April 2012

Keywords:
Excitotoxicity
Motoneurons
Fictive locomotion

ABSTRACT

Overactivity of poly(ADP-ribose) polymerase enzyme 1 (PARP-1) is suggested to be a major contributor to neuronal damage following brain or spinal cord injury, and has led to study the PARP-1 inhibitor 2-(dimethylamino)-N-(5,6-dihydro-6-oxophenanthridin-2yl)acetamide (PJ-34) as a neuroprotective agent. Unexpectedly, electrophysiological recording from the neonatal rat spinal cord in vitro showed that, under control conditions, 1–60 μM PJ-34 per se strongly increased spontaneous network discharges occurring synchronously on ventral roots, persisting for 24 h even after PJ-34 washout. The PARP-1 inhibitor PHE had no similar effect. The action by PJ-34 was reversibly suppressed by glutamate ionotropic receptor blockers and remained after applying strychnine and bicuculline. Fictive locomotion evoked by neurochemicals or by dorsal root stimulation was present 24 h after PJ-34 application. In accordance with this observation, lumbar neurons and glia were undamaged. Neurochemical experiments showed that PJ-34 produced up to 33% inhibition of synaptosomal glutamate uptake with no effect on GABA uptake. In keeping with this result, the glutamate uptake blocker TBOA (5 μM) induced long-lasting synchronous discharges without suppressing the ability to produce fictive locomotion after 24 h. The novel inhibition of glutamate uptake by PJ-34 suggested that this effect may compound tests for its neuroprotective activity which cannot be merely attributed to PARP-1 block. Furthermore, the current data indicate that the neonatal rat spinal cord could withstand a strong, long-lasting rise in network excitability without compromising locomotor pattern generation or circuit structure in contrast with the damage to brain circuits known to be readily produced by persistent seizures.

1. Introduction

Hyperactivation of poly(ADP-ribose) polymerase enzyme 1 (PARP-1) is an important process contributing to brain damage arising from stroke (Andrabi et al., 2008) and acute spinal injury in vivo (Scott et al., 1999; Genovese et al., 2005; Wu et al., 2009). In vitro models of acute spinal cord injury have confirmed the role of this enzyme in the excitotoxic neuronal death (Kuzhandaivel et al., 2010a; Mazzone and Nistri, 2011), and have led to attempts of pharmacological neuroprotection with PARP-1 inhibitors.

Experimental studies have shown that the PARP-1 inhibitor 2-(dimethylamino)-N-(5,6-dihydro-6-oxophenanthridin-2yl)acetamide (PJ-34; Abdelkarim et al., 2001; Kauppinen et al., 2009) could provide a degree of neuroprotection against brain and spinal cord ischemia in which excitotoxicity is thought to play a major role (Virág and Szabó, 2002; Casey et al., 2005; Besson, 2009; Kauppinen et al., 2009; Moroni, 2008; Moroni and Chiarugi, 2009). Nonetheless,

Abbreviations: 5-HT, 5-hydroxytryptamine; ANOVA, analysis of variance; CCF, cross correlation factor; CNQX, 6-cyano-7-nitroquinoxaline-2,3-dione; CV, coefficient of period variation; DAPI, 4′,6-diamidino-2-phenylindole; D-APV, D-(−)-2-Amino-5-phosphonopentanoic acid; DR, dorsal root; EAAT2, excitatory amino acid transporter 2; FFT, fast Fourier transform; GABA, gamma-amino butyric acid; l, left; L, lumbar; mGluR, metabotropic glutamate receptor; *n*, number of preparations; NeuN, neuronal nuclei; NMDA, *N*-methyl–aspartate; PARP-1, poly(ADP-ribose) polymerase enzyme 1; PHE, 6-5(H)-phenathridinone; PJ-34, 2-(dimethylamino)-N-(5,6-dihydro-6-oxophenanthridin-2yl)acetamide; r, right; ROI, region of interest; s.e.m., the standard error of the mean; SD, standard deviation; SMI 32, monoclonal antibody to non-phosphorylated neurofilaments; S100, astrocyte marker monoclonal antibody; TBOA, DL-threo-b-benzyloxyaspartate; VR, ventral root.

* Corresponding author. SISSA, Via Bonomea 265, 34136 Trieste, Italy. Tel.: +39 040 3787718; fax: +39 040 3787702.
E-mail address: nistri@sissa.it (A. Nistri).
[1] Present address: Department of Clinical and Experimental Medicine, Linköping University, Sweden.

0028-3908/$ – see front matter © 2012 Elsevier Ltd. All rights reserved.
doi:10.1016/j.neuropharm.2012.04.014

delayed application of PJ-34 had limited ability to protect rat spinal neurons in vitro as it could efficiently counteract relatively small excitotoxic damage only (Mazzone and Nistri, 2011; Nasrabady et al., 2011a). In the course of those experiments, it became, however, apparent that PJ-34 per se could persistently facilitate spontaneous synaptic transmission in the spinal cord (Nasrabady et al., 2011a). This serendipitous observation led us to investigate the mechanisms underlying such an unexpected phenomenon. Thus, the present report provides new evidence that PJ-34 enhanced glutamatergic transmission and triggered long-lasting network bursting. Our results indicated that the rat spinal cord in vitro could withstand, for at least 24 h, 1/3rd reduction in glutamate transport processes without apparent structural or functional damage.

2. Methods and materials

2.1. Spinal cord preparations

To perform electrophysiological experiments thoracolumbar spinal cords were carefully dissected from neonatal Wistar rats (0–2 days old) in accordance with the guidelines of the National Institutes of Health and the Italian act D.Lgs. 27/1/92 no. 116 (implementing the European Union directives no. 86/609 and 93/88). Under urethane anesthesia (0.2 ml i.p. of a 10% w/v solution) spinal cords were dissected out and superfused (7.5 ml min^{-1}) in a recording chamber with Krebs solution (in mM): NaCl, 113; KCl, 4.5; $MgCl_2 7H_2O$, 1; $CaCl_2$, 2; NaH_2PO_4, 1; $NaHCO_3$, 25; glucose, 11; gassed with 95% O_2 5% CO_2; pH 7.4 at room temperature (for full details see Beato and Nistri, 1999; Taccola and Nistri, 2006a; Margaryan et al., 2009). All efforts were aimed at reducing the number of animals and minimizing their suffering.

2.2. Electrophysiological recordings

DC-coupled recordings were performed through lumbar (L) ventral roots (VRs) with tight-fitting miniature Ag/AgCl suction electrodes (Taccola and Nistri, 2006a). Signals were recorded from left (l) and right (r) L2 VRs (producing mainly flexor motor signals to the hind-limb muscles), and from L5 VRs (which convey mainly extensor motor commands to the same limb) (Kiehn and Kjaerulff, 1998; Kiehn, 2006; Taccola and Nistri, 2006b). Signals acquired at 20 kHz were processed with pClamp (version 9.2; Molecular Devices, Sunnyvale, CA, USA) and MATLAB software (version R2010b). Preparations were electrically stimulated with single or train (30 stimuli at 2 Hz) pulses (0.1 ms duration) applied to the ipsilateral homosegmental dorsal root (DR). To evoke cumulative depolarization with superimposed alternating oscillatory activity typical of fictive locomotion, the stimulation strength was $\geq 2\times$ threshold, whereby threshold was taken as the minimum intensity to elicit a detectable response in the homolateral VR (Taccola et al., 2004; Nasrabady et al., 2011b). On average, threshold was obtained with 1.61 ± 0.58 V stimulus intensity ($n = 6$). VR responses induced by weak stimuli close to threshold were considered to be indicative of monosynaptic reflexes (Fulton and Walton, 1986). The peak amplitude of the responses were calculated by averaging at least 5 events.

Fictive locomotion, defined as rhythmic discharges alternating between homosegmental and left-right lumbar VRs, was induced by co-application of *N*-methyl-D-aspartate (NMDA; 4 or 5 μM) and 5-hydroxytryptamine (5-HT; 10 μM) (Cazalets et al., 1992; Kiehn and Kjaerulff, 1998; Butt et al., 2002). The period value for rhythmic discharges was measured as the time between the onset of two cycles of oscillatory activity (calculated after averaging at least 20 cycles), and its regularity indicated by the coefficient of period variation (CV). Disinhibited bursting (Bracci et al., 1996a,b, 1997) was induced by continuously bath-applied strychnine (1 μM) and bicuculline (20 μM). Full details concerning the definition of bursts and their measurements were as reported before (Bracci et al., 1996a,b). In order to see the changes in network excitability caused by glutamate uptake block, the non-transportable inhibitor DL-threo-b-benzyloxyaspartate (TBOA; 5 μM; Shigeri et al., 2004) was applied for 1 h in a separate batch of experiments. TBOA has an IC_{50} value of circa 7 μM to selectively block the EAAT2 and 3 glial transporters, while at concentration of 100 μM produces a broad-spectrum inhibition of all glutamate uptake systems (Shigeri et al., 2004).

2.3. Study protocol

First, all preparations were tested for their ability to generate locomotor network activity and reflexes. While untreated sham spinal cords were kept for 24 h in Krebs solution (Taccola et al., 2008), parallel preparations were continuously treated with PJ-34 (1 μM or 60 μM) for up to 24 h when, following washout with Krebs solution, all electrophysiological tests were repeated. The higher concentration of PJ-34 was selected as the one producing full block of PARP-1 activity in the rat spinal cord (Nasrabady et al., 2011a). A batch of experiments was also performed by applying a different PARP-1 inhibitor, namely (6-5(H)-phenathridinone; PHE), which we have previously investigated for its potential neuroprotection in the rat spinal cord (Kuzhandaivel et al., 2010a).

2.4. Immunohistochemistry

Each preparation was histologically fixed at the end of the electrophysiological experiment as previously described in detail (Taccola et al., 2008). Thus, paraformaldehye-fixed spinal cords were cryoprotected with 30% sucrose and sectioned (30 μm). The sections were washed in phosphate buffer solution (PBS) and incubated in blocking solution (5% normal goat serum, 5% bovine serum albumin, 0.3% Triton-x 100) for 1 h at room temperature followed by primary antibody (NeuN, 1:50, Millipore, Milan, Italy; SMI 32, 1:200, Convance, Rome, Italy; or S100, 1:100 dilution, Dako, Milan, Italy) incubation at 4 °C overnight. After rinsing with PBS, the sections were incubated with goat antimouse or antirabbit IgG Alexa Fluor 488 or 594 secondary antibodies (1:500; Invitrogen, Milan, Italy) for 1 h at room temperature followed by 20 min of DAPI incubation to label the nuclei. The sections were mounted with Vectashield (Vector Laboratories, Milan, Italy) and analyzed using a Zeiss Axioskop2 microscope and Metavue software.

2.5. Quantification of dead cells

Quantification of dead cells was done as described previously (Margaryan et al., 2009; Kuzhandaivel et al., 2010b). Briefly, pyknotic nuclei (identified with DAPI staining) were counted in the regions of interest (ROIs) comprising ventral, central, dorsal grey matter or ventrolateral white matter. For neuronal or protoplasmic astrocyte counting we used NeuN or S100 immunopositivity, respectively, in ventral, central, or dorsal grey ROIs (Taccola et al., 2008; Margaryan et al., 2009) using "eCELLence" (Glance Vision Tech, Trieste, Italy) software. For each ROI, 3–7 fields of 280 × 280 μm (grey matter) or 100 × 280 μm (white matter) area were analyzed. For each experimental group, 4–11 spinal cords were analyzed and, for each spinal cord, 4–6 different sections from T12 to L3 segments were examined. For estimating motoneuron numbers, SMI32 labelling was performed (Taccola et al., 2008) and Rexed laminae VIII and IX were analyzed.

2.6. PAR ELISA assay

Endogenous PARP-1 activity was determined by measuring PAR levels with an ELISA method as described previously (Nasrabady et al., 2011a). Briefly, tissue lysates were prepared from the spinal cords treated with different concentrations of PJ-34, or from sham preparations. PAR levels were measured using the HT PARP in vivo Pharmacodynamic Assay II kit (http://www.trevigen.com/protocols/pdf/4520-096-K.pdf) following the manufacturer's protocol (Trevigen, Bologna, Italy). PAR levels were always quantified 4 h after application of PJ-34. The present assay is based on the ELISA immunoreactivity resulting in chemiluminescence signals recorded with Glo(R)max multi detection system (Promega, Milan, Italy). All samples were run in triplicate. The net PAR levels were quantified from the known standard concentrations (20–1000 pg/ml) of PAR. Data were expressed as pg/ml per 100 μg of protein.

2.7. Neurochemical measurements of amino acid uptake

Neonatal Wistar rats (0–2 days old) were sacrificed and the spinal cord rapidly removed after exposure of the spinal column. Purified synaptosomes were prepared essentially as previously described (Stigliani et al., 2006). Briefly, the tissue was homogenized in 10 volumes of Tris-buffered sucrose (0.32 M; pH 7.4) using a glass–teflon tissue grinder. The homogenate was centrifuged (5 min, 1000 *g*) to remove nuclei and debris and the supernatant was gently stratified on a discontinuous Percoll® (GE Healthcare) gradient (2, 6, 10 and 20% v/v in Tris-buffered sucrose) and centrifuged at 33,500 *g* for 5 min. The layer between 10 and 20% Percoll® (synaptosomal fraction) was collected and washed by centrifugation. All the procedures were performed at 0–4 °C.

Synaptosomes were resuspended in assay buffer (mM: NaCl, 140; KCl, 3; $MgSO_4$ 1.2; NaH_2PO_4, 1.2; $NaHCO_3$ 5; $CaCl_2$ 1.2; HEPES 10; glucose, 10; pH 7.4). Protein content was measured according to the Bradford method (Bradford, 1976) with bovine serum albumin as standard. Aliquots (0.5 ml) of the synaptosomal suspension were incubated for 5 min at 37 °C; uptake was then started by the addition of [^{3}H]D-aspartate or [^{3}H]GABA to a final concentration of 3 μM and stopped 2 min later by the addition of 5 ml of assay buffer. Samples were immediately filtered under vacuum through cellulose filters and washed twice with 5 ml of assay buffer. PJ-34 (0.1–100 μM), TBOA (0.1–100 μM) or N-(4,4-phenyl-3-butenyl)-nipecotic acid (SKF 89976A; 10 μM; Yunger et al., 1984) was introduced at the beginning of incubation period. Non-specific uptake was determined in presence of 300 μM unlabelled L-glutamate or GABA. Filter radioactivity was evaluated by liquid scintillation counting.

2.8. Data analysis

Statistical analysis was carried out with SigmaStat (SigmaStat 3.1, Systat Software, Chicago, IL, USA) and the data are shown as mean ± SD unless otherwise indicated. Parametric and non-parametric data were first distinguished with a normality test and analyzed with the Student's *t*-test or Mann–Whitney test, respectively, in accordance with the software choice. Uptake data were analyzed by one-way ANOVA followed by Dunnet's or Newman–Keuls test, as appropriate. For the electrophysiological experiments, comparison was made between the data

obtained on the first day (before and after application of the drug) and on second day of each experiment (comparing sham and the group treated with PJ-34). The significant level was always $P < 0.05$ and n indicates the number of preparations.

For analysis of complex spontaneous events elicited by PJ-34, we applied a bootstrap method (Thomson and Chave, 1991; Kass et al., 2003) whereby temporal windows (1 min size) were randomly chosen from the original records (20 kHz sampling; 5 min long) of pairs of VRs. In each pair, cross correlation values were calculated for two windows of simultaneously recorded traces using MATLAB software. We then repeated this procedure 500 times in order to build a distribution of mean cross correlation values for each condition. Thereafter, data from different conditions were compared using t-test (or its non-parametric equivalent). To analyze the frequency of events from different experimental setting, we used 1 min windows, applied the same boot-strapping method indicated above, and calculated the fast Fourier transform (FFT) values.

2.9. Drugs

[^{3}H]D-aspartate (specific activity = 89.5 Ci/mmol) and [^{3}H]GABA (specific activity = 11.3 Ci/mmol) were obtained from Perkin Elmer (Milan, Italy). NMDA and TBOA were purchased from Tocris (Bristol, UK), while PJ-34, PHE, 5-HT, SKF 89976A, and strychnine hydrochloride were from Sigma (Milan, Italy). Bicuculline methiodide was obtained from Fluka (Milan, Italy).

3. Results

3.1. Onset of spontaneous network activity following PJ-34 application

Fig. 1 shows examples of early changes in electrically-evoked and spontaneous network activity recorded from lumbar VRs after PJ-34 application (60 μM). The amplitude of short-latency synaptic responses induced by low threshold stimuli and usually regarded as indicative of monosynaptic transmission (Fulton and Walton, 1986; Evans, 1989; Kerkut and Bagust, 1995) was increased already after 40 min application (Fig. 1A): on average, this increment was nearly two fold (see Table 1). Furthermore, the average decay time also became significantly longer (from 183 ± 45 ms, $n = 5$, to 298 ± 83 ms, $n = 4$; $P = 0.03$). Fig. 1B shows that the peak of polysynaptic responses generated by stronger DR stimuli (>2× threshold) was, however, unchanged after PJ-34 application (see Table 1). Conversely, cumulative depolarization with superimposed oscillations induced by DR stimulus trains (Marchetti et al., 2001) was significantly lower 40 min from the start of PJ-34 application (Fig. 1C and Table 1), even if it was accompanied by a similar number of oscillations (Table 1). In addition to these changes in electrically-evoked synaptic responses, it was noteworthy that, in the presence of PJ-34, the baseline trace had become noisier with spontaneous events appearing at irregular interval (see Fig. 1B–D). These complex events appeared with a latency of approximately 15 min from the start of PJ-34 application.

Fig. 2A shows, on the same preparation, examples of the gradual intensification of spontaneous events after application of PJ-34. Although the mammalian spinal cord in vitro normally expresses random spontaneous discharges (Fulton and Walton, 1986; Kerkut and Bagust, 1995), the events observed after PJ-34 were clearly more numerous and larger as shown in the distribution histograms of Fig. 2B. Thus, 15 min later, large discharges emerged (Fig. 2A, middle) and became very intense 24 h later (Fig. 2A, right). Fig. 2C

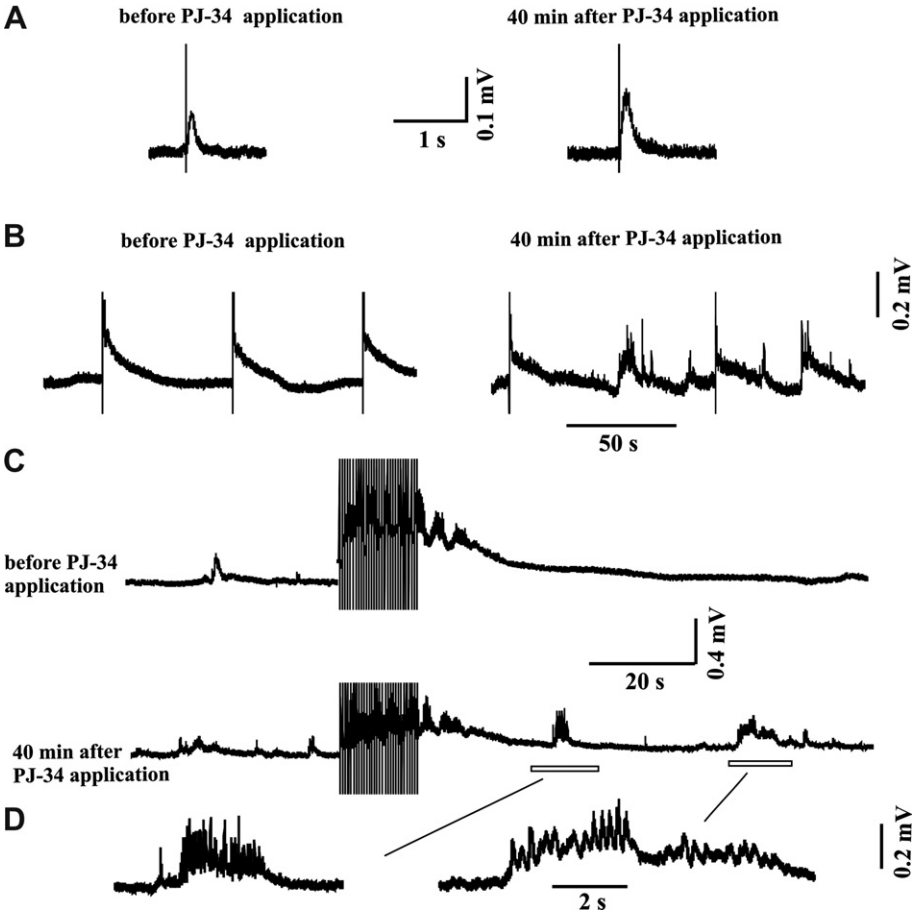

Fig. 1. Electrically-evoked responses recorded from in vitro spinal cord preparations early after PJ-34 (60 μM) application on the first experimental day. (A) Example of average monosynaptic response recorded from L5 homolateral VR in control (left) and after 40 min application of PJ-34. (B) Example of polysynaptic VR responses recorded from the same preparation as in (A). (C) Examples of cumulative depolarization with superimposed oscillatory cycles elicited by train of DR stimuli in control solution and 40 min after the application of PJ-34. (D) Example of spontaneous complex discharges appearing after application of PJ-34 (note faster timebase).

Table 1
Early effects of PJ-34 on VR responses to single (or trains of) DR stimuli.

	Monosynaptic reflex peak amplitude (mV)	Polysynaptic reflex peak amplitude (mV)	Cumulative depolarization amplitude (mV)	Number of oscillations induced by train of stimuli
Control[a]	0.129 ± 0.04 ($n = 5$)	2.59 ± 1.06 ($n = 6$)	0.873 ± 0.228 ($n = 6$)	5.5 ± 1 ($n = 6$)
40 min after application of PJ-34 60 μM	0.277 ± 0.09 ($n = 5$)	2.51 ± 0.87 ($n = 6$)	0.412 ± 0.168 ($n = 6$)	4.5 ± 0.5 ($n = 6$)
P-value	**0.013**	0.889	**0.003**	0.098

[a] Control responses refer to those recorded from the same preparations prior to PJ-34 application. Significant P-values are shown in bold.

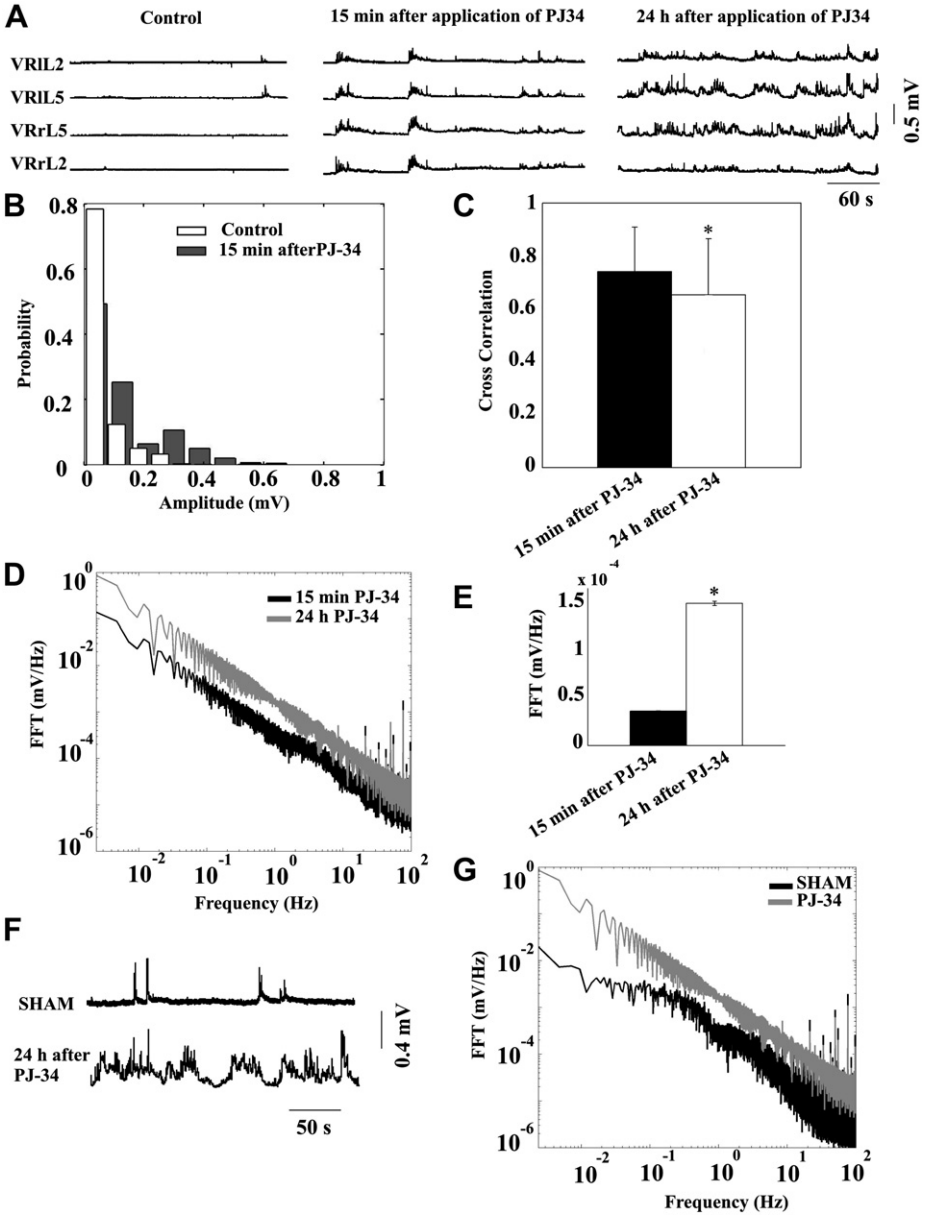

Fig. 2. Persistent effect of PJ-34 on spinal networks. (A) Example of sporadic spontaneous discharges recorded in control solution (before application of PJ-34 60 μM, left) and their gradual intensification after 15 min (middle) and 24 h (right) application of PJ-34. (B) Amplitude probability distribution of depolarizing events in a window of 5 min. Filled bars represent the distribution of the significantly higher average amplitude discharges after PJ-34 application for 15 min ($P < 0.0001$; Mann–Whitney) in comparison with control (open bars); $n = 4$. (C) Histograms demonstrate the significant difference of CCF values between groups treated with PJ-34 for 15 min or 24 h to show discharge synchronicity across segments and across preparations ($^*P < 0.001$; $n = 4$) (D) Plot indicates the mean FFT values of discharges from preparations treated for 15 min or 24 h with PJ-34; $n = 4$. (E) Histograms show increased average FFT values (mean ± s.e.m.) one day after treatment with PJ-34: the frequency power at 15 min PJ-34 application was significantly ($^*P < 0.0001$) smaller than at 24 h ($n = 4$). (F) Example of spontaneous VR discharges recorded on the second day in vitro from a sham (top) or PJ-34 treated (bottom) spinal cord. (G) Plots of mean FFT values show significant ($P < 0.002$) increase after 24 h application of PJ-34.

shows that, on average, events recorded early (filled column) from various VR pairs of different preparations, had a high cross correlation value, indicating their synchronicity across segments and across preparations. Even if 24 h later the cross correlation value was reduced (Fig. 2C, open column), it was still larger than 0.5, suggesting retention of good coupling of electrical discharges between VRs at homo and heterosegmental level.

Fig. 2D plots FFT data from 4 preparations to estimate the prevailing event frequency over a range of 0.1–100 Hz. Thus, for the same spinal cords, the whole frequency power spectrum at 15 min PJ-34 application was significantly ($P < 0.0001$) smaller than 24 h later, indicating the delayed, gradual emergence of slow events (mainly below 10 Hz). This result was accompanied by a significant increase in the average FFT value at 24 h (Fig. 2E) to support a global increment in spontaneous event occurrence.

We also compared, after 24 h in vitro, spontaneous events from sham preparations with those from PJ-34 treated preparations (see example in Fig. 2F). The FFT plot of Fig. 2G demonstrates a significantly ($P < 0.002$) stronger frequency power after PJ-34. In summary, these data suggest that PJ-34 evoked complex and long-lasting synchronous discharges from lumbar VRs, compatible with a substantial rise in network excitability. These delayed effects were, however, absent when spinal cords were treated (for 24 h) with another PARP-1 inhibitor (PHE; 60 μM) that did not induce any detectable change in spontaneous network discharges after 24 h ($n = 5$).

3.2. Relation between PARP-1 inhibition by PJ-34 and network activity

Fig. 3A shows the concentration (1–60 μM)-dependent changes in PARP-1 activity estimated on the amount of measured PAR. In accordance with our previous report (Nasrabady et al., 2011b), after 24 h in vitro, spinal cord samples had a basal PARP-1 activity corresponding to 55.9 ± 7 pg PAR/100 μg protein that fell to 47 ± 6.2 pg PAR/100 μg protein in the presence of 1 μM PJ-34. With 30 μM PJ-34, the PARP-1 activity decreased to 25 ± 8.4 pg PAR/100 μg protein, while with 60 μM PJ-34 it was 26 ± 5.3 pg PAR/100 μg protein, indicating that it had reached a plateau level of inhibition. These values were significantly smaller than those for sham preparations in all three groups ($P = 0.05$ for 1 μM PJ-34, $P = 0.001$ for 30 and 60 μM PJ-34). Fig. 3B shows that even the lowest tested concentration of PJ-34 (1 μM) significantly ($P < 0.001$) increased the FFT values of the spontaneous network discharges after 24 h in comparison with sham preparations, although this effect was less intense than the phenomenon detected after 60 μM PJ-34 (see Fig. 2). As exemplified in Fig. 3C, the onset of the electrophysiological discharges evoked by 1 μM PJ-34 was delayed and fully expressed 24 h later (Fig. 3C) in comparison with the large spontaneous events already detected after 15 min PJ-34 application (see Fig. 2A, middle).

3.3. Effect of PJ-34 on fictive locomotion and disinhibited bursting

We next enquired whether these changes in network excitability evoked by PJ-34 could impact on the ability to generate fictive locomotion. Fig. 4A compares locomotor-like cycles (evoked by co-applied NMDA and 5-HT) recorded, after 24 h, from a sham preparation with those from a PJ-34 treated spinal cord. In fact, fictive locomotion was apparently unperturbed by long-lasting PJ-34 application as indicated by similar cycle period or amplitude values (Fig. 4A, left, right). There was, however, a small, significant increment in the period CV value (Fig. 4A, middle), suggesting a slightly irregular pattern.

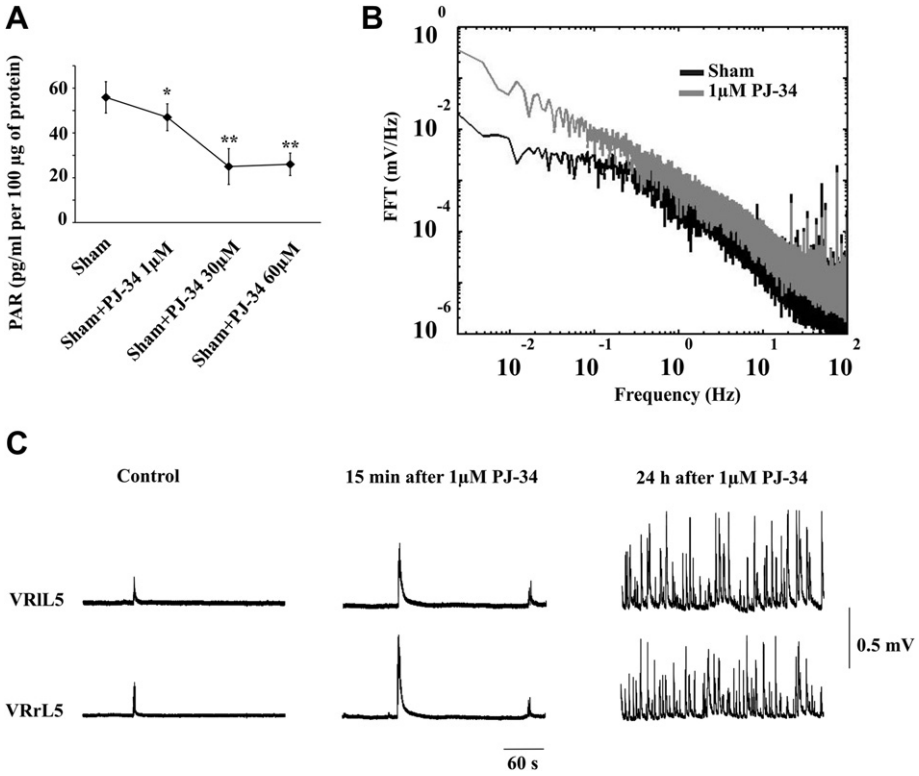

Fig. 3. Concentration-dependent effects of PJ-34 on PAR and network activity. (A) Plot quantifies PAR levels produced by PARP-1 activity of tissue lysates from sham or PJ-34 (1–60 μM) treated spinal cords. The values are significantly smaller than sham in all three groups (*$P = 0.05$ for 1 μM PJ-34, **$P = 0.001$ for 30 and 60 μM PJ-34) ($n = 3$ for each group). (B) FFT plot indicates the higher values of discharges 24 h after application of PJ-34 1 μM ($P < 0.001$, $n = 4$). (C) Example of sporadic spontaneous VR discharges recorded in control (before 1 μM PJ-34 application, left), early after PJ-34 (middle) and 24 h later (right); traces are all from the same preparation.

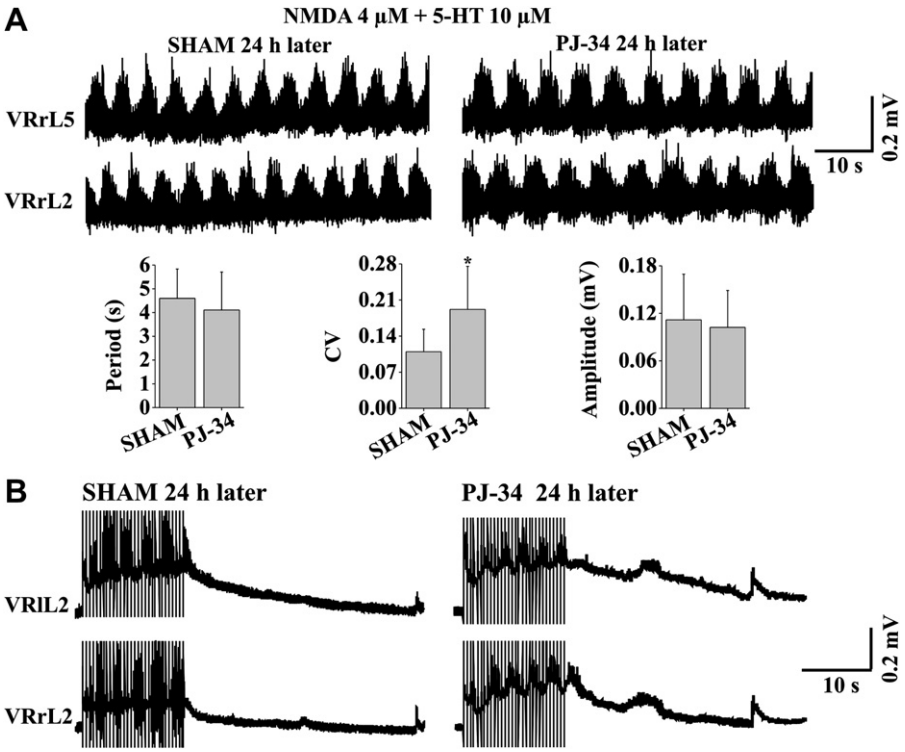

Fig. 4. Chemically or electrically induced fictive locomotion in sham preparations or after 24 h application of PJ-34 60 μM. (A) Examples of fictive locomotion (top traces) induced by NMDA (4 μM) plus 5-HT (10 μM) on sham (left) or PJ-34 treated spinal cord (right). The bottom histograms show similar characteristics of fictive locomotion (except for period CV value, $P = 0.01$, middle) of sham or PJ-34 treated spinal cords ($n = 9$). (B) Examples of alternating oscillatory cycles induced by trains of DR stimuli on sham or PJ-34 treated spinal cords. Number of oscillations and cumulative depolarization amplitude were similar in the two groups.

Fig. 4B shows, for the second day in vitro, examples of cumulative depolarization generated by sham or PJ-34 treated preparations with similar number of superimposed oscillations. Table 2 quantifies such data and also indicates that there was no change in mono and polysynaptic reflexes recorded after 24 h application of 1 or 60 μM PJ-34. Likewise, disinhibited bursting elicited by blocking synaptic inhibition with strychnine and bicuculline was unchanged by 24 h application of PJ-34 since the period was 42 ± 24 s (vs 45 ± 14 sham data; $n = 10$), and burst duration was 15 ± 9 s (vs. 15 ± 7 sham data). Hence, locomotor network activity tested with either neurochemicals or DR stimuli as well as basic circuit rhythmicity were not disrupted by long-lasting PJ-34 application.

3.4. Pharmacological block of PJ-34 evoked discharges

Since glutamate is the main excitatory transmitter of locomotor networks (Cazalets et al., 1992) acting on NMDA and non-NMDA receptors (Beato et al., 1997), we investigated whether block of ionotropic glutamate receptors by CNQX (10 μM) and D-APV (50 μM) could eliminate spontaneous as well as PJ-34 induced events. Fig. 5A (left) shows VR records from a preparation exhibiting strong ongoing discharges in Krebs solution (24 h after application of PJ-34 and washout). When CNQX and APV were applied for 15 min, spontaneous events disappeared (Fig. 4, middle), and returned after 10 min of washout of these antagonists, a result consistent with the dependence of spontaneous events on glutamatergic drive.

We also explored the potential contribution of GABA and glycine receptors to the PJ-34 elicited spontaneous events. This was difficult because the disinhibited bursting arising from block of synaptic inhibition is associated with strong depression of spontaneous excitatory events during the interburst interval (Bracci et al., 1996a), making it unfeasible to test glutamatergic events in isolation. Thus, we took advantage of a previous protocol whereby disinhibited bursts can be entrained on a 1:1 basis by low frequency DR stimulation (0.05 Hz; Bracci et al., 1997) as exemplified in Fig. 5B. Hence, after 24 h application of PJ-34 and washout, spontaneous disinhibited bursting was produced by strychnine and bicuculline, followed by a long (6.5 min) DR stimulus train that regularly entrained bursts. During the electrical stimulation, and unlike the interburst depression typical of control experiments (Bracci et al., 1997), spontaneous synchronous bursts emerged as exemplified, on a faster timebase, in Fig. 5 C. We next calculated whether appearance of such spontaneous events could influence the subsequent electrically-driven one: plotting the evoked burst amplitude (Fig. 5D, top) vs. the time interval from the preceding spontaneous burst showed a linear relation ($r = 0.716$), showing

Table 2
Characteristics of VR responses of sham or PJ-34 treated spinal cord to single (or trains of) DR stimuli on the second day in vitro.

	Monosynaptic reflex peak amplitude (mV)	Polysynaptic reflex peak amplitude (mV)	Cumulative depolarization amplitude (mV)	Number of oscillations induced by train of stimuli
Sham	0.25 ± 0.07 ($n = 7$)	0.73 ± 0.39 ($n = 7$)	0.54 ± 0.27 ($n = 6$)	5.17 ± 0.88 ($n = 6$)
After application of PJ-34 (60 μM)	0.31 ± 0.08 ($n = 6$)	0.82 ± 0.36 ($n = 7$)	0.35 ± 0.1 ($n = 6$)	5.97 ± 1.67 ($n = 7$)
P-value*	0.196	0.664	0.158	0.317
After application of PJ-34 (1 μM)	0.31 ± 0.15 ($n = 4$)	0.80 ± 0.27 ($n = 4$)	0.38 ± 0.05 ($n = 4$)	5.88 ± 1.95 ($n = 4$)
P-value†	0.367	0.770	0.352	0.762

* and † indicate the *P*-value of the comparison between Sham and 60 μM PJ-34 or 1 μM PJ-34 application respectively.

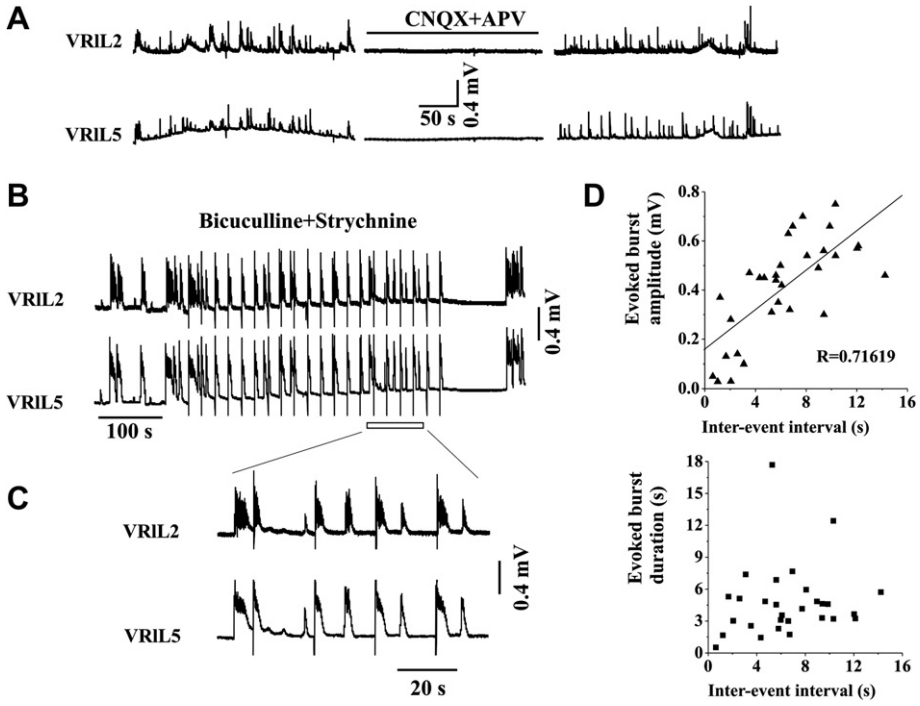

Fig. 5. Ionotropic receptor blockers influence discharges evoked by PJ-34. (A) Examples of spontaneous VR events recorded 24 h after application of PJ-34 and washout which are completely suppressed by co-application of CNQX (10 μM) and APV (50 μM) (middle). The spontaneous events return after 10 min washout with Krebs solution (right). (B) Disinhibited bursting is elicited by application of strychnine and bicuculline one day after PJ-34 application and wash. Although bursts are entrained (1:1) by a DR train of twenty stimuli (2× threshold, 0.05 Hz; see artefacts shown as downward deflections), spontaneous bursts emerge in the intervals between stimuli. (C) Faster timebase example of disinhibited bursting with electrically-driven and spontaneous events taken from (B). (D) A spontaneous burst affects the subsequent electrically-driven one. Top plot indicates that evoked burst amplitude is linearly related to the time interval between a spontaneous burst and the following electrically-evoked one ($P < 0.001$; $n = 5$). Nonetheless, no linear relation (bottom plot) between evoked burst duration and time interval from the previous spontaneous burst is apparent ($P = 0.39$).

that large bursts were preceded by a long quiescent period. Conversely, there was no apparent relation between evoked burst duration and time interval from previous spontaneous burst (Fig. 5D, bottom). Globally, these data were compatible with sustained increase in glutamatergic network activity as the main process responsible for continuous synchronous discharges, and that, when network discharges were fully engaged as bursts, there was a subsequent, transient downregulation of circuit excitability.

3.5. Histochemistry of PJ-34 treated spinal cords

In analogy with our previous studies (Taccola et al., 2008; Nasrabady et al., 2011a), we analyzed four ROIs of spinal cord sections from the same preparations used for our electrophysiological tests. First, we assessed whether pyknosis (condensed chromatin appearance) was more common 24 h after PJ-24 application: Fig. 6A, B indicates that pyknosis was a comparatively rare occurrence (<10%) in all ROIs from sham or treated preparations. Using immunostaining for S100, the main biomarker for grey matter astrocyte precursors in the neonatal rat spinal cord (Kuzhandaivel et al., 2010b; Cifra et al., in press), we also found no difference between sham and treated preparations (Fig. 6E, F). Fig. 6C, D shows no loss of NeuN-stained neurons across spinal cord sections after 24 h application of PJ-34, with good preservation of motoneuron numbers (Fig. 6G, H) evaluated with SMI 32 immunoreactivity (Taccola et al., 2008; Mazzone et al., 2010).

3.6. Effect of the glutamate uptake inhibitor TBOA

The strong increase in network excitability with spontaneous discharges evoked by PJ-34 without concomitant loss of neurons raised the possibility that this drug was partially inhibiting the uptake of glutamate without reaching toxic consequences for network structure and function. To examine this issue, we applied a low concentration of the selective uptake blocker TBOA at a dose close to its IC_{50} value (circa 7 μM) for inhibiting the glutamate glial transporters EAAT2 and 3 (Shigeri et al., 2004). Fig. 7A shows an example of the gradual increase in spontaneous event occurrence developing after the application of TBOA with strong electrical discharges emerging synchronously on L2 and L5 VRs (average CCF value after 40 min = 0.72 ± 0.17, and after 24 *h* = 0.71 ± 0.25; $n = 5$). By performing a FFT analysis of such events from 5 spinal cords and comparing them with the average data from PJ-34 treated preparations (24 h later), the power spectrum appeared overall similar (Fig. 7B) though a small significant ($P < 0.001$) difference was detected as the plot related to the TBOA treated preparations was shifted downwards.

We next investigated the long-term consequences of 24 h TBOA application (5 μM) on fictive locomotion. This pattern was present in 4 out of 5 preparations (see example in Fig. 7C) with characteristics similar to the activity observed in parallel sham preparations (period = 4.16 ± 0.59 s, CV = 0.09 ± 0.03, amplitude = 0.06 ± 0.02 mV after TBOA vs 4.59 ± 1.23 s, 0.10 ± 0.04, 0.11 ± 0.05 mV in sham conditions). The basic network rhythmicity expressed as disinhibited bursting was also present after 24 h application of TBOA. Although the bursts appeared at faster rate (bursts period = 28.6 ± 17.9 s vs 45.8 ± 14.0 s in sham, $P = 0.03$), the other characteristics of network bursting such as CV (0.61 ± 0.22 vs 0.44 ± 0.15 in sham), amplitude (0.75 ± 0.32 mV vs 0.79 ± 0.24 mV in sham), and burst duration (8.51 ± 5.08 s vs 15.78 ± 7.66 s in sham) remained similar. No deleterious action by TBOA (24 h application) on neurons, glia and motoneurons was found on histologically-processed spinal cords (Fig. 6B, D, F, H, open bars).

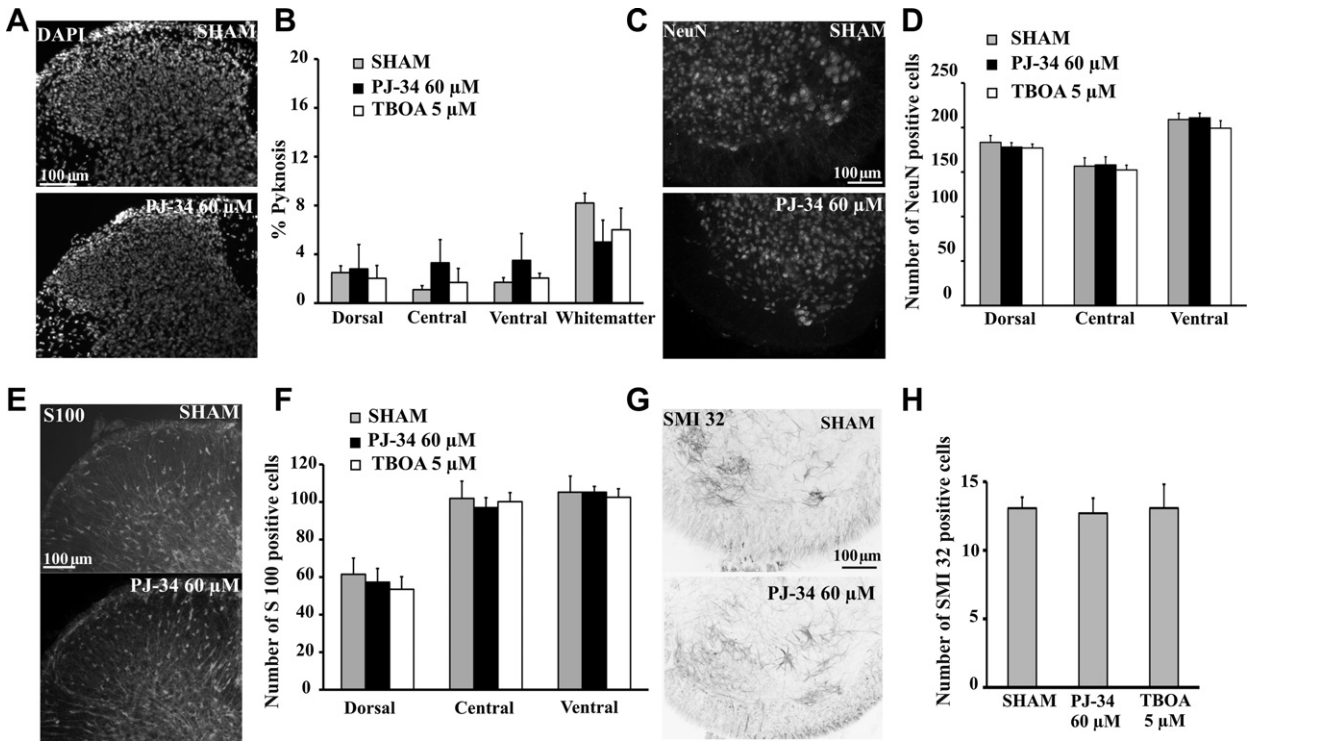

Fig. 6. PJ-34 or TBOA does not induce spinal cord histological damage one day later. (A) Representative images showing DAPI stained dorsal horn of sham or PJ-34 treated spinal cord 24 h later. (B) Histograms plot the low occurrence (<10%) of pyknosis detected in different ROIs of sham, PJ-34 or TBOA treated spinal cords. Pyknosis is normalized with respect to the total number of DAPI sensitive cells. (C) Representative images showing NeuN-stained ventral horn of sham or PJ-34 treated spinal cord. (D) Histogram plots the number of NeuN positive neurons in ROIs from sham, PJ-34 and TBOA treated spinal cords. (E) Representative images showing S100 stained dorsal horn of sham or PJ-34 treated spinal cord. (F) Histogram plots the number of S100 positive protoplasmic astrocytes in ROIs of sham, PJ-34 or TBOA treated spinal cords. (G) Representative images showing SMI 32 stained motoneurons in the ventral horn of sham or PJ-34 treated spinal cord. (H) Histogram plots the number of SMI 32 positive motoneurons in the ventral horn region of sham, PJ-34 or TBOA treated spinal cords. For all the experiments the number of spinal cords was 4, 9, 5 for sham, PJ-34 and TBOA, respectively.

3.7. Neurochemical measurement of glutamate uptake

The uptake of [^{3}H]D-aspartate or [^{3}H]GABA and its inhibition by PJ-34 were evaluated in synaptosomes purified from the spinal cord of 0–2 day old rats. The control uptake of [^{3}H]D-aspartate and of [^{3}H]GABA in synaptosomes exposed to 3 µM of the radioactive tracers amounted to 1355 ± 136 pmol/mg protein/2 min (n = 12) and 3225 ± 191 pmol/mg protein/2 min (n = 5), respectively. Fig. 8 shows the concentration-dependent decrease by PJ-34 (0.1–100 µM) of the uptake of [^{3}H]D-aspartate: the maximal effect amounted to 30% inhibition with IC_{50} value, estimated from the fitted curve, equal to 0.33 µM. [^{3}H]D-aspartate uptake was inhibited also by TBOA (0.1–100 µM) in a concentration-dependent manner (maximal inhibition about 90%: IC_{50} = 2.18 µM. Fig. 8). Synaptosomal [^{3}H]GABA uptake was unaffected by 100 µM PJ-34 (3225 ± 191 nmol/mg protein/2 min in control vs 3089 ± 175 nmol/mg protein/2 min in the presence of PJ-34; n = 5). Conversely, [^{3}H]GABA uptake was decreased from 3225 ± 191 pmol/mg protein/2 min to 225 ± 37 pmol/mg protein/2 min by 10 µM SKF 89976A, a canonical GABA uptake inhibitor (Milanese et al., 2010; n = 5; $P < 0.001$).

4. Discussion

The principal findings of the present report are that: 1. the PARP-1 inhibitor PJ-34 was a partial blocker of glutamate uptake, 2. this action was associated with a strong increase in network discharges persisting even after washout, and 3. it had no neurotoxic consequence, for at least 24 h, on neurons and glia in the neonatal rat spinal cord. These data demonstrate that prolonged electrical discharges per se did not damage complex network activities like the locomotor program.

4.1. PJ-34 as an inhibitor of glutamate uptake: functional consequences

Neurochemical data showed this agent to be a significant blocker of glutamate uptake with no action on GABA transport. It was interesting to detect this effect at micromolar concentrations of PJ-34, implying that this phenomenon might occur with pharmacological rather than toxic doses of this drug. The action of PJ-34 was translated into an early enhancement of glutamate-mediated monosynaptic reflexes, indicating that glutamate uptake was an important process to regulate excitatory transmission. This response was observed together with the smaller amplitude of cumulative depolarization probably due to steadily-depolarized neurons, still capable of generating a standard series of alternating oscillations. Polysynaptic reflexes were unchanged perhaps because of their heterogeneous presynaptic origin.

While the effect of PJ-34 on glutamate uptake and synaptic reflexes was relatively rapid, there was a gradual intensification of spontaneous network discharges: one day later, despite sustained washout of PJ-34, these strong discharges continued, suggesting that spinal circuits had become hyper-excitable.

4.2. Characteristics of spontaneous discharges induced by PJ-34

VR recordings were ill-suited to identify the electrophysiological nature of the PJ-34 evoked events which likely included the activity of several classes of premotoneuron impinging upon motoneurons. Experiments with pharmacological antagonists showed, however, that these discharges were fully dependent on ionotropic glutamate receptor activation, and that, when GABA and glycine receptors were blocked, spontaneous bursts could emerge in the interval between

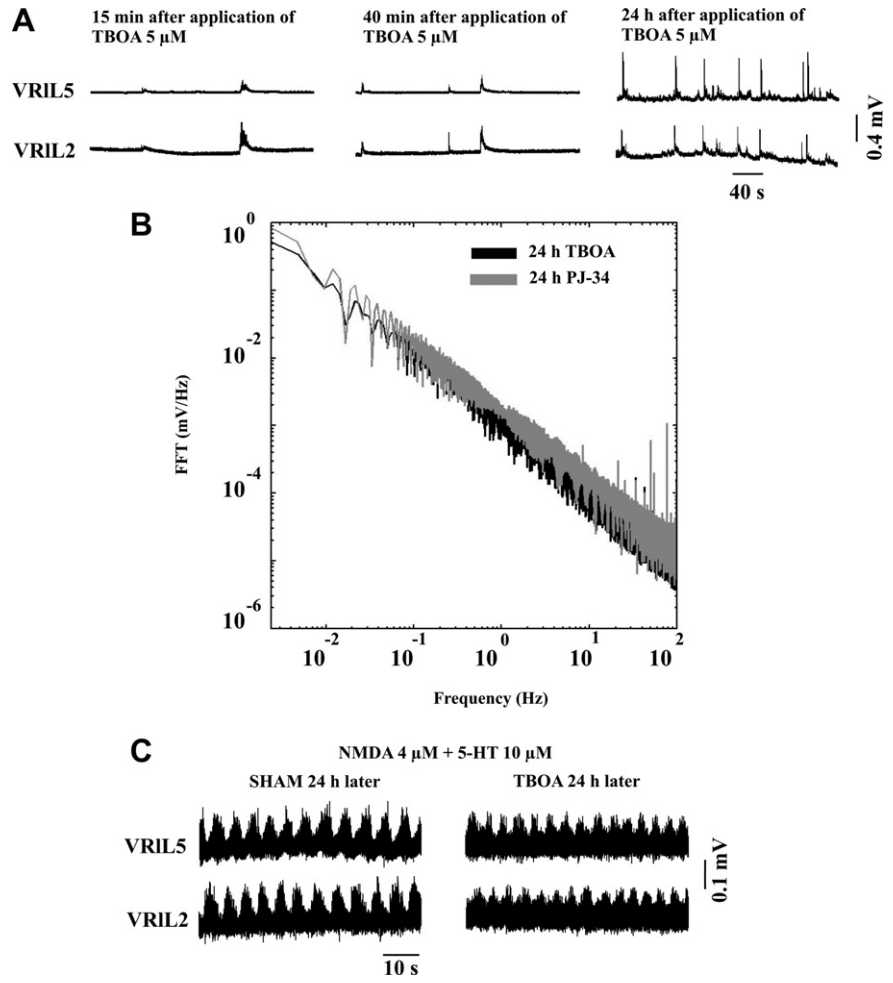

Fig. 7. Effect of TBOA (5 µM) on VR discharges of the spinal network. (A) Traces are examples of early (15 min and 40 min, left and middle, respectively) application of TBOA compared to long-lasting (24 h) application of this drug (right). (B) Comparison of FFT values between 24 h application of TBOA or PJ-34 shows that the TBOA plot is shifted downwards ($P < 0.001$; Mann–Whitney) with a power spectrum slightly different from PJ-34 ($n = 5$). (C) Examples of fictive locomotion induced by NMDA plus 5-HT on a sham and one preparation treated with TBOA for 24 h (and washout). The values of locomotor-like activity in the group treated with TBOA were similar to the sham.

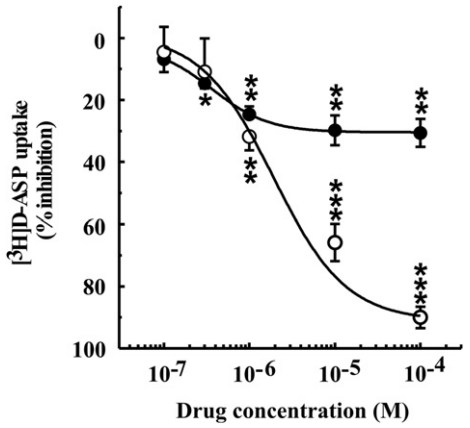

Fig. 8. Effect of PJ-34 (filled circles) or TBOA (open circles) on the uptake of [^{3}H] D-aspartate by synaptosomes from the spinal cord of 0–2 old rats. Data are expressed as percent inhibition of [^{3}H]D-aspartate uptake and represent the mean ± s.e.m of 6 independent experiments run in triplicate. $^*P < 0.05$, $^{**}P < 0.001$, $^{***}P < 0.0001$ vs. the respective controls (ANOVA plus Newman–Keuls test).

electrically-stimulated bursts. The presence of synchronous events across segments is compatible with the possibility of recurrent excitation recruiting a widespread neuronal assembly into collective discharge mode (Streit et al., 2001). In fact, our analysis indicated that these discharges were in general rather slow in accordance with the view that they originated from an ample neuronal population. As previously shown for the rat spinal dorsal horn (Nie and Weng, 2009), impaired glutamate uptake probably induced spill-over of extracellular glutamate outside the active synapses to extensively raise neuronal excitability. The present data cannot distinguish the relative contribution by uptake block and/or facilitated release of this excitatory transmitter to the strong enhancement in spontaneous discharges. In view of the difficulty to probe, in the spinal cord, endogenous glutamate release originating from multiple spinal sites, future experiments based on analysis of synaptic events with patch clamp recording might help to clarify this issue.

The PJ-34 evoked state of spinal cord hyperexcitability did not exert a deleterious action on locomotor-like patterns, nor was it translated into spontaneous bouts of fictive locomotion. Likewise, former studies with the glutamate uptake blocker dihydrokainate have shown that it could only facilitate fictive locomotion induced by bath-applied glutamate to the lamprey spinal cord in vitro (Brodin and Grillner, 1985) or by mesencephalic stimulation of the cat in vivo (Douglas et al., 1993), but rarely could it produce this pattern directly.

4.3. Relative contribution by glutamate uptake inhibition or PARP-1 depression to spontaneous network discharges

A relatively low concentration of PJ-34 (1 μM) produced a partial inhibition of PARP-1 activity amounting to circa 13% reduction in the production of PAR, the compound that (in high concentrations) underlies excitotoxic death (Kuzhandaivel et al., 2011). This rather modest decrease in PARP-1 function was probably unable to explain the strong rise in network excitability: indeed, application of PHE, a different PARP-1 inhibitor (Nasrabady et al., 2011b), did not generate an analogous rise in network discharges. The lowest PJ-34 concentration (1 μM) could, however, induce a significant depression of glutamate uptake (about 25%) which was not very different from the depression (30%) detected with the highest PJ-34 concentrations, and could also evoke delayed onset of strong network discharges. These data, therefore, suggest that partial inhibition of PARP-1 activity was not per se a crucial factor to increase network excitability, an effect more likely attributable to the partial depression of glutamate uptake. Hence, it seems probable that the induction of persistent network discharges was an unexpected property of PJ-34 because of its additional action on the glutamate transport system.

It is difficult to relate the present in vitro findings to the in vivo administration of PJ-34 since, to the best of our knowledge, the actual plasma concentration of this drug and its final redistribution to the brain tissue remain unclear. Since the dose of PJ-34 injected into experimental animal is 3-30 mg/kg (Abdelkarim et al., 2001; Virág and Szabó, 2002; Kauppinen et al., 2009; Crawford et al., 2010), assuming uniform drug distribution throughout body compartments of an adult rat (and ignoring any bound fraction that might lower the free drug concentration), one might estimate a plasma concentration of approximately 37 μM after 10 mg/kg, that is in the range of the concentrations tested in vitro in the present report. Even if the actual concentration of free PJ-34 at neuronal membrane level is likely to be lower, it seems feasible that it would still be compatible with those tested in the present study.

4.4. Downregulation of glutamate transport translated into network plasticity

Following perturbation of neurotransmitter systems, activity-dependent synaptic plasticity regulates brain network excitability (Marder, 1998; Abbott and Nelson, 2000; Neves et al., 2008). This process is known to develop in the spinal cord as well (Parker and Grillner, 2000). We propose that application of PJ-34 biased spinal network activity towards excitation over inhibition as shown by increased random discharges dependent on glutamatergic transmission. It is likely, however, that a degree of homeostatic plasticity had occurred whereby the enhanced level of extracellular glutamate must have led to a compensatory downregulation of glutamatergic transmission as demonstrated by the unchanged size of monosynaptic reflexes (and cumulative depolarization) one day later. Hence, in spinal networks, homeostatic plasticity (Galante et al., 2001; Rosato-Siri et al., 2002) and efficient synaptic inhibition (which enabled locomotor network function; Kiehn, 2006) possibly contributed to prevent any runaway excitation caused by the partial block of glutamate transport. When GABA and glycine receptors were blocked by bicuculline and strychnine, disinhibited bursting following PJ-34 exposure was similar to control. Nonetheless, spontaneous bursts emerged in the interval between electrically-driven bursts and exerted a rapid downregulation of subsequent bursts indicating state-dependent, short term plasticity (Bracci et al., 1997).

4.5. Persistent electrical discharges had no structural consequences on spinal networks

Although excitotoxic damage elicited by impaired glutamate uptake is thought to be a major process to lesion neurons (Kim et al., 2011), and, in particular, motoneurons (Foran and Trotti, 2009), the present study shows that persistently raised network discharges had not caused early loss of neurons or glia in the spinal cord. To account for the structural and functional resilience of spinal networks, it is proposed that build-up of extracellular glutamate might have also activated compensatory processes that have prevented neurotoxicity. In particular, it is likely that wider-scale activation of metabotropic glutamate receptors might have counteracted network hyperexcitability as proposed for brain circuits (Huang et al., 2004; Hartmann et al., 2008; Potier et al., 2010). All main subtypes of metabotropic glutamate receptor are largely expressed by the rat spinal cord (reviewed by Nistri et al., 2006) to regulate synaptic transmission and reflexes (Marchetti et al., 2003). Indeed, a recent study of the rat dorsal horn has shown that inhibition of glutamate transporters enhances group I mGluR-dependent oscillatory activity (Galik et al., 2008). Furthermore, in the rat hippocampus, raised glutamatergic signalling is reported to induce release of endocannabinoids from postsynaptic cells to depress, in a retrograde fashion, further neurotransmitter release (Hofmann et al., 2008; Nahir et al., 2010). Future studies are necessary to explore if a similar process occurs also in the spinal cord as it would represent a powerful system to dampen network excitability. Thus, the most parsimonious explanation is that, as far as locomotor networks were concerned, moderate block of glutamate transport did not trigger neurodegeneration because compensatory mechanisms were likely to contrast the potential risk of excitotoxicity. In support of our suggestion is the report that prolonged elevation of extracellular glutamate due to its transport blockade in vivo is innocuous for spinal motoneurons, while direct activation of glutamate receptors is highly neurotoxic (Tovar-Y-Romo et al., 2009).

4.6. Implications for neurodegeneration in the spinal cord

Previous models of spinal excitotoxicity and allied neurodegeneration had relied on the application of various concentrations of kainate (Mazzone et al., 2010), a glutamate analogue widely employed also for evoking experimental brain lesions with behavioural effects like generalized convulsions (Vincent and Mulle, 2009). Indeed, it is thought that repeated seizures are the cause for chronic epilepsy (Ben-Ari, 2001) since about 1 h of electrically-induced seizures is sufficient to obtain substantial neurodegeneration in the rat hippocampus (Norwood et al., 2011). The present results suggest that, in the rat spinal cord in vitro, intense synchronous discharges were not per se able to produce cell or functional damage. This observation differs from the neurotoxicity data following application of kainate that depolarizes neurons directly by binding to its receptors and it also triggers release of endogenous glutamate from depolarized neurons (Mazzone and Nistri, 2011) to perpetrate a vicious circuit of excitation-neurotoxicity.

In conclusion, strongly and persistently enhanced glutamatergic activity at spinal network level did not trigger neurodegeneration and allowed preservation of locomotor-like function. Thus, these results are consistent with the notion that delayed administration of PJ-34 could protect spinal neurons from excitotoxicity as long as the insult was relatively small (Mazzone and Nistri, 2011; Nasrabady et al., 2011a). It seems probable that, for spinal networks, summating the excitation evoked by PJ-34 to a strong excitotoxic stimulus becomes a tall order to cope with.

Acknowledgements

This study was supported by grants from the government of the Friuli Venezia Giulia Region. The authors state that they have no conflict of interest to declare. AN designed research, SEN, AK, AA, EB and MM made substantial contributions to data acquisition, analysis, and interpretation. SEN, GB and AN drafted the article and revised it critically for intellectual content.

References

Abbott, L.F., Nelson, S.B., 2000. Synaptic plasticity: taming the beast. Nat. Neurosci. 3, 1178–1183.
Abdelkarim, G.E., Gertz, K., Harms, C., Katchanov, J., Dirnagl, U., Szabo, C., Endres, M., 2001. Protective effects of PJ-34, a novel, potent inhibitor of poly(ADP-ribose) polymerase (PARP) in in vitro and in vivo models of stroke. Int. J. Mol. Med. 7, 255–260.
Andrabi, S.A., Dawson, T.M., Dawson, V.L., 2008. Mitochondrial and nuclear cross talk in cell death: parthanatos. Ann. N. Y. Acad. Sci. 1147, 233–241.
Beato, M., Nistri, A., 1999. Interaction between disinhibited bursting and fictive locomotor patterns in the rat isolated spinal cord. J. Neurophysiol. 82, 2029–2038.
Beato, M., Bracci, E., Nistri, A., 1997. Contribution of NMDA and non-NMDA glutamate receptors to locomotor pattern generation in the neonatal rat spinal cord. Proc. Roy. Soc. B 264, 877–884.
Ben-Ari, Y., 2001. Cell death and synaptic reorganizations produced by seizures. Epilepsia 42 (Suppl. 3), 5–7.
Besson, V.C., 2009. Drug targets for traumatic brain injury from poly(ADP-ribose) polymerase pathway modulation. Br. J. Pharmacol. 157, 695–704.
Bracci, E., Ballerini, L., Nistri, A., 1996a. Spontaneous rhythmic bursts induced by pharmacological block of inhibition in lumbar motoneurons of the neonatal rat spinal cord. J. Neurophysiol. 75, 640–647.
Bracci, E., Ballerini, L., Nistri, A., 1996b. Localization of rhythmogenic networks responsible for spontaneous bursts induced by strychnine and bicuculline in the rat isolated spinal cord. J. Neurosci. 16, 7063–7076.
Bracci, E., Beato, M., Nistri, A., 1997. Afferent inputs modulate the activity of a rhythmic burst generator in the rat disinhibited spinal cord in vitro. J. Neurophysiol. 77, 3157–3167.
Bradford, M.M., 1976. A rapid and sensitive method for the quantitation of microgram quantities of protein utilizing the principle of protein dye binding. Anal. Biochem. 72, 248–254.
Brodin, L., Grillner, S., 1985. The role of putative excitatory amino acid neurotransmitters in the initiation of locomotion in the lamprey spinal cord. II. The effects of amino acid uptake inhibitors. Brain Res. 360, 149–158.
Butt, S.J., Lebret, J.M., Kiehn, O., 2002. Organization of left–right coordination in the mammalian locomotor network. Brain Res. Rev. 40, 107–117.
Casey, P.J., Black, J.H., Szabo, C., Frosch, M., Albadawi, H., Chen, M., Cambria, R.P., Watkins, M.T., 2005. Poly(adenosine diphosphate ribose) polymerase inhibition modulates spinal cord dysfunction after thoracoabdominal aortic ischemia-reperfusion. J. Vasc. Surg. 41, 99–107.
Cazalets, J.R., Sqalli-Houssaini, Y., Clarac, F., 1992. Activation of the central pattern generators for locomotion by serotonin and excitatory amino acids in neonatal rat. J. Physiol. 455, 187–204.
Cifra, A., Mazzone, G.L., Nani, F., Nistri, A., Mladinic, M., Postnatal developmental profile of neurons and glia in motor nuclei of the brainstem and spinal cord, and its comparison with organotypic slice cultures. Devel. Neurobiol., in press.
Crawford, R.S., Albadawi, H., Atkins, M.D., Jones, J.E., Yoo, H.J., Conrad, M.F., Austen Jr., W.G., Watkins, M.T., 2010. Postischemic poly (ADP-ribose) polymerase (PARP) inhibition reduces ischemia reperfusion injury in a hind-limb ischemia model. Surgery 148, 110–118.
Douglas, J.R., Noga, B.R., Dai, X., Jordan, L.M., 1993. The effects of intrathecal administration of excitatory amino acid agonists and antagonists on the initiation of locomotion in the adult cat. J. Neurosci. 13, 990–1000.
Evans, R.H., 1989. The pharmacology of segmental transmission in the spinal cord. Prog. Neurobiol. 33, 255–279.
Foran, E., Trotti, D., 2009. Glutamate transporters and the excitotoxic path to motor neuron degeneration in amyotrophic lateral sclerosis. Antioxid. Redox Signal. 11, 1587–1602.
Fulton, B.P., Walton, K., 1986. Electrophysiological properties of neonatal rat motoneurones studied in vitro. J. Physiol. 370, 651–678.
Galante, M., Avossa, D., Rosato-Siri, M., Ballerini, L., 2001. Homeostatic plasticità induced by chronic block of AMPA/kainate receptors modulates the generation of rhythmic bursting in rat spinal cord organotypic cultures. Eur. J. Neurosci. 14, 903–917.
Galik, J., Youn, D.H., Kolaj, M., Randić, M., 2008. Involvement of group I metabotropic glutamate receptors and glutamate transporters in the slow excitatory synaptic transmission in the spinal cord dorsal horn. Neuroscience 154, 1372–1387.
Genovese, T., Mazzon, E., Muia, C., Patel, N.S., Threadgill, M.D., Bramanti, P., De Sarro, A., Thiemermann, C., Cuzzocrea, S., 2005. Inhibitors of poly(ADP-ribose) polymerase modulate signal transduction pathways and secondary damage in experimental spinal cord trauma. J. Pharmacol. Exp. Ther. 312, 449–457.
Hartmann, K., Bruehl, C., Golovko, T., Draguhn, A., 2008. Fast homeostatic plasticity of inhibition via activity-dependent vesicular filling. PLoS One 3, e2979.
Hofmann, M.E., Nahir, B., Frazier, C.J., 2008. Excitatory afferents to CA3 pyramidal cells display differential sensitivity to CB1 dependent inhibition of synaptic transmission. Neuropharmacology 55, 1140–1146.
Huang, Y.H., Sinha, S.R., Tanaka, K., Rothstein, J.D., Bergles, D.E., 2004. Astrocyte glutamate transporters regulate metabotropic glutamate receptor-mediated excitation of hippocampal interneurons. J. Neurosci. 24, 4551–4559.
Kass, R.E., Ventura, V., Cai, C., 2003. Statistical smoothing of neuronal data. Netw. Comput. Neural Syst. 14, 5–15.
Kauppinen, T.M., Suh, S.W., Berman, A.E., Hamby, A.M., Swanson, R.A., 2009. Inhibition of poly(ADP-ribose) polymerase suppresses inflammation and promotes recovery after ischemic injury. J. Cereb. Blood Flow. Metab. 29, 820–829.
Kerkut, G.A., Bagust, J., 1995. The isolated mammalian spinal cord. Prog. Neurobiol. 46, 1–48.
Kiehn, O., Kjaerulff, O., 1998. Distribution of central pattern generators for rhythmic motor outputs in the spinal cord of limbed vertebrates. Ann. N. Y. Acad. Sci. 860, 110–129.
Kiehn, O., 2006. Locomotor circuits in the mammalian spinal cord. Annu. Rev. Neurosci. 29, 279–306.
Kim, K., Lee, S.G., Kegelman, T.P., Su, Z.Z., Das, S.K., Dash, R., Dasgupta, S., Barral, P.M., Hedvat, M., Diaz, P., Reed, J.C., Stebbins, J.L., Pellecchia, M., Sarkar, D., Fisher, P.B., 2011. Role of excitatory amino acid transporter-2 (EAAT2) and glutamate in neurodegeneration: opportunities for developing novel therapeutics. J. Cell. Physiol. 226, 2484–2493.
Kuzhandaivel, A., Nistri, A., Mladinic, M., 2010a. Kainate-mediated excitotoxicity induces neuronal death in the rat spinal cord in vitro via a PARP-1 dependent cell death pathway (Parthanatos). Cell. Mol. Neurobiol. 30, 1001–1012.
Kuzhandaivel, A., Margaryan, G., Nistri, A., Mladinic, M., 2010b. Extensive glial apoptosis develops early after hypoxic-dysmetabolic insult to the neonatal rat spinal cord in vitro. Neuroscience 169, 325–338.
Kuzhandaivel, A., Nistri, A., Mazzone, G., Mladinic, M., 2011. Molecular mechanisms underlying cell death in spinal networks in relation to locomotor activity after acute injury in vitro. Front. Cell. Neurosci. 5, 9.
Marchetti, C., Beato, M., Nistri, A., 2001. Alternating rhythmic activity induced by dorsal root stimulation in the neonatal rat spinal cord in vitro. J. Physiol. 530, 105–112.
Marchetti, C., Taccola, G., Nistri, A., 2003. Distinct subtypes of group I metabotropic glutamate receptors on rat spinal neurons mediate complex facilitatory and inhibitory effects. Eur. J. Neurosci. 18, 1873–1883.
Marder, E., 1998. From biophysics to models of network function. Annu. Rev. Neurosci. 21, 25–45.
Margaryan, G., Mladinic, M., Mattioli, C., Nistri, A., 2009. Extracellular magnesium enhances the damage to locomotor networks produced by metabolic perturbation mimicking spinal injury in the neonatal rat spinal cord in vitro. Neuroscience 163, 669–682.
Mazzone, G.L., Nistri, A., 2011. Effect of the PARP-1 inhibitor PJ-34 on excitotoxic damage evoked by kainate on rat spinal cord organotypic slices. Cell. Mol. Neurobiol. 31, 469–478.
Mazzone, G.L., Margaryan, G., Kuzhandaivel, A., Nasrabady, S.E., Mladinic, M., Nistri, A., 2010. Kainate-induced delayed onset of excitotoxicity with functional loss unrelated to the extent of neuronal damage in the in vitro spinal cord. Neuroscience 168, 451–462.
Milanese, M., Zappettini, S., Jacchetti, E., Bonifacino, T., Cervetto, C., Usai, C., Bonanno, G., 2010. In vitro activation of GAT1 transporters expressed in spinal cord gliosomes stimulates glutamate release that is abnormally elevated in the SOD1/G93A(+) mouse model of amyotrophic lateral sclerosis. J. Neurochem. 113, 489–501.
Moroni, F., Chiarugi, A., 2009. Post-ischemic brain damage: targeting PARP-1 within the ischemic neurovascular units as a realistic avenue to stroke treatment. FEBS J. 276, 36–45.
Moroni, F., 2008. Poly(ADP-ribose)polymerase 1 (PARP-1) and postischemic brain damage. Curr. Opin. Pharmacol. 8, 96–103.
Nahir, B., Lindsly, C., Frazier, C.J., 2010. mGluR-mediated and endocannabinoid-dependent long-term depression in the hilar region of the rat dentate gyrus. Neuropharmacology 58, 712–721.
Nasrabady, S.E., Kuzhandaivel, A., Nistri, A., 2011a. Studies of locomotor network neuroprotection by the selective poly(ADP-ribose) polymerase-1 inhibitor PJ-34 against excitotoxic injury to the rat spinal cord in vitro. Eur. J. Neurosci. 33, 2216–2227.
Nasrabady, S.E., Kuzhandaivel, A., Mladinic, M., Nistri, A., 2011b. Effects of 6(5H)-phenanthridinone, an inhibitor of poly(ADP-ribose)polymerase-1 activity (PARP-1), on locomotor networks of the rat isolated spinal cord. Cell. Mol. Neurobiol. 31, 503–508.
Neves, G., Cooke, S.F., Bliss, T.V., 2008. Synaptic plasticity, memory and the hippocampus: a neural network approach to causality. Nat. Rev. Neurosci. 9, 65–75.
Nie, H., Weng, H.R., 2009. Glutamate transporters prevent excessive activation of NMDA receptors and extrasynaptic glutamate spillover in the spinal dorsal horn. J. Neurophysiol. 101, 2041–2051.
Nistri, A., Ostroumov, K., Sharifullina, E., Taccola, G., 2006. Tuning and playing a motor rhythm: how metabotropic glutamate receptors orchestrate generation of motor patterns in the mammalian central nervous system. J. Physiol. 15, 323–334.
Norwood, B.A., Bauer, S., Wegner, S., Hamer, H.M., Oertel, W.H., Sloviter, R.S., Rosenow, F., 2011. Electrical stimulation-induced seizures in rats: a "dose–response" study on resultant neurodegeneration. Epilepsia 52, e109–112.

Parker, D., Grillner, S., 2000. Neuronal mechanisms of synaptic and network plasticity in the lamprey spinal cord. Prog. Brain Res. 125, 381–398.
Potier, B., Billard, J.M., Rivière, S., Sinet, P.M., Denis, I., Champeil-Potokar, G., Grintal, B., Jouvenceau, A., Kollen, M., Dutar, P., 2010. Reduction in glutamate uptake is associated with extrasynaptic NMDA and metabotropic glutamate receptor activation at the hippocampal CA1 synapse of aged rats. Aging Cell. 9, 722–735.
Rosato-Siri, M., Grandolfo, M., Ballerini, L., 2002. Activity-dependent modulation of GABAergic synapses in developing rat spinal networks in vitro. Eur. J. Neurosci. 16, 2123–2135.
Scott, G.S., Jakeman, L.B., Stokes, B.T., Szabó, C., 1999. Peroxynitrite production and activation of poly (adenosine diphosphate-ribose) synthetase in spinal cord injury. Ann. Neurol. 45, 120–124.
Shigeri, Y., Seal, R.P., Shimamoto, K., 2004. Molecular pharmacology of glutamate transporters, EAATs and VGLUTs. Brain Res. Rev. 45, 250–265.
Stigliani, S., Zappettini, S., Raiteri, L., Passalacqua, M., Melloni, E., Venturi, C., Tacchetti, C., Diaspro, A., Usai, C., Bonanno, G., 2006. Glia re-sealed particles freshly prepared from adult rat brain are competent for exocytotic release of glutamate. J. Neurochem. 96, 656–668.
Streit, J., Tscherter, A., Heuschkel, M.O., Renaud, P., 2001. The generation of rhythmic activity in dissociated cultures of rat spinal cord. Eur. J. Neurosci. 14, 191–202.
Taccola, G., Nistri, A., 2006a. Fictive locomotor patterns generated by tetraethylammonium application to the neonatal rat spinal cord in vitro. Neuroscience 137, 659–670.
Taccola, G., Nistri, A., 2006b. Oscillatory circuits underlying locomotor networks in the rat spinal cord. Crit. Rev. Neurobiol. 18, 25–36.
Taccola, G., Marchetti, C., Nistri, A., 2004. Modulation of rhythmic patterns and cumulative depolarization by group I metabotropic glutamate receptors in the neonatal rat spinal cord in vitro. Eur. J. Neurosci. 19, 533–541.
Taccola, G., Margaryan, G., Mladinic, M., Nistri, A., 2008. Kainate and metabolic perturbation mimicking spinal injury differentially contribute to early damage of locomotor networks in the in vitro neonatal rat spinal cord. Neuroscience 155, 538–555.
Thomson, D.J., Chave, A.D., 1991. Jackknife error estimates for spectra, coherences, and transfer functions. In: Haykin, S. (Ed.), Advances in Spectral Analysis and Array Processing. Prentice-Hall, Englewood Cliffs, NJ, pp. 58–113.
Tovar-Y-Romo, L.B., Santa-Cruz, L.D., Zepeda, A., Tapia, R., 2009. Chronic elevation of extracellular glutamate due to transport blockade is innocuous for spinal motoneurons in vivo. Neurochem. Int. 54, 186–191.
Vincent, P., Mulle, C., 2009. Kainate receptors in epilepsy and excitotoxicity. Neuroscience 158, 309–323.
Virág, L., Szabó, C., 2002. The therapeutic potential of poly(ADP-ribose) polymerase inhibitors. Pharmacol. Rev. 54, 375–429.
Wu, K.L., Hsu, C., Chan, J.Y., 2009. Nitric oxide and superoxide anion differentially activate poly(ADP-ribose) polymerase-1 and bax to induce nuclear translocation of apoptosis-inducing factor and mitochondrial release of cytochrome c after spinal cord injury. J. Neurotrauma 26, 965–977.
Yunger, L.M., Fowler, P.J., Zarevics, P., Setler, P.E., 1984. Novel inhibitors of gamma-aminobutyric acid (GABA) uptake: anticonvulsant actions in rats and mice. J. Pharmacol. Exp. Ther. 228, 109–115.

Methods, materials and results

Section 3

ATF3 is a novel nuclear marker for migrating ependymal stem cells in the rat spinal cord.

Mladinic M, **Bianchetti E**, Dekanic A, Mazzone GL, Nistri A.

Manuscript under review (2013).

ATF3 is a novel nuclear marker for migrating ependymal stem cells in the rat spinal cord

Miranda Mladinic[1,2,3], Elena Bianchetti [1], Ana Dekanic[1,3], Graciela L. Mazzone[1], and Andrea Nistri[1,2]

[1]Neuroscience Dept., International School for Advanced Studies (SISSA), Trieste, Italy;
[2]SPINAL (Spinal Person Injury Neurorehabilitation Applied Laboratory), Istituto di Medicina Fisica e Riabilitazione, Udine, Italy;
[3]Department of Biotechnology, University of Rijeka, Rijeka, Croatia

Corresponding author:
Miranda Mladinic PhD
Department of Biotechnology, University of Rijeka
Radmile Matejčić 2, 51000 Rijeka, Croatia
Phone: +39 040 3787770
Fax: +385 51 584599
Email: mirandamp@uniri.hr

Highlights:

- ATF3 is expressed in rat ependymal stem/progenitor cells from neonatal to adult age.
- In quiescent ependymal cells ATF3 immunostaining overlaps with nestin and vimentin.
- Migrating spinal stem cells show nuclear ATF3 immunostaining.
- Migrating cells make chain formation termed funicular migratory stream.
- MAPK-p38 and JNK/c-Jun inhibitors prevent the migration of ATF3 positive cells

Keywords: Activating transcription factor 3, quiescent stem cells, spinal cord injury, in vitro rat spinal cord, excitotoxicity, oxygen-glucose deprivation

Abbreviations: ATF3, activating transcription factor; AU, arbitrary units; bHLH, basic helix-loop-helix; bZIP, Basic Leucine Zipper; CC, central canal; CREB, cAMP responsive element-binding; CSF, cerebrospinal fluid; DAPI, 4,6-diamidino-2-phenylindole; DCX, doublecourtin; DIV, days in vitro; EdU, 5-ethynyl-20-deoxyuridine; FMS, funicular migratory stream; GFAP, glial fibrillary acidic protein; MAPK, mitogen-activated protein kinases; PM, pathological medium; RMS, rostral migratory stream; SPCs, stem and progenitor cells; TBP, TATA binding protein.

Acknowledgments: We thank Mrs Jessica Franzot for technical support with Western blotting. This work was supported by grants from the government of the Friuli Venezia Giulia Region (SPINAL project), the Fund for Transregional Cooperation (MINA project), and the IBRO Return Home Programme Grant (to MM). AD was supported by the project DIANET, 2007/2013 Operational Program of the European Social Fund of the autonomous Region Friuli Venezia Giulia.

ABSTRACT

The present study identified the ATF3 as a novel dynamic marker for ependymal stem/progenitor cells (nestin, vimentin and SOX2 positive) around the central canal of the neonatal or adult rat spinal cord. While quiescent ependymal cells showed cytoplasmic ATF3 expression, during 6-24 h in vitro these cells mobilized and acquired intense nuclear ATF3 staining. Their migratory pattern followed a centrifugal pathway toward the dorsal and ventral funiculi, reminiscent of the rostral migratory stream of the brain subventricular stem cells. Thus, the chain cell formation was, by analogy, termed funicular migratory stream (FMS). The FMS process preceded the strong proliferation of ependymal cells occurring only after 24 h in vitro. Pharmacological inhibition of MAPK-p38 and JNK/c-Jun (upstream effectors of ATF3 activation) prevented the FMS mobilization of ATF3 nuclear-positive cells. Excitotoxicity or ischemia-like conditions, reported to evoke neuronal and glial injury, did not further enhance migration of ependymal cells at 24 h, suggesting that, at this early stage of damage, the FMS phenomenon had peaked and that more extensive repair processes are delayed beyond this time point. ATF3 is, therefore, useful to identify activation and migration of endogenous stem cells of the rat spinal cord in vitro.

1. INTRODUCTION

The ependymal region of the adult spinal cord in mammals harbours a pool of stem and progenitor cells (SPCs) readily activated and recruited by spinal damage (Weiss at al.,1996; Hugnot and Franzen, 2011). Even though their adult neurogenesis has not been observed (Hugnot and Franzen, 2011; Sabourin et al., 2009), the neural stem cells present in the adult spinal cord are recruited and proliferate after spinal cord injury (Yamamoto et al., 2001b),

producing scar-forming astrocytes and myelinating oligodendrocytes (Meletis et al., 2008). The manipulation of endogenous spinal stem cells after injury could represents one valid alternative to stem cell transplantation, since it is noninvasive and avoids the need for immune suppression (Meletis et al., 2008).

Spinal stem cells are difficult to identify due to their heterogeneity and lack of specific expressional markers, since the ones currently used significantly overlap with those of mature astrocytes (McDonough and Martinez-Cardeno, 2012). Furthermore, there is no specific marker to discriminate between quiescent and activated ependymal spinal cells, or to monitor migratory ependymal cells. Moreover, the signaling pathways and genes controlling the spinal SPC fate in normal and pathological conditions, remain largely unknown (Hugnot and Franzen, 2011).

Brain transcription factors that regulate formation and proliferation of neural SPCs depend on the Sox family of genes, in particular Sox2 (Liu et al., 2013). Genomics and proteomics technologies have recently identified Wnt/beta-catenin, Notch, sonic hedgehog and growth factor networks as major signaling pathways involved in maintainance, self-renewal, proliferation and neurogenesis of the neural SPCs, and have demonstrated cross-talk between key molecules of these pathways and their modulations by transcription factors, miRNA and histone modifications (Yun et al., 2010).

At variance with the wealth of brain data, transcription factors controlling spinal cord stem cells remain incompletely understood as they have been studied with in vitro primary cultures, showing common expression of various homeodomain-type (Pax6, Pax7, Nkx2.2, and Prox1) and basic helix-loop-helix (bHLH)-type (Ngn2, Mash1, NeuroD1, and Olig2) regulatory factors in adult and embryonic rat spinal neural progenitors (Yamamoto et al., 2001b). In the course of

our studies with biomarkers of neuronal damage (Khuzhandaivel et al., 2011) we serendipitously discovered intense immunostaining of ependymal cells for the activating transcription factor 3 (ATF3): this observation led us to explore its expression in control or damage-induced protocols.

ATF3 belongs to the mammalian ATF/cAMP responsive element-binding (CREB) protein family of the Basic Leucine Zipper (bZIP) transcription factors (Hashimoto et al., 2002) that generate a wide range of either repressors or activators of transcription (Thompson et al., 2009). ATF3 is thought to be an immediate early gene, a stress inducible gene and an adaptive response gene, which, when activated by various stimuli, can control cell cycle and cell death machinery (Hunt et al., 2012).

ATF3 expression is normally very low in central neurons and glia, but it is markedly upregulated in response to injury and closely linked to survival and regeneration of peripheral axons (Hunt et al., 2012). Both cytoplasmic and nuclear ATF3 immunostaining has been reported with variations related to cell type, species, and injury state when it becomes prevalently nuclear (Hunt et al., 2012). ATF3 is supposed to have a role in neurite growth and regeneration (Moore et al., 2011) and it has been identified as regulator of neuronal survival against excitotoxic and ischemic brain damage (Zhang et al., 2011). ATF3 knockout exacerbates inflammation and brain injury after transient focal cerebral ischemia (Wang et al., 2012).

ATF3 has no known role in neuronal development of the intact nervous system, neither its expression has been reported in SPCs. The present study is the first report of ATF3 as a reliable marker of activated neuroprogenitor cells in the rat spinal cord.

2. MATERIAL AND METHODS

2.1. Animals

The experiments were performed on neonatal or adult Wistar rats in accordance with the guidelines of the National Institutes of Health and the Italian act D.Lgs. 27/1/92 no. 116 (implementing the European Community directives no. 86/609 and 93/88), and with approval by the SISSA ethical committee for animal experimentation. All efforts were aimed at reducing the number of animals used and at minimizing their suffering. Spinal cords were dissected out from neonatal animals under urethane anesthesia (0.2 ml i.p. of a 10% w/v solution) with continuous superfusion with Kreb's solution containing (in mM): NaCl, 113; KCl, 4.5; $MgCl_27H_2O$, 1; $CaCl_2$, 2; NaH_2PO_4, 1; $NaHCO_3$, 25; glucose, 11; gassed with 95% O_2/5% CO_2, pH 7.4 at room temperature, as described previously (Mladinic et al., 2013). The adult spinal cord was dissected out from adult pregnant females, anaesthetized with the 10.5% chloral hydrate, 0.4 ml/100 g i.m. and subsequently killed by an intracardiac injection (2 ml) of chloral hydrate.

2.2. Experimental protocols

The dissected spinal cords were immediately fixed or maintained for the preset times in Kreb's solution (up to 24 h) and then fixed. The p38 inhibitor SB203580 or the JNK/c-Jun inhibitor SP600125 (both form Calbiochem/ Millipore, Milan, Italy) was added to the Kreb's solution for 12 or 24 h. To induce moderate or severe excitotoxic spinal cord injury, either 50 μM or 1 mM kainate was added to the Kreb's solution for 1 h and then washed out in Kreb's solution for further 24 h (this procedure has previously been described in detail (Mladinic et al., 2013; Taccola et al., 2008)). The ischemia-like metabolic perturbation was induced as previously described (Mladinic et al., 2013; Taccola et al., 2008; Bianchetti et al., 2013) by incubating the tissue for 1 h in pathological medium (PM), namely Kreb's solution containing 10 mM H_2O_2,

500 mM sodium nitroprusside, lacking oxygen and glucose, with 6.75–6.80 pH and 230–240 mOsm osmolarity. When the spinal cord was maintained in vitro for >24 h, the tissue was kept in oxygenated (95% O_2/5% CO_2) BME Eagle's basal medium (Sigma-Aldrich, St. Louis, MM, USA) supplemented with 0.2% fetal calf serum, 30 ng/ml 7S nerve growth factor, 10 μg/ml insulin and 0.1 mg/ml gentamycin (Mladinic, 2007).

2.3. Fluorescence immunostaining procedure

The free-floating immuno-fluorescence protocol was as previously described (Mladinic et al., 2013; Taccola et al., 2008). The primary antibodies (Supplemental Table 1) were visualized using appropriate secondary fluorescent Alexa Fluor 488 or 594 antibodies (1:500 dilution, Invitrogen, Carlsbad, CA, USA). Sections were stained in 1 g/ml solution of 4,6-diamidino-2-phenylindole (DAPI) for 20 min to visualize cell nuclei and mounted on Superfrost Plus (Menzel-Glaser, Braunschweig, Germany) slides. The immunostaining signal was analysed by Zeiss Axioskop2 microscope (Oberkochen, Germany) or TCS SP2 LEICA confocal microscope (Wetzlar, Germany), using 1 μm z sectioning. The ATF-3 (C-19, sc-188) antibody (Santa Cruz Biotech, CA, USA) has previously been used as a reliable marker for immunostaining (Tsujino et al., 2000; Tsuzuki et al., 2001; Zhang et al., 2012). Its specificity for rat ependymal spinal cells was tested by incubating the antibody with the specific blocking peptide (Santa Cruz Biotech, sc-188P; dilution 1:5) for 2h at room temperature, prior to the immunostaining procedure (Supplemental Figure 1). Quantification of immunofluorescence signals (gray level intensity expressed in arbitrary units, AU) was performed with Meta-Vue imaging software (Molecular Devices, Sunnyvale, CA, USA) using the densitometry function to calculate mean signal intensities for areas of interest reactive to ATF3 or SOX2 (1000 μm^2 covering the ependymal

zone as shown in Fig. 4A; white rectangles). The values are mean±SD (at least three different fields in each one of three different sections from two different spinal cords).

2.4. Quantification of ATF3, Ki67 or EdU positive cell nuclei

To analyze mobilization of stained cells, ATF3, Ki67 or 5-ethynyl-20-deoxyuridine (EdU) nuclearly labeled cells were counted in a central spinal region (termed funicular migratory stream, FMS; 150 μm wide) that, as shown in Figure 3C, included a sagittal area from the apex of the dorsal funiculus to the apex of the ventral funiculus. The proliferation assay Click‑iT® EdU (Invitrogen) was used in accordance with the manufacturers' instructions as recently detailed (Mazzone et al., 2013). Thus, the spinal cords were incubated for 12 h in Kreb's solution containing EdU (10 μM), fixed, cryopreserved and microtome-sectioned. Incorporated EdU was detected with the fluorescent azide coupling reaction. Sections were then washed twice with 3% BSA in PBS and immunostained with ATF3 or Ki67 antibody.

2.5. Western blotting

Cytoplasmic and nuclear fractions were separated by a standard procedure (Kuzhandaivel et al., 2010). Quantification of protein content was performed using a bicinchoninic acid test. Gel electrophoresis was performed on 12% acrylamide SDS gels. As a size standard, Page Ruler Prestained Protein Ladder (Fisher Scientific SAS, Illkirch Cedex, France) from 10 KDa to 170 KDa was used. As positive control, we used RAW 264.7 Cell Lysate (sc- 2211, Santa Cruz Biotech). The membrane was incubated with anti-ATF3 (ATF-3, C-19, sc-188, Santa Cruz Biotech) diluted 1:100 in blocking solution. For the negative control, the primary antibody was pre-incubated with the specific blocking peptide (Santa Cruz Biotech, sc-188P; dilution 1:5). Blots were incubated overnight at 4°C. The signal was visualized using fluorescence-labeled

secondary antibodies anti-rabbit, produced in goat, with the 1: 2000 dilution (Dako Italia, Milan, Italy). The results were acquired using Alliance LD2-77WL (Uvitec, Cambridge, UK) and analyzed with Uviband software (Uvitec). ATF3 levels for the cytoplasmic fractions were normalized for β-actin using a β-Actin−Peroxidase antibody (A3854, Sigma-Aldrich), while the nuclear fractions were normalized for TATA binding protein (AB62126, Abcam, Cambridge, UK).

2.6. Data analysis

All data are expressed as mean±SD, except for the Western blotting where the data are mean±S.E. Statistical analysis was carried out with SigmaStat 3.1 (Systat Software, Chicago, IL, USA). The statistical analysis of the ATF3 immunostaining intensity measurements in spinal cords of various aged rats were performed using One Way Analysis of Variance test, and then, for the pairwise multiple comparison procedures, the Tukey Test was used. The number of measurements in each group was >20 (at least two measurements in each of ten different spinal cord sections from three different animals). For the statistical comparison of the ATF3 and SOX2 immunostaining intensity measurements, the *t*-test was used. The number of measurements in each group was 10 (at least three measurements in each of three different spinal cord sections from two different animals). For the statistical analysis of the number of cells with the ATF3, Ki67 or EdU positive nuclei, the *t*-test was also used. The number of sections on which the counting was performed ranged from 6 to 20 for each experimental protocol. For the statistical analysis of the Western blotting ATF3 signal, data were first assessed as parametric with a normality test (Anova Tukey) and then analyzed with the paired and two tailed distribution Student *t*-test. The signals obtained from two different blots were analyzed, and in

each experiment, different protein samples, coming from the three different animals, were collected. Thus, the total number of animals for each experimental group was six.

3. RESULTS

3.1. Postnatal ATF3 expression in spinal ependymal cells overlaps with nestin, vimentin and SOX2

Strong ATF3 immunostaining was detected in the cytoplasm of ependymal cells around the spinal central canal of rats aged from postnatal day (P) 1 up to adulthood (Figure 1A,B,D). The ATF3 filamentous staining in the ependymal zone is clearly observed at higher magnification in Figure 1B. The intensity of the ATF3 immunostaining in the area of interest of ependymal zone (see methods) was measured in tissues from animals of different age, and was found to increase postnatally, and remain elevated in adulthood (Figure 1C). ATF3 staining overlapped with vimentin (Figure 1Ad-f,) and nestin (Figure 1Dc,d), markers previously shown to be expressed in stem cells of the spinal ependymal region (Hugnot and Franzen, 2011). As previously reported by (Mokry et al., 2008), in adult rats nestin staining was observed not only in the ependymal region, but also in blood vessels (Fig. 1Dc,d), while the ATF3 staining remained restricted to the ependymal zone (Figure 1Db). Ependymal cells from embryonic and P0 tissue did not show ATF3 staining.

Both neonatal and adult ependymal cells were co-stained for ATF3 and the transcription factor SOX2 (Figure 2A,B). Figure 2D shows, at higher magnification, a central section from a stack of z-plane confocal images of adult spinal ependymal cells that confirmed the cytoplasmic ATF3 and nuclear SOX2 stainings of densely packed cells.

Outside the ependymal zone, no significant ATF3 staining was observed in the grey matter as shown by the spinal cord cross section in Figure 2C. It is noteworthy, however, that, in the lateral and ventral regions of the white matter, cytoplasmic ATF3 staining was detected in sparse cells at early postnatal age (P1-P4) (Figure 2C). In these white matter cells (showing ramified morphology similar to the NG2/BrdU positive cells (Horner et al., 2000), the cytoplasmic ATF3 staining again coincided with nuclear SOX2 staining (Figure 2C).

ATF3 staining in the ependymal region did not overlap with any of the following cell-specific markers: NeuN (neurons), DCX (neuronal precursors and immature neurons), GFAP (astrocytes), NG2 (astrocyte precursor cells), O4 (oligodendrocytes and their precursors), CD68 (activated microglia) (Supplemental Figure 2). It should be noted that the same ATF3 antibody did not show any immunopositive cells in the ependymal spinal cord region of the mouse (results not shown). It has been previously reported that ATF3 immunostaining (cytoplasmic and nuclear) is species-specific (rat or mouse) (Hunt et al., 2012).

3.2. In vitro mobilization of ependymal spinal cord cells and nuclear ATF3 expression

Previous studies have indicated that the spinal cord preparation survives in vitro for at least 24 h with functional network activity clearly observed as locomotor-like patterns recorded from multisegmental motor pools (Kuzhandaivel et al., 2011). Figure 3 shows that such in vitro protocol stimulated mobilization of ependymal cells from the central canal zone toward the dorsal and ventral funiculi (Figure 3B-D), creating, at 24 h, a characteristic pattern reminiscent of the rostral migratory stream (RMS) of the brain subventricular stem cells (Coskun and Luskin, 2002; Murase and Horwitz, 2004). By analogy, the spinal cord ependymal migration was termed

FMS (see methods), and was clearly restricted to this 150 μm wide area (Fig. 3C, red lines). The time course of nuclear ATF3 staining is shown in Figure 3E, and plotted in Figure 3F. Thus, a detectable ATF3 nuclear signal appeared 4h after dissection and reached a plateau between 14 and 24 h. Likewise, the occurrence of ATF3 positive cells in the FMS area (indicated by the blue rectangle in Figure 3C) had a similar time course (Figure 3G). The ATF3-nuclear positive migratory cells were nestin (Supplemental Figure 3A), vimentin (Supplemental Figure 3B) and SOX2 (Supplemental Figure 3C) positive. Figure 4A demonstrates the differential distribution of ependymal cell ATF3 staining that was strong around the central canal of fresh tissue (top row in A; region of interest quantified in Figure 4 B), whereas it significantly ($P<0.001$) decreased (Figure 4 A, bottom row, and Figure 4 B) at 24 h in vitro. Figure 4 C,D compares the ATF3 expression in two areas of interest (indicated by hatched squares in Figure 4A, bottom left) and demonstrates that mobilized cells (Figure 4 D) showed nuclear ATF3. On the other hand, nuclear SOX2 staining was consistently found in cells surrounding the central canal in fresh tissue (Figure 4 A, top row) or after 24 h in vitro (Figure 4 A, bottom row) and remained expressed even in the migrated cells (Figure 4 B, D). These results suggest that, while SOX2 was a general stem cell marker, ATF3 preferentially stained nuclei of those ependymal cells undergoing mobilization.

ATF3 is widely used as a marker for axotomized motoneurons (Tsujino et al., 2000), or injured dorsal root ganglion neurons (Tsuzuki et al., 2001). The present study examined ATF3 expression in motoneurons at various times in vitro. ATF3 was detected in the motoneuron cytoplasm already 2 h after dissection, reached a peak at 4 h, after which it decreased with no nuclear staining (Supplemental Figure 4A). Supplemental Figure 4B shows, in the same spinal section, strong ATF3 signal in the FMS area (right edge) in contrast with lack of signal from

motoneurons (left edge) at 24 h in vitro. At this time point motoneurons were well preserved as shown by their SMI32 staining (Supplemental Figure 4C) and remain functionally viable (Kuzhandaivel et al., 2011). These results validate ample survival of motoneurons at 24 h in control conditions with no nuclear ATF3 staining characteristic for the injured motoneurons.

3.3. Proliferative markers of the ependymal region in vitro

The time-dependent redistribution of ATF3 stained cells might have suggested not only mobilization, but also cell proliferation developing during a few hours in vitro. To examine this possibility, we first investigated in the FMS region of interest (see Figure 3 C) if cells, which had incorporated EdU as a DNA marker of cell proliferation (Mazzone et al., 2013) also showed ATF3 positivity at 6 or 24 h in vitro. At 6 h, we detected 50±10 EdU positive cells (Figure 5 B) and a lower number of ATF3 nuclear-positive cells (20±7; n=6). Figure 5 A shows the mismatch between ATF3 and EdU nuclear positive cells in the FMS at 24 h. In fact, while the number of EdU positive cells in the FMS area had not changed (52±5; n=6) vs the value at 6 h (Figure 5 B), the number of ATF3 nuclearly-positive cells increased more than four times (83±18, n=20). In support of this observation we also studied the number of cells with their nucleus positive for the proliferative marker Ki67 (Mazzone et al., 2013) or ATF3. Figure 5 C shows a similar number of Ki67 or ATF3 positive nuclei at 24 h in the FMS region, while a significant rise was detected at 48 h only. Even if double immunostaining with Ki67 and ATF3 was not possible for lack of compatible antibodies, these data are consistent with ependymal cell proliferation occurring mainly after the first 24 h. Thus, our results suggest that ATF3 nuclearly-stained cells migrated away from the central canal with a time profile distinct from local cell proliferation.

3.4. Signaling pathways underlying ATF3 activation

ATF3 activation has been previously shown to be dependent on c-Jun phosphorylation (Lindwall et al., 2004) or the mitogen-activated protein kinases (MAPK)/p38 pathway (Lu et al., 2007). In keeping with this notion, the MAPK-p38 inhibitor SB203580 or the JNK/c-Jun inhibitor SP600125 prevented the rise in the number of ATF3 nuclear-positive cells in the FMS region at 12 h in vitro (Figure 6A,B). In fact, application of SB203580 (1μM) or SP600125 (50-100μM) treatment (12 h) led to absence of nuclear ATF3 signal that was replaced by filament-like staining (Figure 6A).

We next investigated ATF3 protein levels in the nuclear and cytoplasmic extracts from freshly frozen spinal tissue, or maintained for 24 h in Kreb's solution (with or without SB203580 or SP600125). To this end, we used the same anti-ATF3 antibody used for immunostaining previously validated to detect ATF3 protein by Western blotting in cancer tissue (Buganim et al., 2011). The 22 kDa band, corresponding to the full-length ATF3 (Hashimoto et al., 2002; Buganim et al., 2011; Chen et al., 1994), was of the highest intensity in nuclear lysates (loading control was TBP) from spinal tissue maintained in vitro for 24 h (sham; Figure 6C, top lane, and Figure 6D), very low from fresh tissue, and significantly ($P>0.01$) weaker 24 h after SB203580 (1 μM) or SP600125 (100 μM) treatment (Figure 6 C,D). As a positive control, the lysate from RAW 264.7 cells (Abelson murine leukemia virus-induced tumor) was employed, as suggested by the ATF3 antibody manufacturer (see Figure 6C, right lanes), to produce a strong ATF3 band. Thus, the change in the intensity of the ATF3 specific nuclear expression mirrored the pattern of the ATF3 immunofluorescence signal observed in the nuclei of mobilized cells. Regardless of the protocol used, a band of 28 kDa (as reported by the ATF3 antibody manufacturer) was observed with unchanged intensity in cytoplasmic lysates (β-actin loading control; Figure 6C, lower lanes).

3.5. ATF3 activation after experimental SCI

We recently reported that in vitro spinal cord lesions like excitotoxic injury (Mazzone et al., 2013) or oxygen-glucose deprivation (Bianchetti et al., 2013) applied for a short time (1 h), induce a slowly developing process of cell death that peaks at 24 h. We, therefore, wondered if these paradigms could activate ependymal cell early mobilization. Figure 7A shows the presence of ATF3 positive cells in the FMS area 24 h after 50 μM kainate application (1 h). Likewise, Figure 7B depicts, in the same region, ATF3-positive cells 24 h following ischemic-like injury (1 h application of a pathological medium lacking oxygen and glucose and containing reactive oxygen species (Bianchetti et al., 2013)). Such cells, with ATF3 positive nuclear staining, were also nestin and vimentin positive (Figure 7 A,B). Figure 7D shows that, with either protocol, the number of cells with the ATF3 positive nucleus in the FMS area was similar to control at 24 h in vitro. Only when the concentration of kainate was raised to 1mM to apply a very intense excitotoxic stimulus, the number of ATF3-nuclear positive cells significantly ($P=0.005$) fell by one third, suggesting substantial cell loss (Figure 7C,D).

4. DISCUSSION

The current study is the first report of the dynamic expression of the ATF3 by ependymal spinal stem cells, as this protein was localized to the cytoplasm when such cells were quiescent, but was found in their nucleus when cells became activated. This property enabled us to follow up activated ependymal cells that migrated from the central canal toward the ventral and dorsal white matter, forming the FMS that resembles the RMS of the brain SPCs.

The fact that ATF3 immunostaining coincided with well-known SPC markers, such as nestin, vimentin and SOX2, suggests that ATF3 labeling in the spinal cord was primarily expressed by intrinsic stem cells, typically found around the central canal (Hugnot and Franzen, 2011). ATF3 was mainly expressed in the cytoplasm and processes of these cells from P1 onwards, grew during the first postnatal week and remained elevated later. Such ATF3 stained cells in fresh tissue had small diameter, large egg-shaped nucleus, and were closely packed together. Grey matter cells remained, however, devoid of ATF3 staining, adding specificity to the role of this protein for stem cell labeling.

Previous reports of the role of ATF3 in the regulation of SPCs are scant. Recent studies (Gao et al., 2013; Gargiulo et al., 2013) have indicated involvement of ATF3 in the control of genes like SOX2 or BMI1, critical for pluripotency and reprogramming of the human embryonic stem cells or glioblastoma stem-like cells. The present observation of ATF3 and SOX2 co-staining is consistent with this possibility. Moreover, the CREB transcription factor family, of which the ATF3 is a member, has an established role in the SPC regulation and neurogenesis (Merz et al., 2011; Mantamadiotis et al., 2012). Our results suggest, however, a new role of ATF3 not only in the maintenance of the spinal ependymal cells but also in their activation.

When spinal cords were kept in vitro for 24 h, we observed a novel phenomenon, namely centrifugal mobilization of ependymal stem cells which formed a migratory chain analogous to the brain RMS (Lois et al., 1996; Wichterle et al., 1997; Tanvig et al., 2009) as they moved away from the central canal to the adjacent ventral and dorsal white matter. When this occurred, ATF3 was clearly expressed in the cell nucleus. This phenomenon developed gradually after 4 h and was clearly observed at 24 h. Interestingly, ependymal cells which did not mobilize, retained their SOX2 nuclear staining, yet lost the ATF3 cytoplasmic one. Hence, ATF3 nuclear labeling

could be interpreted as a novel marker of migrating ependymal cells. The fact that in vitro conditions induce mobilization of stem cells has been earlier reported with organotypic brain slices (Tanvig et al., 2009): in such a case RMS toward the olfactory bulb is occurring after several days, while the present report shows a much faster process developing within hours. The unchanged occurrence of Ki67 or EdU positive cells in FMS at 24 h in vitro is consistent with a process of ependymal cell early mobilization rather than proliferation that occurred at later time. In support of this hypothesis is the recent observation that, in rat organotypic slices, significant proliferation of neuroprogenitors was detected only after a few days in culture (Mazzone et al., 2013).

The question then arises regarding the mechanism(s) responsible for activation and mobilization of ependymal cells in vitro, given that spinal networks are fully preserved and viable during this timeframe, including electrophysiological activity of locomotor networks (Taccola et al., 2008). In vivo the ependymal cells are in direct contact with the cerebrospinal fluid (CSF) and numerous blood vessels (Hugnot and Franzen, 2011). Thus, their delayed activation in vitro might be due to the disappearance of yet-unclear signals from the CSF or blood (Menezes et al., 2002), which might normally keep the ependymal cells quiescent (Cheung et al., 2013). Additionally, the activating signal might come from a few cells injured during dissection, even if systematic analysis of in vitro tissue showed minimal pyknosis at 24 h in vitro (Taccola et al., 2008). A recent review has highlighted how stem cell quiescence is a state maintained by signaling pathways ready to allow rapid activation (Cheung et al., 2013). Deciphering the molecular mechanisms regulating stem cell quiescence is, therefore, an important goal for future studies to increase our understanding of tissue regeneration mechanisms in pathological conditions (Cheung et al., 2013). Identification of the factors underlying even brain RMS

remains incomplete as various chemo-attractants, chemo-repellents, growth factors and cell adhesion molecules have been proposed to guide migrating cells (Tanvig et al., 2009; Menezes et al., 2002). The intracellular presence of other ATF/CREB family members with which ATF3 forms heterodimers may ultimately decide the functional role of ATF3 (Thompson et al., 2009), as much as the influence of regulators like other transcription factors, miRNA or histone modifications (Yun et al., 2010).

Previous studies have demonstrated that the signal transduction pathways mediating ATF3 expression include c-Jun co-expressed with ATF3 in the nervous system after injury and stress (Hunt et al., 2012). The selective JNK/c-Jun inhibitor SP600125 fully blocks ATF3 induction in adult rat ganglion neurons and inhibits outgrowth of their axons (Lindwall et al., 2004). Furthermore, the MAPK/p38 pathway is also required for ATF3 expression in several non-neuronal cell lines undergoing apoptosis, an effect suppressed by the specific MAPK/p38 inhibitor SB203580 (Lu et al., 2007). In accordance with these results, our current data showed the involvement of both molecular pathways (JNK/c-Jun and MAPK/p38) in the control of the ATF3 nuclear expression in mobilized spinal ependymal cells. This observation was also supported by Western blotting analysis indicating ATF3 expression (of molecular weight in full accordance with reports by (Hashimoto et al., 2002; Chen et al., 1994) in nuclear fractions at 24 h in vitro. The origin of the variation in the molecular weight between the nuclear and cytoplasmic ATF3 protein remains unclear and will need future work.

Excitotoxic or ischemic-like protocols, that are reported to produce moderate damage to the spinal cord (Taccola et al., 2008; Bianchetti et al., 2013; Mazzone et al., 2010), did not enhance the number of activated and migrating ATF3 positive cells 24 h later. When the excitotoxic stimulus was very strong (1 mM kainate), the number of activated ependymal cells actually

decreased in line with widespread neurotoxicity (Taccola et al., 2008). Our previous investigations have indicated that, in the rat spinal cord, neuronal and glial death occurs mainly during the first 24 h (Taccola et al., 2008; Bianchetti et al., 2013; Mazzone et al., 2013). Any attempt to repair cell damage might perhaps require an intervention by stem cells occurring over several days after the primary injury. This process has been examined with long-term organotypic cultures in which stem cell activation two weeks after excitotoxic stimulation failed to produce significant neurogenesis (Mazzone et al., 2013). While ATF3 is reported as a marker for the axotomy-dependent motoneuronal injury in the rat (Zhang et al., 2012), we detected transient, rather early cytoplasmic (never nuclear) staining for ATF3 in motoneurons, a phenomenon that disappeared by 24 h in vitro. Our data, thus, confirm that maintaining the rat spinal cord in vitro did not per se lead to neuron damage as clearly indicated by fully preserved network responses (Taccola et al., 2008) and that ependymal cell mobilization was probably a reaction to changes in the extracellular milieu.

We propose that the role of ATF3 might be different in the neuronal (postmitotic) and ependymal (mitotic) spinal cells. In neurons ATF3 is viewed as a late marker for injury (Tsujino et al., 2000; Tsuzuki et al., 2001; Francis et al., 2004), with a neuroprotective and pro-survival influence (Zhang et al., 2011; Wang et al., 2012). The role of ATF3 in proliferation and migration of ependymal cells could be similar to the ATF3 role in cancer cells in which ATF3 promotes proliferation, motility and invasiveness of certain cancer cell lines (Thompson et al., 2009; Wang et al., 2008).

5. CONCLUSIONS

In lower vertebrates the spinal cord can regenerate after injury, a process in which ependymal cells play a major role (Hugnot and Franzen, 2011). The mammalian spinal cord, however, cannot regenerate after lesion: hence, intense efforts are in progress to develop new, noninvasive, endogenous-stem cells based strategies for the treatment of spinal injury (Barnabe-Heider et al., 2008; Sahni and Kessler, 2010; Ruff and al., 2012). The discovery of ATF3 as a marker not only for quiescent but particularly for activated, migrating spinal SPCs should help future work to monitor their migration and fate (neurogenesis or gliogenesis) after injury and to test drugs to change the outcome. One might even imagine that it would be possible to up-regulate the ATF3 gene in ependymal spinal cells after injury to find out the impact on the neuronal tissue repair.

REFERENCES

Barnabé-Heider F, Frisén, J. Stem cells for spinal cord repair. Cell Stem Cell 2008;3:16-24.

Bianchetti E, Mladinic M, Nistri A. Mechanisms underlying cell death in ischemia-like damage to the rat spinal cord in vitro. Cell Death Dis 2013;4:e707.

Buganim Y, Madar S, Rais Y, Pomeraniec L, Harel E, Solomon H, Kalo E, Goldstein I, Brosh R, Haimov O, Avivi C, Polak-Charcon S, Goldfinger N, Barshack I, Rotter V. Transcriptional activity of ATF3 in the stromal compartment of tumors promotes cancer progression. Carcinogenesis 2011;32:1749-1757.

Chen BP, Liang G, Whelan J, Hai T. ATF3 and ATF3 delta Zip. Transcriptional repression versus activation by alternatively spliced isoforms. J Biol Chem 1994;269:15819-15826.

Cheung TH, Rando TA. Molecular regulation of stem cell quiescence. Nat Rev Mol Cell Biol. 2013;14:329-340.

Coskun V, Luskin MB. Intrinsic and extrinsic regulation of the proliferation and differentiation of cells in the rodent rostral migratory stream. J Neurosci Res 2002;69:795-802.

Francis JS, Dragunow M, During MJ. Over expression of ATF-3 protects rat hippocampal neurons from in vivo injection of kainic acid. Brain Res Mol Brain Res 2004;124:199-203.

Gao F, Wei Z, An W, Wang K, Lu W. The interactomes of POU5F1 and SOX2 enhancers in human embryonic stem cells. Sci Rep 2013;3:1588.

Gargiulo G, Cesaroni M, Serresi M, de Vries N, Hulsman D, Bruggeman SW, Lancini C, van Lohuizen M. In vivo RNAi screen for BMI1 targets identifies TGF-β/BMP-ER stress pathways as key regulators of neural- and malignant glioma-stem cell homeostasis. Cancer Cell 2013;23:660-676.

Hashimoto Y, Zhang C, Kawauchi J, Imoto I, Adachi MT, Inazawa J, Amagasa T, Hai T, Kitajima S. An alternatively spliced isoform of transcriptional repressor ATF3 and its induction by stress stimuli. Nucleic Acids Res 2002;30:2398-2406.

Horner PJ, Power AE, Kempermann G, Kuhn HG, Palmer TD, Winkler J, Thal LJ, Gage FH. Proliferation and differentiation of progenitor cells throughout the intact adult rat spinal cord. J Neurosci 2000;20:2218-2228.

Hugnot JP, Franzen R. The spinal cord ependymal region: a stem cell niche in the caudal central nervous system. Front Biosci 2011;16:1044-1059.

Hunt D, Raivich G, Anderson PN. Activating transcription factor 3 and the nervous system. Front Mol Neurosci 2012;5:7.

Kuzhandaivel A, Nistri A, Mazzone GL, Mladinic M. Molecular mechanisms underlying cell death in spinal networks in relation to locomotor activity after acute injury in vitro. Front Cell Neurosci 2011;5:9.

Kuzhandaivel A, Nistri A, Mladinic M. Kainate-mediated excitotoxicity induces neuronal death in the rat spinal cord in vitro via a PARP-1 dependent cell death pathway (Parthanatos). Cell Mol Neurobiol 2010;30:1001-1012.

Lindwall C, Dahlin L, Lundborg G, Kanje M. Inhibition of c-Jun phosphorylation reduces axonal outgrowth of adult rat nodose ganglia and dorsal root ganglia sensory neurons. Mol Cell Neurosci 2004;27:267-279.

Liu K, Lin B, Zhao M, Yang X, Chen M, Gao A, Liu F, Que J, Lan X. The multiple roles for Sox2 in stem cell maintenance and tumorigenesis. Cell Signal 2013;25:1264-1271.

Lois C, García-Verdugo JM, Alvarez-Buylla A. Chain migration of neuronal precursors. Science. 1996;271:978-981.

Lu D, Chen J, Hai T. The regulation of ATF3 gene expression by mitogen-activated protein kinases. Biochem J 2007;401:559-567.

Mantamadiotis T, Papalexis N, Dworkin S. CREB signalling in neural stem/progenitor cells: recent developments and the implications for brain tumour biology. Bioessays 2012;34:293-300.

Mazzone GL, Margaryan G, Kuzhandaivel A, Nasrabady SE, Mladinic M, Nistri A. Kainate-induced delayed onset of excitotoxicity with functional loss unrelated to the extent of neuronal damage in the in vitro spinal cord. Neuroscience 2010;168:451-462.

Mazzone GL, Mladinic M, Nistri A. Excitotoxic cell death induces delayed proliferation of endogenous neuroprogenitor cells in organotypic slice cultures of the rat spinal cord. Cell Death Dis 2013;4:e902

McDonough A, Martínez-Cerdeño V. Endogenous proliferation after spinal cord injury in animal models. Stem Cells Int 2012;2012:387513.

Meletis K, Barnabé-Heider F, Carlén M, Evergren E, Tomilin N, Shupliakov O, Frisén J. Spinal cord injury reveals multilineage differentiation of ependymal cells. PLoS Biol 2008;6:e182.

Menezes JR, Marins M, Alves JA, Froes MM, Hedin-Pereira C. Cell migration in the postnatal subventricular zone. Braz J Med Biol Res 2002;35:1411-1421.

Merz K, Herold S, Lie DC. CREB in adult neurogenesis--master and partner in the development of adult-born neurons? Eur J Neurosci 2011;33:1078-1086.

Mladinic M. Changes in cyclic AMP levels in the developing opossum spinal cord at the time when regeneration stops being possible. Cell Mol Neurobiol. 2007;27:883-888.

Mladinic M, Nistri A, Taccola G. Acute spinal cord injury in vitro: insight into basic mechanisms. In: Aldskogius H. Animal Models in Spinal Cord Repair, Neuromethods 76. Springer Science+Business Media, Humana Press, 2013:39-63.

Mokrý J, Ehrmann J, Karbanová J, Cízková D, Soukup T, Suchánek J, Filip S, Kolár Z. Expression of intermediate filament nestin in blood vessels of neural and non-neural tissues. Acta Medica (Hradec Kralove) 2008;51:173-179.

Moore DL, Goldberg JL. Multiple transcription factor families regulate axon growth and regeneration. Dev Neurobiol 2011;71:1186-1211.

Murase S, Horwitz AF. Directions in cell migration along the rostral migratory stream: the pathway for migration in the brain. Curr Top Dev Biol 2004;61:135-152.

Ruff CA, Wilcox JT, Fehlings MG. Cell-based transplantation strategies to promote plasticity following spinal cord injury. Exp Neurol 2012;235:78-90.

Sahni V, Kessler JA. Stem cell therapies for spinal cord injury. Nat Rev Neurol 2010;6:363–372.

Sabourin JC, Ackema KB, Ohayon D, Guichet PO, Perrin FE, Garces A, Ripoll C, Charité J, Simonneau L, Kettenmann H, Zine A, Privat A, Valmier J, Pattyn A, Hugnot JP. A

mesenchymal-like ZEB1(+) niche harbors dorsal radial glial fibrillary acidic protein-positive stem cells in the spinal cord. Stem Cells 2009;27:2722-2733.

Taccola G, Margaryan G, Mladinic M, Nistri A. Kainate and metabolic perturbation mimicking spinal injury differentially contribute to early damage of locomotor networks in the in vitro neonatal rat spinal cord. Neuroscience 2008;155:538-555.

Tanvig M, Blaabjerg M, Andersen RK, Villa A, Rosager AM, Poulsen FR, Martinez-Serrano A, Zimmer J, Meyer M. A brain slice culture model for studies of endogenous and exogenous precursor cell migration in the rostral migratory stream. Brain Res 2009;1295:1-12.

Thompson MR, Xu D, Williams BR. ATF3 transcription factor and its emerging roles in immunity and cancer. J Mol Med (Berl) 2009;87:1053-1060.

Tsujino H, Kondo E, Fukuoka T, Dai Y, Tokunaga A, Miki K, Yonenobu K, Ochi T, Noguchi K. Activating transcription factor 3 (ATF3) induction by axotomy in sensory and motoneurons: A novel neuronal marker of nerve injury. Mol Cell Neurosci 2000;15:170-182.

Tsuzuki K, Kondo E, Fukuoka T, Yi D, Tsujino H, Sakagami M, Noguchi K. Differential regulation of P2X(3) mRNA expression by peripheral nerve injury in intact and injured neurons in the rat sensory ganglia. Pain 2001;91:351-360.

Wang A, Arantes S, Yan L, Kiguchi K, McArthur MJ, Sahin A, Thames HD, Aldaz CM, Macleod MC. The transcription factor ATF3 acts as an oncogene in mouse mammary tumorigenesis. BMC Cancer 2008;8:268.

Wang L, Deng S, Lu Y, Zhang Y, Yang L, Guan Y, Jiang H, Li H. Increased inflammation and brain injury after transient focal cerebral ischemia in activating transcription factor 3 knockout mice. Neuroscience 2012;220:100-108.

Weiss S, Dunne C, Hewson J, Wohl C, Wheatley M, Peterson AC, Reynolds BA. Multipotent CNS stem cells are present in the adult mammalian spinal cord and ventricular neuroaxis. J Neurosci 1996;16:7599-7609.

Wichterle H, Garcia-Verdugo JM, Alvarez-Buylla A. Direct evidence for homotypic, glia-independent neuronal migration. Neuron 1997;18:779-791.

Yamamoto S, Nagao M, Sugimori M, Kosako H, Nakatomi H, Yamamoto N, Takebayashi H, Nabeshima Y, Kitamura T, Weinmaster G, Nakamura K, Nakafuku M. Transcription factor expression and Notch-dependent regulation of neural progenitors in the adult rat spinal cord. J Neurosci 2001a;21:9814-9823.

Yamamoto S, Yamamoto N, Kitamura T, Nakamura K, Nakafuku M. Proliferation of parenchymal neural progenitors in response to injury in the adult rat spinal cord. Exp Neurol 2001b;172:115-127.

Yun SJ, Byun K, Bhin J, Oh JH, Nhung le TH, Hwang D, Lee B. Transcriptional regulatory networks associated with self-renewal and differentiation of neural stem cells. J Cell Physiol 2010;225:337-347.

Zhang SJ, Buchthal B, Lau D, Hayer S, Dick O, Schwaninger M, Veltkamp R, Zou M, Weiss U, Bading H. A signaling cascade of nuclear calcium-CREB-ATF3 activated by synaptic NMDA receptors defines a gene repression module that protects against extrasynaptic NMDA receptor-induced neuronal cell death and ischemic brain damage. J Neurosci 2011;31:4978-4990.

Zhang ZJ, Dong YL, Lu Y, Cao S, Zhao ZQ, Gao YJ. Chemokine CCL2 and its receptor CCR2 in the medullary dorsal horn are involved in trigeminal neuropathic pain. J Neuroinflammation 2012;9:136.

FIGURE LEGENDS

Figure 1. Age-related expression of ATF3 by spinal ependymal cell and its co-expression with nestin and vimentin immunostaining. (**A):** Top row shows cytoplasmic ATF3 immunostaining (red) of the ependymal region around the central canal (CC) of P4 (a), P7 (b) and P21 (c) rat spinal cord cross-sections (30 μm thick). Bottom row shows ATF3 immunostaining (red) overlapping with vimentin staining (green) in P4 (d), P7 (e) and P21 (f) sections. Cell nuclei are counterstained with the nuclear dye DAPI (blue). (**B**): Higher magnification of ATF3 immunostaining (with DAPI nuclear counterstaining) of ependymal cells in P4 spinal cord. For image clarity fluorescent stainings (left and middle panels) were converted to grayscale and their negatives are shown to reveal the fibrillary, cytoplasmic ATF3 staining of ependymal cells. In right panel, ATF3 (red) and DAPI (blue) fluorescent stainings are merged. (**C**): Histograms show the intensity of ATF3 immunostaining (AU) in an area of interest covering the 1000 μm^2 of the ependymal zone (from postnatal day 2, P2, until adult age) as shown with a white rectangle in Fig. 4A.) The values are mean±SD (at least three different fields in each one of three different sections from two different spinal cords). The data from P2 and adult spinal cords are significantly different from those obtained from those of P4-7 ($P<0.001$; One Way Analysis of Variance test). (**D**): Cross-section (30 μm thick) of adult female rat spinal cord showing the zone around the central canal (CC) stained with DAPI (a; fluorescent blue staining was converted to grayscale), ATF3 (green; b), nestin (red; c), and merged image (d). Scale bars = 50 μm.

Figure 2. ATF3 immunostaining of ependymal spinal cord cells overlaps with SOX2 in neonatal and adult rats. (**A, B**): Spinal cord cross-sections (30 μm thick) of neonatal (A, top row) or adult (B, bottom row) spinal cord immunostained with SOX2 and ATF3. The left panels show cell nuclei stained with DAPI (grayscale conversion). In the right panels the fluorescent signals with DAPI (blue), SOX2 (green) and ATF3 (red) are merged. (**C**): Half-section of the P1 spinal cross-section reconstructed from 6 different images (10x). Note that ATF3/SOX2 staining is localized to the ependymal zone, with scattered positive cells in the white matter. (**D**): central section from a stack of z-plane confocal images showing (highly magnification) the ependymal zone of adult spinal cord stained with cytoplasmic ATF3 (red), nuclear SOX2 (green) and counterstained with DAPI (blue). Scale bar is 100 μm in A-C and 10 μm in D.

Figure 3. Nuclear ATF3 immunostaining of activated, mobilized stem cells**. (A-D**): ATF3 immunostaining (grayscale) in 30 μm thick sections from the central zone around the central spinal canal (CC) of P2 rat spinal cord. Note fresh tissue with fibrilar, cytoplasmic ATF3 staining of ependymal cells (**A**) and nuclear ATF3 staining of cells after 24 h in vitro (**B-D**) demonstrating migration from the central canal toward dorsal and ventral spinal funiculi. (**C**): Half-section of the spinal cord shows the 150 μm wide zone (delimited by red lines) through which the spinal ependymal cells migrate to form the funicular migratory stream (FMS). (**D**): FMS zone (reconstructed from two images taken at 10 x). (**E**): Grayscale conversion of ATF3 fluorescent immunostaining of P2 rat spinal cords maintained in vitro for 0-24 h, indicating the time course of ependymal cell migration. (**F**): Number of cells in FMS zone with the nuclear ATF3 staining show migration started between 4 and 6 h in vitro, and peaked after 24 h. (**G**): Time-dependent occurrence of ATF3 nucleary-positive cells in the FMS zone (blue rectangle)

150 μm away from the central canal. Scale bar is 50 μm in **A, B** and **D**, 200 μm in **C** and 100 μm in **E**.

Figure 4. Differential ATF3 and SOX2 immunostaining in ependymal zone of spinal tissue maintained in vitro. (**A**): Central region of the spinal cord (30 μm thick cross-sections) stained with ATF3 (red) and SOX2 (green) and counterstained with DAPI (grayscale); upper panels show freshly fixed tissue (FF), while lower panels show spinal cord tissue after 24 h in vitro. In right panels the ATF3 (red), SOX2 (green) and DAPI (blue) fluorescent stainings are merged. Note the fibrillary, cytoplasmic ATF3 staining in ependymal cells of fresh tissue, which largely disappears after 24 h in vitro. On the contrary, the nuclear SOX staining remains similarly intense in fresh tissue and after 24 h in vitro. (**B**): Histograms of signal intensity (AU) in the area of interest of the ependymal zone indicated by the white rectangles in (**A**). Note significant drop of ATF3 signal ($P<0.001$) after 24 h in vitro while the SOX2 signal did not change. Data are mean ± SD from 10 sections for each group. (**C**): Confocal images of DAPI (blue), SOX2 (green) and ATF3 (red) staining of ependymal cells of the spinal cord maintained in vitro for 24h. Bottom hatched box (**A**, left) indicates the ependymal region used for confocal microscopy. Note the absence of the ATF3 immunostaining signal in (**C**). (**D**): DAPI (blue), SOX2 (green) and ATF3 (red) staining of the region apical to the central canal, to which ATF3 nucleary-positive cells migrate. Note nuclear ATF3 staining overlapping SOX2 nuclear staining. Scale bar = 50 μm in A and 10 μm in C and D.

Figure 5. Proliferative cells in funicular migratory stream (FMS). (**A**): Nuclear co-immunostaining of ATF3 (red) and EdU (green) in spinal section (30 μm thick) of spinal cord maintained in vitro for 24 h. The labeled cells belong to the FMS (CC). Note that the green EdU signal does not overlap with ATF3 positive nucleus. Scale bar = 50 μm. (**B**): EdU positive nuclei

in FMS region of spinal cords maintained in vitro for 6 or 24 h (n=6-20 sections from 3 spinal cords). (**C**): ATF3 or Ki67 positive nuclei in the FMS region of spinal cords maintained one or two days in vitro (DIV), showing significant increase by the second day (P=0.039 for ATF3 and P=0.004 for Ki67; n=6-20 sections from 3 spinal cords).

Figure 6. The p38 inhibitor SB203580 or the JNK/c-Jun inhibitor SP600125 blocks nuclear ATF3 staining in spinal cords after 24 h in vitro. (**A**): Control ATF3 immunostaining (grayscale) in the region near the central canal (CC) after 12 h in Kreb's solution (left, sham; note the intense nuclear ATF3 staining), after treatment with the p38 inhibitor SB203580, or the JNK/c-Jun inhibitor SP600125 for the 12 h. Note filamental ATF3 staining (middle and right panels). Scale bar = 50 μm. (**B**): Number of cells with nuclear ATF3 staining in the FMS region (delineated with red lines in Figure 3C) are plotted to show inhibition of cell occurrence after SB203580 or SP600125 treatment (n=6-20 sections from 3 spinal cords for each condition). (**C**): Western blots show ATF3 in the nuclear (upper band) and cytoplasmic (lower band) protein fractions from the freshly frozen tissue (FF) or the tissue maintained in vitro for 24 h with or without (SHAM) SB203580 or SP600125 inhibitors. As a positive control, the lysate from RAW 264.7 cells (Abelson murine leukemia virus-induced tumor) is used and the negative control are the results obtained after incubating the ATF3 antibody with the specific blocking peptide prior to immunostaining the Western blot. The loading control for the cytoplasmic fractions was β-actin and for the nuclear fractions TATA binding protein (TBP). (**D**): Intensity of 22 kDa band ATF3 is of the highest value in nuclear lysates from spinal tissue maintained in vitro for 24 h, when compared to fresh tissue or the tissue treated with the inhibitors (P>0.01; data are duplicate experiments for 6 spinal cords for each condition).

Figure 7. ATF3 positive cells after excitotoxic or ischemia-like spinal injury**.** (**A**): ATF3 (red) and nestin (green) double staining of FMS region around the central canal of 30 μm thick sections of spinal cord 24 h after exposure to moderate (1 h long) excitotoxic injury with 50 μM kainate. (**B**): similar experiment as in A using ATF3 and vimentin co-staining, although the toxic stimulus was 1h application of pathological medium (PM) mimicking ischemia conditions. (**C**): very strong excitotoxic stimulus with 1 mM kainate leads to decrease ATF3 signal in the FMS region. (**D**): The number of the cells with nuclear ATF3 staining in the FMS region (delineated with red lines in Figure 3C) is significantly (P=0.005) smaller in 1 mM kainate treated spinal cords with 1 mM kainate (n=6-20 sections from at least 3 spinal cords for each group).

Supplementary Figure 1. Negative control for the Activating transcription factor 3 (ATF3) immunostaining. Sections of P1 rat spinal cord kept for 24 h in Kreb's solution were immunostained with ATF3 antibody (green; upper panels) or with ATF3 antibody pre-incubated with the specific blocking peptide (lower panels). Sections are counterstained with DAPI to shown cell nuclei (original DAPI blue fluorescence is converted to a grayscale for clarity; left panels). The DAPI (blue) and ATF3 signals (green) are merged in the right panels. Note the disappearance of the ATF3 signal after the incubation with the specific blocking peptide. Scale bar= 50 μm.

Supplementary Figure 2. ATF3 staining does not overlap with NeuN, DCX, GFAP, NG2, O4 or CD68 staining. Double immunostaining of ATF3 (red) and different neuronal or glial markers shown in green pseudocolor [NeuN for neurons; doublecourtin (DCX) for neuronal precursors and immature neurons; glial fibrillary acidic protein (GFAP) for astrocytes; NG2 for astrocyte

precursor cells; O4 for oligodendrocytes and their precursors; CD68 for activated microglia] are shown in the ependymal zone of P1 rat transverse spinal cord sections (30 μm thick). Scale bars = 100 μm.

Supplementary Figure 3. The activated, migrating ATF3 cells are nestin, vimentin and SOX2 positive. The central area of the 30 μm thin sections cut from P2 spinal cords maintained for 24 h in Kreb's solution and double immunostained for ATF3 (red) and nestin (**A**), vimentin (**B**) or SOX2 (**C**) (green) is shown. The sections were counterstained with DAPI (blue) to reveal cell nuclei. Scale bars = 100μm in A and 50μm in B and C.

Supplementary Figure 4. Time course of ATF3 activation in spinal cord motoneurons maintained in vitro. Thirty μm sections from P2 rat spinal cords maintained in vitro for 0-24 h were immunostained for ATF3. (**A**): Images are from the ventral horn area that contains motoneurons. The fluorescent ATF3 signal is converted to a grayscale signal, the negative of which is shown for clarity. Note absence of nuclear signal and presence of cytoplasmic ATF3 with peak at 4h. (**B**): Spinal cord section comprising motoneurons (left side) and ependymal cells (right side) stained for ATF3. At 4 h (left panel) cytoplasmic ATF3 staining is observed in motoneurons and the ependymal region. At 24 h (right panel), ATF3 signal disappears from motoneurons, while the signal becomes nuclear in the ependymal cells that migrate from the central canal (CC) versus ventral funiculus in an ordinate chain formation. (**C**): Motoneurons are shown with SMI32 immunostaining (green) as large cells in the ventral horn of the spinal cord kept in vitro for 24 h. The section is counterstained with DAPI to visualize cell nuclei. Note good preservation of star-like motoneuronal cells. Scale bar = 100 μm.

Figure 1

Click here to download high resolution image

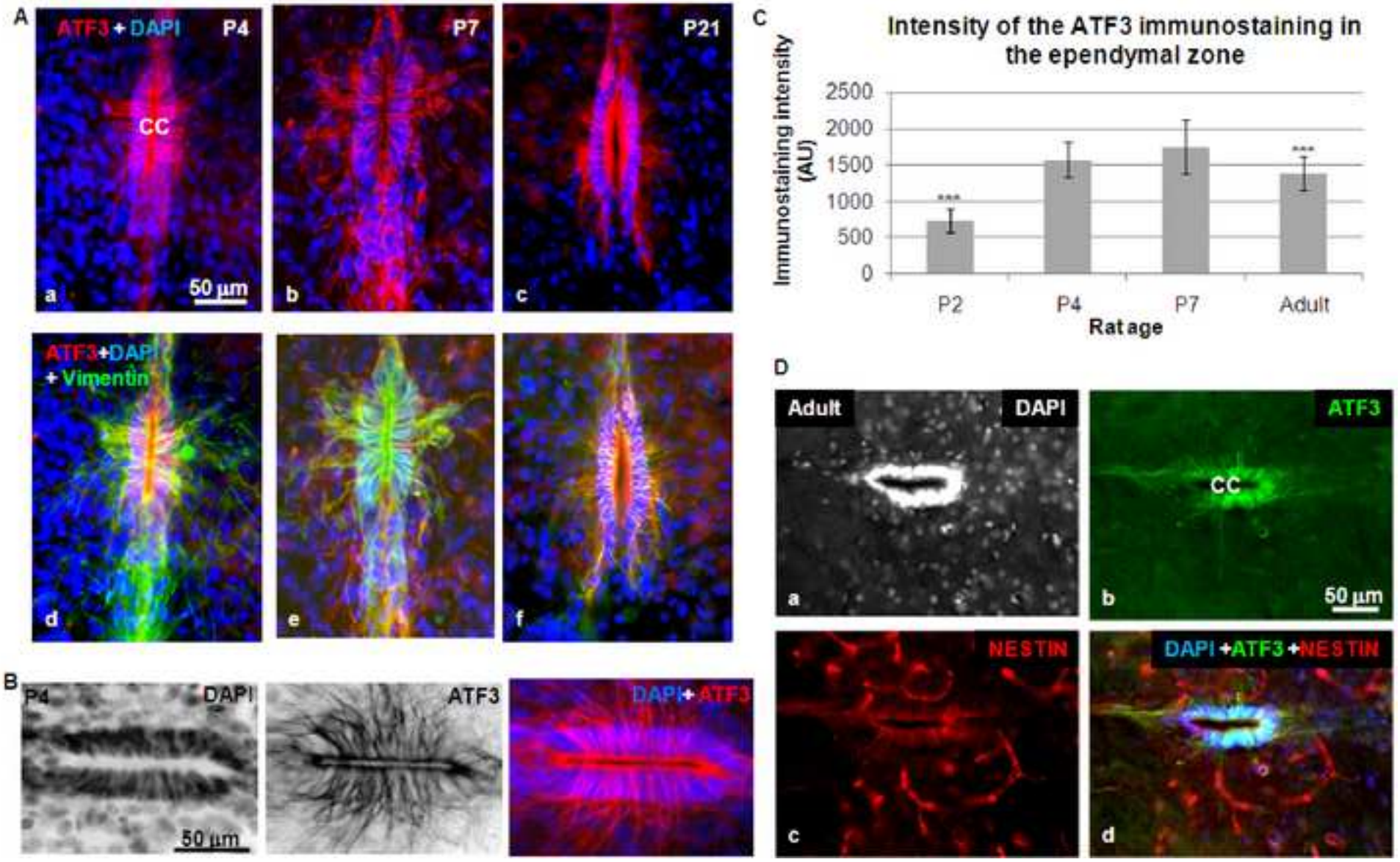

Figure 2

Click here to download high resolution image

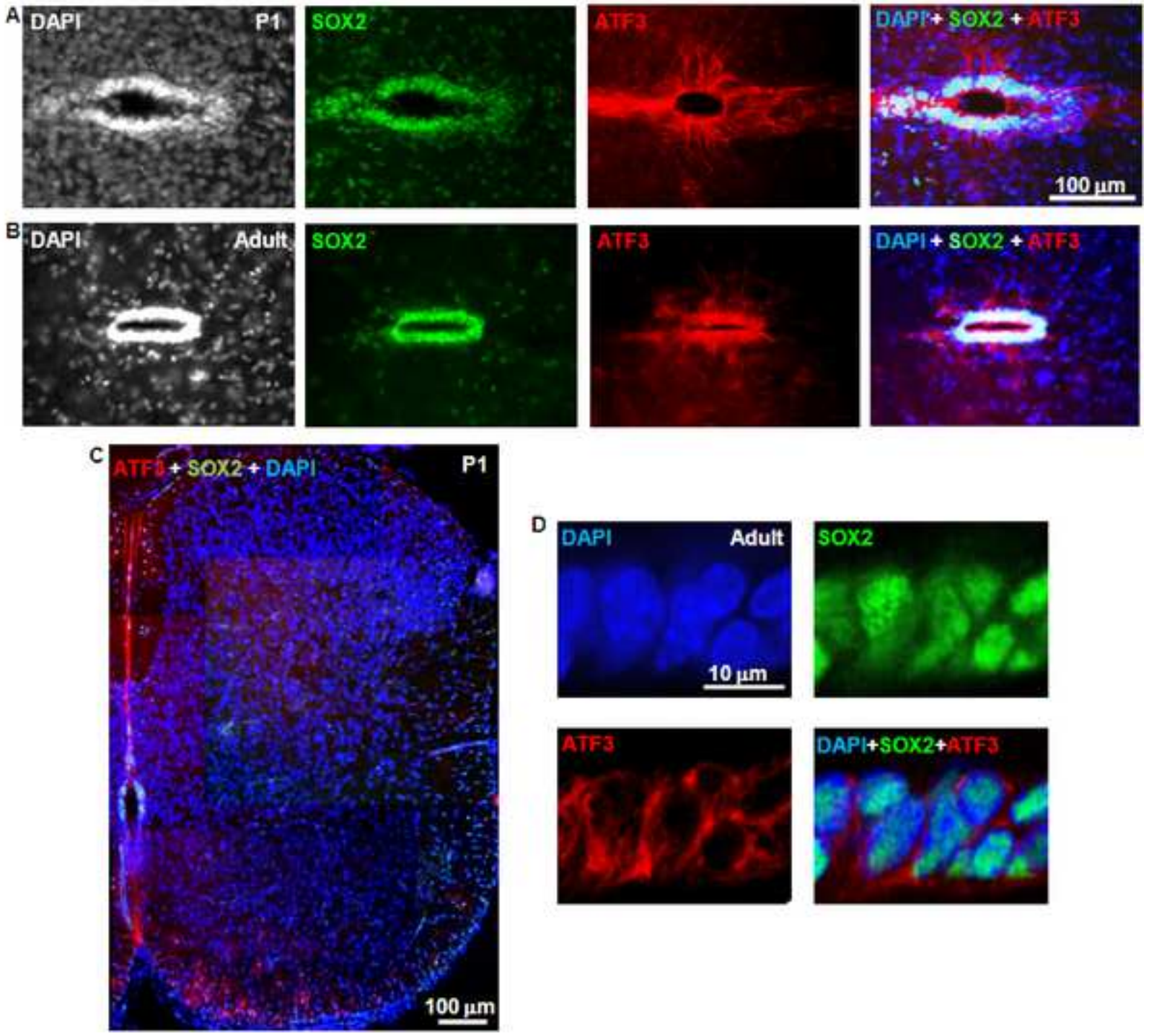

Figure 3

Click here to download high resolution image

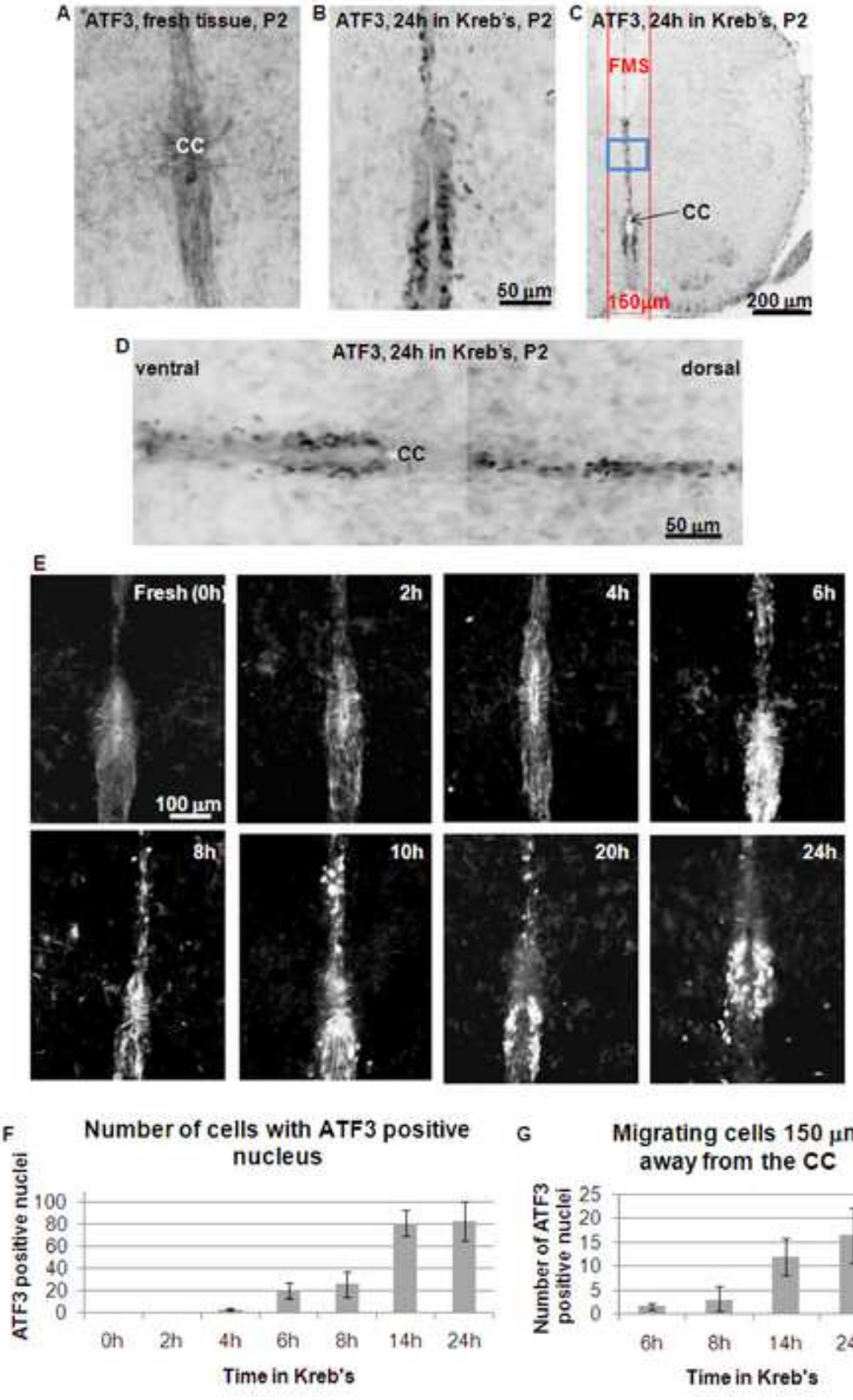

Figure 4

Click here to download high resolution image

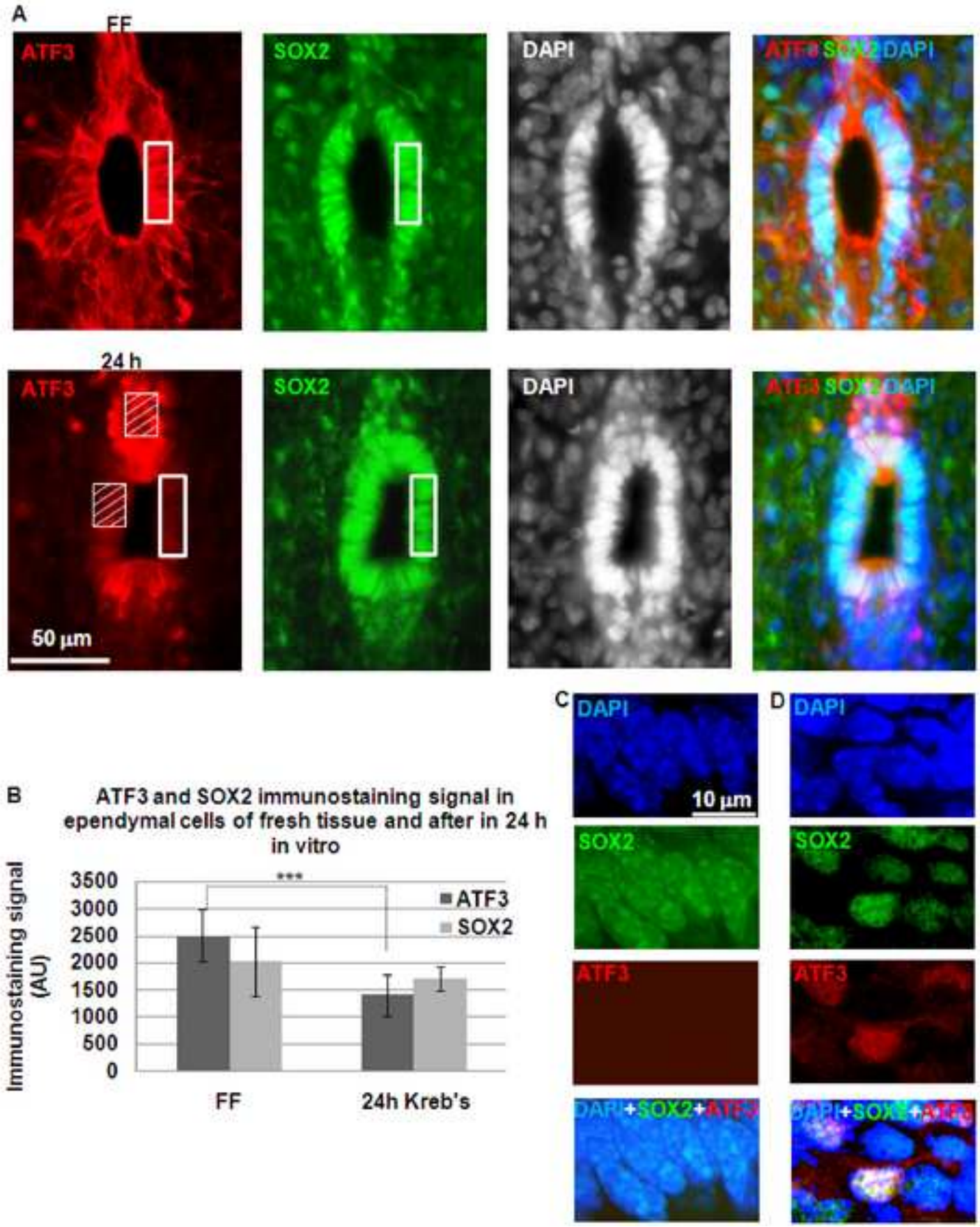

Figure 5

Click here to download high resolution image

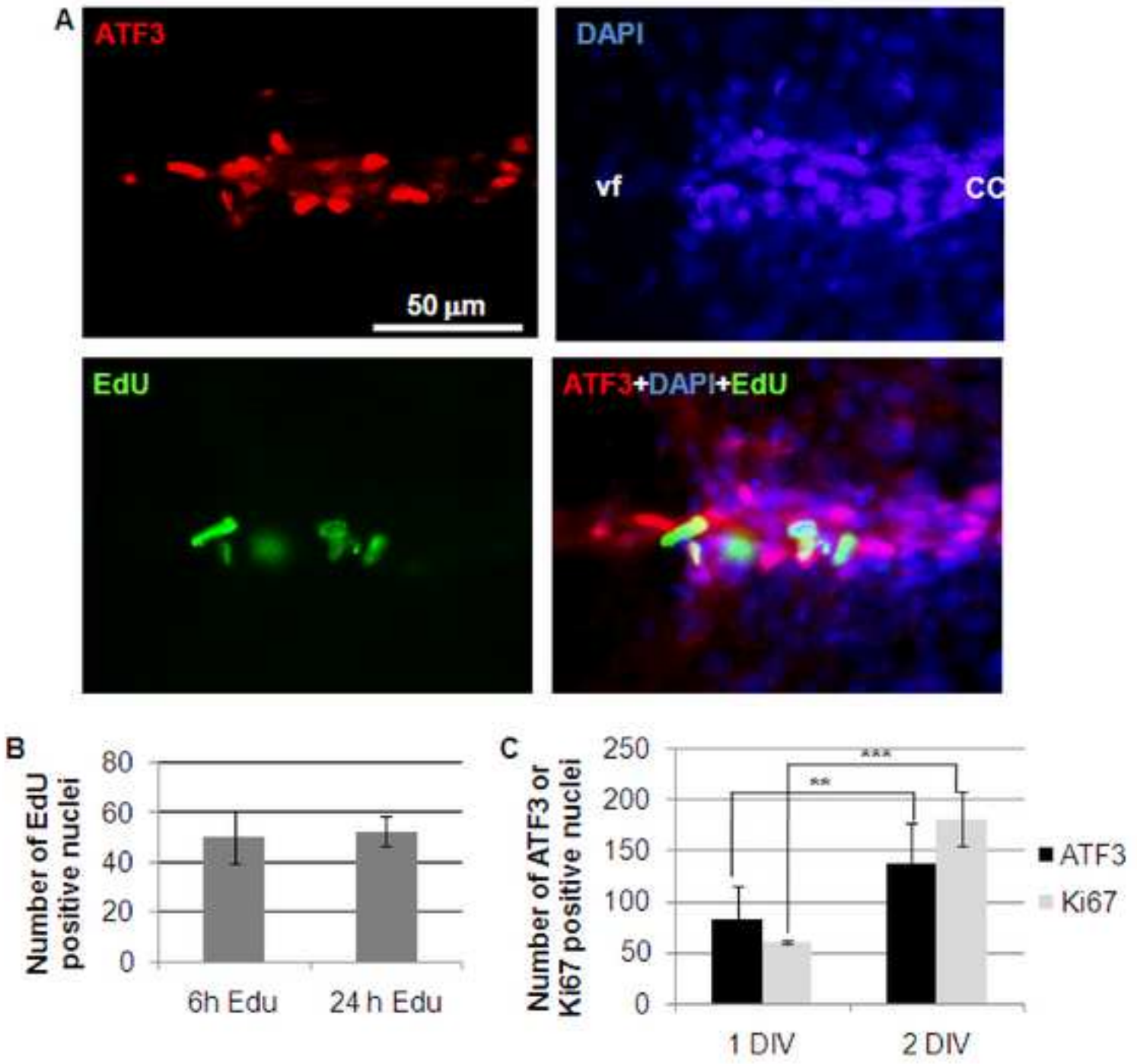

Figure 6

Click here to download high resolution image

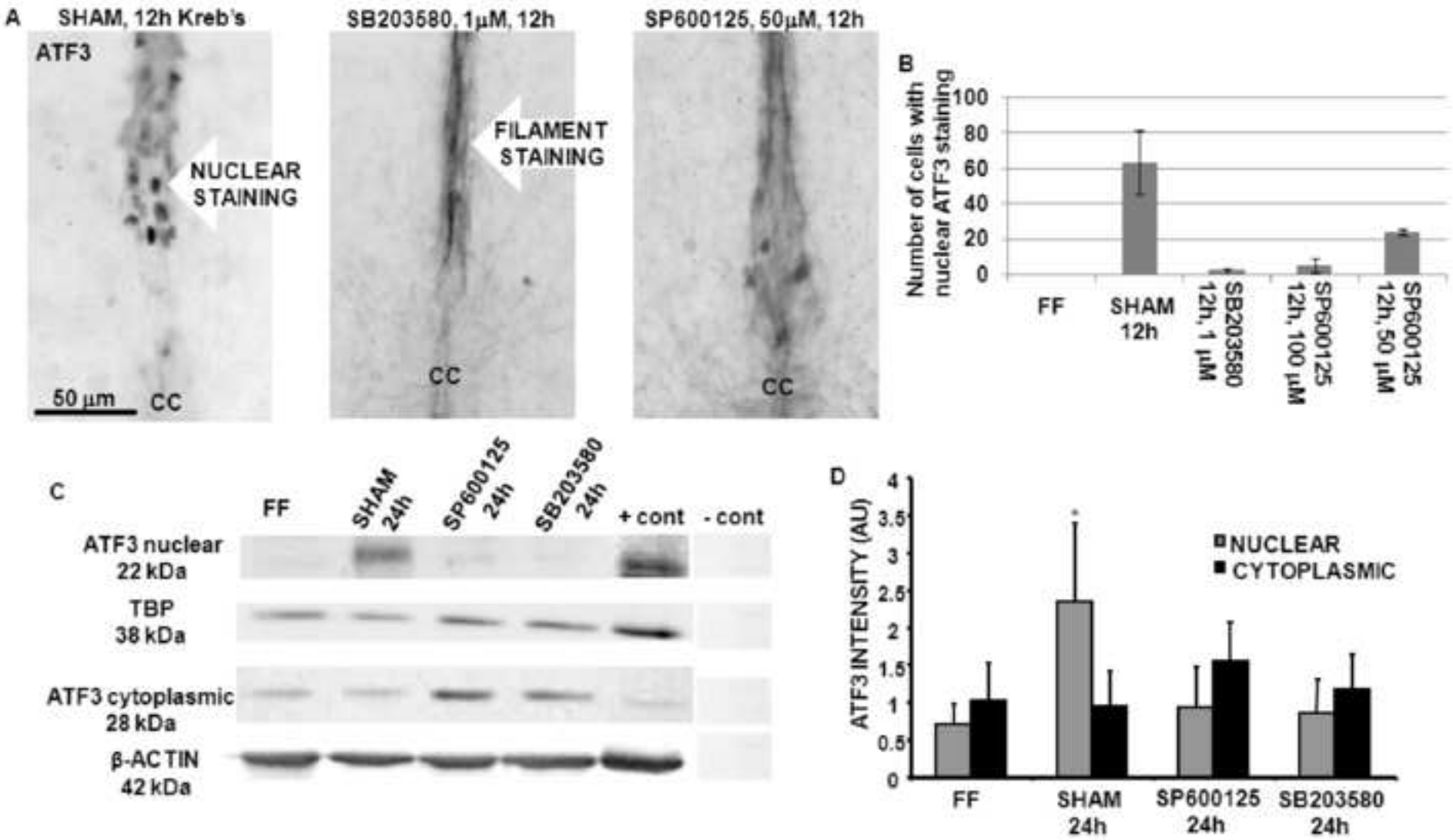

Figure 7

Click here to download high resolution image

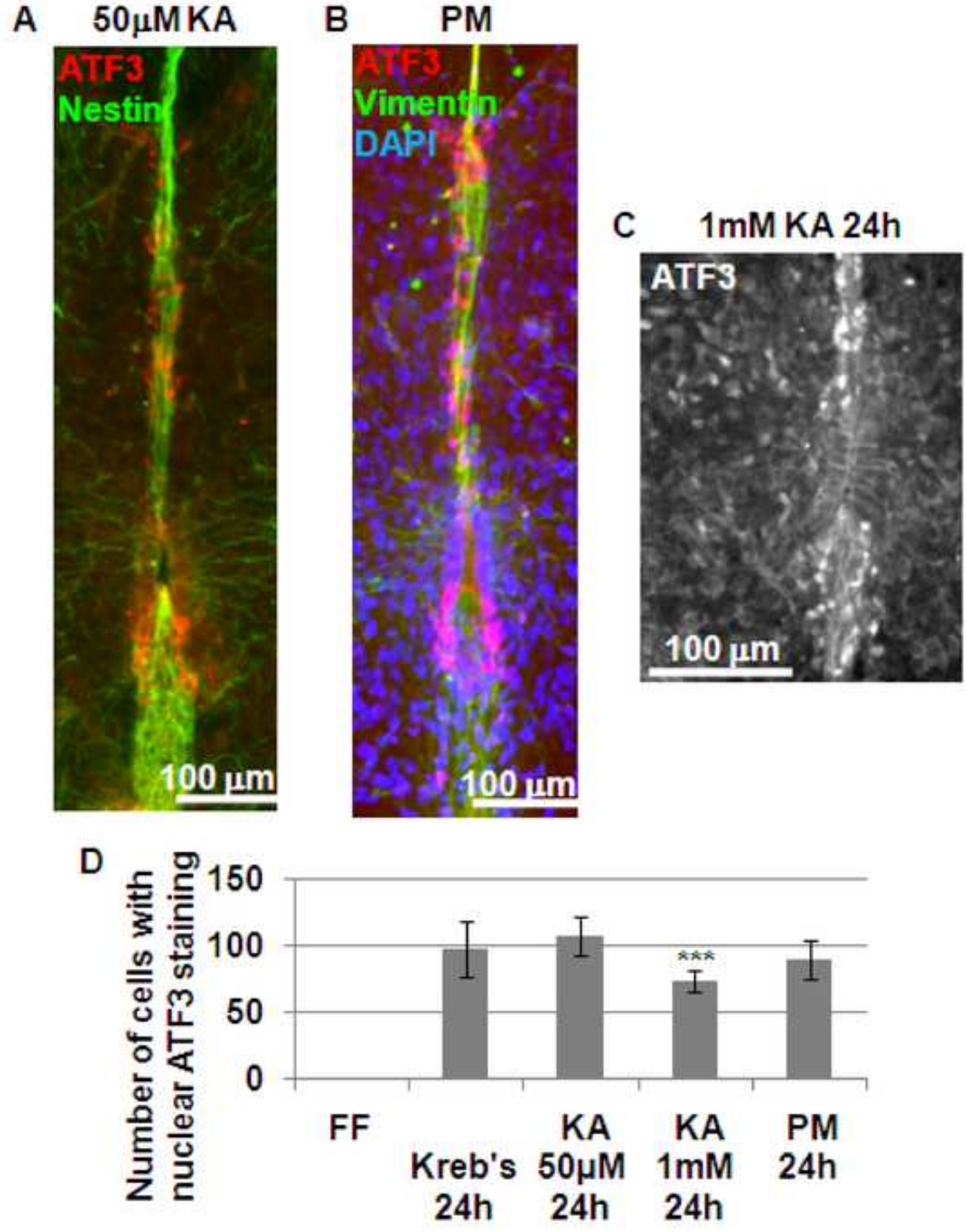

Supplemental Table 1. Antibodies used for immunofluorescent staining

Name	Company	Code	Type	Dilution
ATF-3 (C-19)	Santa Cruz Biotech	sc-188	rabbit polyclonal	1:200
CD68	Abcam	ab31630	mouse monoclonal	1:750
DCX Doublecourtin	Santa Cruz Biotech	sc-8066	goat polyclonal	1:20
GFAP Glial fibrillary acidic protein	Sigma	G3893	mouse monoclonal	1:200
Ki67	Abcam	ab15580	rabbit polyclonal	1:100
Nestin	Millipore	MAB353	mouse monoclonal	1:100
NeuN	Millipore	MAB377	mouse monoclonal	1:50
NG-2	Millipore	AB5320	rabbit polyclonal	1:100
Oligodendrocyte Marker O4	R&D Systems	MAB1326	mouse monoclonal	1:200
SOX2,	Abcam	ab79351	mouse monoclonal	1:1000
Vimentin	Abcam	ab8069	mouse monoclonal	1:100
SMI32	Millipore	NE1023	mouse monoclonal	1:200

Supplemental Figure 1

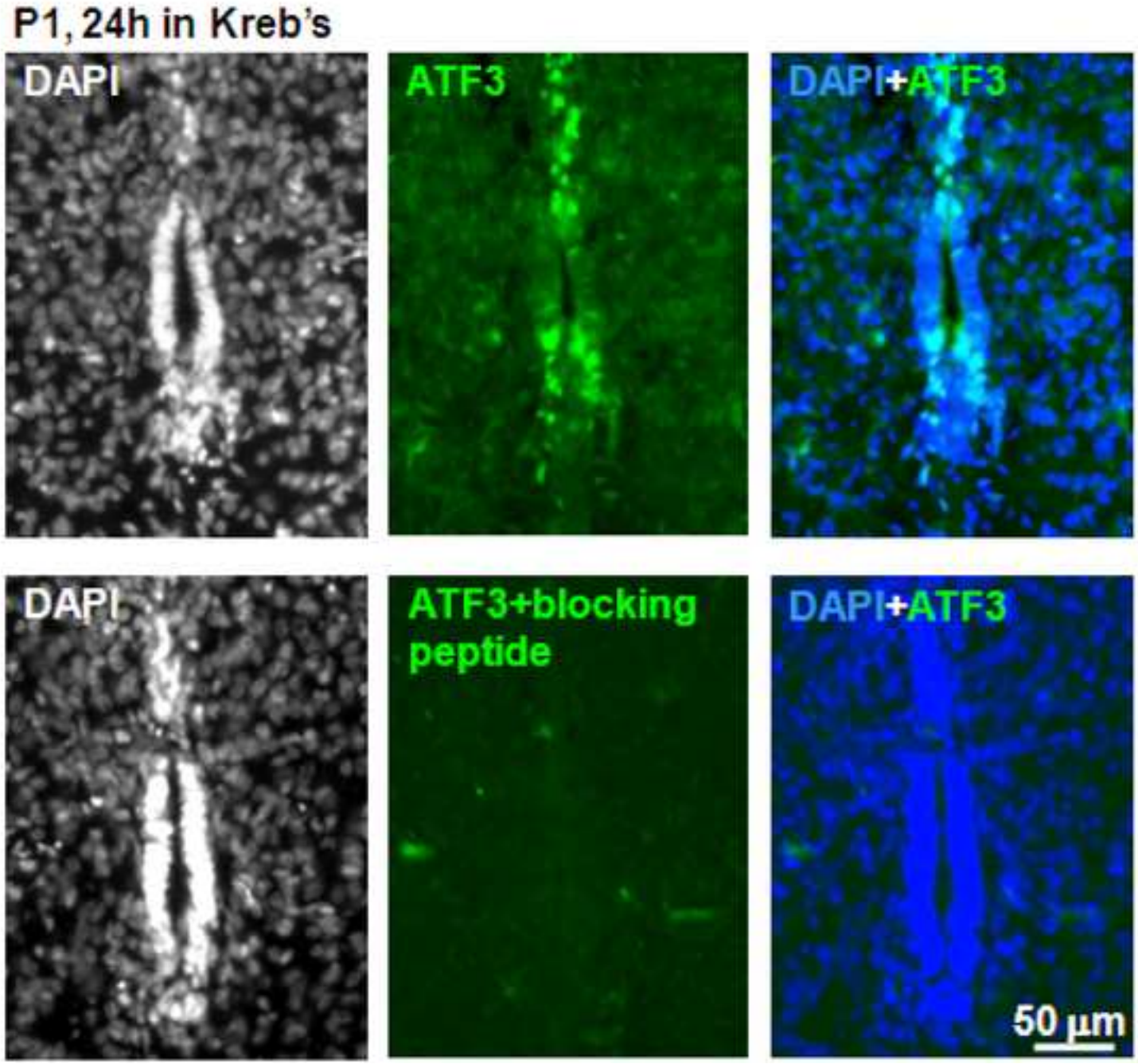

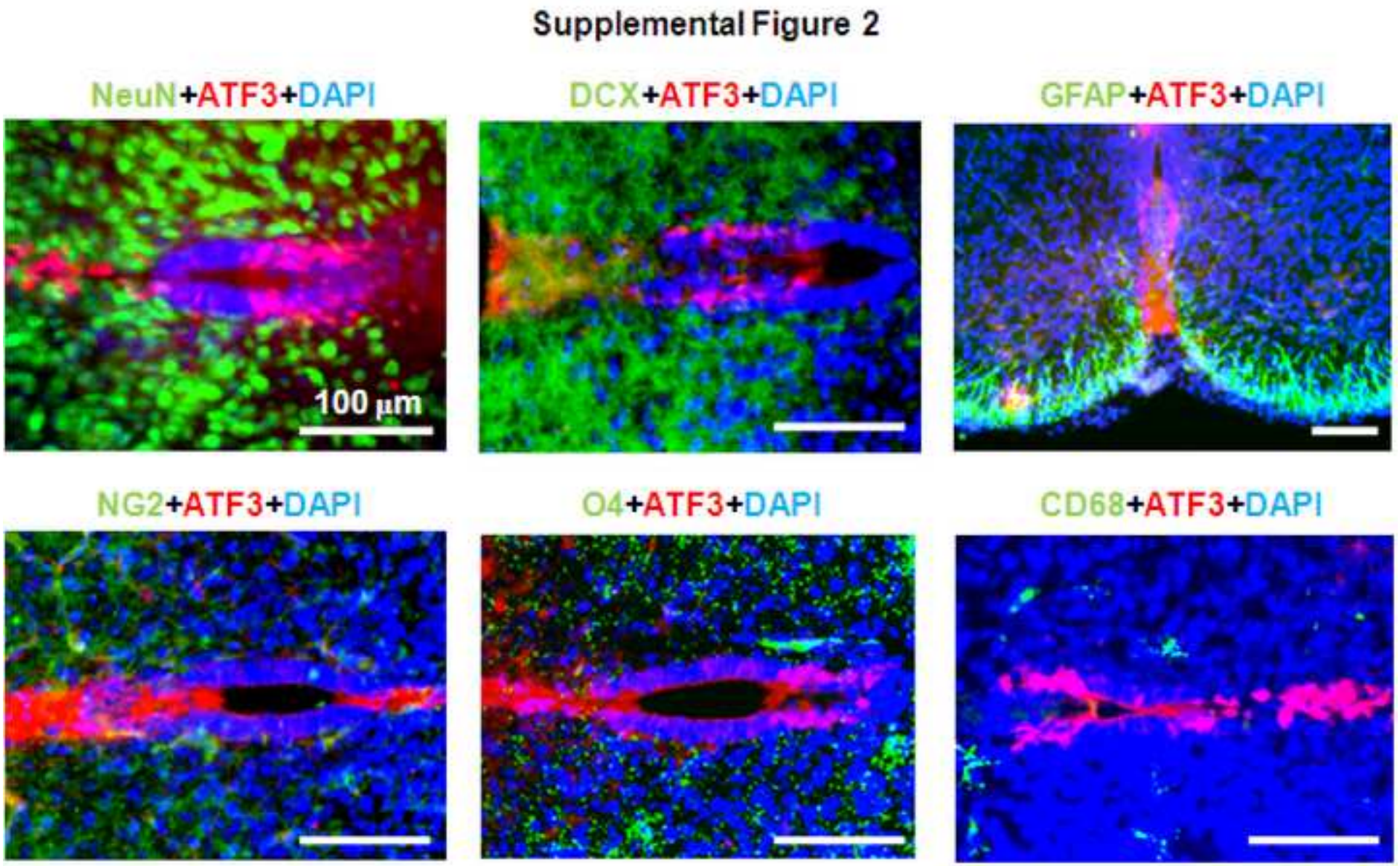
Supplemental Figure 2
NeuN+ATF3+DAPI
DCX+ATF3+DAPI
GFAP+ATF3+DAPI
100 μm
NG2+ATF3+DAPI
O4+ATF3+DAPI
CD68+ATF3+DAPI

Supplemental Figure 3

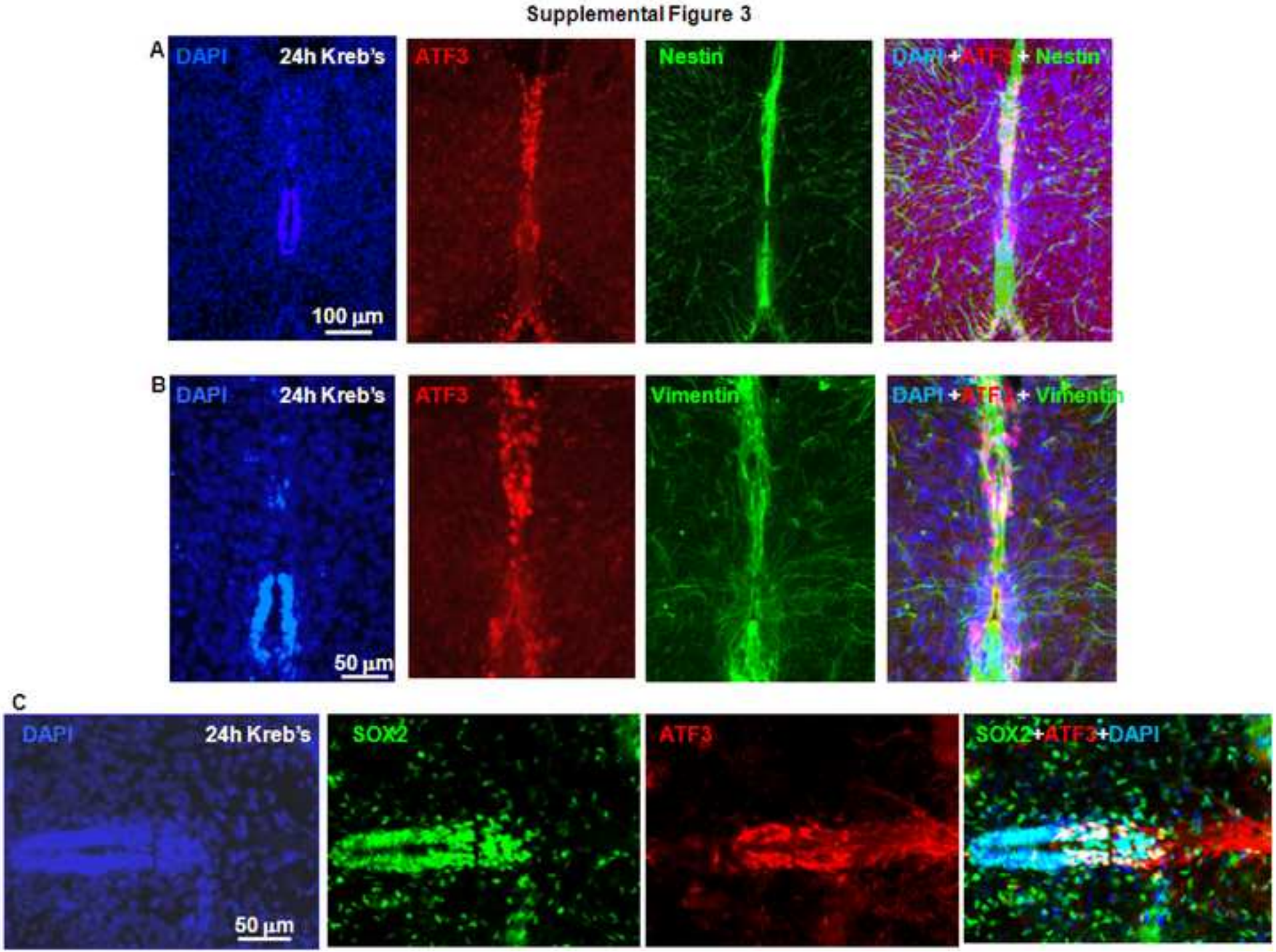

Supplemental Figure 4

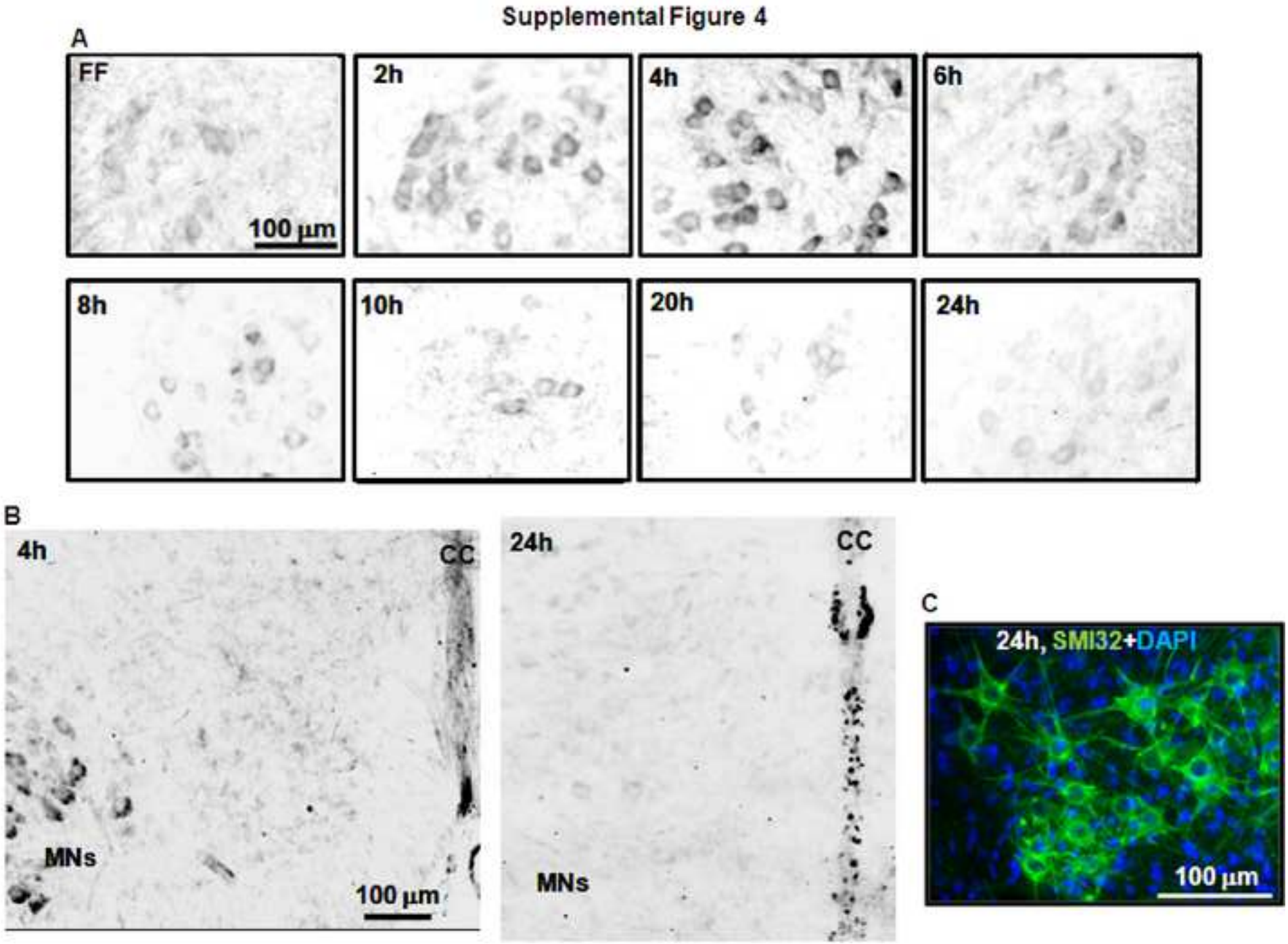

DISCUSSION

In relation to the aims of my project, I achieved the following points:

The principle focus of the present study was understand the role of extracellular Mg^{2+} in the genesis of neurotoxicity after transient application of a medium mimicking ischemia-anoxic conditions. The present data indicate that the presence of this divalent cation contributed to enhance the delayed damage to the white matter spreading it to the grey matter of the rat spinal cord via distinct cell death pathways. The addition of Mg^{2+} to the Kreb's solution did not lead to damage, indicating that this ion is not toxic by itself but it worsens an ischemic-like condition. We investigated the potential TRPM2 and TRPM7 involvement in the damage mediated by Mg^{2+}, and found a significant dichotomy in TRPM7 and TRPM2 channel expression. In order to find new neuroprotective or/and neuroregenerative strategies, we tested the potential neuroprotective effect of PARP-1 inhibitors on SCI models and we probed the efficacy of ATF3 as a marker for the migration of ependymal stem cells of the spinal cord.

A model of non-traumatic injury has been developed in our laboratory. Non-traumatic causes of SCI are recently incrising in number and importance (van den Berg et al., 2010; McKinley et al., 2002; Nair et al., 2005; Sekhon and Fehlings, 2001). This point led us to develop a specific rat model, in order to examine the processes responsible for cell death early after the insult. This is a difficult goal with *in vivo* preparations, due to the need of anesthesia, the difficulty to induce metabolic perturbations targeted to a specific region of the spinal cord and complexity of electrophysiological analysis. Therefore, we have recently employed an *in vitro* model that can express electrical oscillations typical of locomotion and can allow detailed analysis of the underlying pathophysiological mechanisms (Kuzhandaivel et al., 2011; Mladinic and Nistri, 2013). This i*n vitro* model is largely versatile, permitting to study a particular process underlying injury, such us excitotoxicity or ischemia-like tests. After an excitotoxic damage induced by Kainate, an analog of glutamate (Taccola et al., 2008), we have observed that neurons are the most affected, rather than white matter in which the damage is limited, and the principle mechanism leading to neuronal death is parthanatos (Kuzhandaivel et al., 2010a). Different concentrations of KA, from 1 to 1000 µM, were tested; KA at the concentration of 50 µM is already sufficient to induce an irreversible loss of fictive locomotion even if spinal reflexes persist (Mazzone et al., 2010). Conversely, white matter elements are the most affected by the methabolic perturbation evoked in our model by PM, a toxic solution

containing free oxygen radicals with no oxygen or glucose supply (Taccola et al., 2008). It has also been demonstrated by previous experiments done in our lab that the predominant mechanism by which white matter dies after PM insult is apoptosis (Kuzhandaivel et al., 2010b). After PM, the grey matter region is more preserved compared to white matter, with moderate impairment of locomotor-like patterns that were still present at regular frequency, but with clearly lower amplitude (Margaryan et al., 2009; Taccola et al., 2008). Nonetheless, the addition to the PM solution of standard extracellular Mg^{2+} concentration of 1 mM is enought to worsen the white matter lesion and to extend the histological damage to neurons (Bianchetti et al., 2013; Margaryan et al., 2009), with the inhibition of the locomotor patterns (Margaryan et al., 2009). Data collected during my PhD sought to characterize the processes responsible for this damage enhancement.

PM+Mg^{2+} extends damage of white matter elements. The original PM medium (without Mg^{2+}) produces a strong damage in the white matter. The addition of Mg^{2+} worsened this damage, inducing pyknosis in about 80 % of white matter elements. This pyknosis was accompanied by early phosphohistone positivity, indicating an ongoing DNA damage (Plesca et al., 2008). Caspase 3, the tipical marker of apoptosis (Cohen, 1997), was evident in a small persentage of white matter cells only. In keeping with this view was our observation that a pharmacological inhibitor of apoptosis, named the caspase-3 inhibitor (Vandenabeele et al., 2006), arrested pyknosis in the 5% only of the total white matter cells. Almost half of the white matter elements showed positivity for PAR, indicating a switch of cell death mechanism from apoptosis after PM application to parthanatos after PM+Mg^{2+}. In fact, the caspase-3 inhibitor reduced cell death when it was coapplied with PJ34, an inhibitor of PARP-1 (Abdelkarim et al., 2001). While PARP-1 is essential for DNA damage repair, its hyperactivation generates the toxic product PAR (Abdelkarim et al., 2001; Andrabi et al., 2006; Berger, 1985; Yu et al., 2006). PAR increased strongly already 3 h after the end of PM+Mg^{2+} application suggesting a narrow time window before irreversible cell damage could occur. Co-localization of PAR and pyknosis supported this hypothesis. Neuroprotection remained, however, incomplete probably for a variety of reasons like rate of access of exogenous drugs to intracellular targets, speed of lethal cascade reactions, and multiple effectors of cell damage. In general, the present results suggest that the presence of Mg^{2+} during the ischemic-anoxic like protocol aggravated the damage to the white matter cells by promoting the activation of at least one major cell death pathway, namely parthanatos (David et al., 2009).

PM+Mg^{2+} extended the damage to the grey matter. It was interesting that grey matter elements were much less sensitive to PM+Mg^{2+} damage than white matter ones. Morphological analysis indicated low-scale pyknosis and persistence of most NeuN positive neurons, even though the damage was relatively more intense in the ventral horn area. The number of motoneurons, however, did not decrease, as their typical marker ChAT was preserved even 24 h later. These cells were, nevertheless, showing sign of distress because the intensity of SMI32 signal was decreased, suggesting an ongoing damage of their cytoskeleton. It is interesting to note that, shortly after a metabolic insult, the SMI32 signal decreased despite unaltered expression of ChAT, whereas a traumatic lesion *in vivo* is associated with loss of ChAT followed by hyperexpression of SMI32 by surviving motoneurons, taken as an index to cell repair (Penas et al., 2009). The differential expression of ChAT and SMI32 in the present study compared to the *in vivo* experiments could be due to the motoneuronal maturation. However, neonatal motoneurons already show somatic size (Carrascal et al., 2005) and there is evidence asserting that in the *in vitro* rat spinal cord the number of SMI32- and ChAT- positive cells and their staining pattern remain constant during the first week of life (Cifra et al., 2012). Hence, dynamic changes in these biomarkers may indicate distinct processes and timecourse of degenerative mechanisms and restoration. AIF-dependent cell death mediates neuronal death after hypoxia-ischemia in the neonatal rat brain (Zhu et al., 2003) like in the adult rat brain (Wang et al., 2009). In our PM+Mg^{2+} model too, concomitant with the fall in SMI32 signal, was the detection of rising PAR immunoreactivity in the same cells. This was likely a sign of an ongoing damage, in fact it was accompanied by strong AIF translocation into the nucleus, a known effector of cell death by parthanatos (Yu et al., 2006). It was interesting that AIF translocation into the nucleus was closely associated with loss of NeuN positivity, an intrinsic component of the neuronal nuclear matrix indeed (Dent et al., 2010). The degradation of the neuronal nuclear matrix occurs already at 1 h after injury (Giordano et al., 2005) so it precedes cytoscheletal changes (observed in our studies by a SMI32 staining) in injured motoneurons (Penas et al., 2009). These results imply that various motoneuron biomarkers should be tested for assessing damage in pathological conditions as their significance for diagnosis of cell death is time-dependent. Thus, our view is that the development of parthanatos in motoneurons occurred on a slower time base than in the white matter, maybe due to the more complex methabolism of large cells such as motoneurons. Nonetheless, these pathological changes have a strong negative impact on locomotor network function (Margaryan et al., 2009).

TRPM2 and TRPM7 role in the PM+Mg^{2+} effects. TRPM2 and TRPM7 are membrane channels recently investigated for their contribution to ischemic cell death in the brain under a variety of experimental conditions (Aarts and Tymianski, 2005a, 2005b; Aarts et al., 2003; Sun et al., 2009). These channels show persistent permeability to mono and divalent cations, whose influx is believed to trigger neuronal death mechanisms. In normal conditions they are minimally activated, as they are gated open by various ions and agents including intracellular PAR, reactive oxygen species and Mg^{2+} (Aarts and Tymianski, 2005b; Chen et al., 2012; Cook et al., 2009; Kühn et al., 2005; Scharenberg, 2005). Because of their ability to respond to PAR and Mg^{2+}, both of them present in our experimental model, and because of their involvement in the ischemic damage, we decided to investigate how these channels were expressed during our experimental protocol. Evidence in the literature reports the ubiquitous occurrence of TRPM7 expression (Penner and Fleig, 2007), therefore their immunohistochemical absence in the white matter under sham conditions was not anticipated. Analogous lack of signal was found when the tissue was immediately put in PFA (for the istological analisis) after dissection, so we exclude that this phenomenon could be attributed to loss of protein expression by keeping the preparation *in vitro*. It seems probable that a factor for poor TRPM7 expression was the immaturity of the neonatal spinal cord; however, already 3 h after PM+Mg^{2+} exposure, a large number of white matter cells, characterized by pyknotic nucleus, were positive to TRPM7. Our interpretation is that metabolic distress in the presence of Mg^{2+} triggered rapid trafficking of TRPM7 proteins to the cell membrane where their activation might have contributed to the observed damage. This will have to be studied with membrane biotynilation experiments. Unlike white matter cells, motoneurons and other spinal neurons showed baseline expression of TRPM7 that was decreased lately after PM+Mg^{2+} when pyknosis was not yet manifested. The reason for the differential timecourse of TRPM7 expression between white and grey matter remains obscure. However, we observed, in the case of TRPM2 expression, a mirror-like situation whereby late fall in TRPM7 corresponded to late rise in TRPM2 in grey matter neurons, especially strong in central region, whereas large increment of TRPM7 in white matter corresponded to lack of detectable TRPM2 expression. It is important to note that the intensity of immunoreactivity cannot be related to channel activation, so the present results about differential TRPM7 and TRPM2 signal intensities cannot be extrapolated to a specific role of these proteins in neuronal survival or death. Despite this limitation, the present results indicate a significant dichotomy in TRPM7 and TRPM2 channel expression, whose molecular mechanism remains to be clarified through future studies. Unfortunately,

investigating the functional activity of TRPM2 or TRPM7 channels under our experimental protocols is, however, complex because of the difficulty to isolate, in an intact network system, the contribution of these conductances, especially in the absence of selective inhibitors, the widespread dysfunction of motoneurons and the lack of knockout rat models. As TRPM2 channels are inhibited by intracellular glutathione (Belrose et al., 2012), TRPM2 overexpression was perhaps related to metabolic dysfunction that developed early for superficially located motoneurons. The effects of the toxic solution on deep central neurons were likely delayed with morphological preservation of such cells that had shown the strongest TRPM2 expression. One hypothesis is that the TRPM2 activation would eventually lead to central neuron damage occurring at a time point beyond the 24 h *in vitro* survival of the isolated spinal cord, and thus outside our experimental range. In analogy with data from brain neurons under *in vitro* ischemia-like conditions, we may propose that persistent activation of TRPM2 channels in spinal neurons could determine a long-lasting rise in intracellular free Ca^{2+} and Mg^{2+} to activate cell death pathways. Since TRPM2 channels are characterized by small conductance (Kühn et al., 2005), it would follow that a small scale influx of these cations might determine the delayed trigger of parthanatos.

Role of extracellular Mg^{2+} during ischemia-anoxia. Various clinical and *in vivo* animal studies have shown that, during brain ischemia, there is an early and reversible fall in the extracellular Mg^{2+} concentration of the cerebrospinal fluid (Lin et al., 2004; Wei et al., 2007). Longitudinal clinical studies have actually reported that the administration of Mg^{2+} in various injury models including acute stroke, SCI in rabbit and traumatic brain injury might has negative effect on the injury outcome (Maas and Murray, 2007; Muir et al., 2004; Saeki et al., 2004; Temkin et al., 2007). Analogous observations for the rat spinal cord were not available prior, till our investigations (Bianchetti et al., 2013). From the point of view of an *in vitro* model, it is apparent that the standard concentration (1 mM) of Mg^{2+} led to tissue damage, amplified the white matter lesion and extended it to the grey matter. The reason for this diversity of damage sensitivity, between white and grey matter, remains unclear and might be related to differential expression of TRPM7 and TRPM2 expression as well as to the degree of PAR hyperproduction at an early stage. PAR and Mg^{2+} are in fact potent modulators of the activity of these channels (Aarts and Tymianski, 2005b; Xie et al., 2010). Recent studies with *in vitro* brainstem neurons have proposed that changes in intracellular Mg^{2+} concentrations occurring during pathological states can affect the conductance of neuronal Cx36 gap junctions48 (Palacios-Prado et al., 2013) and can

presumably shape the damage outcome. Although chemical synaptic inputs and Cx36-dependent electrical synapses contribute to synchronization of spinal motoneuron function (Tresch and Kiehn, 2002), the expressions of Cx36 and Cx32 mRNA and proteins are sparse and unchanged after rat SCI (Lee et al., 2005). Notwithstanding the resolution of this issue, the present study suggests potential risks in administering Mg^{2+} during early ischemia-anoxia of the spinal cord as tissue damage might actually increase (Bianchetti et al., 2013), in accordance with reports of the lack of effectiveness of Mg^{2+} administration on rabbit ischemic spinal injury (Saeki et al., 2004). Such clinical results have actually shown that many patients receiving Mg^{2+} infusion fared worse than untreated patients, a result unexpectedly found also for stroke patients (Muir et al., 2004). In conclusion, the complexity of the processes underlying ischemia-anoxia damage in the spinal cord even when studied with an *in vitro* model, implies diversity of molecular pathways with distinct time dependence and cell-specificity, factors that contribute to the difficulty of implementing successful neuroprotection *in vivo* (Faden and Stoica, 2007; Savitz and Fisher, 2007; Thuret et al., 2006). The present study suggests that the phisiological extracellular level of Mg^{2+} during an ischemic damage largely affects cell death mechanisms in the spinal cord and extends damage to motoneurons by facilitating the onset of parthanatos.

Neuroprotection tested in our *in vitro* model. Overactivitation of PARP-1 is suggested to be a major contributor to neuronal damage following brain or spinal cord injury. Thus, we investigated the PARP-1 inhibitor PJ34 (Abdelkarim et al., 2001; Kauppinen et al., 2009) as a neuroprotective agent. Unexpectedly, preliminary electrophysiological experiments showed that, under control conditions, 1-60 μM PJ34 per se strongly increased spontaneous network discharges occurring synchronously on ventral roots, persisting for 24 h even after PJ34 washout. Another PARP-1 inhibitor named PHE (6-5(H)-phenathridinone; Nasrabady et al., 2011b; Kuzhandaivel et al., 2010a) had no similar effect. These discharges were fully dependent on ionotropic glutamate receptor activation, because this action by PJ34 was reversibly suppressed by glutamate receptor blockers and remained after applying strychnine and bicuculline. Fictive locomotion evoked by neurochemicals or by dorsal root stimulation was present 24 h after PJ34 application. In accordance with this observation, lumbar neurons and glia were undamaged. Neurochemical experiments showed that PJ34 per se produced up to 33% inhibition of synaptosomal glutamate uptake with no effect on GABA uptake. In keeping with this result, the glutamate uptake blocker TBOA (5 μM) induced long-lasting synchronous discharges

without suppressing the ability to produce fictive locomotion after 24 h. The novel inhibition of glutamate uptake by PJ34 suggested that this effect may compound tests for its neuroprotective activity which cannot be merely attributed to PARP-1 block. Furthermore, the data published by Nasrabadi et al., (2012) indicate that the neonatal rat spinal cord could withstand a strong, long-lasting rise in network excitability without compromising locomotor pattern generation or circuit structure in contrast with the damage to brain circuits known to be readily produced by persistent seizures. As our results after the addition of PM+Mg^{2+} showed the presence of parthanatos even in grey than in white matter, PJ34 was added during the washout after PM+Mg^{2+} insult, in order to neuroprotect the SCI immediately after damage. As we expected, it decreased significantly the piknosis at 24 h, above all in the white matter elements. The SCI condition seemed to be improved especially when PJ34 was administered in association with caspase-3 inhibitor, protecting the spinal cord from the induction of apoptosis and parthanatos by the PM+Mg^{2+} insult. Further experiments have to be done, in order to understand if this result is associated with an electrophysiological improvement too. Previous results demonstrated that, when PJ34 is administered early during the lesion protocol, a degree of neuroprotection is observed (Nasrabady et al., 2011a) in accordance with the present data.

ATF3 as a marker for migrating ependymal stem cells. The manuscript presently under review, is the first report of the dynamic expression of the ATF3 by ependymal spinal stem cells. In our experimental conditions, this protein was localized to the cytoplasm when such cells were quiescent, but was found in their nucleus when cells became activated. This property enabled us to follow up activated ependymal cells that migrated from the central canal toward the ventral and dorsal white matter, forming the funicular migratory stream (FMS) that resembles the rostral migratory stream (RMS) of the brain neural brain stem/progenitor cells (SPCs). The fact that ATF3 immunostaining coincided with well-known SPC markers, such as nestin, vimentin and SOX2, suggests that ATF3 labeling in the spinal cord was primarily expressed by intrinsic stem cells, typically found around the central canal (Hugnot and Franzen, 2011). Although virtually absent in embryonic and P0 ependymal cells, ATF3 was mainly expressed in the cytoplasm and processes of these cells from P1 onwards, grew during the first postnatal week and remained elevated later with a small decrement only. Such ATF3 stained cells in fresh tissue had small diameter, large egg-shaped nucleus, and were closely packed together. However, grey matter cells remained devoid of ATF3 staining, adding specificity to the role of this protein for stem cell labeling.

Role of ATF3 in the regulation of SPCs. There is lack of information on ATF3 in the regulation of SPCs. Recent evidence (Gao et al., 2013; Gargiulo et al., 2013) shows the involvement of ATF3 in the control of genes like SOX2 or BMI1. These genes are critical for pluripotency and reprogramming of the human embryonic stem cells or glioblastoma stem-like cells, and ATF3 and SOX2 co-staining seen in the present study supports this hypotesis. Moreover, the CREB transcription factor family, of which the ATF3 is a member, has an established role in the SPC regulation and neurogenesis (Mantamadiotis et al., 2012; Merz et al., 2011). Our speculation, thus, includes a new role of ATF3 not only in the maintenance of the spinal ependymal cells but also in their activation.

***In vitro* conditions induce mobilization of stem cells.** When spinal cords were kept *in vitro* for 24 h, we observed a novel phenomenon, namely centrifugal mobilization of ependymal stem cells which formed a migratory chain analogous to the brain RMS (Lois et al., 1996; Tanvig et al., 2009; Wichterle et al., 1997) as they moved away from the central canal to the adjacent ventral and dorsal white matter. When this occurred, ATF3 was clearly expressed in the cell nucleus. This phenomenon developed gradually after 4 h and was clearly observed at 24 h. Interestingly, ependymal cells which did not mobilize, retained their SOX2 nuclear staining, yet lost the ATF3 cytoplasmic one. Hence, ATF3 nuclear labeling could be interpreted as a novel marker of migrating ependymal cells. The fact that *in vitro* conditions induce mobilization of stem cells has been earlier reported with organotypic brain slices (Tanvig et al., 2009): in such case RMS toward the olfactory bulb is occurring after several days, while the present report shows a much faster process developing within hours. The unchanged occurrence of Ki67 or EdU positive cells in FMS at 24 h *in vitro* is consistent with a process of ependymal cell mobilization rather than proliferation that occurs at later time. In support of this hypothesis is the recent observation that, in rat organotypic slices, significant proliferation of neuroprogenitors was detected only after a few days in culture (Mazzone et al., 2013). Spinal networks are fully preserved and viable during this timeframe, including electrophysiological activity of locomotor networks (Taccola et al., 2008), so we focused our attention on the mechanisms responsible for activation and mobilization of ependymal cells *in vitro*. *In vivo* ependymal cells are in direct contact with the cerebrospinal fluid (CSF) and numerous blood vessels (Hugnot and Franzen, 2011). Thus, their delayed activation *in vitro* might be due to the disappearance of yet-unclear signals from the CSF or blood (Menezes et al., 2002), which might normally keep the ependymal cells quiescent (Cheung and Rando, 2013). Additionally, the activating signal might come from a few cells injured during dissection,

even if systematic analysis of *in vitro* tissue showed minimal pyknosis at 24 h *in vitro* (Taccola et al., 2008). A recent review has highlighted how stem cell quiescence is a state maintained by signaling pathways ready to allow rapid activation (Cheung and Rando, 2013).

Pathways mediating ATF3 expression. Previous studies have demonstrated that the signal transduction pathways mediating ATF3 expression include c-Jun co-expressed with ATF3 in the nervous system after injury and stress (Hunt et al., 2012). The selective JNK/c-Jun inhibitor SP600125 fully blocks ATF3 induction in adult rat ganglion neurons and inhibits outgrowth of their axons (Lindwall et al., 2004). Furthermore, the MAPK/p38 pathway is also required for ATF3 expression in several non-neuronal cell lines undergoing apoptosis, an effect suppressed by the specific MAPK/p38 inhibitor SB203580 (Lu et al., 2007). In accordance with these results, our current data showed the involvement of both molecular pathways (JNK/c-Jun and MAPK/p38) in the control of the ATF3 nuclear expression in mobilized spinal ependymal cells. This observation was also supported by Western blotting analysis indicating ATF3 expression (of molecular weight in full accordance with reports by Chen et al. (1994) and Hashimoto et al. (2002) in nuclear fractions at 24 h *in vitro*. The origin of the variation in the molecular weight between the nuclear and cytoplasmic ATF3 protein remains unclear and will need future work.

ATF3 expression and migration after excitotoxic and ischemic-like conditions. Excitotoxic or ischemic-like protocols, that are reported to produce moderate damage to the spinal cord (Bianchetti et al., 2013; Mazzone et al., 2010; Taccola et al., 2008), did not enhance the number of activated and migrating ATF3 positive cells 24 h later. When the excitotoxic stimulus was very strong (1 mM kainate), the number of activated ependymal cells actually decreased in line with widespread neurotoxicity (Taccola et al., 2008). Our previous investigations have indicated that, in the rat spinal cord, neuronal and glial death occurs mainly during the first 24 h (Bianchetti et al., 2013; Mazzone et al., 2013; Taccola et al., 2008). Any attempt to repair cell damage might perhaps require an intervention by stem cells occurring over several days after the primary injury. This process has been examined with long-term organotypic cultures in which stem cell activation two weeks after excitotoxic stimulation failed to produce significant neurogenesis (Mazzone et al., 2013). Our speculation is that the role of ATF3 might be different in the neuronal (postmitotic) and ependymal (mitotic) spinal cells. In neurons ATF3 is viewed as a late marker for injury (Francis et al., 2004; Tsujino et al., 2000; Tsuzuki et al., 2001), with a neuroprotective and pro-survival influence (Wang et al., 2012; Zhang et al., 2011). The role of ATF3 in

proliferation and migration of ependymal cells could be similar to the ATF3 role in cancer cells in which ATF3 promotes proliferation, motility and invasiveness of certain cancer cell lines (Thompson et al., 2009; Wang et al., 2008).

CONCLUSIONS AND FUTURE PROSPECTS

My project has demonstrated the feasibility of producing an *in vitro* model that mimics ischemia in the spinal cord, thus extending former studies using OGD on brain slices to simulate stroke. Our model can reproduce clinical conditions of spinal ischemic damage with partial loss of neurons and glia associated with severe functional impairment. In this experimental setting, various cell death processes were observed, especially parthanatos. Furthermore, PJ34, an inhibitor of PARP-1, produce partial neuroprotection despite its ability to induce network persistent activity. Within the field of cell neurorepair, we characterized spinal stem/progenitor cells, demonstrating ATF3 as a marker for their presence and activation. Future studies concerning pharmacological and cellular approaches are thus necessary to test the outcome of our SCI model.

REFERENCES

Aarts, M.M., and Tymianski, M. (2003). Novel treatment of excitotoxicity: targeted disruption of intracellular signalling from glutamate receptors. Biochem. Pharmacol. *66*, 877–886.

Aarts, M.M., and Tymianski, M. (2005a). TRPM7 and ischemic CNS injury. Neurosci. Rev. J. Bringing Neurobiol. Neurol. Psychiatry *11*, 116–123.

Aarts, M.M., and Tymianski, M. (2005b). TRPMs and neuronal cell death. Pflüg. Arch. Eur. J. Physiol. *451*, 243–249.

Aarts, M., Iihara, K., Wei, W.-L., Xiong, Z.-G., Arundine, M., Cerwinski, W., MacDonald, J.F., and Tymianski, M. (2003). A key role for TRPM7 channels in anoxic neuronal death. Cell *115*, 863–877.

Abdelkarim, G.E., Gertz, K., Harms, C., Katchanov, J., Dirnagl, U., Szabó, C., and Endres, M. (2001). Protective effects of PJ34, a novel, potent inhibitor of poly(ADP-ribose) polymerase (PARP) in in vitro and in vivo models of stroke. Int. J. Mol. Med. *7*, 255–260.

Abe, Y., Yamamoto, T., Sugiyama, Y., Watanabe, T., Saito, N., Kayama, H., and Kumagai, T. (1999). Apoptotic cells associated with Wallerian degeneration after experimental spinal cord injury: a possible mechanism of oligodendroglial death. J. Neurotrauma *16*, 945–952.

Andrabi, S.A., Kim, N.S., Yu, S.-W., Wang, H., Koh, D.W., Sasaki, M., Klaus, J.A., Otsuka, T., Zhang, Z., Koehler, R.C., et al. (2006). Poly(ADP-ribose) (PAR) polymer is a death signal. Proc. Natl. Acad. Sci. U. S. A. *103*, 18308–18313.

Andrabi, S.A., Dawson, T.M., and Dawson, V.L. (2008). Mitochondrial and nuclear cross talk in cell death: parthanatos. Ann. N. Y. Acad. Sci. *1147*, 233–241.

Araque, A., Li, N., Doyle, R.T., and Haydon, P.G. (2000). SNARE protein-dependent glutamate release from astrocytes. J. Neurosci. Off. J. Soc. Neurosci. *20*, 666–673.

Ariumi, Y., Masutani, M., Copeland, T.D., Mimori, T., Sugimura, T., Shimotohno, K., Ueda, K., Hatanaka, M., and Noda, M. (1999). Suppression of the poly(ADP-ribose) polymerase activity by DNA-dependent protein kinase in vitro. Oncogene *18*, 4616–4625.

Baptiste, D.C., and Fehlings, M.G. (2008). Emerging drugs for spinal cord injury. Expert Opin. Emerg. Drugs *13*, 63–80.

Barres, B.A., Jacobson, M.D., Schmid, R., Sendtner, M., and Raff, M.C. (1993). Does oligodendrocyte survival depend on axons? Curr. Biol. CB *3*, 489–497.

Beattie, M.S., Farooqui, A.A., and Bresnahan, J.C. (2000). Review of current evidence for apoptosis after spinal cord injury. J. Neurotrauma *17*, 915–925.

Beattie, M.S., Hermann, G.E., Rogers, R.C., and Bresnahan, J.C. (2002). Cell death in models of spinal cord injury. Prog. Brain Res. *137*, 37–47.

Becker, E.B.E., and Bonni, A. (2004). Cell cycle regulation of neuronal apoptosis in development and disease. Prog. Neurobiol. *72*, 1–25.

Beckman, J.S., Beckman, T.W., Chen, J., Marshall, P.A., and Freeman, B.A. (1990). Apparent hydroxyl radical production by peroxynitrite: implications for endothelial injury from nitric oxide and superoxide. Proc. Natl. Acad. Sci. U. S. A. *87*, 1620–1624.

Belrose, J.C., Xie, Y.-F., Gierszewski, L.J., MacDonald, J.F., and Jackson, M.F. (2012). Loss of glutathione homeostasis associated with neuronal senescence facilitates TRPM2 channel activation in cultured hippocampal pyramidal neurons. Mol. Brain *5*, 11.

Van den Berg, M.E.L., Castellote, J.M., Mahillo-Fernandez, I., and de Pedro-Cuesta, J. (2010). Incidence of spinal cord injury worldwide: a systematic review. Neuroepidemiology *34*, 184–192; discussion 192.

Berger, N.A. (1985). Poly(ADP-ribose) in the cellular response to DNA damage. Radiat. Res. *101*, 4–15.

Berger, F., Ramírez-Hernández, M.H., and Ziegler, M. (2004). The new life of a centenarian: signalling functions of NAD(P). Trends Biochem. Sci. *29*, 111–118.

Bianchetti, E., Mladinic, M., and Nistri, A. (2013). Mechanisms underlying cell death in ischemia-like damage to the rat spinal cord in vitro. Cell Death Dis. *4*, e707.

Bovolenta, P., Wandosell, F., and Nieto-Sampedro, M. (1992). CNS glial scar tissue: a source of molecules which inhibit central neurite outgrowth. Prog. Brain Res. *94*, 367–379.

Bredesen, D.E. (2000). Apoptosis: overview and signal transduction pathways. J. Neurotrauma *17*, 801–810.

Bredesen, D.E., Rao, R.V., and Mehlen, P. (2006). Cell death in the nervous system. Nature *443*, 796–802.

Carrascal, L., Nieto-Gonzalez, J.L., Cameron, W.E., Torres, B., and Nunez-Abades, P.A. (2005). Changes during the postnatal development in physiological and anatomical characteristics of rat motoneurons studied in vitro. Brain Res. Brain Res. Rev. *49*, 377–387.

Chen, B.P., Liang, G., Whelan, J., and Hai, T. (1994). ATF3 and ATF3 delta Zip. Transcriptional repression versus activation by alternatively spliced isoforms. J. Biol. Chem. *269*, 15819–15826.

Chen, H.-C., Su, L.-T., González-Pagán, O., Overton, J.D., and Runnels, L.W. (2012). A key role for Mg(2+) in TRPM7's control of ROS levels during cell stress. Biochem. J. *445*, 441–448.

Cheung, T.H., and Rando, T.A. (2013). Molecular regulation of stem cell quiescence. Nat. Rev. Mol. Cell Biol. *14*, 329–340.

Chiarugi, A. (2005). Intrinsic mechanisms of poly(ADP-ribose) neurotoxicity: three hypotheses. Neurotoxicology *26*, 847–855.

Chinnaiyan, A.M., O'Rourke, K., Tewari, M., and Dixit, V.M. (1995). FADD, a novel death domain-containing protein, interacts with the death domain of Fas and initiates apoptosis. Cell *81*, 505–512.

Cho, Y.S., Challa, S., Moquin, D., Genga, R., Ray, T.D., Guildford, M., and Chan, F.K.-M. (2009). Phosphorylation-driven assembly of the RIP1-RIP3 complex regulates programmed necrosis and virus-induced inflammation. Cell *137*, 1112–1123.

Cifra, A., Mazzone, G.L., Nani, F., Nistri, A., and Mladinic, M. (2012). Postnatal developmental profile of neurons and glia in motor nuclei of the brainstem and spinal cord, and its comparison with organotypic slice cultures. Dev. Neurobiol. *72*, 1140–1160.

Clark, R.S., Kochanek, P.M., Schwarz, M.A., Schiding, J.K., Turner, D.S., Chen, M., Carlos, T.M., and Watkins, S.C. (1996). Inducible nitric oxide synthase expression in cerebrovascular smooth muscle and neutrophils after traumatic brain injury in immature rats. Pediatr. Res. *39*, 784–790.

Cohen, G.M. (1997). Caspases: the executioners of apoptosis. Biochem. J. *326 (Pt 1)*, 1–16.

Cohen, J.J. (1993). Apoptosis. Immunol. Today *14*, 126–130.

Colak, A., Karaoğlan, A., Barut, S., Köktürk, S., Akyildiz, A.I., and Taşyürekli, M. (2005). Neuroprotection and functional recovery after application of the caspase-9 inhibitor z-LEHD-fmk in a rat model of traumatic spinal cord injury. J. Neurosurg. Spine *2*, 327–334.

Cook, N.L., Van Den Heuvel, C., and Vink, R. (2009). Are the transient receptor potential melastatin (TRPM) channels important in magnesium homeostasis following traumatic brain injury? Magnes. Res. Off. Organ Int. Soc. Dev. Res. Magnes. *22*, 225–234.

Crowe, M.J., Bresnahan, J.C., Shuman, S.L., Masters, J.N., and Beattie, M.S. (1997). Apoptosis and delayed degeneration after spinal cord injury in rats and monkeys. Nat. Med. *3*, 73–76.

D'Amours, D., Desnoyers, S., D'Silva, I., and Poirier, G.G. (1999). Poly(ADP-ribosyl)ation reactions in the regulation of nuclear functions. Biochem. J. *342 (Pt 2)*, 249–268.

Van Damme, P., Van Den Bosch, L., Van Houtte, E., Callewaert, G., and Robberecht, W. (2002). GluR2-dependent properties of AMPA receptors determine the selective vulnerability of motor neurons to excitotoxicity. J. Neurophysiol. *88*, 1279–1287.

David, S., and Kroner, A. (2011). Repertoire of microglial and macrophage responses after spinal cord injury. Nat. Rev. Neurosci. *12*, 388–399.

David, K.K., Andrabi, S.A., Dawson, T.M., and Dawson, V.L. (2009). Parthanatos, a messenger of death. Front. Biosci. Landmark Ed. *14*, 1116–1128.

Davis, A.R., Lotocki, G., Marcillo, A.E., Dietrich, W.D., and Keane, R.W. (2007). FasL, Fas, and death-inducing signaling complex (DISC) proteins are recruited to membrane rafts after spinal cord injury. J. Neurotrauma *24*, 823–834.

Davis, S.M., Lees, K.R., Albers, G.W., Diener, H.C., Markabi, S., Karlsson, G., and Norris, J. (2000). Selfotel in acute ischemic stroke : possible neurotoxic effects of an NMDA antagonist. Stroke J. Cereb. Circ. *31*, 347–354.

Dawson, V.L., and Dawson, T.M. (2004). Deadly conversations: nuclear-mitochondrial cross-talk. J. Bioenerg. Biomembr. *36*, 287–294.

Dawson, T.M., Dawson, V.L., and Snyder, S.H. (1994). Molecular mechanisms of nitric oxide actions in the brain. Ann. N. Y. Acad. Sci. *738*, 76–85.

Dawson, V.L., Dawson, T.M., London, E.D., Bredt, D.S., and Snyder, S.H. (1991). Nitric oxide mediates glutamate neurotoxicity in primary cortical cultures. Proc. Natl. Acad. Sci. U. S. A. *88*, 6368–6371.

Degterev, A., Huang, Z., Boyce, M., Li, Y., Jagtap, P., Mizushima, N., Cuny, G.D., Mitchison, T.J., Moskowitz, M.A., and Yuan, J. (2005). Chemical inhibitor of nonapoptotic cell death with therapeutic potential for ischemic brain injury. Nat. Chem. Biol. *1*, 112–119.

Van Den Bosch, L., Vandenberghe, W., Klaassen, H., Van Houtte, E., and Robberecht, W. (2000). Ca(2+)-permeable AMPA receptors and selective vulnerability of motor neurons. J. Neurol. Sci. *180*, 29–34.

Dent, M.A.R., Segura-Anaya, E., Alva-Medina, J., and Aranda-Anzaldo, A. (2010). NeuN/Fox-3 is an intrinsic component of the neuronal nuclear matrix. FEBS Lett. *584*, 2767–2771.

Dirnagl, U., Iadecola, C., and Moskowitz, M.A. (1999). Pathobiology of ischaemic stroke: an integrated view. Trends Neurosci. *22*, 391–397.

Donnelly, D.J., and Popovich, P.G. (2008). Inflammation and its role in neuroprotection, axonal regeneration and functional recovery after spinal cord injury. Exp. Neurol. *209*, 378–388.

Ehlers, M.D. (2004). Deconstructing the axon: Wallerian degeneration and the ubiquitin-proteasome system. Trends Neurosci. *27*, 3–6.

Eliasson, M.J., Sampei, K., Mandir, A.S., Hurn, P.D., Traystman, R.J., Bao, J., Pieper, A., Wang, Z.Q., Dawson, T.M., Snyder, S.H., et al. (1997). Poly(ADP-ribose) polymerase gene disruption renders mice resistant to cerebral ischemia. Nat. Med. *3*, 1089–1095.

Emery, E., Aldana, P., Bunge, M.B., Puckett, W., Srinivasan, A., Keane, R.W., Bethea, J., and Levi, A.D. (1998). Apoptosis after traumatic human spinal cord injury. J. Neurosurg. *89*, 911–920.

Faden, A.I., and Stoica, B. (2007). Neuroprotection: challenges and opportunities. Arch. Neurol. *64*, 794–800.

Figoni, S.F. (1984). Cardiovascular and haemodynamic responses to tilting and to standing in tetraplegic patients: a review. Paraplegia *22*, 99–109.

Foret, A., Quertainmont, R., Botman, O., Bouhy, D., Amabili, P., Brook, G., Schoenen, J., and Franzen, R. (2010). Stem cells in the adult rat spinal cord: plasticity after injury and treadmill training exercise. J. Neurochem. *112*, 762–772.

Francis, J.S., Dragunow, M., and During, M.J. (2004). Over expression of ATF-3 protects rat hippocampal neurons from in vivo injection of kainic acid. Brain Res. Mol. Brain Res. *124*, 199–203.

Fuentes-Prior, P., and Salvesen, G.S. (2004). The protein structures that shape caspase activity, specificity, activation and inhibition. Biochem. J. *384*, 201–232.

Galluzzi, L., Vitale, I., Abrams, J.M., Alnemri, E.S., Baehrecke, E.H., Blagosklonny, M.V., Dawson, T.M., Dawson, V.L., El-Deiry, W.S., Fulda, S., et al. (2012). Molecular definitions of cell death subroutines: recommendations of the Nomenclature Committee on Cell Death 2012. Cell Death Differ. *19*, 107–120.

Gao, F., Wei, Z., An, W., Wang, K., and Lu, W. (2013). The interactomes of POU5F1 and SOX2 enhancers in human embryonic stem cells. Sci. Rep. *3*, 1588.

Gargiulo, G., Cesaroni, M., Serresi, M., de Vries, N., Hulsman, D., Bruggeman, S.W., Lancini, C., and van Lohuizen, M. (2013). In vivo RNAi screen for BMI1 targets identifies TGF-β/BMP-ER stress pathways as key regulators of neural- and malignant glioma-stem cell homeostasis. Cancer Cell *23*, 660–676.

Genovese, T., and Cuzzocrea, S. (2008). Role of free radicals and poly(ADP-ribose)polymerase-1 in the development of spinal cord injury: new potential therapeutic targets. Curr. Med. Chem. *15*, 477–487.

Genovese, T., Mazzon, E., Muià, C., Patel, N.S.A., Threadgill, M.D., Bramanti, P., De Sarro, A., Thiemermann, C., and Cuzzocrea, S. (2005). Inhibitors of poly(ADP-ribose) polymerase modulate signal transduction pathways and secondary damage in experimental spinal cord trauma. J. Pharmacol. Exp. Ther. *312*, 449–457.

Giordano, G., Sánchez-Pérez, A.M., Montoliu, C., Berezney, R., Malyavantham, K., Costa, L.G., Calvete, J.J., and Felipo, V. (2005). Activation of NMDA receptors induces protein kinase A-mediated phosphorylation and degradation of matrin 3. Blocking these effects prevents NMDA-induced neuronal death. J. Neurochem. *94*, 808–818.

Grant, E.R., Bacskai, B.J., Pleasure, D.E., Pritchett, D.B., Gallagher, M.J., Kendrick, S.J., Kricka, L.J., and Lynch, D.R. (1997). N-methyl-D-aspartate receptors expressed in a nonneuronal cell line mediate subunit-specific increases in free intracellular calcium. J. Biol. Chem. *272*, 647–656.

Gross, A., McDonnell, J.M., and Korsmeyer, S.J. (1999). BCL-2 family members and the mitochondria in apoptosis. Genes Dev. *13*, 1899–1911.

Guzmán-Lenis, M.-S., Navarro, X., and Casas, C. (2009). Drug screening of neuroprotective agents on an organotypic-based model of spinal cord excitotoxic damage. Restor. Neurol. Neurosci. *27*, 335–349.

Hagberg, H., Wilson, M.A., Matsushita, H., Zhu, C., Lange, M., Gustavsson, M., Poitras, M.F., Dawson, T.M., Dawson, V.L., Northington, F., et al. (2004). PARP-1 gene disruption in mice preferentially protects males from perinatal brain injury. J. Neurochem. *90*, 1068–1075.

Hall, E.D. (1993). The role of oxygen radicals in traumatic injury: clinical implications. J. Emerg. Med. *11 Suppl 1*, 31–36.

Hall, E.D. (1996). Lipid peroxidation. Adv. Neurol. *71*, 247–257; discussion 257–258.

Hall, E.D., and Springer, J.E. (2004). Neuroprotection and acute spinal cord injury: a reappraisal. NeuroRx J. Am. Soc. Exp. Neurother. *1*, 80–100.

Hamada, Y., Ikata, T., Katoh, S., Tsuchiya, K., Niwa, M., Tsutsumishita, Y., and Fukuzawa, K. (1996). Roles of nitric oxide in compression injury of rat spinal cord. Free Radic. Biol. Med. *20*, 1–9.

Harkey, H.L., 3rd, White, E.A., 4th, Tibbs, R.E., Jr, and Haines, D.E. (2003). A clinician's view of spinal cord injury. Anat. Rec. B. New Anat. *271*, 41–48.

Hashimoto, Y., Zhang, C., Kawauchi, J., Imoto, I., Adachi, M.T., Inazawa, J., Amagasa, T., Hai, T., and Kitajima, S. (2002). An alternatively spliced isoform of transcriptional repressor ATF3 and its induction by stress stimuli. Nucleic Acids Res. *30*, 2398–2406.

Hayaishi, O., and Ueda, K. (1977). Poly(ADP-ribose) and ADP-ribosylation of proteins. Annu. Rev. Biochem. *46*, 95–116.

He, S., Wang, L., Miao, L., Wang, T., Du, F., Zhao, L., and Wang, X. (2009). Receptor interacting protein kinase-3 determines cellular necrotic response to TNF-alpha. Cell *137*, 1100–1111.

Herrmann, J.E., Imura, T., Song, B., Qi, J., Ao, Y., Nguyen, T.K., Korsak, R.A., Takeda, K., Akira, S., and Sofroniew, M.V. (2008). STAT3 is a critical regulator of astrogliosis and scar formation after spinal cord injury. J. Neurosci. Off. J. Soc. Neurosci. *28*, 7231–7243.

Hill, C.E., Beattie, M.S., and Bresnahan, J.C. (2001). Degeneration and sprouting of identified descending supraspinal axons after contusive spinal cord injury in the rat. Exp. Neurol. *171*, 153–169.

Hitomi, J., Christofferson, D.E., Ng, A., Yao, J., Degterev, A., Xavier, R.J., and Yuan, J. (2008). Identification of a molecular signaling network that regulates a cellular necrotic cell death pathway. Cell *135*, 1311–1323.

Hugnot, J.P., and Franzen, R. (2011). The spinal cord ependymal region: a stem cell niche in the caudal central nervous system. Front. Biosci. Landmark Ed. *16*, 1044–1059.

Huletsky, A., de Murcia, G., Muller, S., Hengartner, M., Ménard, L., Lamarre, D., and Poirier, G.G. (1989). The effect of poly(ADP-ribosyl)ation on native and H1-depleted chromatin. A role of poly(ADP-ribosyl)ation on core nucleosome structure. J. Biol. Chem. *264*, 8878–8886.

Hulsebosch, C.E. (2002). Recent advances in pathophysiology and treatment of spinal cord injury. Adv. Physiol. Educ. *26*, 238–255.

Hunt, D., Raivich, G., and Anderson, P.N. (2012). Activating transcription factor 3 and the nervous system. Front. Mol. Neurosci. *5*, 7.

Ince, P., Stout, N., Shaw, P., Slade, J., Hunziker, W., Heizmann, C.W., and Baimbridge, K.G. (1993). Parvalbumin and calbindin D-28k in the human motor system and in motor neuron disease. Neuropathol. Appl. Neurobiol. *19*, 291–299.

Ishii, M., Oyama, A., Hagiwara, T., Miyazaki, A., Mori, Y., Kiuchi, Y., and Shimizu, S. (2007). Facilitation of H2O2-induced A172 human glioblastoma cell death by insertion of oxidative stress-sensitive TRPM2 channels. Anticancer Res. *27*, 3987–3992.

Itoh, N., Yonehara, S., Ishii, A., Yonehara, M., Mizushima, S., Sameshima, M., Hase, A., Seto, Y., and Nagata, S. (1991). The polypeptide encoded by the cDNA for human cell surface antigen Fas can mediate apoptosis. Cell *66*, 233–243.

Jagtap, P., and Szabó, C. (2005). Poly(ADP-ribose) polymerase and the therapeutic effects of its inhibitors. Nat. Rev. Drug Discov. *4*, 421–440.

Jürgensmeier, J.M., Xie, Z., Deveraux, Q., Ellerby, L., Bredesen, D., and Reed, J.C. (1998). Bax directly induces release of cytochrome c from isolated mitochondria. Proc. Natl. Acad. Sci. U. S. A. *95*, 4997–5002.

Kakulas, B.A. (2004). Neuropathology: the foundation for new treatments in spinal cord injury. Spinal Cord *42*, 549–563.

Kalia, L.V., Kalia, S.K., and Salter, M.W. (2008). NMDA receptors in clinical neurology: excitatory times ahead. Lancet Neurol. *7*, 742–755.

Kameshita, I., Matsuda, Z., Taniguchi, T., and Shizuta, Y. (1984). Poly (ADP-Ribose) synthetase. Separation and identification of three proteolytic fragments as the substrate-binding domain, the DNA-binding domain, and the automodification domain. J. Biol. Chem. *259*, 4770–4776.

Kaneko, S., Kawakami, S., Hara, Y., Wakamori, M., Itoh, E., Minami, T., Takada, Y., Kume, T., Katsuki, H., Mori, Y., et al. (2006). A critical role of TRPM2 in neuronal cell death by hydrogen peroxide. J. Pharmacol. Sci. *101*, 66–76.

Katoh, K., Ikata, T., Katoh, S., Hamada, Y., Nakauchi, K., Sano, T., and Niwa, M. (1996). Induction and its spread of apoptosis in rat spinal cord after mechanical trauma. Neurosci. Lett. *216*, 9–12.

Kauppinen, T.M., Suh, S.W., Berman, A.E., Hamby, A.M., and Swanson, R.A. (2009). Inhibition of poly(ADP-ribose) polymerase suppresses inflammation and promotes recovery after ischemic injury. J. Cereb. Blood Flow Metab. Off. J. Int. Soc. Cereb. Blood Flow Metab. *29*, 820–829.

Kaushal, V., and Schlichter, L.C. (2008). Mechanisms of microglia-mediated neurotoxicity in a new model of the stroke penumbra. J. Neurosci. Off. J. Soc. Neurosci. *28*, 2221–2230.

Kim, M.Y., Zhang, T., and Kraus, W.L. (2005). Poly(ADP-ribosyl)ation by PARP-1: “PAR-laying” NAD+ into a nuclear signal. Genes Dev. *19*, 1951–1967.

Knoblach, S.M., Huang, X., VanGelderen, J., Calva-Cerqueira, D., and Faden, A.I. (2005). Selective caspase activation may contribute to neurological dysfunction after experimental spinal cord trauma. J. Neurosci. Res. *80*, 369–380.

Koda, M., Murakami, M., Ino, H., Yoshinaga, K., Ikeda, O., Hashimoto, M., Yamazaki, M., Nakayama, C., and Moriya, H. (2002). Brain-derived neurotrophic factor suppresses delayed apoptosis of oligodendrocytes after spinal cord injury in rats. J. Neurotrauma *19*, 777–785.

Koh, D.W., Dawson, T.M., and Dawson, V.L. (2005). Mediation of cell death by poly(ADP-ribose) polymerase-1. Pharmacol. Res. Off. J. Ital. Pharmacol. Soc. *52*, 5–14.

Kraus, W.L., and Lis, J.T. (2003). PARP goes transcription. Cell *113*, 677–683.

Kühn, F.J.P., Heiner, I., and Lückhoff, A. (2005). TRPM2: a calcium influx pathway regulated by oxidative stress and the novel second messenger ADP-ribose. Pflüg. Arch. Eur. J. Physiol. *451*, 212–219.

Kumar, K.N., Tilakaratne, N., Johnson, P.S., Allen, A.E., and Michaelis, E.K. (1991). Cloning of cDNA for the glutamate-binding subunit of an NMDA receptor complex. Nature *354*, 70–73.

Kun, E., Kirsten, E., and Ordahl, C.P. (2002). Coenzymatic activity of randomly broken or intact double-stranded DNAs in auto and histone H1 trans-poly(ADP-ribosylation), catalyzed by poly(ADP-ribose) polymerase (PARP I). J. Biol. Chem. *277*, 39066–39069.

Kuzhandaivel, A., Nistri, A., and Mladinic, M. (2010a). Kainate-mediated excitotoxicity induces neuronal death in the rat spinal cord in vitro via a PARP-1 dependent cell death pathway (Parthanatos). Cell. Mol. Neurobiol. *30*, 1001–1012.

Kuzhandaivel, A., Margaryan, G., Nistri, A., and Mladinic, M. (2010b). Extensive glial apoptosis develops early after hypoxic-dysmetabolic insult to the neonatal rat spinal cord in vitro. Neuroscience *169*, 325–338.

Kuzhandaivel, A., Nistri, A., Mazzone, G.L., and Mladinic, M. (2011). Molecular Mechanisms Underlying Cell Death in Spinal Networks in Relation to Locomotor Activity After Acute Injury in vitro. Front. Cell. Neurosci. *5*, 9.

Lautier, D., Lagueux, J., Thibodeau, J., Ménard, L., and Poirier, G.G. (1993). Molecular and biochemical features of poly (ADP-ribose) metabolism. Mol. Cell. Biochem. *122*, 171–193.

Lee, I.-H., Lindqvist, E., Kiehn, O., Widenfalk, J., and Olson, L. (2005). Glial and neuronal connexin expression patterns in the rat spinal cord during development and following injury. J. Comp. Neurol. *489*, 1–10.

Lees, K.R., Asplund, K., Carolei, A., Davis, S.M., Diener, H.C., Kaste, M., Orgogozo, J.M., and Whitehead, J. (2000). Glycine antagonist (gavestinel) in neuroprotection (GAIN International) in patients with acute stroke: a randomised controlled trial. GAIN International Investigators. Lancet *355*, 1949–1954.

Lewén, A., Matz, P., and Chan, P.H. (2000). Free radical pathways in CNS injury. J. Neurotrauma *17*, 871–890.

Li, S., and Stys, P.K. (2001). Na(+)-K(+)-ATPase inhibition and depolarization induce glutamate release via reverse Na(+)-dependent transport in spinal cord white matter. Neuroscience *107*, 675–683.

Li, H., Zhu, H., Xu, C.J., and Yuan, J. (1998). Cleavage of BID by caspase 8 mediates the mitochondrial damage in the Fas pathway of apoptosis. Cell *94*, 491–501.

Lin, M.-C., Huang, Y.-L., Liu, H.-W., Yang, D.-Y., Lee, C.-P., Yang, L.-L., and Cheng, F.-C. (2004). On-line microdialysis-graphite furnace atomic absorption spectrometry in the determination of brain magnesium levels in gerbils subjected to cerebral ischemia/reperfusion. J. Am. Coll. Nutr. *23*, 561S–565S.

Lindwall, C., Dahlin, L., Lundborg, G., and Kanje, M. (2004). Inhibition of c-Jun phosphorylation reduces axonal outgrowth of adult rat nodose ganglia and dorsal root ganglia sensory neurons. Mol. Cell. Neurosci. *27*, 267–279.

Lipton, S.A., and Rosenberg, P.A. (1994). Excitatory amino acids as a final common pathway for neurologic disorders. N. Engl. J. Med. *330*, 613–622.

Liu, K., Lin, B., Zhao, M., Yang, X., Chen, M., Gao, A., Liu, F., Que, J., and Lan, X. (2013). The multiple roles for Sox2 in stem cell maintenance and tumorigenesis. Cell. Signal. *25*, 1264–1271.

Liu, X., Kim, C.N., Yang, J., Jemmerson, R., and Wang, X. (1996). Induction of apoptotic program in cell-free extracts: requirement for dATP and cytochrome c. Cell *86*, 147–157.

Liu, X.Z., Xu, X.M., Hu, R., Du, C., Zhang, S.X., McDonald, J.W., Dong, H.X., Wu, Y.J., Fan, G.S., Jacquin, M.F., et al. (1997). Neuronal and glial apoptosis after traumatic spinal cord injury. J. Neurosci. Off. J. Soc. Neurosci. *17*, 5395–5406.

Lo, E.H., Bosque-Hamilton, P., and Meng, W. (1998). Inhibition of poly(ADP-ribose) polymerase: reduction of ischemic injury and attenuation of N-methyl-D-aspartate-induced neurotransmitter dysregulation. Stroke J. Cereb. Circ. *29*, 830–836.

LOCKSHIN, R.A., and WILLIAM, C.M. (1965). PROGRAMMED CELL DEATH. 3. NEURAL CONTROL OF THE BREAKDOWN OF THE INTERSEGMENTAL MUSCLES OF SILKMOTHS. J. Insect Physiol. *11*, 601–610.

Lois, C., García-Verdugo, J.M., and Alvarez-Buylla, A. (1996). Chain migration of neuronal precursors. Science *271*, 978–981.

Lorenzo, H.K., and Susin, S.A. (2007). Therapeutic potential of AIF-mediated caspase-independent programmed cell death. Drug Resist. Updat. Rev. Comment. Antimicrob. Anticancer Chemother. *10*, 235–255.

Lu, D., Chen, J., and Hai, T. (2007). The regulation of ATF3 gene expression by mitogen-activated protein kinases. Biochem. J. *401*, 559–567.

Lu, J., Ashwell, K.W., and Waite, P. (2000). Advances in secondary spinal cord injury: role of apoptosis. Spine *25*, 1859–1866.

Maas, A.I.R., and Murray, G.D. (2007). Magnesium for neuroprotection after traumatic brain injury. Lancet Neurol. *6*, 20–21.

Mancini, M., Machamer, C.E., Roy, S., Nicholson, D.W., Thornberry, N.A., Casciola-Rosen, L.A., and Rosen, A. (2000). Caspase-2 is localized at the Golgi complex and cleaves golgin-160 during apoptosis. J. Cell Biol. *149*, 603–612.

Mandir, A.S., Przedborski, S., Jackson-Lewis, V., Wang, Z.Q., Simbulan-Rosenthal, C.M., Smulson, M.E., Hoffman, B.E., Guastella, D.B., Dawson, V.L., and Dawson, T.M. (1999). Poly(ADP-ribose) polymerase activation mediates 1-methyl-4-phenyl-1, 2,3,6-tetrahydropyridine (MPTP)-induced parkinsonism. Proc. Natl. Acad. Sci. U. S. A. *96*, 5774–5779.

Mandir, A.S., Poitras, M.F., Berliner, A.R., Herring, W.J., Guastella, D.B., Feldman, A., Poirier, G.G., Wang, Z.Q., Dawson, T.M., and Dawson, V.L. (2000). NMDA but not non-

NMDA excitotoxicity is mediated by Poly(ADP-ribose) polymerase. J. Neurosci. Off. J. Soc. Neurosci. *20*, 8005–8011.

Mantamadiotis, T., Papalexis, N., and Dworkin, S. (2012). CREB signalling in neural stem/progenitor cells: recent developments and the implications for brain tumour biology. BioEssays News Rev. Mol. Cell. Dev. Biol. *34*, 293–300.

Margaryan, G., Mladinic, M., Mattioli, C., and Nistri, A. (2009). Extracellular magnesium enhances the damage to locomotor networks produced by metabolic perturbation mimicking spinal injury in the neonatal rat spinal cord in vitro. Neuroscience *163*, 669–682.

Masson, M., Niedergang, C., Schreiber, V., Muller, S., Menissier-de Murcia, J., and de Murcia, G. (1998). XRCC1 is specifically associated with poly(ADP-ribose) polymerase and negatively regulates its activity following DNA damage. Mol. Cell. Biol. *18*, 3563–3571.

Mattson, M.P. (2000). Activin to the rescue for overexcited neurons. Nat. Med. *6*, 739–741.

Mattson, M.P. (2003). Excitotoxic and excitoprotective mechanisms: abundant targets for the prevention and treatment of neurodegenerative disorders. Neuromolecular Med. *3*, 65–94.

Mazzone, G.L., Margaryan, G., Kuzhandaivel, A., Nasrabady, S.E., Mladinic, M., and Nistri, A. (2010). Kainate-induced delayed onset of excitotoxicity with functional loss unrelated to the extent of neuronal damage in the in vitro spinal cord. Neuroscience *168*, 451–462.

Mazzone, G.L., Mladinic, M., and Nistri, A. (2013). Excitotoxic cell death induces delayed proliferation of endogenous neuroprogenitor cells in organotypic slice cultures of the rat spinal cord. Cell Death Dis. *4*, e902.

McDonald, J.W., and Sadowsky, C. (2002). Spinal-cord injury. Lancet *359*, 417–425.

McDonough, A., and Martínez-Cerdeño, V. (2012). Endogenous proliferation after spinal cord injury in animal models. Stem Cells Int. *2012*, 387513.

McKinley, W.O., Tewksbury, M.A., and Godbout, C.J. (2002). Comparison of medical complications following nontraumatic and traumatic spinal cord injury. J. Spinal Cord Med. *25*, 88–93.

McNulty, S., and Fonfria, E. (2005). The role of TRPM channels in cell death. Pflüg. Arch. Eur. J. Physiol. *451*, 235–242.

Meletis, K., Barnabé-Heider, F., Carlén, M., Evergren, E., Tomilin, N., Shupliakov, O., and Frisén, J. (2008). Spinal cord injury reveals multilineage differentiation of ependymal cells. PLoS Biol. *6*, e182.

Menezes, J.R.L., Marins, M., Alves, J.A.J., Froes, M.M., and Hedin-Pereira, C. (2002). Cell migration in the postnatal subventricular zone. Braz. J. Med. Biol. Res. Rev. Bras. Pesqui. Médicas E Biológicas Soc. Bras. Biofísica Al *35*, 1411–1421.

Merz, K., Herold, S., and Lie, D.C. (2011). CREB in adult neurogenesis--master and partner in the development of adult-born neurons? Eur. J. Neurosci. *33*, 1078–1086.

Mladinic, M., and Nistri, A. (2013). Microelectrode arrays in combination with in vitro models of spinal cord injury as tools to investigate pathological changes in network activity: facts and promises. Front. Neuroengineering *6*.

Muir, K.W., Lees, K.R., Ford, I., Davis, S., and Intravenous Magnesium Efficacy in Stroke (IMAGES) Study Investigators (2004). Magnesium for acute stroke (Intravenous Magnesium Efficacy in Stroke trial): randomised controlled trial. Lancet *363*, 439–445.

Muzio, M., Chinnaiyan, A.M., Kischkel, F.C., O'Rourke, K., Shevchenko, A., Ni, J., Scaffidi, C., Bretz, J.D., Zhang, M., Gentz, R., et al. (1996). FLICE, a novel FADD-homologous ICE/CED-3-like protease, is recruited to the CD95 (Fas/APO-1) death--inducing signaling complex. Cell *85*, 817–827.

Nagata, S. (1997). Apoptosis by death factor. Cell *88*, 355–365.

Nair, K.P.S., Taly, A.B., Maheshwarappa, B.M., Kumar, J., Murali, T., and Rao, S. (2005). Nontraumatic spinal cord lesions: a prospective study of medical complications during in-patient rehabilitation. Spinal Cord *43*, 558–564.

Nakagawa, T., Zhu, H., Morishima, N., Li, E., Xu, J., Yankner, B.A., and Yuan, J. (2000). Caspase-12 mediates endoplasmic-reticulum-specific apoptosis and cytotoxicity by amyloid-beta. Nature *403*, 98–103.

Nasrabady, S.E., Kuzhandaivel, A., and Nistri, A. (2011a). Studies of locomotor network neuroprotection by the selective poly(ADP-ribose) polymerase-1 inhibitor PJ-34 against excitotoxic injury to the rat spinal cord in vitro. Eur. J. Neurosci. *33*, 2216–2227.

Nasrabady, S.E., Kuzhandaivel, A., Mladinic, M., and Nistri, A. (2011b). Effects of 6(5H)-phenanthridinone, an inhibitor of poly(ADP-ribose)polymerase-1 activity (PARP-1), on locomotor networks of the rat isolated spinal cord. Cell. Mol. Neurobiol. *31*, 503–508.

Nasrabady, S.E., Kuzhandaivel, A., Akrami, A., Bianchetti, E., Milanese, M., Bonanno, G., and Nistri, A. (2012). Unusual increase in lumbar network excitability of the rat spinal cord evoked by the PARP-1 inhibitor PJ-34 through inhibition of glutamate uptake. Neuropharmacology *63*, 415–426.

Nistri, A., Taccola, G., Mladinic, M., Margaryan, G., and Kuzhandaivel, A. (2010). Deconstructing locomotor networks with experimental injury to define their membership. Ann. N. Y. Acad. Sci. *1198*, 242–251.

Norenberg, M.D., Smith, J., and Marcillo, A. (2004). The pathology of human spinal cord injury: defining the problems. J. Neurotrauma *21*, 429–440.

Oei, S.L., and Shi, Y. (2001). Poly(ADP-ribosyl)ation of transcription factor Yin Yang 1 under conditions of DNA damage. Biochem. Biophys. Res. Commun. *285*, 27–31.

Ogata, N., Ueda, K., Kawaichi, M., and Hayaishi, O. (1981). Poly(ADP-ribose) synthetase, a main acceptor of poly(ADP-ribose) in isolated nuclei. J. Biol. Chem. *256*, 4135–4137.

Olney, J.W. (1969). Glutaate-induced retinal degeneration in neonatal mice. Electron microscopy of the acutely evolving lesion. J. Neuropathol. Exp. Neurol. *28*, 455–474.

Onifer, S.M., Rabchevsky, A.G., and Scheff, S.W. (2007). Rat models of traumatic spinal cord injury to assess motor recovery. ILAR J. Natl. Res. Counc. Inst. Lab. Anim. Resour. *48*, 385–395.

Palacios-Prado, N., Hoge, G., Marandykina, A., Rimkute, L., Chapuis, S., Paulauskas, N., Skeberdis, V.A., O'Brien, J., Pereda, A.E., Bennett, M.V.L., et al. (2013). Intracellular magnesium-dependent modulation of gap junction channels formed by neuronal connexin36. J. Neurosci. Off. J. Soc. Neurosci. *33*, 4741–4753.

Papa, S., Rossi, F., Ferrari, R., Mariani, A., De Paola, M., Caron, I., Fiordaliso, F., Bisighini, C., Sammali, E., Colombo, C., et al. (2013). Selective Nanovector Mediated Treatment of Activated Proinflammatory Microglia/Macrophages in Spinal Cord Injury. ACS Nano.

Park, E., Velumian, A.A., and Fehlings, M.G. (2004). The role of excitotoxicity in secondary mechanisms of spinal cord injury: a review with an emphasis on the implications for white matter degeneration. J. Neurotrauma *21*, 754–774.

Pavri, R., Lewis, B., Kim, T.-K., Dilworth, F.J., Erdjument-Bromage, H., Tempst, P., de Murcia, G., Evans, R., Chambon, P., and Reinberg, D. (2005). PARP-1 determines specificity in a retinoid signaling pathway via direct modulation of mediator. Mol. Cell *18*, 83–96.

Penas, C., Casas, C., Robert, I., Forés, J., and Navarro, X. (2009). Cytoskeletal and activity-related changes in spinal motoneurons after root avulsion. J. Neurotrauma *26*, 763–779.

Penner, R., and Fleig, A. (2007). The Mg2+ and Mg(2+)-nucleotide-regulated channel-kinase TRPM7. Handb. Exp. Pharmacol. 313–328.

Perederiy, J.V., Luikart, B.W., Washburn, E.K., Schnell, E., and Westbrook, G.L. (2013). Neural injury alters proliferation and integration of adult-generated neurons in the dentate gyrus. J. Neurosci. Off. J. Soc. Neurosci. *33*, 4754–4767.

Perlman, J.M. (2006). Intervention strategies for neonatal hypoxic-ischemic cerebral injury. Clin. Ther. *28*, 1353–1365.

Perraud, A.L., Fleig, A., Dunn, C.A., Bagley, L.A., Launay, P., Schmitz, C., Stokes, A.J., Zhu, Q., Bessman, M.J., Penner, R., et al. (2001). ADP-ribose gating of the calcium-permeable LTRPC2 channel revealed by Nudix motif homology. Nature *411*, 595–599.

Pineau, I., and Lacroix, S. (2007). Proinflammatory cytokine synthesis in the injured mouse spinal cord: multiphasic expression pattern and identification of the cell types involved. J. Comp. Neurol. *500*, 267–285.

Plesca, D., Mazumder, S., and Almasan, A. (2008). DNA damage response and apoptosis. Methods Enzymol. *446*, 107–122.

Poirier, G.G., de Murcia, G., Jongstra-Bilen, J., Niedergang, C., and Mandel, P. (1982). Poly(ADP-ribosyl)ation of polynucleosomes causes relaxation of chromatin structure. Proc. Natl. Acad. Sci. U. S. A. *79*, 3423–3427.

Pop, C., and Salvesen, G.S. (2009). Human caspases: activation, specificity, and regulation. J. Biol. Chem. *284*, 21777–21781.

Que, H., Liu, Y., Jia, Y., and Liu, S. (2011). Establishment and assessment of a simple and easily reproducible incision model of spinal cord neuron cells in vitro. In Vitro Cell. Dev. Biol. Anim. *47*, 558–564.

Quencer, R.M., Sheldon, J.J., Post, M.J., Diaz, R.D., Montalvo, B.M., Green, B.A., and Eismont, F.J. (1986). MRI of the chronically injured cervical spinal cord. AJR Am. J. Roentgenol. *147*, 125–132.

Raff, M.C., Barres, B.A., Burne, J.F., Coles, H.S., Ishizaki, Y., and Jacobson, M.D. (1993). Programmed cell death and the control of cell survival: lessons from the nervous system. Science *262*, 695–700.

Rempe, D.A., Takano, T., and Nedergaard, M. (2009). TR(I)Pping towards treatment for ischemia. Nat. Neurosci. *12*, 1215–1216.

Reynolds, B.A., and Weiss, S. (1992). Generation of neurons and astrocytes from isolated cells of the adult mammalian central nervous system. Science *255*, 1707–1710.

Rink, A., Fung, K.M., Trojanowski, J.Q., Lee, V.M., Neugebauer, E., and McIntosh, T.K. (1995). Evidence of apoptotic cell death after experimental traumatic brain injury in the rat. Am. J. Pathol. *147*, 1575–1583.

Rowland, J.W., Hawryluk, G.W.J., Kwon, B., and Fehlings, M.G. (2008). Current status of acute spinal cord injury pathophysiology and emerging therapies: promise on the horizon. Neurosurg. Focus *25*, E2.

Abu-Rub, M., McMahon, S., Zeugolis, D.I., Windebank, A., and Pandit, A. (2010). Spinal cord injury in vitro: modelling axon growth inhibition. Drug Discov. Today *15*, 436–443.

Ruscetti, T., Lehnert, B.E., Halbrook, J., Le Trong, H., Hoekstra, M.F., Chen, D.J., and Peterson, S.R. (1998). Stimulation of the DNA-dependent protein kinase by poly(ADP-ribose) polymerase. J. Biol. Chem. *273*, 14461–14467.

Ryazanova, L.V., Rondon, L.J., Zierler, S., Hu, Z., Galli, J., Yamaguchi, T.P., Mazur, A., Fleig, A., and Ryazanov, A.G. (2010). TRPM7 is essential for Mg(2+) homeostasis in mammals. Nat. Commun. *1*, 109.

Saeki, H., Matsumoto, M., Kaneko, S., Tsuruta, S., Cui, Y.J., Ohtake, K., Ishida, K., and Sakabe, T. (2004). Is intrathecal magnesium sulfate safe and protective against ischemic spinal cord injury in rabbits? Anesth. Analg. *99*, 1805–1812, table of contents.

Salvesen, G.S., and Dixit, V.M. (1997). Caspases: intracellular signaling by proteolysis. Cell *91*, 443–446.

Savitz, S.I., and Fisher, M. (2007). Future of neuroprotection for acute stroke: in the aftermath of the SAINT trials. Ann. Neurol. *61*, 396–402.

Scharenberg, A.M. (2005). TRPM2 and TRPM7: channel/enzyme fusions to generate novel intracellular sensors. Pflüg. Arch. Eur. J. Physiol. *451*, 220–227.

Schmitz, C., Perraud, A.-L., Johnson, C.O., Inabe, K., Smith, M.K., Penner, R., Kurosaki, T., Fleig, A., and Scharenberg, A.M. (2003). Regulation of vertebrate cellular Mg2+ homeostasis by TRPM7. Cell *114*, 191–200.

Schreiber, V., Dantzer, F., Ame, J.-C., and de Murcia, G. (2006). Poly(ADP-ribose): novel functions for an old molecule. Nat. Rev. Mol. Cell Biol. *7*, 517–528.

Scott, G.S., Szabó, C., and Hooper, D.C. (2004). Poly(ADP-ribose) polymerase activity contributes to peroxynitrite-induced spinal cord neuronal cell death in vitro. J. Neurotrauma *21*, 1255–1263.

Sekhon, L.H., and Fehlings, M.G. (2001). Epidemiology, demographics, and pathophysiology of acute spinal cord injury. Spine *26*, S2–12.

Selvarajah, S., Hammond, E., Haider, A.H., Abularrage, C.J., Becker, D., Hyder, O., Dhiman, N., Gupta, D., Black Iii, J.H., and Schneider, E.B. (2013). The Burden of Acute Traumatic Spinal Cord Injury among Adults in the United States: an Update. J. Neurotrauma.

Shuman, S.L., Bresnahan, J.C., and Beattie, M.S. (1997). Apoptosis of microglia and oligodendrocytes after spinal cord contusion in rats. J. Neurosci. Res. *50*, 798–808.

Sibilla, S., and Ballerini, L. (2009). GABAergic and glycinergic interneuron expression during spinal cord development: dynamic interplay between inhibition and excitation in the control of ventral network outputs. Prog. Neurobiol. *89*, 46–60.

Silani, V., Braga, M., Ciammola, A., Cardin, V., and Scarlato, G. (2000). Motor neurones in culture as a model to study ALS. J. Neurol. *247 Suppl 1*, I28–36.

Singleton, R.H., and Povlishock, J.T. (2004). Identification and characterization of heterogeneous neuronal injury and death in regions of diffuse brain injury: evidence for multiple independent injury phenotypes. J. Neurosci. Off. J. Soc. Neurosci. *24*, 3543–3553.

Smulson, M.E., Simbulan-Rosenthal, C.M., Boulares, A.H., Yakovlev, A., Stoica, B., Iyer, S., Luo, R., Haddad, B., Wang, Z.Q., Pang, T., et al. (2000). Roles of poly(ADP-ribosyl)ation and PARP in apoptosis, DNA repair, genomic stability and functions of p53 and E2F-1. Adv. Enzyme Regul. *40*, 183–215.

Springer, J.E., Azbill, R.D., and Knapp, P.E. (1999). Activation of the caspase-3 apoptotic cascade in traumatic spinal cord injury. Nat. Med. *5*, 943–946.

Stifani, N., Freitas, A.R.O., Liakhovitskaia, A., Medvinsky, A., Kania, A., and Stifani, S. (2008). Suppression of interneuron programs and maintenance of selected spinal motor neuron fates by the transcription factor AML1/Runx1. Proc. Natl. Acad. Sci. U. S. A. *105*, 6451–6456.

Sumoza-Toledo, A., and Penner, R. (2011). TRPM2: a multifunctional ion channel for calcium signalling. J. Physiol. *589*, 1515–1525.

Sun, H.-S., Jackson, M.F., Martin, L.J., Jansen, K., Teves, L., Cui, H., Kiyonaka, S., Mori, Y., Jones, M., Forder, J.P., et al. (2009). Suppression of hippocampal TRPM7 protein prevents delayed neuronal death in brain ischemia. Nat. Neurosci. *12*, 1300–1307.

Susin, S.A., Lorenzo, H.K., Zamzami, N., Marzo, I., Snow, B.E., Brothers, G.M., Mangion, J., Jacotot, E., Costantini, P., Loeffler, M., et al. (1999). Molecular characterization of mitochondrial apoptosis-inducing factor. Nature *397*, 441–446.

Szabó, C., and Dawson, V.L. (1998). Role of poly(ADP-ribose) synthetase in inflammation and ischaemia-reperfusion. Trends Pharmacol. Sci. *19*, 287–298.

Szydlowska, K., and Tymianski, M. (2010). Calcium, ischemia and excitotoxicity. Cell Calcium *47*, 122–129.

Taccola, G., Margaryan, G., Mladinic, M., and Nistri, A. (2008). Kainate and metabolic perturbation mimicking spinal injury differentially contribute to early damage of locomotor networks in the in vitro neonatal rat spinal cord. Neuroscience *155*, 538–555.

Taccola, G., Mladinic, M., and Nistri, A. (2010). Dynamics of early locomotor network dysfunction following a focal lesion in an in vitro model of spinal injury. Eur. J. Neurosci. *31*, 60–78.

Takagi, T., Takayasu, M., Mizuno, M., Yoshimoto, M., and Yoshida, J. (2003). Caspase activation in neuronal and glial apoptosis following spinal cord injury in mice. Neurol. Med. Chir. (Tokyo) *43*, 20–29; discussion 29–30.

Tanvig, M., Blaabjerg, M., Andersen, R.K., Villa, A., Rosager, A.M., Poulsen, F.R., Martinez-Serrano, A., Zimmer, J., and Meyer, M. (2009). A brain slice culture model for studies of endogenous and exogenous precursor cell migration in the rostral migratory stream. Brain Res. *1295*, 1–12.

Tator, C.H. (1972). Acute spinal cord injury: a review of recent studies of treatment and pathophysiology. Can. Med. Assoc. J. *107*, 143–145 passim.

Tator, C.H. (1995). Update on the pathophysiology and pathology of acute spinal cord injury. Brain Pathol. Zurich Switz. *5*, 407–413.

Tator, C.H., and Koyanagi, I. (1997). Vascular mechanisms in the pathophysiology of human spinal cord injury. J. Neurosurg. *86*, 483–492.

Taylor, A.R., Robinson, M.B., and Milligan, C.E. (2007). In vitro methods to prepare astrocyte and motoneuron cultures for the investigation of potential in vivo interactions. Nat. Protoc. *2*, 1499–1507.

Temkin, N.R., Anderson, G.D., Winn, H.R., Ellenbogen, R.G., Britz, G.W., Schuster, J., Lucas, T., Newell, D.W., Mansfield, P.N., Machamer, J.E., et al. (2007). Magnesium sulfate for neuroprotection after traumatic brain injury: a randomised controlled trial. Lancet Neurol. *6*, 29–38.

Thayer, S.A., and Wang, G.J. (1995). Glutamate-induced calcium loads: effects on energy metabolism and neuronal viability. Clin. Exp. Pharmacol. Physiol. *22*, 303–304.

Thompson, M.R., Xu, D., and Williams, B.R.G. (2009). ATF3 transcription factor and its emerging roles in immunity and cancer. J. Mol. Med. Berl. Ger. *87*, 1053–1060.

Thuret, S., Moon, L.D.F., and Gage, F.H. (2006). Therapeutic interventions after spinal cord injury. Nat. Rev. Neurosci. *7*, 628–643.

Tresch, M.C., and Kiehn, O. (2002). Synchronization of motor neurons during locomotion in the neonatal rat: predictors and mechanisms. J. Neurosci. Off. J. Soc. Neurosci. *22*, 9997–10008.

Tsujino, H., Kondo, E., Fukuoka, T., Dai, Y., Tokunaga, A., Miki, K., Yonenobu, K., Ochi, T., and Noguchi, K. (2000). Activating transcription factor 3 (ATF3) induction by axotomy in sensory and motoneurons: A novel neuronal marker of nerve injury. Mol. Cell. Neurosci. *15*, 170–182.

Tsuzuki, K., Kondo, E., Fukuoka, T., Yi, D., Tsujino, H., Sakagami, M., and Noguchi, K. (2001). Differential regulation of P2X(3) mRNA expression by peripheral nerve injury in intact and injured neurons in the rat sensory ganglia. Pain *91*, 351–360.

Tymianski, M., Wallace, M.C., Spigelman, I., Uno, M., Carlen, P.L., Tator, C.H., and Charlton, M.P. (1993). Cell-permeant Ca2+ chelators reduce early excitotoxic and ischemic neuronal injury in vitro and in vivo. Neuron *11*, 221–235.

Valadka, A.B., Goodman, J.C., Gopinath, S.P., Uzura, M., and Robertson, C.S. (1998). Comparison of brain tissue oxygen tension to microdialysis-based measures of cerebral ischemia in fatally head-injured humans. J. Neurotrauma *15*, 509–519.

Vandenabeele, P., Vanden Berghe, T., and Festjens, N. (2006). Caspase inhibitors promote alternative cell death pathways. Sci. STKE Signal Transduct. Knowl. Environ. *2006*, pe44.

Vandenabeele, P., Galluzzi, L., Vanden Berghe, T., and Kroemer, G. (2010). Molecular mechanisms of necroptosis: an ordered cellular explosion. Nat. Rev. Mol. Cell Biol. *11*, 700–714.

Vander Heiden, M.G., and Thompson, C.B. (1999). Bcl-2 proteins: regulators of apoptosis or of mitochondrial homeostasis? Nat. Cell Biol. *1*, E209–216.

Wang, A., Arantes, S., Yan, L., Kiguchi, K., McArthur, M.J., Sahin, A., Thames, H.D., Aldaz, C.M., and Macleod, M.C. (2008). The transcription factor ATF3 acts as an oncogene in mouse mammary tumorigenesis. BMC Cancer *8*, 268.

Wang, L., Deng, S., Lu, Y., Zhang, Y., Yang, L., Guan, Y., Jiang, H., and Li, H. (2012). Increased inflammation and brain injury after transient focal cerebral ischemia in activating transcription factor 3 knockout mice. Neuroscience *220*, 100–108.

Wang, Y., Dawson, V.L., and Dawson, T.M. (2009). Poly(ADP-ribose) signals to mitochondrial AIF: a key event in parthanatos. Exp. Neurol. *218*, 193–202.

Wang, Y., Kim, N.S., Haince, J.-F., Kang, H.C., David, K.K., Andrabi, S.A., Poirier, G.G., Dawson, V.L., and Dawson, T.M. (2011). Poly(ADP-ribose) (PAR) binding to apoptosis-inducing factor is critical for PAR polymerase-1-dependent cell death (parthanatos). Sci. Signal. *4*, ra20.

Wei, W.-L., Sun, H.-S., Olah, M.E., Sun, X., Czerwinska, E., Czerwinski, W., Mori, Y., Orser, B.A., Xiong, Z.-G., Jackson, M.F., et al. (2007). TRPM7 channels in hippocampal neurons detect levels of extracellular divalent cations. Proc. Natl. Acad. Sci. U. S. A. *104*, 16323–16328.

Weiss, S., Dunne, C., Hewson, J., Wohl, C., Wheatley, M., Peterson, A.C., and Reynolds, B.A. (1996). Multipotent CNS stem cells are present in the adult mammalian spinal cord and ventricular neuroaxis. J. Neurosci. Off. J. Soc. Neurosci. *16*, 7599–7609.

Whalen, M.J., Clark, R.S., Dixon, C.E., Robichaud, P., Marion, D.W., Vagni, V., Graham, S.H., Virag, L., Hasko, G., Stachlewitz, R., et al. (1999). Reduction of cognitive and motor deficits after traumatic brain injury in mice deficient in poly(ADP-ribose) polymerase. J. Cereb. Blood Flow Metab. Off. J. Int. Soc. Cereb. Blood Flow Metab. *19*, 835–842.

Wichterle, H., Garcia-Verdugo, J.M., and Alvarez-Buylla, A. (1997). Direct evidence for homotypic, glia-independent neuronal migration. Neuron *18*, 779–791.

Wrathall, J.R., Teng, Y.D., and Choiniere, D. (1996). Amelioration of functional deficits from spinal cord trauma with systemically administered NBQX, an antagonist of non-N-methyl-D-aspartate receptors. Exp. Neurol. *137*, 119–126.

Wu, K.L.H., Hsu, C., and Chan, J.Y.H. (2007). Impairment of the mitochondrial respiratory enzyme activity triggers sequential activation of apoptosis-inducing factor-dependent and caspase-dependent signaling pathways to induce apoptosis after spinal cord injury. J. Neurochem. *101*, 1552–1566.

Xia, Y., Dawson, V.L., Dawson, T.M., Snyder, S.H., and Zweier, J.L. (1996). Nitric oxide synthase generates superoxide and nitric oxide in arginine-depleted cells leading to peroxynitrite-mediated cellular injury. Proc. Natl. Acad. Sci. U. S. A. *93*, 6770–6774.

Xie, Y.-F., Macdonald, J.F., and Jackson, M.F. (2010). TRPM2, calcium and neurodegenerative diseases. Int. J. Physiol. Pathophysiol. Pharmacol. *2*, 95–103.

Xiong, Y., Rabchevsky, A.G., and Hall, E.D. (2007). Role of peroxynitrite in secondary oxidative damage after spinal cord injury. J. Neurochem. *100*, 639–649.

Yamamoto, K., Ishikawa, T., Sakabe, T., Taguchi, T., Kawai, S., and Marsala, M. (1998). The hydroxyl radical scavenger Nicaraven inhibits glutamate release after spinal injury in rats. Neuroreport *9*, 1655–1659.

Yamamoto, S., Yamamoto, N., Kitamura, T., Nakamura, K., and Nakafuku, M. (2001a). Proliferation of parenchymal neural progenitors in response to injury in the adult rat spinal cord. Exp. Neurol. *172*, 115–127.

Yamamoto, S., Nagao, M., Sugimori, M., Kosako, H., Nakatomi, H., Yamamoto, N., Takebayashi, H., Nabeshima, Y., Kitamura, T., Weinmaster, G., et al. (2001b). Transcription factor expression and Notch-dependent regulation of neural progenitors in the adult rat spinal cord. J. Neurosci. Off. J. Soc. Neurosci. *21*, 9814–9823.

Ye, H., Cande, C., Stephanou, N.C., Jiang, S., Gurbuxani, S., Larochette, N., Daugas, E., Garrido, C., Kroemer, G., and Wu, H. (2002). DNA binding is required for the apoptogenic action of apoptosis inducing factor. Nat. Struct. Biol. *9*, 680–684.

Yong, C., Arnold, P.M., Zoubine, M.N., Citron, B.A., Watanabe, I., Berman, N.E., and Festoff, B.W. (1998). Apoptosis in cellular compartments of rat spinal cord after severe contusion injury. J. Neurotrauma *15*, 459–472.

Yoshino, O., Matsuno, H., Nakamura, H., Yudoh, K., Abe, Y., Sawai, T., Uzuki, M., Yonehara, S., and Kimura, T. (2004). The role of Fas-mediated apoptosis after traumatic spinal cord injury. Spine *29*, 1394–1404.

Yu, S.-W., Andrabi, S.A., Wang, H., Kim, N.S., Poirier, G.G., Dawson, T.M., and Dawson, V.L. (2006). Apoptosis-inducing factor mediates poly(ADP-ribose) (PAR) polymer-induced cell death. Proc. Natl. Acad. Sci. U. S. A. *103*, 18314–18319.

Yu, W., Ginjala, V., Pant, V., Chernukhin, I., Whitehead, J., Docquier, F., Farrar, D., Tavoosidana, G., Mukhopadhyay, R., Kanduri, C., et al. (2004). Poly(ADP-ribosyl)ation regulates CTCF-dependent chromatin insulation. Nat. Genet. *36*, 1105–1110.

Yuan, J., Lipinski, M., and Degterev, A. (2003). Diversity in the mechanisms of neuronal cell death. Neuron *40*, 401–413.

Yun, S.J., Byun, K., Bhin, J., Oh, J.-H., Nhung, L.T.H., Hwang, D., and Lee, B. (2010). Transcriptional regulatory networks associated with self-renewal and differentiation of neural stem cells. J. Cell. Physiol. *225*, 337–347.

Zagami, C.J., Zusso, M., and Stifani, S. (2009). Runx transcription factors: lineage-specific regulators of neuronal precursor cell proliferation and post-mitotic neuron subtype development. J. Cell. Biochem. *107*, 1063–1072.

Zhang, D.-W., Shao, J., Lin, J., Zhang, N., Lu, B.-J., Lin, S.-C., Dong, M.-Q., and Han, J. (2009). RIP3, an energy metabolism regulator that switches TNF-induced cell death from apoptosis to necrosis. Science *325*, 332–336.

Zhang, J., Dawson, V.L., Dawson, T.M., and Snyder, S.H. (1994). Nitric oxide activation of poly(ADP-ribose) synthetase in neurotoxicity. Science *263*, 687–689.

Zhang, J., O'Carroll, S.J., Wu, A., Nicholson, L.F.B., and Green, C.R. (2010). A model for ex vivo spinal cord segment culture--a tool for analysis of injury repair strategies. J. Neurosci. Methods *192*, 49–57.

Zhang, S.-J., Buchthal, B., Lau, D., Hayer, S., Dick, O., Schwaninger, M., Veltkamp, R., Zou, M., Weiss, U., and Bading, H. (2011). A signaling cascade of nuclear calcium-CREB-ATF3 activated by synaptic NMDA receptors defines a gene repression module that protects against extrasynaptic NMDA receptor-induced neuronal cell death and ischemic brain damage. J. Neurosci. Off. J. Soc. Neurosci. *31*, 4978–4990.

Zhu, C., Qiu, L., Wang, X., Hallin, U., Candé, C., Kroemer, G., Hagberg, H., and Blomgren, K. (2003). Involvement of apoptosis-inducing factor in neuronal death after hypoxia-ischemia in the neonatal rat brain. J. Neurochem. *86*, 306–317.

Zipfel, G.J., Babcock, D.J., Lee, J.M., and Choi, D.W. (2000). Neuronal apoptosis after CNS injury: the roles of glutamate and calcium. J. Neurotrauma *17*, 857–869.